



## **LIPOSOMES AS VERSATILE TOOLS: NANOREACTORS, MEMBRANE MODELS AND DRUG DELIVERY CARRIERS.**

**Gael Clergeaud Veiga**

**Dipòsit Legal: T 154-2015**

**ADVERTIMENT.** L'accés als continguts d'aquesta tesi doctoral i la seva utilització ha de respectar els drets de la persona autora. Pot ser utilitzada per a consulta o estudi personal, així com en activitats o materials d'investigació i docència en els termes establerts a l'art. 32 del Text Refós de la Llei de Propietat Intel·lectual (RDL 1/1996). Per altres utilitzacions es requereix l'autorització prèvia i expressa de la persona autora. En qualsevol cas, en la utilització dels seus continguts caldrà indicar de forma clara el nom i cognoms de la persona autora i el títol de la tesi doctoral. No s'autoritza la seva reproducció o altres formes d'explotació efectuades amb finalitats de lucre ni la seva comunicació pública des d'un lloc aliè al servei TDX. Tampoc s'autoritza la presentació del seu contingut en una finestra o marc aliè a TDX (framing). Aquesta reserva de drets afecta tant als continguts de la tesi com als seus resums i índexs.

**ADVERTENCIA.** El acceso a los contenidos de esta tesis doctoral y su utilización debe respetar los derechos de la persona autora. Puede ser utilizada para consulta o estudio personal, así como en actividades o materiales de investigación y docencia en los términos establecidos en el art. 32 del Texto Refundido de la Ley de Propiedad Intelectual (RDL 1/1996). Para otros usos se requiere la autorización previa y expresa de la persona autora. En cualquier caso, en la utilización de sus contenidos se deberá indicar de forma clara el nombre y apellidos de la persona autora y el título de la tesis doctoral. No se autoriza su reproducción u otras formas de explotación efectuadas con fines lucrativos ni su comunicación pública desde un sitio ajeno al servicio TDR. Tampoco se autoriza la presentación de su contenido en una ventana o marco ajeno a TDR (framing). Esta reserva de derechos afecta tanto al contenido de la tesis como a sus resúmenes e índices.

**WARNING.** Access to the contents of this doctoral thesis and its use must respect the rights of the author. It can be used for reference or private study, as well as research and learning activities or materials in the terms established by the 32nd article of the Spanish Consolidated Copyright Act (RDL 1/1996). Express and previous authorization of the author is required for any other uses. In any case, when using its content, full name of the author and title of the thesis must be clearly indicated. Reproduction or other forms of for profit use or public communication from outside TDX service is not allowed. Presentation of its content in a window or frame external to TDX (framing) is not authorized either. These rights affect both the content of the thesis and its abstracts and indexes.

# Liposomes as versatile tools: nanoreactors, membrane models and drug delivery carriers

Gael Clergeaud Veiga

Doctoral Thesis



UNIVERSITAT  
ROVIRA I VIRGILI

Department of Chemical Engineering

2014



# Liposomes as versatile tools: nanoreactors, membrane models and drug delivery carriers

Doctoral Thesis supervised by

Dr. Mayreli Ortiz and Dr. Ciara O'Sullivan



UNIVERSITAT  
ROVIRA I VIRGILI

Department of Chemical Engineering  
University Rovira i Virgili  
Tarragona  
Spain

2014





# Liposomes as versatile tools: nanoreactors, membrane models and drug delivery carriers

## Tribunal members:

**Prof. Pau Ballester**

(Institute of Chemical Research of Catalonia, University of Rovira i Virgili)

**Prof. Daniel Maspoch Comamala**

(Catalan Institute of Nanoscience and Nanotechnology, Autonomous University of Barcelona)

**Prof. Fatouros Dimitrios**

(Aristotle University of Thessaloniki)

**Prof. Alex Fragoso**

(University of Rovira i Virgili)

**Dr. César Fernández Sánchez**

(Barcelona Microelectronics Institute, CNM-CSIC, Autonomous University of Barcelona)

**Dr. Rukan Genç**

(University of Mersin)

## External examiners:

**Prof. Thomas Lars Andresen**

(Technical University of Denmark)

**Dr. Neil Keegan**

(Institute of Cellular Medicine, University of Newcastle)



UNIVERSITAT  
ROVIRA I VIRGILI

Department of Chemical Engineering  
University Rovira i Virgili  
Tarragona  
Spain

2014





Department of Chemical Engineering

Universitat Rovira i Virgili

Av. Països Catalans 26

43007 Tarragona, Spain

Tel: 977 55 96 58

Fax: 977 55 96 67

I STATE that the present study, entitled "Liposomes as versatile tools: nanoreactors, membrane models and drug delivery carriers", presented by Gael Clergeaud Veiga for the award of the degree of Doctor, has been carried out under my supervision at the Department of Chemical Engineering of this university, and that it fulfils all the requirements to be eligible for the International Doctorate Award.

Tarragona, 15<sup>th</sup> October 2014

Doctoral Thesis Supervisor/s

Dr. Ciara O'Sullivan

Dr. Mayreli Ortiz

UNIVERSITAT ROVIRA I VIRGILI

LIPOSOMES AS VERSATILE TOOLS: NANOREACTORS, MEMBRANE MODELS AND DRUG DELIVERY CARRIERS.

Gael Clergeaud Veiga

Dipòsit Legal: T 154-2015

## Acknowledgments

The present doctoral thesis covers the work carried out through my three years as a Ph.D. student in the Nanobiotechnology & Bioanalysis group at the Department of Chemical Engineering of the University Rovira i Virgili. First of all I would like to thank my supervisors Dr. Ciara K. O'Sullivan and Dr. Mayreli Ortiz for their inspirational talks, great guidance and enormous support during my Master and Ph.D. thesis. They offered me the tools to construct what I am now. I would especially render my gratitude to Dr. Ciara K. O'Sullivan for believing in me for pursuing the Ph.D. within the group.

I would also want to express my gratitude to Prof. Thomas L. Andresen for giving me the chance to work in his lab, for the valuable discussions and for the priceless experiences garnered. I would also like to thank all the colleagues from the Colloids & Biological Interface group at the Technical University of Denmark for the constructive and friendly environment rendered up during my stay in Denmark, especially to my colleague Houman.

I could not forget to give huge thanks to all the past and present members from the Nanobiotechnology & Bioanalysis group I have met along this "trip" for the enthusiastic research and friendly atmosphere rendered. To all the technicians, administratives and postdocs for their kindly help, and to all the Ph.D. students that we shared this great experience... Special mention goes to Jonathan for those irreplaceable and insanely good moments laughing out loud. I would also like to thank all the people from the URV microscopy unit for their helpful collaboration. In general, to all those people that have added something during this stage... you know who you are.

I would also want to appreciate the great support received from all my family, for always being so generous and open-minded, especially from my father Francis and my mother Teresa, whom have always believed on me and pushed me forward to achieve my goals. Infinitely grateful...

Last but not least, I want to thank immensely my girlfriend Alba, for her huge support, her wise advices and her unconditional love. She has been and is the accomplice of my life, and throughout this Ph.D. *trip* has made even finish a thesis possible.

## Agradecimientos

La presente tesis doctoral abarca el trabajo llevado a cabo durante mis tres años como estudiante de doctorado en el grupo *Nanobiotechnology & Bioanalysis* en el Departamento de Ingeniería Química de la Universidad Rovira i Virgili. En primer lugar me gustaría dar las gracias a mis supervisores Dr. Ciara K. O'Sullivan y Dr. Mayreli Ortiz por sus charlas inspiradoras, su gran orientación y su enorme apoyo durante mi tesis de master y doctorado. Me ofrecieron las herramientas para construir este proyecto. Me gustaría agradecer especialmente a la Dr. Ciara K. O'Sullivan por creer en mí para continuar con el doctorado dentro del grupo.

También me gustaría expresar mi gratitud al Prof. Thomas L. Andresen por darme la oportunidad de trabajar en su laboratorio, por las valiosas discusiones y las impagables experiencias recolectadas. También me gustaría dar las gracias a todos los miembros de su grupo *Colloids & Biological Interface* en la Universidad Técnica de Dinamarca por el amigable y constructivo ambiente creado durante mi estancia en Dinamarca, especialmente a mi colega Houman.

No podría olvidar agradecer enormemente a todos los colegas, pasados y presentes del grupo *Nanobiotechnology & Bioanalysis* que he conocido a lo largo de este "viaje", por crear un ambiente agradable y mostrar una entusiasta actividad investigadora. Gracias a todos los técnicos, personal administrativo y postdocs por su enorme y amable ayuda, y a todos los estudiantes de doctorado que hemos compartido esta gran experiencia... mención especial va para Jonathan, por esos momentos irremplazables e increíblemente buenos compartiendo risas y carcajadas. También me gustaría dar las gracias a todas las personas de la unidad de microscopía de la URV por su gran colaboración. En general, a todas aquellas personas que me han aportado algo durante esta etapa... ya sabeis quienes sois.

También me gustaría apreciar el gran apoyo recibido de toda mi familia, por estar siempre tan "abiertos de mente" y ser increíblemente generosos, especialmente de mi padre Francis y mi madre Teresa, quienes siempre han creído en mí y me han empujado hacia adelante para poder alcanzar mis metas. Gracias infinitamente...

Por último, pero no menos importante, quiero agradecer inmensamente a mi novia Alba, por su enorme apoyo, sus sabios consejos y su amor incondicional. Ella ha sido y es la cómplice de mi vida, y a lo largo de este doctorado ha hecho que incluso terminar una tesis sea posible.

## Table of contents

<b>SUMMARY</b> .....	<b>1</b>
<b>RESUMEN</b> .....	<b>4</b>
<b>LIST OF PUBLICATIONS</b> .....	<b>7</b>
<b>LIST OF SYMBOLS AND ABBREVIATIONS</b> .....	<b>9</b>
<b>LIST OF FIGURES</b> .....	<b>11</b>
<b>LIST OF TABLES</b> .....	<b>13</b>
<b>CHAPTER I - INTRODUCTION</b> .....	<b>15</b>
1.1. LIPOSOMES .....	17
1.1.1. <i>Lipids</i> .....	17
1.1.2. <i>Vesicle formation</i> .....	18
1.1.3. <i>Classification</i> .....	22
1.1.3.1. <i>Structural parameters</i> .....	22
1.1.3.2. <i>Liposome composition and functionalization</i> .....	23
1.2. METHODS FOR LIPOSOME PREPARATION AND CHARACTERIZATION .....	25
1.2.1. <i>Preparation of liposomes</i> .....	25
1.2.1.1. <i>Curvature-tuned method</i> .....	26
1.2.1.2. <i>Lipid thin-film hydration and extrusion method</i> .....	26
1.2.2. <i>Characterization of liposomes</i> .....	27
1.2.2.1. <i>Size and particle distribution</i> .....	27
1.2.2.2. <i>Lamellarity</i> .....	27
1.2.2.3. <i>Lipid composition and concentration</i> .....	28
1.2.2.4. <i>Surface charge</i> .....	28
1.2.2.5. <i>Phase transition temperature</i> .....	28
1.2.2.6. <i>Encapsulation efficiency</i> .....	29
1.3. APPLICATIONS .....	29
1.3.1. <i>Liposomes as nanoreactors for the controlled synthesis of metal nanoparticles</i> .....	31
1.3.2. <i>Liposomes as cell membrane models for the study of zinc ionophores</i> .....	32
1.3.3. <i>Liposomes as drug delivery carriers for anti-cancer therapy</i> .....	33
1.4. CONCLUDING REMARKS .....	35
1.5. THESIS OBJECTIVES .....	36
1.6. REFERENCES.....	37
<b>CHAPTER II - GREEN SYNTHESIS OF GOLD NANOPARTICLES USING GLYCEROL-INCORPORATED NANOSIZED LIPOSOMES</b> .....	<b>49</b>
<b>CHAPTER III - LIPOSOMAL NANOREACTORS FOR THE SYNTHESIS OF MONODISPERSE PALLADIUM NANOPARTICLES USING GLYCEROL</b> .....	<b>67</b>
<b>CHAPTER IV - SHAPE DIRECTED BIOMINERALIZATION OF GOLD NANOPARTICLES USING SELF-ASSEMBLED LIPID STRUCTURES</b> .....	<b>89</b>
<b>CHAPTER V - ZINC IONOPHORE ACTIVITY OF QUERCETIN AND EPIGALLOCATECHIN-GALLATE: FROM HEP1-6 CELLS TO A LIPOSOME MODEL</b> .....	<b>107</b>
<b>CHAPTER VI - A SIMPLE LIPOSOME ASSAY FOR THE SCREENING OF ZINC IONOPHORE ACTIVITY OF POLYPHENOLS</b> .....	<b>127</b>
<b>CHAPTER VII - ACTIVITY AND TOLERABILITY OF OXALIPLATIN FORMULATED IN SECRETORY PHOSPHOLIPASE A<sub>2</sub>-SENSITIVE LIPOSOMES AS ANTICANCER DRUGS</b> .....	<b>147</b>
<b>GENERAL CONCLUSIONS</b> .....	<b>173</b>



UNIVERSITAT ROVIRA I VIRGILI

LIPOSOMES AS VERSATILE TOOLS: NANOREACTORS, MEMBRANE MODELS AND DRUG DELIVERY CARRIERS.

Gael Clergeaud Veiga

Dipòsit Legal: T 154-2015

## Summary

The biocompatible, biodegradable and non-immunogenic nature of liposomes, together with their ability to encapsulate both hydro- and lipo-philic molecules in the aqueous core and within the lipid membrane, results in remarkably attractive structures for many scientific disciplines. In addition, liposomes are incredibly versatile structures that can be easily produced and functionalized in order to fit requirements for a large number of different applications.

The overall objective of the present doctoral thesis is to exploit the advantageous properties of liposomes and demonstrate their versatility as multifaceted tools in several applications.

This doctoral thesis is divided in seven chapters. A general introduction which covers the liposome state of the art as well as different topics of the thesis is presented in Chapter I. The following Chapter II, III and IV are related with the use of liposomes as nanoreactors for the controlled synthesis of metallic nanoparticles. Chapter V and VI involve the study of the zinc-ionophore activity of dietary polyphenols exploiting liposomes as cell membrane systems. Finally, Chapter VII covers the development of an enzyme-sensitive liposome carrier for the site-specific delivery of chemotherapeutics for cancer therapy.

In Chapter II, the use of glycerol within liposomal nanoreactors was explored for the green synthesis of gold nanoparticles. The liposomal nanoreactors composed of DOPG lipids were demonstrated to provide a nanoenvironment surrounded by a fluid-like membrane where semi-mobile glycerol molecules provide nucleation sites for subsequent controlled nanoparticle growth. In addition, reaction parameters such as temperature, glycerol concentration and the effect of additional capping agent were studied in terms of their effect on the size and the homogeneity of nanoparticles formed and were compared to the solution-based synthesis studied under the same conditions.

Chapter III explores the use of liposomes as nanoreactors for the development of an environmentally-friendly method for preparation of very small palladium nanoparticles exploiting glycerol as both reducing and capping agent. The synthesised palladium nanoparticles were compared in terms of size, shape and homogeneity between the ones produced via solution-based methods and within liposomal nanoreactors under the same conditions. In addition, we have demonstrated the strong influence of the membrane composition characteristics of the nanoreactors, such as transition temperature, head group and surface charge, in modulating the reduction kinetics of the nanoparticle synthesis, thus affecting their final size, shape and homogeneity. Furthermore, glycerol was postulated to act as a capping agent to stabilize small nanoparticles and prevent nanoparticle growth. The palladium nanoparticles were characterized using transmission electron microscopy, selected area electron diffraction, Fourier transform infrared and Raman spectroscopies, X-ray diffraction and dynamic light scattering to determine their morphology, size, charge, surface chemistry and crystal structure. The catalytic activity of the nanoparticles was also demonstrated for the reduction of p-nitrophenol to p-aminophenol as a model reaction.

Lipid molecules are also known to form a wide number of supramolecular structures by self-assembly. The ability of lipid molecules to form such polymorphic arrangements was explored in Chapter IV for the preparation of lipid templates by carefully selecting lipids with specific shapes and transition temperatures, in which the reduction of gold nanoparticles by citrate was shaped by those structures. The prepared lipid templates, including rectangular, hexagonal and twisted ribbons nanostructures, were demonstrated to function as effective templates for the

synthesis of shape-tuned gold nanoparticles, such as planar or hexagonal disks, and twisted ribbons or chain-like structures.

Dietary polyphenols have been reported to modulate the intracellular levels of labile zinc, consequently affecting the activity of numerous signalling and metabolic cellular pathways. In Chapter V we have demonstrated the capacity of two of the most consumed phenolic compounds present in the human diet, quercetin and epigallocatechin-gallate, to increase the amount of labile zinc within mouse hepatocarcinoma Hepa 1-6 cells, and compared the results with the well-reported ionophore clioquinol. However, in order to confirm that the polyphenols transport zinc cations across the plasma membrane independently of cell transport mechanisms, such as zinc transporters or endocytosis, we explored the use of FluoZin-3 loaded liposomes as simple membrane systems that mimic the cell membrane. The zinc ionophore activity was determined as the capacity of polyphenols to transport zinc inside the liposomes and increase the zinc-specific fluorescence of the encapsulated fluorophore FluoZin-3. Characterization studies including dynamic light scattering, zeta potential, and confocal and transmission electron microscopy were also performed in order to confirm that the fluorescent signal emerges from the inner part of the liposomes and to check their stability after treatments.

In Chapter VI we studied the zinc ionophore activity of a selected library consisting of the most relevant dietary polyphenols by exploiting the same liposomal system. The zinc ionophore effect relies on the ability of the compounds to bind zinc cations and facilitate its transport across the lipid bilayer. Therefore, we first evaluated the zinc-chelating strength of the phenolic compounds in a competition assay based on the fluorescence quenching of zinc-dependent fluorescence emitted by zinc-FluoZin-3 complex, and in the second part of the work, we classified the phenolic compounds according to their ionophore activity by means of fluorescence emanating from FluoZin-3 encapsulated within liposomes. The correlation between the chelation capacity and ionophore activity underlines the different behaviours phenolic compounds can display, sequestering or ionophoric, thus, giving us a better knowledge of the importance of the structural conformation versus their biological activity.

Finally, Chapter VII consists of the work carried out in the group of Thomas L. Andresen (Colloids & Biological Interfaces Group) at the Technical University of Denmark (DTU). In this work, an enzyme-sensitive pegylated liposome drug delivery system was developed for the site-specific delivery of oxaliplatin, a chemotherapeutic agent, to treat colon cancer. Long circulating pegylated liposomal oxaliplatin confirmed to have the ability to confine the drug, thus limiting its' toxic side-effects, and to enhance drug accumulation in the tumor tissue by the EPR effect. In addition, the membrane of the liposome carrier was designed to be enzyme-sensitive towards its degradation by secretory phospholipase A<sub>2</sub> (sPLA<sub>2</sub>), an overexpressed enzyme in many cancer cells, thus resulting in a site-specific release of oxaliplatin only in cancer tissue. At first, we have demonstrated in a calcein release study that by modulating the ratio between DPPC and DPPG lipid present in the liposome membrane, we were able to tune its' sensitivity towards sPLA<sub>2</sub> activity and modify the drug release profile. *In vitro* treatment of cancer cell lines with sPLA<sub>2</sub>-sensitive liposomes loaded with oxaliplatin resulted in a superior growth inhibition compared to free drug or drug loaded within conventional liposomes. In addition, we have shown that the hydrolysis by-products formed by sPLA<sub>2</sub>, lysolipids and fatty acids, are capable of acting as cell permeability enhancers and display toxic effect. Finally, *in vivo* studies performed in mice with sPLA<sub>2</sub>-secreting human colon cancer xenograft models resulted in an improvement in tumor growth delay compared to the free drug, but not to conventional liposomal drug. In conclusion, the developed enzyme-sensitive liposomal oxaliplatin carrier was able to effectively enhance the

pharmacokinetics of the drug, but suffered from a reduced triggered release response in the complex *in vivo* scenario.

## Resumen

La propia naturaleza biocompatible, biodegradable y no inmunogénica de los liposomas, junto con su capacidad para encapsular tanto moléculas hidrofílicas como lipofílicas en el núcleo acuoso o dentro de la membrana lipídica, dan como resultado estructuras muy atractivas para numerosas disciplinas científicas. Además, los liposomas son estructuras muy versátiles que pueden ser fácilmente producidos y funcionalizados con el fin de ser adaptados a los requisitos de un gran número de aplicaciones diferentes.

El objetivo principal de la presente tesis doctoral es aprovechar las propiedades ventajosas de los liposomas y demostrar su versatilidad como herramienta multifacética en varias aplicaciones.

Esta tesis doctoral se divide en siete capítulos. Una introducción general que cubre el estado del arte sobre los liposomas, así como diferentes temas tratados a lo largo de la tesis, se presentan en el capítulo I. Los siguientes capítulos II, III y IV están relacionados con el uso de liposomas como nanoreactores para la síntesis controlada de nanopartículas metálicas. Capítulos V y VI envuelven el estudio de la actividad de ionófora de zinc que poseen ciertos polifenoles presentes en la dieta mediante el uso de liposomas como sistemas de membrana celular. Finalmente, el Capítulo VII cubre el desarrollo de liposomas que son sensibles a la degradación por una enzima como vehículos para la entrega específica de agentes quimioterapéuticos para el tratamiento del cáncer.

En el Capítulo II, se exploró el uso de glicerol dentro nanoreactores liposomales para la síntesis de nanopartículas de oro de forma respetuosa para el medio ambiente. Los nanoreactores compuestos de lípidos DOPG se demostró que proporcionan un nano-espacio rodeado por la membrana en un estado fluídico donde las moléculas de glicerol se desplazan semi-libremente proporcionando sitios de nucleación para el crecimiento posterior de nanopartículas de una forma más controlada. Además, ciertos parámetros de la reacción se estudiaron, tales como la temperatura, concentración de glicerol y el efecto de la presencia adicional de un agente de protección, y sus consecuencias fueron analizadas en relación a su efecto sobre el tamaño y la homogeneidad de las nanopartículas formadas. Además las nanopartículas producidas fueron comparadas con las producidas en solución bajo las mismas condiciones estudiadas.

El capítulo III explora el uso de liposomas como nanoreactores para el desarrollo de un método respetuoso con el medio ambiente para la preparación de nanopartículas muy pequeñas de paladio usando glicerol como agente reductor y protector. Las nanopartículas de paladio sintetizadas se compararon en términos de tamaño, forma y homogeneidad, y bajo las mismas condiciones, con las producidas a través del método de síntesis en solución y con el método de nanoreactores liposomales. Además, se ha demostrado la fuerte influencia que las características de la membrana de los nanoreactores, tales como la temperatura de transición, el grupo presente en la cabeza de los lípidos y la carga de la superficie, tienen en la modulación de la cinética de reducción de la síntesis de nanopartículas, lo que afectará a su tamaño, su forma y la homogeneidad de la población final. Por otra parte, el glicerol se postuló como posible agente de protección para estabilizar las pequeñas nanopartículas y evitar su crecimiento. Las nanopartículas de paladio producidas se caracterizaron mediante microscopía electrónica de transmisión, difracción de electrones en área seleccionada, espectroscopía de Raman e infrarrojos por transformada de Fourier, difracción de rayos X y dispersión de luz dinámica para la determinación de su estructura en términos de morfología, tamaño, carga, química de

superficie y estructura cristalina. La actividad catalítica de las nanopartículas también se demostró para la reducción de p-nitrofenol a p-aminofenol como reacción modelo.

Las moléculas de lípidos también son conocidas por formar, gracias a sus propiedades de auto-ensamblaje, un gran número de estructuras supramoleculares. La capacidad de estas moléculas lipídicas para formar tales configuraciones polimórficas se exploró en el Capítulo IV para la preparación de plantillas de lipídicas, seleccionando cuidadosamente los lípidos con formas y temperaturas de transición específicas, en los que la reducción por citrato de nanopartículas de oro ocurre de forma guiada por dichas estructuras. Las plantillas de lípidos preparadas, incluyendo nanoestructuras rectangulares, hexagonales y cintas retorcidas, han demostrado funcionar como eficaces plantillas para la síntesis de nanopartículas de oro con una forma específica, como discos planos, hexagonales, cintas retorcidas o estructuras en forma de cadena.

Los polifenoles presentes en la dieta han sido descritos como moduladores de los niveles intracelulares de zinc lábil, en consecuencia, afectando a la actividad de numerosas vías celulares de señalización y rutas metabólicas. En el capítulo V hemos demostrado la capacidad de dos de los compuestos fenólicos presentes y más consumidos en la dieta humana, la quercetina y el epigallocatequina-galato, de aumentar la cantidad de zinc lábil dentro de células de hepatocarcinoma en ratón Hepa 1-6. Dichos resultados se compararon con los resultados obtenidos con clioquinol, un bien conocido ionóforo del zinc. Sin embargo, con el fin de confirmar que los polifenoles son capaces de transportar los cationes de zinc a través de la membrana plasmática de forma independiente a los mecanismos de transporte celular, tales como transportadores de zinc o endocitosis, hemos explorado el uso de liposomas con FluoZin-3 encapsulado como simples sistemas de membrana que imitan la membrana celular. La actividad ionófora de zinc se determinó como la capacidad de los polifenoles para transportar zinc dentro de los liposomas y, en consecuencia, aumentar la fluorescencia producida por el fluoroforo encapsulado, FluoZin-3, al interactuar con el zinc. Diferentes estudios de caracterización incluyendo dispersión de luz dinámica, el potencial zeta, y microscopía confocal y electrónica de transmisión, se realizaron con el fin de confirmar que la señal fluorescente emerge de la parte interior de los liposomas y para verificar su estabilidad después de los tratamientos.

En el capítulo VI se presenta un estudio de la actividad ionófora de zinc de una biblioteca de los polifenoles más relevantes mediante la explotación del mismo sistema liposomal. El efecto ionóforo de zinc se basan en la capacidad de los compuestos para unirse a cationes de zinc y facilitar su transporte a través de la bicapa lipídica. Por lo tanto, primeramente se ha evaluado la fuerza de quelación entre el zinc y los compuestos fenólicos en un ensayo de competición basado en la disminución de la fluorescencia específica emitida por el complejo zinc-FluoZin-3. En la segunda parte del trabajo, se han clasificado el compuestos fenólicos por su actividad ionófora por medio del incremento en la fluorescencia procedente del FluoZin-3 encapsulado dentro de liposomas. La correlación entre la capacidad de quelación y la actividad ionóforo subraya los diferentes comportamientos que dichos compuestos fenólicos pueden mostrar, secuestradores o ionóforos del zinc, por lo tanto, mostrando un mejor conocimiento de la importancia entre la conformación estructural y su actividad biológica.

Por último, el capítulo VII consiste en el trabajo llevado a cabo en el grupo de Thomas L. Andresen (Grupo de Coloides y Biología de Interfaces) de la Universidad Técnica de Dinamarca (DTU). En este trabajo, un sistema de suministro de medicamento basado en liposomas pegilados sensibles a una enzima fue desarrollado para la entrega específica de oxaliplatino, un agente quimioterapéutico, para el tratamiento d cáncer de colon. Liposomas de larga circulación

y que encapsulan oxaliplatino tienen la capacidad de confinar el fármaco, lo que limita sus efectos secundarios tóxicos, y mejora la acumulación del fármaco en el tejido del tumor gracias a el efecto EPR. Además, la membrana de los liposomas fue diseñado para ser sensible a la degradación por una enzima, la secretada fosfolipasa A<sub>2</sub> (sPLA<sub>2</sub>), enzima que se sobreexpresa en muchas células cancerosas, lo que resulta en una liberación deliberada y específica de oxaliplatino solamente en el tejido de canceroso. Primeramente, se ha demostrado en un estudio de liberación de calceína que la modulación de la cantidad de lípidos DPPC y DPPG presentes en la membrana del liposoma es capaz de afinar su sensibilidad hacia la actividad de la sPLA<sub>2</sub> y por lo tanto modificar el perfil de liberación del fármaco. En el tratamiento *in vitro* de líneas celulares cancerosas con liposomas sensibles a la sPLA<sub>2</sub> cargados con oxaliplatino da lugar a una inhibición del crecimiento superior en comparación con el fármaco libre o encapsulado dentro de liposomas convencionales. Además, hemos demostrado que los subproductos formados por la hidrólisis causada por la sPLA<sub>2</sub>, lisolípidos y ácidos grasos, son capaces de actuar como potenciadores de la permeabilidad celular y también muestran un efecto tóxico para las células. Finalmente, los estudios *in vivo* realizados en ratones con modelos xenoinjertados de células de cáncer de colon humanas secretoras de sPLA<sub>2</sub> demostraron una mejoría en el retraso del crecimiento tumoral en el ratón en comparación con el fármaco libre, pero no en relación al fármaco encapsulado en liposomas convencional. En conclusión, el desarrollo de oxaliplatino encapsulado en liposomas sensibles a la enzima fue capaz de mejorar de manera efectiva la farmacocinética del compuesto, pero sin embargo, la liberación del fármaco, en el complejo escenario *in vivo*, sufre una reducción en la velocidad de liberación.

## List of publications

Genç R.; **Clergeaud G.**; Ortiz M.; O'Sullivan C.K. *Green synthesis of gold nanoparticles using glycerol-incorporated nanosized liposomes*. *Langmuir* 2011, 27, 10894-10900.

**Clergeaud G.**; Genç R.; Ortiz M.; O'Sullivan C.K. *Liposomal Nanoreactors For The Synthesis Of Monodisperse Palladium Nanoparticles Using Glycerol*. *Langmuir* 2013, 29, 15405–15413.

Genç R.; **Clergeaud G.**; Ortiz M.; O'Sullivan C.K. *Shape directed biomineralization of gold nanoparticles using self-assembled lipid structures*. *Biomater. Sci.* 2014, 2, 1128-1134.

Dabbagh-Bazarbachi H.; **Clergeaud G.**; Quesada I.M.; Ortiz M.; O'Sullivan C.K.; Fernández-Larrea J.B. *Zinc Ionophore Activity of Quercetin and Epigallocatechin-gallate: From Hepa 1-6 Cells to a Liposome Model*. *J. Agric. Food Chem.* 2014, 62, 8085–8093.

**Clergeaud G.**; Dabbagh-Bazarbachi H.; Ortiz M.; Fernández-Larrea J.B.; O'Sullivan C.K. *A simple liposome assay for the screening of zinc ionophore activity of polyphenols*. For submission to RSC Adv.

Pourhassan H.; **Clergeaud G.**; Hansen A.E.; Østrem R.G.; Fliedner F.P.; O'Sullivan C.K.; Kjær A.; Andresen T.L. *Activity and tolerability of oxaliplatin formulated in secretory phospholipase A<sub>2</sub>-sensitive liposomes as anticancer drugs*. For submission to ACS Nano.





## List of symbols and abbreviations

AFM	Atomic force microscopy	FI	Fluorescence intensity
Ag	Silver	FILIA	Flow-injection liposome immunoanalysis
AOT	Dioctylsulfosuccinate sodium salt	FTIR	Fourier transform infrared
Au	Gold	GAL	Gallic acid
CAF	Caffeic acid	GEN	Genistein
CAT	Catechol	GUV	Giant unilamellar vesicles
CAT	Catechin hydrate	HPLC	High-performance liquid chromatography
HYD		HSPC	hydrogenated L- $\alpha$ -phosphatidylcholine
CMC	Critical micelle concentration	ICP	Inductively coupled plasma
CQ	Clioquinol	KCl	Potassium chloride
CT	Computed tomography	LIA	Liposome immunoassay
CTAB	Cetyltrimethylammonium bromide	LILA	Liposome immunolysis assay
CTP	Curvature-tuned preparation	LISA	Liposome immunosorbent assay
Cu	Copper	LUT	Luteolin
DLS	Dynamic light scattering	LUV	Large unilamellar vesicles
DLVO	Derjaguin and Landau, Verwey and Overbeek	LysoPPC	1-palmitoyl-2-hydroxy-sn-glycero-3-phosphocholine
DMEM	Dulbecco's Modified Eagle Medium	LysoPPG	1-palmitoyl-2-hydroxy-sn-glycero-3-phospho-(1'-rac-glycerol)
DMSO	Dimethyl sulfoxide	M	Molar
DNA	Deoxyribonucleic acid	MCH	6-mercapto-1-hexanol
DOPE	1,2-dioleoyl-sn-glycero-3-phosphoethanolamine	MLV	Multilamellar vesicles
DOPG	1,2-dioleoyl-sn-glycero-3-phosphor-rac-(1-glycerol)	Mn	Magnesium
DPPC	1,2-dipalmitoyl-sn-glycero-3-phosphocholine	Mn(OH) <sub>2</sub>	Manganese hydroxide
DPPG	1,2-dipalmitoyl-sn-glycero-3-phosphorac-(1-glycerol)	MnCO <sub>3</sub>	Manganese carbonate
DSC	Differential scanning calorimetry	MPS	Mononuclear phagocyte system
DSPC	1,2-distearoyl-sn-glycero-3-phosphocholine	MR	Magnetic resonance
DSPE	1,2-distearoyl-sn-glycero-3-phosphoethanolamine	MS	Mass spectrometry
DSPG	1,2-distearoyl-sn-glycero-3-phospho-(1'-rac-glycerol)	MT	Metallothionein
$E_b$	Bending elasticity	Mv	Milivolt
EE	Encapsulation efficiency	MVV	Multivesicular vesicles
EGCG	Epigallocatechin-3-gallate	Na <sub>2</sub> HPO <sub>4</sub>	Disodium phosphate
ELSD	Evaporative light scattering detection	NaBH <sub>4</sub>	Sodium hydroxide
EM	Electron microscope	NaCl	Sodium chloride
EPR	Enhanced permeability and retention	NAR	Naringenin
ESEM	Environmental scanning electron microscope	nm	Nanometre
EXAFS	X-ray absorption fine-structure	NMR	Nuclear magnetic resonance
FAAS	Flame atomic absorption spectroscopy	NP	Nanoparticle
FBS	Fetal bovine serum	OLV	Oligolamellar vesicles
fcc	Face-centered-cubic	$P$	Packing parameter
FDA	Food and drug administration	PA	Phosphotungstic acid hydrate
FFF	Field-flow fractionation	PBS	Phosphate buffered saline
PdCl <sub>2</sub>	Palladium chloride	PC	Phosphocholine
		PCS	Photon correlation
		Pd	Palladium
		PYR	Pyrrhione

PEG	Polyethylene glycol	QCT	Quercetin
PG	Phosphoglycerol	RES	Reticuloendothelial system
PVP	Polyvinylpyrrolidone	REV	Reverse-phase evaporation
RNA	Ribonucleic acid	SUV	Small unilamellar vesicles
ROS	Reactive oxygen species	TAN	Tannic acid
RSV	Resveratrol	TAX	Taxifolin
RT	Room temperature	TEM	Transmission electron microscope
Ru	Ruthenium	Tio <sub>2</sub>	Titanium dioxide
RUT	Rutin	TLC	Thin-layer chromatography
SAED	Selected area electron diffraction	Tm	Phase transition temperature
SAXS	Small-angle X-ray spectroscopy	TPEN	N,N,N',N'-tetrakis (2-pyridylmethyl) ethylenediamine
SEC	Size-exclusion chromatography	XRD	X-ray diffraction
SERS	Surface enhanced Raman scattering	Zn	Zinc
SPECT	Single photon emission computed tomography	ZnCl <sub>2</sub>	Zinc chloride
sPLA <sub>2</sub>	Secreted phospholipase A <sub>2</sub>		

## List of figures

### CHAPTER I

Figure 1.1. Schematic illustration of a liposome encapsulating both hydrophilic (blue) and hydrophobic (orange) molecules. ....	17
Figure 1.2. Structural representation of a phospholipid with the different alcohol head groups and one saturated and mono-unsaturated fatty acid chains. ....	18
Figure 1.3. Schematic showing the different lipid shapes, their packing parameters and related structures of aggregates. ....	20
Figure 1.4. Schematic lipid phase transition diagram driven by the water concentration. ....	21
Figure 1.5. Schematic representation of the lipid phase transition temperature ( $T_m$ ). ....	22
Figure 1.6. Schematic classification of liposomes taking into account structural parameters. ....	23
Figure 1.7. Schematic illustration of different types of liposomes classified by their composition and surface functionalization. ....	23
Figure 1.8. Techniques for the preparation of liposomes of different sizes and lamellae. ....	25
Figure 1.9. Preparation of liposomes using the curvature-tuned method. ....	26
Figure 1.10. Preparation of liposomes employing the thin-film method. ....	27
Figure 1.11. Application of liposomes in many diverse fields. ....	29
Figure 1.12. Schematic illustration of the liposome passive-targeting phenomena via EPR effect. ....	34

### CHAPTER II

Figure 2.1. Table of contents figure.....	53
Figure 2.2. TEM images of the particles synthesized using the direct synthesis of gold nanoparticles using glycerol in PBS after 24 h of incubation.....	57
Figure 2.3. Schematic of the designed liposomal nanoreactor. ....	58
Figure 2.4. Formation stages of gold nanoparticles inside the glycerol-incorporated liposomes. ....	59
Figure 2.5. Effect of capping agent and glycerol concentration.....	61
Figure 2.6. Effect of temperature on the particle size and shape synthesized in glycerol (15% v/v)-incorporated liposomes in the presence of capping agent MCH at changing temperatures.....	62

### CHAPTER III

Figure 3.1. Table of contents figure.....	71
Figure 3.2. Structure of the lipid molecules used for the liposomal nanoreactor study.....	74
Figure 3.3. UV-vis spectra of $[PdCl_4]^{2-}$ and Pd NPs produced by glycerol in solution. ....	76
Figure 3.4. Effect of the concentration of glycerol on the solution-based synthesis of Pd nanoparticles. 77	
Figure 3.5. Schematic design of the glycerol-incorporated DOPG liposomal nanoreactor for the synthesis of Pd NPs.....	78
Figure 3.6. TEM images of Pd NPs obtained in solution (A) and within DOPG liposomes (B) using 10 % (v/v) glycerol and their corresponding size distribution graphs calculated using iTEM ( $n = 100$ ). ....	78
Figure 3.7. Lipid composition effect on the synthesis of Pd nanoparticles. ....	80
Figure 3.8. XRD pattern and SAED of the prepared Pd nanoparticles from glycerol-incorporated DOPG liposomes. ....	81
Figure 3.9. Schematic illustration of glycerol acting as a capping agent for nanoparticle stabilization. ....	82
Figure 3.10. FTIR spectra of (A) glycerol and (B) Pd NPs. ....	82
Figure 3.11. Raman spectra of glycerol, DOPG, and Pd nanoparticles. ....	83
Figure 3.12. Reduction of p-nitrophenolate (pNP) catalysed by palladium nanoparticles (Pd NPs) studied by UV-vis. ....	84

## CHAPTER IV

Figure 4.1. Proposed growth path of nanoparticle formation through membrane fusion of reactant encapsulating lipid structures.....	97
Figure 4.2. TEM images representing the square shaped templates, the purified gold nanoparticles and their XRD pattern.....	98
Figure 4.3. TEM images representing the hexagonal shaped templates, the purified gold nanoparticles and their XRD pattern.....	99
Figure 4.4. TEM images of twisted ribbon-shaped DMPG lipid self-assembly prepared at an operating temperature of 25 °C.....	100
Figure 4.5. Schemes outlining the different strategies for the use of twisted ribbon shaped lipid templates for the preparation of ribbon-like gold nanostructures and TEM images of gold nanostructures formed as a result of the methodology used.....	101
Figure 4.6. XRD pattern of nanostructures synthesized.....	102

## CHAPTER V

Figure 5.1. Table of contents figure.....	111
Figure 5.2. Schematic representation of zinc homeostasis.....	115
Figure 5.3. Effect of QCT, EGCG, and CQ on the cytoplasmic pool of labile zinc in Hepa 1-6 cells.....	116
Figure 5.4. Intensity of FluoZin-3 fluorescence signal from images in Figure 2 was quantified using quanta program and considering an equal number of cells in each field.....	117
Figure 5.5. Subcellular localization of FluoZin-3 detectable zinc in Hepa 1-6 cells after 4 h treatment in the same samples as in Figure 2 showed at a greater magnification.....	117
Figure 5.6. Schematic design of the FluoZin-3 loaded liposomes and the ionophore-like effect interpretation.....	118
Figure 5.7. Effect of QCT, EGCG and CQ on the uptake of zinc cations by liposomes.....	119
Figure 5.8. Three-dimensional confocal microscopy images of zinc dependent fluorescence emission of FluoZin-3 loaded within liposomes treated with zinc cations, polyphenols and CQ.....	120
Figure 5.9. Transmission electron micrographs of liposomes with encapsulated FluoZin-3 after treatment with ZnCl <sub>2</sub> , QCT, EGCG and CQ.....	120

## CHAPTER VI

Figure 6.1. Table of contents figure.....	131
Figure 6.2. Chelation strength of zinc cations by the polyphenols, clioquinol, pyrithione and TPEN.....	137
Figure 6.3. Liposome assay for the determination of zinc ionophore activity of polyphenols, clioquinol and pyrithione.....	138
Figure 6.4. Time-dependent fluorescence emission of FluoZin-3 loaded liposomes.....	139
Figure 6.5. Schematic comparison between zinc chelating strength and ionophore activity.....	141

## CHAPTER VII

Figure 7.1. Table of contents figure.....	151
Figure 7.2. In vitro sPLA <sub>2</sub> -dependent release kinetic of calcein from liposomal formulations.....	157
Figure 7.3. In vitro cytotoxicity of sPLA <sub>2</sub> -labile liposomes loaded with L-OHP against sPLA <sub>2</sub> -secreting Colo205 cells (A) and sPLA <sub>2</sub> -deficient HT-29 cells in the presence of Colo205 cell conditioned medium (contain sPLA <sub>2</sub> ) (B).....	158
Figure 7.4. In vitro cytotoxicity of unloaded sPLA <sub>2</sub> -sensitive liposomes comes predominantly from cellular lysis following sPLA <sub>2</sub> -driven hydrolysis and formation of permeability enhancing components.....	159
Figure 7.5. Inhibitory effect of sPLA <sub>2</sub> -sensitive liposomes on HT-29 cell proliferation is modulated by presence of serum components.....	160
Figure 7.6. Effect of sPLA <sub>2</sub> -degradable liposomal L-OHP against colorectal tumor growth in vivo.....	162

## List of tables

### CHAPTER I

Table 1.1. Summary of several surface chemistry approaches for the functionalization of liposomes. ....	24
Table 1.2. List of liposomal drugs clinically approved for marketing. ....	30

### CHAPTER II

Table 2.1. Particle size after 24 h of incubation at different glycerol concentrations in the presence and absence of a capping agent at 25 °C <sup>a</sup> . ....	60
--	----

### CHAPTER III

Table 3.1. Methodologies to produce palladium nanoparticles. ....	73
Table 3.2. Effect of the lipidic composition of the liposomal nanoreactor on the size and distribution of the palladium nanoparticles produced. ....	81

### CHAPTER IV

Table 4.1. Properties of the phospholipids studied and conditions for the preparation of differently shaped lipid templates. ....	95
---	----

### CHAPTER V

Table 5.1. Dynamic light scattering and $\zeta$ Potential measurements of liposomes loaded with FluoZin-3 before and after treatments. ....	118
---	-----

### CHAPTER VI

Table 6.1. Summary of the phenolic compounds used and divided according to class, food source, chemical structure and the number of hydroxyl groups present. ....	136
Table 6.2. Dynamic light scattering and Zeta-potential measurements of the liposomes loaded with FluoZin-3, as well as the fluorescence increment ( $\Delta$ ) caused by each compound, after the treatment with 10 $\mu$ M ZnCl <sub>2</sub> and polyphenols, clioquinol, pyrithione and TPEN at 50 $\mu$ M. ....	140

### CHAPTER VII

Table 7.1. In vivo evaluated liposomal formulations of oxaliplatin. ....	156
Table 7.2. Comparison of oxaliplatin and liposomal oxaliplatin against early-stage human Colo205 colorectal carcinoma. ....	163



---



CHAPTER I

# Introduction

---





## 1.1. Liposomes

Liposomes, from Greek etymology *lipos* meaning fat and *soma* meaning body, are spherical-shaped lipid vesicles that have garnered enormous interest due to their unique properties since they were discovered in the early 1960's by Alec D. Bangham<sup>1</sup>. Due to the amphiphilic nature of their lipidic building blocks, liposomes are formed by closed membrane-like bilayers that arrange concentrically around a hydrophilic cavity (Figure 1.1). This particular structural organization, offering hydrophilic (core) and hydrophobic (within the membrane) environments, as well as their biocompatible, biodegradable and non-immunogenic own nature, make liposomes one of the cornerstones of nanobiotechnology.

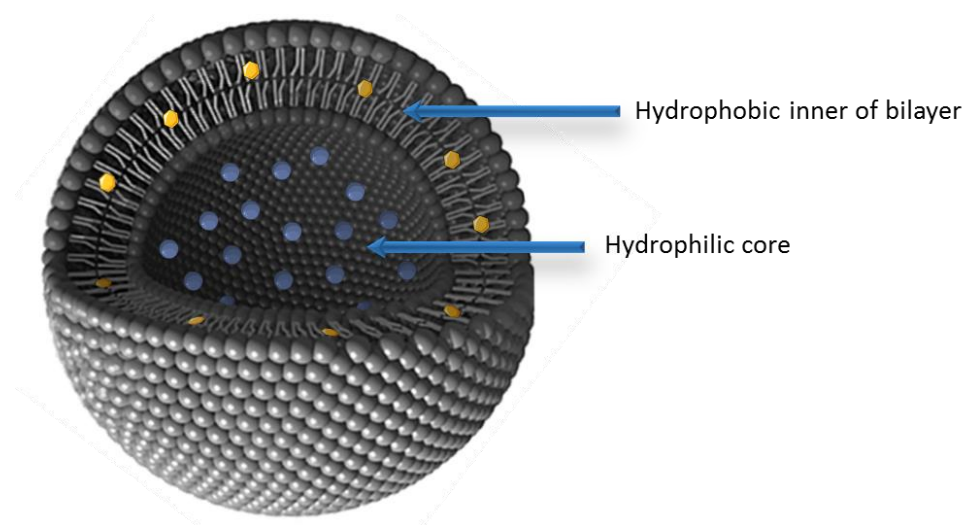


Figure 1.1. Schematic illustration of a liposome encapsulating both hydrophilic (blue) and hydrophobic (orange) molecules.

Liposomes are structurally and functionally some of the most versatile supramolecular assemblies in existence, thus offering advantageous properties that have positioned liposomes as well established structures in a large number of applications including drug/gene delivery platforms in pharmaceuticals<sup>2</sup> and cosmetics<sup>3</sup>, food technology<sup>4</sup>, models as biological cell membranes<sup>5</sup>, in analytical sciences as signal amplifiers (immunoassays)<sup>6</sup> amongst a plethora of further applications<sup>7</sup>.

### 1.1.1. Lipids

Lipids constitute part of the essential naturally-occurring biomolecules for the structure and function of any living organism, presenting a key biological role in energy storage, signalling and as structural membrane components. The main characteristic of lipids group together a diverse classification of organic molecules with appreciable structural differences, including fats, oils, hormones and phospholipids, that are related by their solubility in organic solvents and display water-insoluble properties.

Phospholipids are amphiphilic molecules containing both a hydrophilic and hydrophobic moiety that act as the main building blocks of biological membranes. In general, they are composed of four components, the fatty acids, a glycerol or sphingosine backbone, a phosphate and an alcohol attached to it. In the case of phosphoglycerids, two of the hydroxyl groups present in

the glycerol-backbone (at C-1 and C-2 positions) are esterified to the carboxyl groups of the fatty acid chains (saturated or unsaturated) forming the non-polar tails of the lipid that acts as a hydrophobic barrier. The remaining hydroxyl group of the glycerol backbone (at C-3) is esterified to the phosphoric acid, which at the same time, could be further linked by an ester bond between its phosphate group to the hydroxyl group of one of different alcohols, thus offering the hydrophilic properties required to enable interaction with the environment. Figure 1.2 depicts the structural formula of the phosphoglycerides with the common alcohol components, choline, ethanolamine, glycerol, inositol and serine.

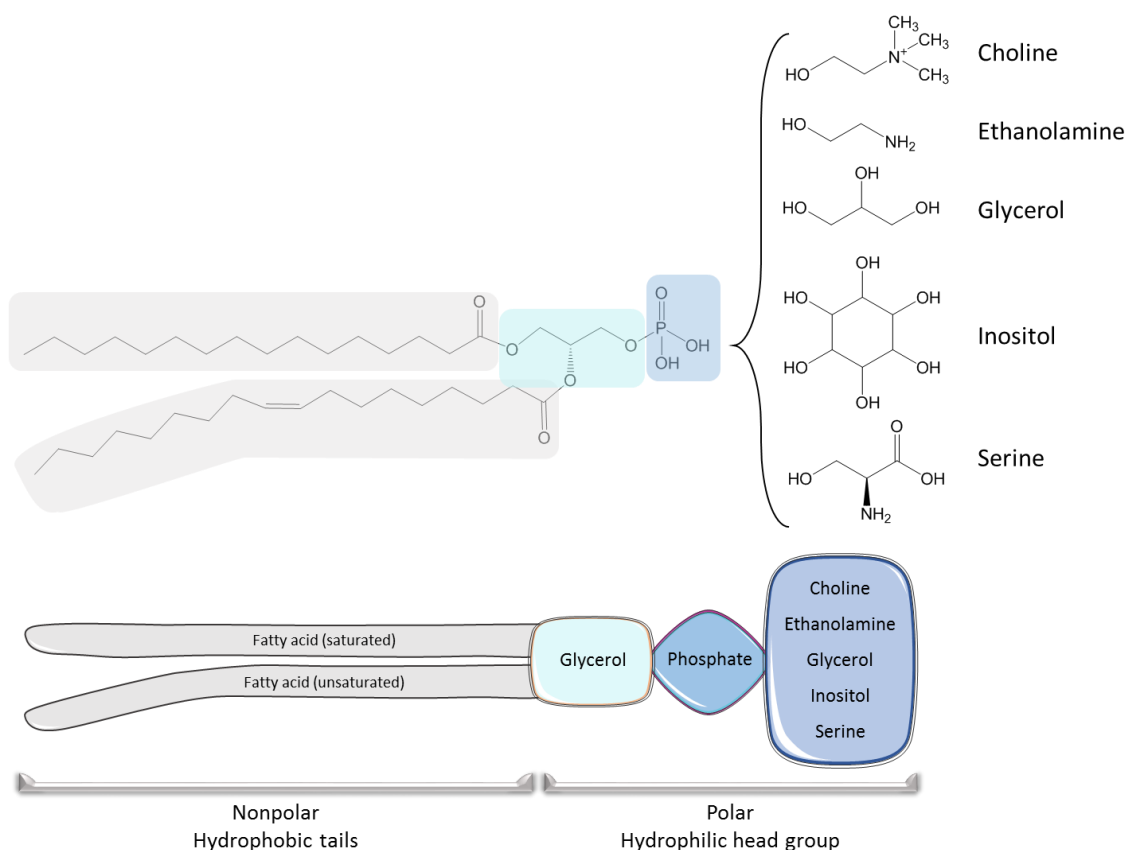


Figure 1.2. Structural representation of a phospholipid with the different alcohol head groups and one saturated and mono-unsaturated fatty acid chains.

Lipids can form an extraordinarily rich multitude of polymorphic structures through their self-assembly properties when surrounded in aqueous environments and, as highlighted by Luzzati<sup>8</sup>, lead a class of molecules displaying such a variety of structures in such a narrow range of physicochemical parameters.

### 1.1.2. Vesicle formation

The amphiphilic nature of phospholipids can be explained by their dual preference for water. In 1972, Singer and Nicholson presented the “fluid mosaic model” in which they reported that the lipids head groups can be exposed to aqueous environments due to their hydrophilic nature, while the lipids tails are hydrophobic and therefore orientate towards each other<sup>9</sup>. In aqueous solution, very low concentrations of lipids tend to be dissolved, but as the lipid concentration increases beyond the critical micelle concentration (CMC), they spontaneously self-assemble due to the increasing unfavourable entropy of the water-hydrocarbon interactions. This lipid

organization produces a rich diversity of non-covalent lipid architectures, such as lamellar and non-lamellar structures including micelles, tubes, bilayers, liposomes, disks, ribbons, hexagonal phases and cubic phases<sup>10, 11, 11b, 12</sup>. The resulting structures reflect the optimal packing of the lipids at a minimum energy balancing the hydrophobic forces and the repulsive forces between the confined head groups. Thermodynamic interactions mentioned above, as well as the attractive-repulsive forces described in the DLVO Theory (named after Derjaguin, Landau, Verwey and Overbeek) are not the only governing factors (Mouritsen 2005), since the molecular parameters of the lipids, such as their chemical and geometrical properties, as well as physical conditions, e.g. temperature, pH, salinity and pressure are decisive factors affecting the resulting lipid structures.

The self-assembly of lipids into liposome vesicles relies on two main phenomena, spontaneous vesiculation and the curvature theory. The spontaneous vesiculation process is mainly governed by thermodynamics and intermolecular forces. From a thermodynamic point of view, the hydrophobic effect that drives the assembling of lipid molecules into supramolecular structures by reducing the overall Gibbs free energy of the system does not, however, specify the final aggregation structure. The hydration of the polar head groups by hydrogen bonding produces an enthalpic gain in solvation that minimizes the potential energy and a gain in entropy of bulk water, thus increasing the stabilization of the phospholipids within the aggregated structures<sup>13</sup>. In addition, attractive-repulsive London forces (ion-dipole) between charged head groups and water molecules plays an important role in the aggregation process and further stabilization of the polar head groups (Tomohiro, Shoko and Masahiko 2006).

In 1976, Israelachvili et al.<sup>14</sup> introduced the concept of a molecular packing parameter ( $P$ ) as a first attempt to correlate the molecular structure of the amphiphile with the curvature of a membrane. The concept describes the geometry of the volume occupied by a lipid and its ability to pack into different structures. Simplified as  $P$  value, the packing parameter is defined by the ratio between the volume occupied by the hydrophobic tails ( $v$ ) with respect to their length ( $l$ ) and the surface of the polar head group ( $a$ ), equation 1. These three parameters depend on the lipid geometry as well as on the attraction and repulsion forces between them once packed into aggregates<sup>15</sup>, and will directly influence the resulting lipid aggregation structure.

$$P = v / l \cdot a \qquad \text{Equation 1}$$

( $P$ ) is the packing parameter, ( $v$ ) is the effective volume occupied by the hydrocarbon tails, ( $l$ ) is the length of the tails and ( $a$ ) is the head group surface area.

In that sense, when  $P < 1/3$  the lipid exhibits a cone-like shape and will pack into micelles. If  $1/3 < P < 1/2$ , the lipid adopts a truncated cone shape and forms cylindrical micelles (hexagonal phases). If  $1/2 < P \leq 1$ , the shape of the lipid is between a truncated cone and a cylinder, and will pack into vesicles or lamellar bilayers. Finally, if  $P > 1$ , the lipid displays an inverted truncated cone shape and inverted micelles will form (Figure 1.3).

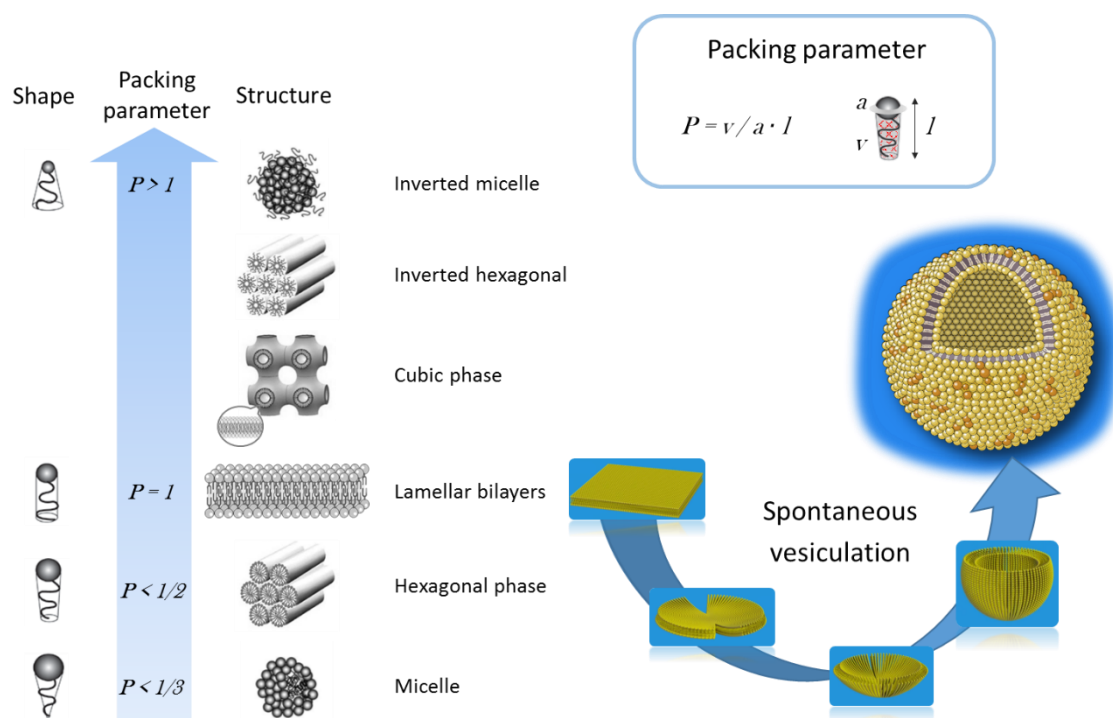


Figure 1.3. Schematic showing the different lipid shapes, their packing parameters and related structures of aggregates. Lamellar phases forming liposome structures by the process called spontaneous vesiculation is also depicted.

The spontaneous vesiculation process has been described recently as a multi-step process, starting from the formation of lamellar disk-like structures that bend once they have grown above a critical dimension in order to minimize the high energy at their edges, therefore, forming enclosed vesicles<sup>16</sup>. This bending energy or elastic energy, plays a fundamental role in reducing the edges' energy but also implies an energy cost due to the modification of the Gaussian curvature of the sheet. In this sense, membranes with higher spontaneous curvatures minimize the energy required to curve them and form vesicles under a spontaneous process, but symmetric membranes (spontaneous curvature = 0) prefer to be flat and energy is required to curve them<sup>17</sup>. The bending elasticity per unit area ( $E_b$ ) with both principal curvatures being equal is approximated by equation 2.

$$E_b = \frac{1}{2} K (2C - C_0)^2 + kC^2 \quad \text{Equation 2}$$

( $E_b$ ) is the elastic binding energy, ( $K_b$ ) is the binding elastic constant, ( $C$ ) is the curvature of the radius ( $C = 1/\text{radius}$ ), ( $C_0$ ) is the spontaneous curvature and ( $k$ ) is the Gaussian curvature modulus.

In addition to the considerations mentioned above, other important factors should also be addressed as they have a strong effect on the final size and shape of the lipid aggregates. These

factors include the lipid chemical structure, the concentration ratio between lipid and water molecules, the temperature and others such as pH, salinity (Seddon and Templer 1995).

The chemical structure of the lipids is one of the most important parameters impacting on the aggregate structure. For instance, the lipid chain length has a strong effect on the hydrophobicity, thus lowering the CMC value, increasing the lipid transition temperature and favouring the formation of inverse non-lamellar phases<sup>18</sup>. In addition, the presence of *cis*- or *trans*-double bonds in the hydrocarbon chains lead to a drastic decrease of the chain melting transition temperature<sup>19</sup>. A major effect on the lipid polymorphism is also caused by the head group of the lipid, in which its' polarity, charge and steric characteristics play a very important role<sup>20</sup>.

The lipid concentration in the aqueous solution has also a great effect on their supramolecular organization and can be mainly explained by the CMC value. Below the CMC, the very low concentrations of lipids are dissolved as monomers first and as the lipid concentration increases beyond the CMC value, the lipids organize into micelles, hexagonal phases, cubic phases, lamellar phases, inverted cubic phases, inverted hexagonal phases and inverted micelles respectively (figure 1.4). The CMC value decreases as the hydrophobic hydrocarbon lipid chains increase in size and therefore it is strongly dependent on the lipid architecture<sup>13,21</sup>.

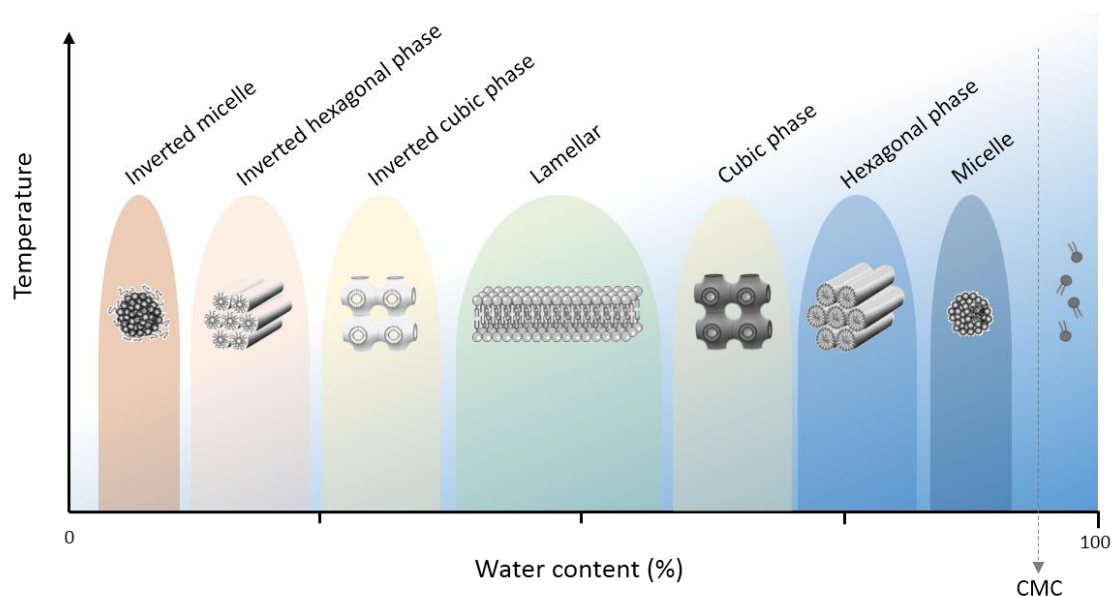


Figure 1.4. Schematic lipid phase transition diagram driven by the water concentration.

In addition to the lipid concentration or water content, the temperature is also a critical variable that influences the resulting lipid supramolecular structures. Each lipid molecule has a specific phase transition temperature (also called melting temperature or  $T_m$ ) in which the lipid changes its' physical state from solid-gel phase to liquid phase. This temperature-dependent behaviour correlates with the degree of lipid organization within a lamellar bilayer, from ordered solid-gel phases when the temperature is below the  $T_m$ , to disordered liquid phase when the temperature is above the  $T_m$  (Figure 1.5). In solid-gel phases the lipids are packed together in a regular and rigid arrangement, whilst in liquid phases the disorder in the membrane enhances

the relative fluidity or mobility of their single lipid molecules within the bilayer, thus increasing its' permeability to small molecules<sup>21, 22, 23</sup>.

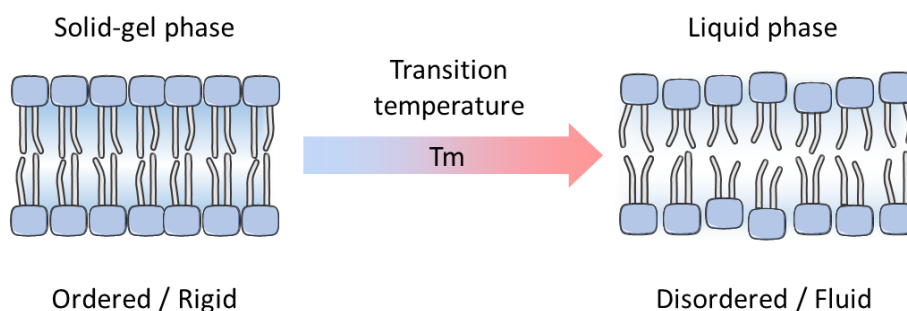


Figure 1.5. Schematic representation of the lipid phase transition temperature ( $T_m$ ). Schematic representation of the lipid phase transition temperature ( $T_m$ ). If the temperature of the system is below the main  $T_m$ , the lipid bilayer will be a solid-gel phase with ordered configuration, whilst if the temperature of the system is above the main  $T_m$ , the lipid bilayer will be a liquid phase with a higher degree of disorder.

Lipid vesicles or liposomes are one of the most studied polymorphic lipid structures, however, the full understanding and control on the vesicle formation is still a matter of research in the scientific and industrial community. These soft aggregates composed of flexible lipid bilayers, display a multitude of varying morphologies with diverse sizes and shapes.

### 1.1.3. Classification

Liposomes can be classified into a wide number of varying categories. Due to their flexible possibilities to easily modulate their structural and physicochemical characteristics, liposomes may surpass other colloidal carrier systems. This versatility offers researchers the possibility to fine-tune the liposome properties towards specific applications. Most frequently, liposomes are classified based on structural parameters, but other alternative classifications rely on their composition or sensitivity.

#### 1.1.3.1. Structural parameters

Taking into account structural parameters, liposomes are divided depending on the number of lipid bilayers (lamellae) and the size of the vesicle. Unilamellar liposomes are of major interest in research due to their facile preparation and the simplicity in understanding their membrane properties. These single-bilayer vesicles are, at the same time, classified into three size subtypes (Figure 1.6). Vesicles smaller than hundred nanometres are called small unilamellar vesicles (SUV), when ranging from hundred nanometres to one micrometre large unilamellar vesicles (LUV), and larger than one micron giant unilamellar vesicles (GUV). Although unilamellar vesicles have been largely studied in many fields, the ones smaller than two hundred nanometres are the most explored and of particular interest as drug/gene delivery carriers in pharmaceutical applications, whilst the GUV are mostly used as simple membrane models to study properties of living cell membranes. In addition to the single-lamellae vesicles, alternative larger structures are formed when composed of many bilayers, i.e. oligolamellar vesicles (OLV), multilamellar vesicles (MLV) and multivesicular vesicles (MVV). All these multi-lamellar vesicles usually adopt very different behaviours from the unilamellar species due to the changes in their physical properties. In addition, the difficulties in producing homogeneous specimens of those multi-



layered structures place this liposomes in a less explored category as compared to the unilamellar liposomes.

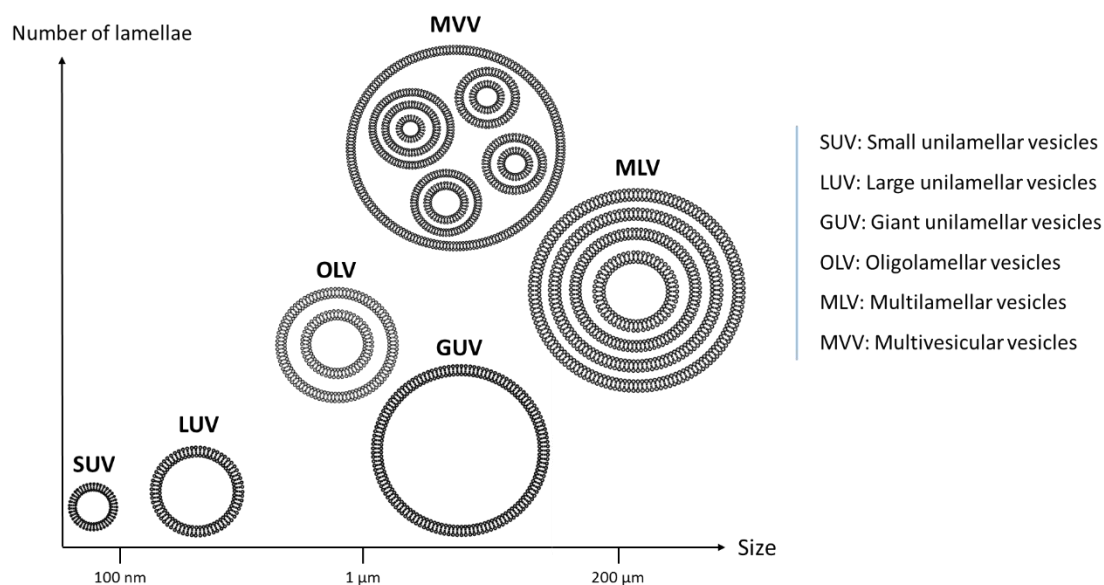


Figure 1.6. Schematic classification of liposomes taking into account structural parameters, the size and the number of lamellar.

#### 1.1.3.2. Liposome composition and functionalization

Liposomes are often distinguished from each other taking into account their surface functionalization, and therefore their further applicability. In this case, the different membrane compositions giving distinctive features to the entire liposome are used to classify as: conventional, cationic, targeted and stealth liposomes (Figure 1.7).

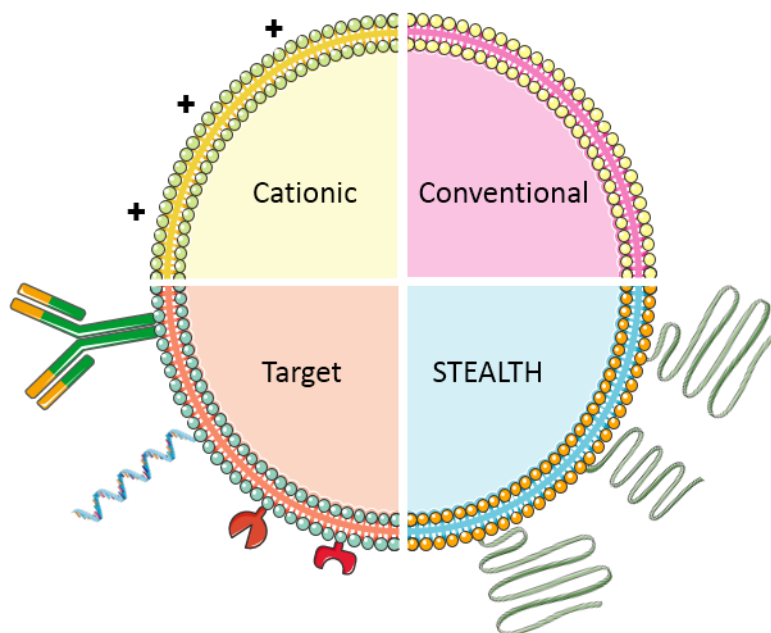


Figure 1.7. Schematic illustration of different types of liposomes classified by their composition and surface functionalization.



Conventional liposomes are the simplest liposomes which are generally composed by one, or a mixture, of neutral or negatively charged phospholipids forming a bilayer surrounding the aqueous inner core. On the other hand, when the net charge of the vesicle is positive, they are called cationic liposomes, and this subgroup is of particular interest as genetic delivery systems, as the cationic lipids interact with the negatively-charged DNA/RNA forming stable lipid-DNA/RNA complexes<sup>24</sup>. Target liposomes group together all the liposomes that are functionalized with some ligand to direct them towards a specific receptor. This is commonly done by functionalizing a few phospholipids of the membrane with an antibody or antibody fragment, so called immunoliposomes. Liposomes offered great versatility for the design of functional surface groups exploiting several surface chemistry approaches<sup>25</sup>. Generally, the ligand coupling is achieved by three different strategies: covalent binding to the lipid in organic solvent, preparation of lipid-conjugate micelles which will transfer to the outer liposome membrane after co-incubation (post-insertion method)<sup>26</sup> or direct conjugation on preformed liposomes (post-functionalization approach). A summary of several strategies are outlined in table 1.1.

Table 1.1. Summary of several surface chemistry approaches for the functionalization of liposomes.

Surface functionalization	References
Aldehyde-modified liposomes	27
Alkyne-modified liposomes	28, 29
Amine-modified liposomes	30, 31
Bromoacetyl-modified liposomes	32, 33
Carboxyl-modified liposomes	34, 35
Cyanur-modified liposomes	36
Cysteine-modified liposomes	37
Hydrazide-modified liposomes	38, 39
Maleimide-modified liposomes	40, 41
p-Nitrophenylcarbonyl-modified liposomes	42
Thiol-modified liposomes	43, 44
Triphosphine-modified liposomes	45

Last but not least, the stealth liposomes, also known as stearic liposomes or long-circulating liposomes, represent one of the cornerstones in liposomal drug delivery research. They benefit from a coat of hydrophilic polyethylene glycol (PEG) chains covalently attached to the outer phospholipids to massively decrease their fast and efficient clearance from the body by the phagocytes of the mononuclear phagocyte system (MPS), or also called reticuloendothelial system (RES), and by creating a stearic layer around the liposome that protects it from destabilization<sup>46</sup>.

## 1.2. Methods for liposome preparation and characterization

### 1.2.1. Preparation of liposomes

Since the pioneering demonstration by Alec D. Bangham that dispersions of phospholipids in aqueous environments form enclosed arrangements<sup>1</sup>, a multitude of potential methods have been widely described in the literature for the preparation of liposomes<sup>47, 47b</sup>. Some of the mechanisms involve more complex procedures than others but the selection of the correct method will influence the size and lamellarity of the resulting liposomal vesicles. In that sense, the correct selection should depend on: i) the physicochemical properties and concentrations of the lipids and the substance to be encapsulated, ii) the size, polydispersity and lamellarity of the vesicles, iii) the medium composition of the liposomal dispersion and iv) batch to batch reproducibility.

Most of the procedures are based on the preparation of a dry lipid film followed by hydration with an aqueous solution containing the encapsulating material (Bangham method)<sup>48</sup> to obtain MLV dispersions, and then, taking advantage of size reducing and homogenization techniques, such as sonication<sup>49</sup>, extrusion<sup>50</sup> or pH jump<sup>51</sup> to obtain LUV or SUV. In addition, other commonly reported methodologies involve the use of solvent microinjection techniques<sup>52</sup>, detergent dialysis<sup>53</sup> and reverse-phase evaporation methods (REV)<sup>54</sup>. Moreover, alternative methods reported on the literature are based on electroformation<sup>55</sup>, heating<sup>56</sup>, microfluidic methods<sup>57</sup>, supercritical fluidic technology<sup>58</sup>, dual asymmetric centrifugation<sup>59</sup>, membrane contactor technology<sup>60</sup>, freeze-drying double emulsions<sup>61</sup>

Despite the vast amount of literature regarding liposome preparation, the common preparation techniques are outlined in Figure 1.8, but only the methodology used to prepare liposomes throughout this thesis is going to be further discussed.

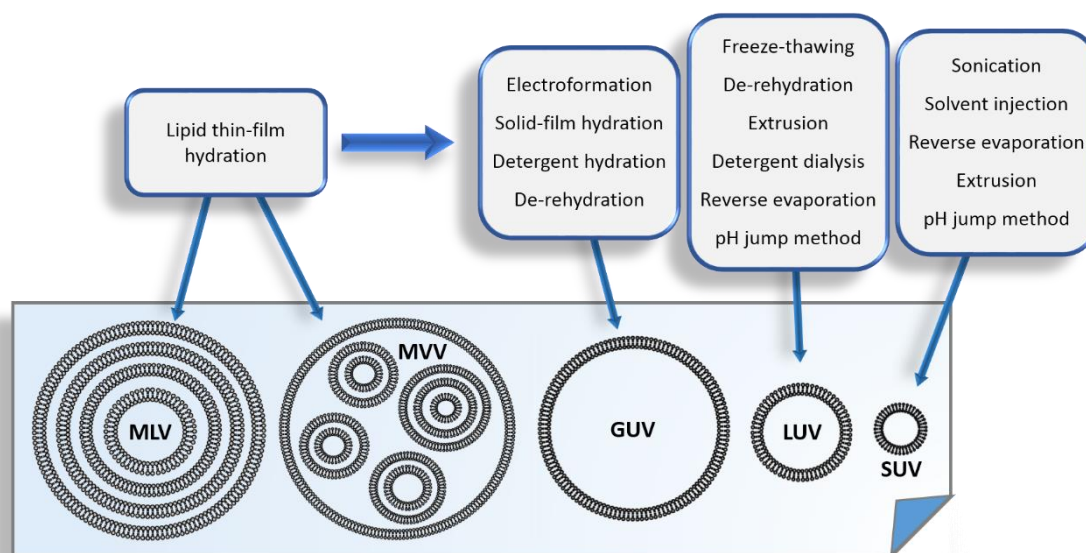


Figure 1.8. Techniques for the preparation of liposomes of different sizes and lamellae.

### 1.2.1.1. Curvature-tuned method

Taking into consideration the phenomenon of spontaneous vesiculation and the theory of curvature, in 2009 Genç et al.<sup>62</sup> presented a rapid and simple, solvent-free method for the preparation of SUV solutions using both charged and zwitterionic lipids. The method obviates the time-consuming prerequisite of preparing a lipid film, and therefore, the use of organic solvents (i.e. chloroform or methanol). The formation of the liposomes is based on the synergistic effect of a rapid change in pH, from pH 7.4 to 11 and back to 7.4, termed “pH jump”, as the main driving force followed by a defined equilibration time where lipids curl into vesicles, and a centrifugation step to obtain the SUV (Figure 1.9). The fine-tuning of the pH jump time interval, the equilibration time, the temperature, the buffer type and lipid characteristics determines the final liposome size and homogeneity.

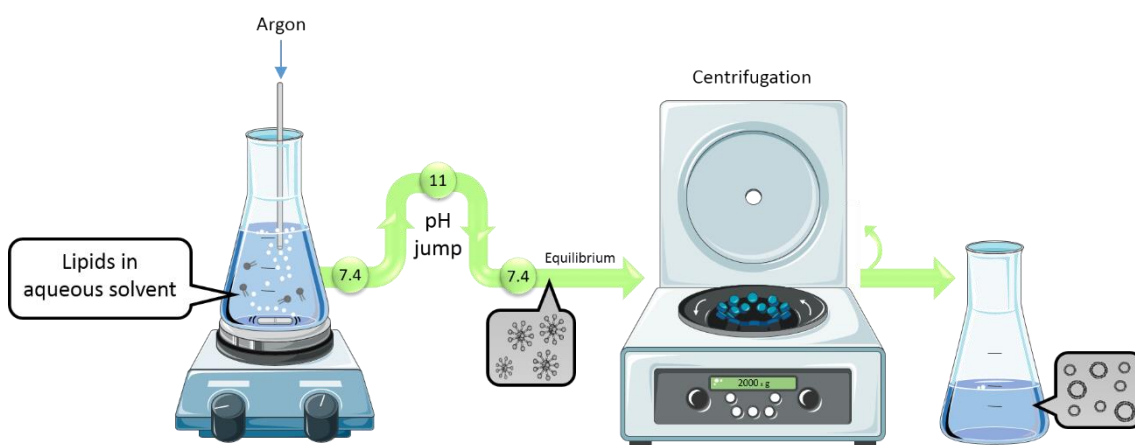


Figure 1.9. Preparation of liposomes using the curvature-tuned method.

This method was used through the thesis work for the preparation of liposomal nanoreactors for the synthesis of nanoparticles (Chapter II, III and IV) and for the preparation of zinc-fluorophore loaded liposomes as membrane models (Chapter V and VI). However, when preparing liposomes composed of complex mixtures of lipids, the lipids must first be dissolved and mixed in an organic solvent, such as chloroform:methanol 9:1 (v/v) solution, to ensure a perfect homogenization, and therefore, homogeneous organization in the membrane of the liposome. This is the case of the liposomes prepared for drug delivery (Chapter VII), where a complete homogeneous membrane of the carrier plays special importance for the drug release. Thus, the liposomes were prepared using the thin-film hydration method followed by extrusion.

### 1.2.1.2. Lipid thin-film hydration and extrusion method

The thin-film method is the most widely used method for liposome preparation and forms MLV with high encapsulation efficiency but yields heterogeneous populations of varying sizes and shapes. In this method, a lipid mixture is dissolved in an organic solvent until homogenization is complete (note that several lipids may need some heat to be completely dissolved). The organic solvent is then evaporated and a dried film of lipids starts to form in a glass flask. Finally, the dried lipid film is hydrated with an aqueous solution containing the molecules to be encapsulated under vigorous agitation and vortexing at a temperature above the main lipid transition temperature. The formed heterogeneous MLV is then extruded in order to obtain a well-defined size of homogeneous unilamellar vesicles. MLV are thus forced to pass through the

pores of a polycarbonate membrane filter while maintaining the temperature above the transition temperature until unilamellar liposomes of uniform size are obtained<sup>63</sup> (Figure 1.10).

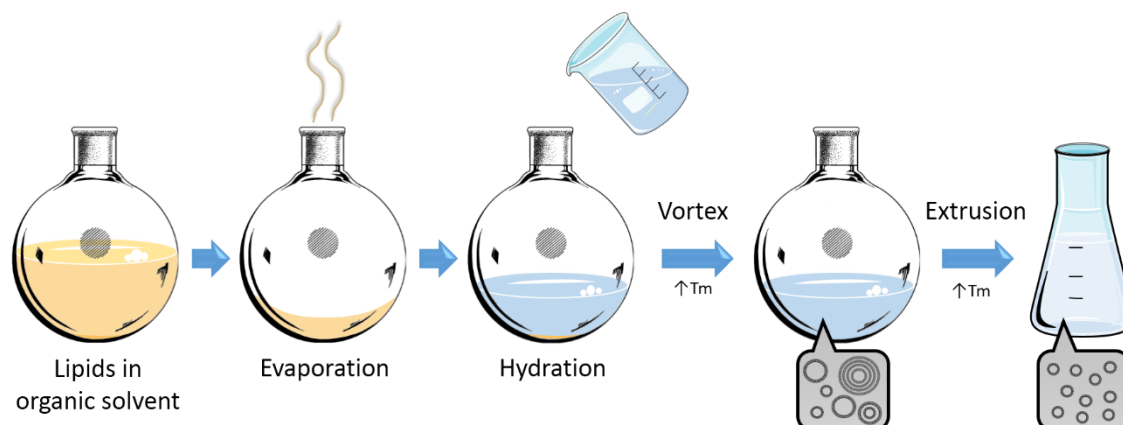


Figure 1.10. Preparation of liposomes employing the thin-film method.

### 1.2.2. Characterization of liposomes

In order to validate the batch-to-batch reproducibility and quality of liposome samples, various parameters should be carefully controlled. Therefore, a full physicochemical characterization is required to assess liposome size, particle distribution, lamellarity, lipid concentration, lipid formulation composition, surface charge of the vesicles, membrane phase transition and encapsulation efficiency.

#### 1.2.2.1. Size and particle distribution

Liposome mean size, size distribution and particle dispersion are among the most relevant parameters when describing a liposome sample. Several techniques have been described including dynamic light scattering (DLS)<sup>64</sup>, microscopy techniques<sup>65</sup>, size-exclusion chromatography (SEC)<sup>66</sup>, field-flow fractionation (FFF)<sup>67</sup>, centrifugation<sup>68</sup>, flow-cytometry<sup>69</sup>, capillary electrophoresis<sup>70</sup> and turbidity<sup>71</sup>. Among those commonly used techniques, DLS is the most broadly used for the determination of liposome size distribution, and it is based on the time-dependent fluctuations of the light scattered at 90° from the particles undergoing Brownian motion. However, DLS analysis does not allow the determination of the liposomes shape, whilst microscopy techniques do. In this sense, a set of diverse electron microscopic (EM) techniques, such as transmission electron microscopy (TEM)<sup>72</sup>, freeze-fracture EM<sup>73</sup>, cryo-TEM<sup>74</sup>, environmental scanning electron microscopy (ESEM)<sup>75</sup> and atomic force microscopy (AFM)<sup>76</sup>, act as complementary methods to provide valuable information on the liposome morphology, as well as resolving different particle sizes.

#### 1.2.2.2. Lamellarity

The lamellarity of the liposomes is an important parameter to investigate whether the vesicles are unilamellar (UV) or multilamellar (MLV or MVV), and also, to obtain a quantifiable signal to estimate the number of bilayers that the liposomes contain. The lamellarity value is often measured by <sup>31</sup>P-NMR, in which the addition of Mn<sup>2+</sup> ions quenches the <sup>31</sup>P-NMR signal of the phospholipids pointing the outer face of the liposome bilayer by broadening their resonance beyond detection<sup>77</sup>. Taking into account that the fraction of phospholipids exposed to the

external medium ranges from 5% in large MLV to 70% in SUV<sup>78</sup>, liposome lamellarity can be calculated by the ratio of <sup>31</sup>P-NMR signal before and after addition of Mn<sup>2+</sup>. The lamellarity can also be determined by EM techniques, such as freeze-fracture EM<sup>79</sup> or cryo-EM<sup>80</sup>, and by spectroscopic techniques, such as X-ray diffraction (XRD)<sup>81</sup> or small-angle X-ray spectroscopy (SAXS)<sup>82</sup>.

#### 1.2.2.3. Lipid composition and concentration

The characterization of the final lipid formulation present in the liposomes should be analysed, since often it may not correlate with the starting lipid mixtures, in both qualitative and quantitative terms, however, most of the literature focuses on the quantitative studies and obviates qualitative analysis. The lipid concentration is commonly determined by wet chemistry protocols that estimate the total phosphorous content, such as the Bartlett method<sup>83</sup>, or the Stewart assay through the formation of a coloured complex between the phospholipid and ammonium ferrothiocyanate<sup>84</sup>. In addition, more accurate results can be obtained by measuring the phospholipids content using high-performance liquid chromatography coupled with evaporative light scattering detection (HPLC-ELSD)<sup>85</sup> or inductively coupled plasma mass spectrometry (ICP-MS)<sup>86</sup>. While these methods provide information on the concentration of phospholipids, the accuracy in lipid composition is not addressed. The exact lipid composition present in the liposomes membrane can be qualitatively assessed by firstly disrupting the lipid bilayers prior to their analysis using HPLC<sup>87</sup> or thin-layer chromatography (TLC)<sup>88</sup>.

#### 1.2.2.4. Surface charge

The stability and interaction of the liposome vesicles with the environment can be critically accentuated by the surface charge present in the lipid membrane. The control over the surface charge of the liposomes has always garnered huge importance, especially in pharmaceutical applications where the correct surface charge may revoke the therapeutic potential. For example, cationic liposomes are widely used as transfection vectors in gene therapy due to their attractive surface interactions with negatively charged DNA/RNA and cell membranes.<sup>89</sup> The liposome charge is often related with the zeta-potential value, an indicator of the surface potential of the particle in suspension that gives information regarding the overall charge that the particle acquires in a particular medium. Zeta-potential analysis are commonly done in the liposome field due to its easiness.<sup>90, 90b</sup> In addition, zeta-potential is also used as an indicator of liposome aggregation, due to the fact that vesicles with a zeta-potential value of above/below +/- 30mV will suffer from strong electrostatic repulsive interactions, thus enhancing their stability as a colloidal dispersion.<sup>91</sup>

#### 1.2.2.5. Phase transition temperature

The phase transition temperature, also referred as melting temperature (T<sub>m</sub>), is the temperature at which a lipid changes its' physical state from an ordered solid phase to a disordered liquid phase. This temperature is therefore an essential parameter to be aware of since it affects the behaviour of the liposome membrane and thus its' fluidity and permeability to small molecules. Generally, this transition temperature is studied using differential scanning calorimetry (DSC) technique, based on the amount of heat needed to increase the temperature of the sample<sup>92</sup>.

#### 1.2.2.6. Encapsulation efficiency

The encapsulation efficiency (EE) is a measure of the percentage of total encapsulated material, and is defined as the total amount of encapsulating material found in the liposome solution versus the total amount of the encapsulate. Encapsulation efficiency is commonly measured by spectrophotometry<sup>93</sup>, fluorescence spectroscopy<sup>94</sup>, enzyme-based methods<sup>95</sup>, electrochemical techniques<sup>96</sup>, NMR spectroscopy<sup>97</sup> and ICP-MS<sup>98</sup>.

The EE value depends not only on the initial amount of the encapsulate or the ability of the liposomes to entrap the molecules, but also if a remote-loading technique is used. The general methods for the preparation of loaded liposomes are based on passive loading of the drug during the liposome formation, whilst active loading techniques take advantage of transmembrane pH gradients to actively entrap protonable molecules.<sup>99</sup> The trapping effectiveness can vastly differ from less than 30% to almost 100% of the starting material when using remote-loading techniques.

### 1.3. Applications

Since the early discover by Alec D. Bangham, liposomes were firstly proposed as models of lipid membranes, however it was not until few years later when Gregory Gregoriadis expanded their future applicability by establishing the idea that liposomes can entrap molecules and outlining their huge potential as carriers in different fields<sup>100</sup>. In addition, their particular structural organization offering the possibility to carry and protect both hydro- and lipo-philic compounds in the core and within the bilayer respectively, as well as their biocompatible, biodegradable and non-immunogenic nature, have positioned liposomes as incredibly versatile tools in a vast range of scientific disciplines (Figure 1.11).

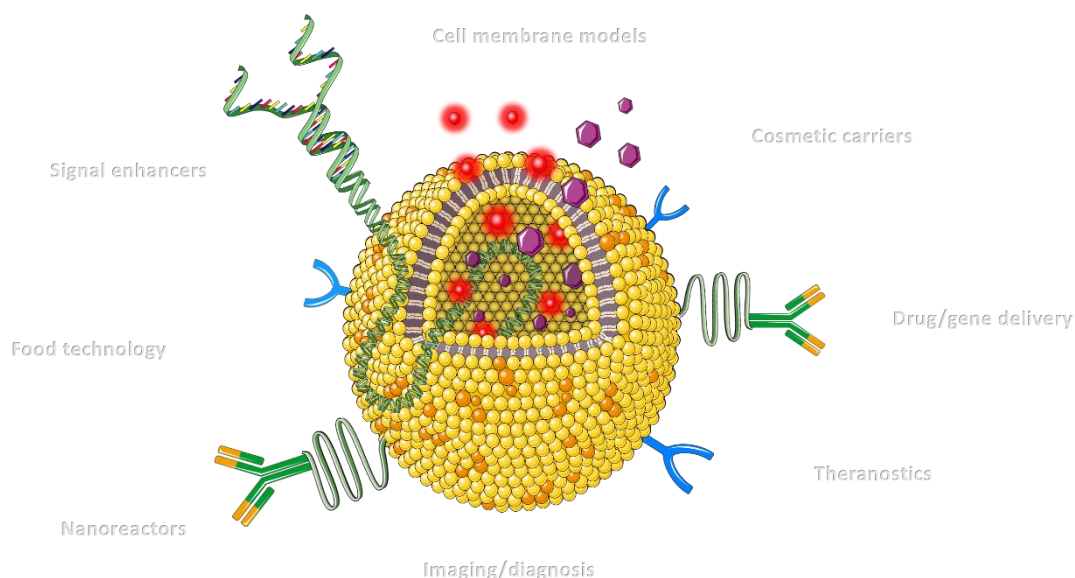


Figure 1.11. Application of liposomes in many diverse fields.

Liposome research mainly focuses on medical and pharmacological applications. They have been extensively explored as carriers for the delivery of a vast range of different drugs, including anti-cancer chemotherapeutics<sup>101</sup>, bactericides<sup>102</sup>, fungicides<sup>103</sup>, hormones<sup>104</sup>, enzymes<sup>105</sup>, genetic



material<sup>106</sup> amongst others. Within the therapeutic field, it has been widely reported that encapsulating a drug within liposomal nanocarriers can prevent its' toxic side-effects and enhance its' efficacy by optimizing the drug biodistribution and pharmacokinetic dynamics, thus helping the delivery of the drug to a desired target and reducing the amount of drug needed to achieve a therapeutic effect. Liposomes are currently the most used and promising drug delivery carriers, as demonstrated by the large number of clinically approved liposomal drugs (Table 1.2), with many more in clinical trials, due to their accomplishment in drug-protection, long-circulation in blood, specific-targeting and specific drug release<sup>107, 108</sup>.

Table 1.2. List of liposomal drugs clinically approved for marketing.

Product	Drug	Indication	Year approved	References
AmBisome	Amphotericin B	Fungal infections Leishmaniasis	1990	I.M. Hann and H.G. Prentice (2001)
Doxil/Caelyx	Doxorubicin	Karposi's sarcoma	1995	N.D. James <i>et al.</i> (1994)
		Ovarian cancer	1999	
		Breast cancer	2003	
		Myeloma	2007	
DaunoXome	Daunorubicin	Karposi's sarcoma	1996	C.E. Petre and D.P. Dittmer (2007)
Myocet	Doxorubicin	Breast cancer	2000	G. Batist <i>et al.</i> (2001)
Amphotec	Amphotericin B	Fungal infections	1996	R. Bowden <i>et al.</i> (2002)
Abelcet	Amphotericin B	Fungal infections	1995	T.J. Walsh <i>et al.</i> (1998)
Visudyne	Verteporphin	Wet macular degeneration	2000	N.M. Bressler (2001)
DepoDur	Morphine sulfate	Pain following surgery	2004	D. Gambling <i>et al.</i> (2005)
Depocyt	Cytarabine	Lymphomatous meningitis	1999	M.J. Glantz <i>et al.</i> (1999)
Diprivan	Propofol	Anesthesia	1986	M.R. Patrick <i>et al.</i> (1985)
Estrasorb	Estrogen	Menopausal therapy	2003	J.A. Simon (2006)
Exparel	Bupivacaine	Analgesia	2011	S.R. Gorfine <i>et al.</i> (2011)
Marqibo	Vincristine	Lymphoblastic leukemia	2012	A.H. Sarris <i>et al.</i> (2000)

Liposomes have also been widely explored in the field of vaccination<sup>109, 110</sup> and as immunological adjuvants to enhance the immunogenicity of small antigens<sup>111</sup>, of particular interest when used as carriers of genetic material. Cationic liposomes have been largely used in gene therapy as effective candidates for the easy encapsulation, protection and delivery of genetic material due to the ability of cationic lipids to bind and carry polyanionic DNA/RNA molecules<sup>112, 113</sup>, often called lipoplexes<sup>114</sup>, and as non-viral transfecting vectors<sup>115</sup>. The application of liposomes as cosmetic carriers started with the first proposal in 1980 by Mezei and Gulasekharam as skin delivery platforms<sup>116</sup>. Since then, intensive research on the cosmetic and cosmoceutic fields have placed liposomes as efficient delivery carriers due to their ability to protect the carrying molecule from degradation and enhance its' skin penetration through their transdermal properties<sup>117, 118, 119, 120</sup>.

In addition to the therapeutic purposes, liposomes are also widely studied as useful imaging tools for diagnosis. It has been shown that liposomes are valuable tools that enhance the target-specificity of image-based diagnosis for the effective screening of diseases, such as in computed tomography (CT), single photon emission computed tomography (SPECT) and magnetic resonance (MR), by encapsulating contrast agents<sup>121</sup>, radioactive tracers<sup>122</sup> and paramagnetic

agents<sup>123</sup> within the targeted liposomes. The alliance of both diagnostic and therapeutic fields, referred to theranostics, has resulted in a revolutionary new field pursuing personalized medicine, in which liposomes emerge with great potential as multifunctional carriers<sup>124, 125, 126</sup>.

Although liposome research is mainly focused on medical applications, it should be emphasised that liposomes are also largely explored in numerous scientific disciplines. They have been used as mathematical models for modelling the drug release from liposomes<sup>127</sup> and in theoretical physics, for the analysis of aggregation behaviour, membrane phase segregation, vesicle morphology<sup>128</sup>. In colloidal science, liposomes are used for the study of aggregation processes, colloidal stability and DLVO theory<sup>129</sup>. Application of liposomes in chemical disciplines, include their use in catalysis<sup>130</sup>, energy conversion<sup>131, 132</sup>, and as reactors or templates for controlled chemical reactions<sup>133, 134</sup>. In addition, due to the fact that liposomes are synthetic analogues of biological membranes, they have been extensively used as membrane models for understanding many cell membrane functions<sup>135, 136</sup>.

The food industry has also exploited the use of liposome technology due to their ability to encapsulate hydrophilic and hydrophobic molecules. Biocompatible and biodegradable liposomes have been extensively used for entrapping and shielding the functionality of unstable compounds, such as enzymes, vitamins, antioxidants and flavours, as well as for the delivery of toxins and pesticides, in the nutritional and agricultural fields<sup>137</sup>. The textile industry has also joined the trend of applying liposome technology to their processes, mainly in wool dyeing, durable fragrance, protective textile, insect repellents, antimicrobial agents and phase-change materials<sup>138</sup>.

Liposomes have demonstrated to have huge potential in many analytical applications. In biosensors or bioanalysis, where the detection sensitivity is of essential importance, liposomes offer the ability to entrap large quantities of signalling molecules and, therefore, amplify the signal. A multitude of different variations in liposome-based bioassays has been described in the literature, including liposome immunoassay (LIA)<sup>139</sup>, liposome immunolysis assay (LILA)<sup>140</sup>, liposome immunosorbent assay (LISA)<sup>141</sup> and flow-injection liposome immunoanalysis (FILIA)<sup>142</sup>, as well as in biosensors<sup>143</sup>.

### 1.3.1. Liposomes as nanoreactors for the controlled synthesis of metal nanoparticles

During the last decades, metallic nanoparticles (NP) with controlled size and shape have witnessed enormous research interest due to their exceptional unique chemical, electronic, magnetic and optical properties, which are not observable in their bulk state<sup>144</sup>. Those nano-dependent features have resulted in their extensive application in many diverse disciplines, including catalysis<sup>145</sup>, electronics<sup>146</sup>, plasmonics<sup>147</sup>, sensors<sup>148</sup> and biomedical fields<sup>149</sup>.

The development of synthesis methods to produce homogeneous size- and shape-tunable NPs is still a challenge. Many different techniques have been reported in the literature, including photolytic<sup>150</sup> and thermal<sup>151</sup> decomposition, sonochemical<sup>152</sup> and hydrogen reduction<sup>153</sup>, electrochemical deposition<sup>154</sup>, one-phase<sup>155</sup> and two-phase<sup>156</sup> reduction methods, and biogenic methods<sup>157</sup>. The most common methods utilize reducing agents such as borohydrides, aminoboranes, hydrazine, formaldehyde, hydroxylamine, saturated and unsaturated alcohols,



citric and oxalic acids, polyols, sugars, hydrogen peroxide, sulphites, carbon monoxide, hydrogen, acetylene and mono-electronic reducing agents, often in combination with capping agents such as citrates, sulphur ligands, phosphorus ligands, nitrogen-based ligands, oxygen-based ligands, dendrimers, polymers and surfactants, to mediate the reduction reaction and avoid uncontrolled aggregation into larger particles<sup>158, 159</sup>.

Despite the large variety of methods described, very few techniques allow a precise and fine control over the size and shape of the resulting NPs. The use of templates or reactors offer the possibility to confine the reduction reaction in a controllable environment, thus modifying the reduction and growth kinetics of the NPs as compared to bulk solution. Surfactants and reverse micelles used as templates were shown to provide good control over the produced NPs. The use of the surfactants cetyltrimethylammonium bromide (CTAB) or dioctylsulfosuccinate sodium salt (AOT) for the preparation of size- and shape-tuned NPs have been widely reported<sup>160, 161, 162</sup>. Polyelectrolytes have also been described as nanoreactors for the synthesis of Pd NPs<sup>163</sup>. Regarding the use of reverse micelles, a large number of studies are available but among a vast variety, polyvinylpyrrolidone (PVP) polymer micelles are the most commonly used for the preparation of small NPs<sup>164, 165, 166</sup>.

The structure of liposomes also offers a system to compartmentalise chemical reactions in order to control the reduction of NPs. In this sense, they can be used as nanosized reactors for the synthesis of colloid NPs in a more controlled way within the confined environment. There are few studies in the literature using liposomes as nanoreactors for the synthesis of metallic NPs, e.g. the use of liposomes for the synthesis and stabilization of Au NPs<sup>167</sup>, the synthesis of Au NPs via phospholipid membrane-bound Pd catalysed reduction by hypophosphite<sup>168</sup>, the use of liposomes for the preparation of several platinum nanostructures inside<sup>169, 170</sup>, or the preparation of Au NPs by ascorbic acid in liposomes of several compositions (GUVs)<sup>171</sup>. It has been also described that phosphoglycerol lipids can act as stabilizers for Au and Cu nanoparticles and Au-Cu bimetallic nanoparticles<sup>172, 173</sup>.

Liposomes appear as suitable candidates as nanoreactors for the controlled synthesis of NPs in an environmentally-friendly manner, however the fine tuning of critical parameters involved in the control of the kinetics of the reduction reaction, such as the permeability of the nanoreactor membrane, are still required in order to reveal their full potential as templates.

### 1.3.2. Liposomes as cell membrane models for the study of zinc ionophores

Liposomes are one of the simplest cell models consisting only of a spherical lipid bilayer enclosing an aqueous buffer. Being synthetic analogues of biological membranes, liposomes have been extensively used as membrane models for understanding many of the cell membrane functions<sup>135, 136, 174</sup>. One of those membrane functions, is the ability to control the internalization of different compounds across the bilayer into the cytosol. This uptake can be achieved by means of membrane transporters or endocytosis processes. However, there are a class of molecules called ionophores which are able to bind small ions and transport them across lipid membranes without the help of any cell transporting mechanisms. These ionophore molecules generally are lipo-soluble compounds that can be found in nature or chemically synthesised, and

have been widely explored as therapeutic agents since they can modulate the concentration of metal ions within the cells, such as clioquinol or pyrithione<sup>175</sup>.

Interestingly, a class of phenolic compounds found in several human diet products, such as in fruits, wine and green tea, have been reported to modulate the levels of labile zinc metal ions within the cells. Zinc labile ions are known to modulate the activity of numerous enzymes and thus signalling and metabolic pathways and cellular processes, including cell fate and apoptosis<sup>176, 177</sup>. Therefore, polyphenols have been considered bioactive micronutrients whose regular consumption either as food components or as dietary supplements (nutraceuticals)<sup>178</sup>, entails benefits for human health including cancer prevention<sup>179</sup>, diabetes<sup>180</sup>, and cardiovascular<sup>181</sup> and neurodegenerative<sup>182</sup> diseases. However no effort has been made in order to understand whether polyphenolic compounds can modulate cell levels of zinc ions by transporting them across the lipid membrane without the help of any cell transport mechanism.

Few publications in the literature have reported the use of liposomes as simple cell membrane systems for the demonstration of ion transport across lipid bilayers, known as the ionophore effect<sup>183, 184, 185, 186</sup>. Therefore, liposomes show great potential and can be exploited as simple membrane models for the determination of the ionophore activity of various molecules, including the phenolic compounds, in order to characterize them as independent ion transporters.

### 1.3.3. Liposomes as drug delivery carriers for anti-cancer therapy

Liposomes started to attract notable clinical acceptance and to be recognized as leading drug delivery platforms after the first liposomal anti-cancer drug, Doxil<sup>®</sup>, was clinically approved by the FDA in 1995<sup>187</sup>. Since then, the field has continuously progressed in the development of bioengineered liposomes to fulfil the needs of a robust and effective drug delivery system. In that sense, one of the major advances was the ability to overcome their relatively rapid clearance from the body by the reticuloendothelial system (RES), by modifying the liposome surface with a polyethylene-glycol (PEG) layer<sup>188</sup>. The PEGylation of liposomes demonstrated a prolonged circulation behaviour by enhancing their stability and avoiding their opsonisation and clearance<sup>46</sup>. In addition, these long circulating liposomes benefits from increased accumulation in the tumor tissue (passive-targeting) via the enhanced permeability and retention (EPR) effect, in which particles smaller than 200 nm are able to exploit the EPR effect and diffuse across the leaky tumor blood vessels to accumulate in the tumour tissue<sup>189</sup> (Figure 1.12).

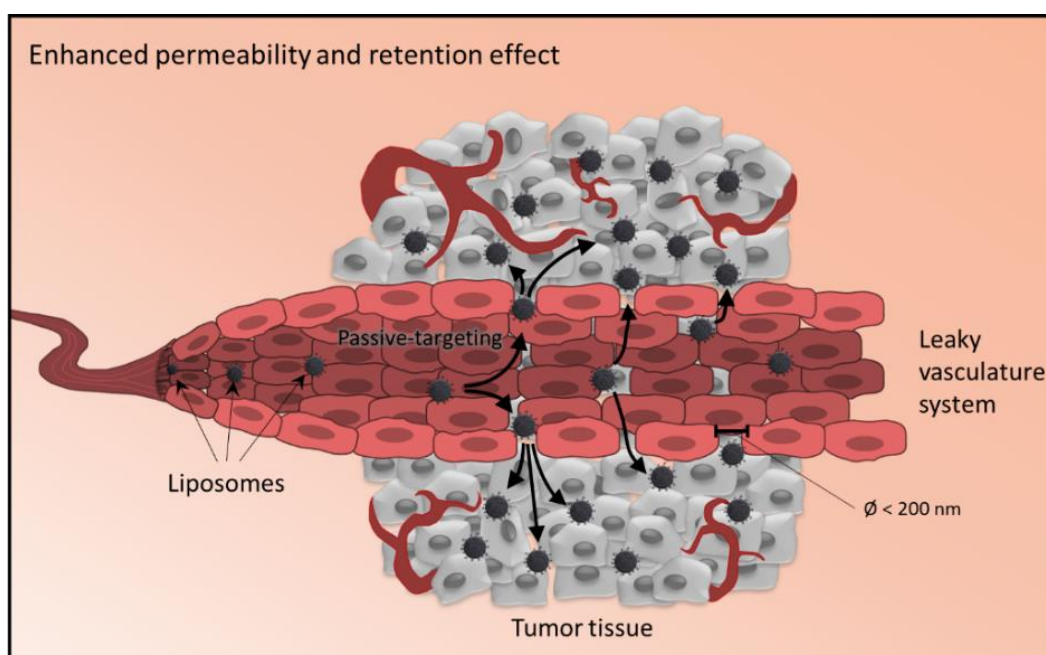


Figure 1.12. Schematic illustration of the liposome passive-targeting phenomena via EPR effect.

Other methodologies based on active-targeting, imply the modification of the liposome surface to specifically-bind the target and minimize unspecific interactions. Liposomes offer great advantages due to their facility to functionalize their lipid membrane by attaching different target ligands, including proteins, peptides, polysaccharides, glycolipids, glycoproteins, antibodies and pro-drug molecules, that can actively modify the liposome biodistribution patterns and enhance their cellular internalization<sup>190,191,192</sup>. However, enough drug bioavailability in the target cell to perform its therapeutic effect still depends on the drug release from the liposomes and further uptake by the cells. Several strategies are based on specific stimuli that triggers the degradation of the membrane and therefore the release of the cargo. The main specific triggered-release mechanisms are based on the sensitivity of the liposome membrane towards its degradation by acid pH<sup>193</sup>, heat<sup>194</sup>, light<sup>195</sup> or enzyme<sup>196</sup> (mainly proteases such as phospholipases<sup>197</sup>, phosphatases<sup>198</sup>, elastases<sup>199</sup>, metalloproteinases<sup>200</sup>).

The enzyme-driven release of the drug from enzyme-sensitive liposome carriers is probably the most selective and robust drug release system to effectively achieve site-specific release by enzymes secreted by the target cells. However, a careful design of the liposome membrane sensitivity towards enzyme-degradation is of crucial importance to ensure complete and full drug release without compromising their stability in non-targeted environments.

#### 1.4. Concluding remarks

Amphipathic lipid molecules have been shown to display the ability to self-assemble into diverse polymorphic structures due to their dual preference for solvents. One of those supramolecular arrangements, liposomes, result from the curling process of lamellar aggregates into vesicles due to several physicochemical phenomena including spontaneous vesiculation and curvature processes.

The biocompatible, biodegradable and non-immunogenic nature of liposomes, together with their ability to encapsulate both hydro- and lipo-philic molecules in the aqueous core and within the lipid membrane, results in remarkably attractive structures for many scientific disciplines. In addition, liposomes are incredibly versatile structures that can be easily produced and functionalized in order to fit requirements in a large number of different applications.

Current efforts in the controlled synthesis of metallic nanoparticles focus on the use of templates to provide confined nanoenvironments in which the reduction, nucleation and nanoparticle growth happens in a restricted way. The use of liposomal nanoreactors has been postulated to offer similar conditions, modulating the reduction kinetics and having a direct effect on the final characteristics of the produced nanoparticles.

Dietary polyphenols have been demonstrated to have direct effect on the modulation of the labile zinc levels within the cells, thus affecting many zinc related metabolic pathways including apoptosis. However the ability of polyphenols to bind zinc cations and transport them across biological membranes devoid of cell transport mechanisms, thus acting as zinc ionophores, still remind unknown. Therefore, the use of liposomes as simple cell membrane systems could be exploited to determine the zinc ionophore effect displayed by several phenolic compounds.

Although the use of chemotherapy in cancer therapy is widely recognized, it is often restricted by the dose-limiting toxic side-effects and also from rapid circulatory removal. Long circulating pegylated liposomes offer the ability to confine and enhance drug exposure specifically to target cancer tissue. In addition, the development of site-specific triggered release systems, such as enzyme-degradable liposomes, results in a local drug release only where high expression levels of the enzyme appear. The application of enzyme-sensitive liposomal drug delivery carriers for anti-cancer treatment aim to improve chemotherapeutic indexes.

## 1.5. Thesis objectives

The overall objective of the present doctoral thesis is to demonstrate the versatility of liposomes and explore their use as multifaceted tools in different applications, including nanoreactors, membrane models and smart drug delivery carriers. To accomplish this, the following specific objectives have been set:

- Evaluation of different liposomal nanoreactors for the glycerol-mediated synthesis of metallic nanoparticles to provide confined nanoenvironments thus modulating the nanoparticle reduction kinetics and having a direct effect on the final size, shape and homogeneity of the nanoparticles produced.
- Determination of the zinc ionophore activity of a library of dietary polyphenols by exploiting zinc-specific fluorophore loaded liposomes as a simple cell membrane system.
- Development of a liposomal drug delivery system that exploits increased secretory phospholipase A<sub>2</sub> type IIA (sPLA<sub>2</sub>) enzyme activity found in a wide variety of cancers to mediate the deliver and release of chemotherapeutics specifically in the tumor interstitium.

## 1.6. References

1. Weissman, G.; Sessa, G.; Standish, M.; Bangham, A. D. A DIRECT EFFECT OF STEROIDS ON PERMEABILITY OF LIPID MEMBRANES (LIPOSOMES). *J. Clin. Invest.* **1965**, *44* (6), 1109-8.
2. Torchilin, V. P. Recent advances with liposomes as pharmaceutical carriers. *Nature Reviews Drug Discovery* **2005**, *4* (2), 145-160.
3. Müller, R. H.; Petersen, R. D.; Hommoss, A.; Pardeike, J. Nanostructured lipid carriers (NLC) in cosmetic dermal products. *Advanced Drug Delivery Reviews* **2007**, *59* (6), 522-530.
4. Keller, B. C. Liposomes in nutrition. *Trends in Food Science & Technology* **2001**, *12* (1), 25-31.
5. Fenz, S. F.; Sengupta, K. Giant vesicles as cell models. *Integrative Biology* **2012**, *4* (9), 982-995.
6. Rongen, H. A. H.; Bult, A.; van Bennekom, W. P. Liposomes and immunoassays. *Journal of Immunological Methods* **1997**, *204* (2), 105-133.
7. Jesorka, A.; Orwar, O. Liposomes: Technologies and Analytical Applications. In *Annual Review of Analytical Chemistry*, 2008; Vol. 1, pp 801-832.
8. Luzzati, V.; Spegel, P. A. Polymorphism of Lipids. *Nature* **1967**, *215* (5102), 701-704.
9. Singer, S. J.; Nicolson, G. L. The fluid mosaic model of the structure of cell membranes. *Science* **1972**, *175* (4023), 720-31.
10. Garg, G.; Saraf, S. Cubosomes: an overview. *Biological & pharmaceutical bulletin* **2007**, *30* (2), 350-3.
11. (a) Barauskas, J.; Johnsson, M.; Tiberg, F. Self-Assembled Lipid Superstructures: Beyond Vesicles and Liposomes. *Nano Letters* **2005**, *5* (8), 1615-1619; (b) Koynova R, T. B. Transitions between lamellar and non-lamellar phases in membrane lipids and their physiological roles. *OA Biochemistry* **2013**, *01*, 1-9.
12. Simons, K.; Sampaio, J. L. Membrane Organization and Lipid Rafts. *Cold Spring Harbor Perspectives in Biology* **2011**, *3* (10).
13. Šegota, S.; Težak, D. u. i. Spontaneous formation of vesicles. *Advances in Colloid and Interface Science* **2006**, *121* (1-3), 51-75.
14. Israelachvili, J. N.; Mitchell, D. J.; Ninham, B. W. Theory of self-assembly of hydrocarbon amphiphiles into micelles and bilayers. *Journal of the Chemical Society, Faraday Transactions 2: Molecular and Chemical Physics* **1976**, *72* (0), 1525-1568.
15. Tanford, C. Micelle shape and size. *The Journal of Physical Chemistry* **1972**, *76* (21), 3020-3024.
16. Leng, J.; Egelhaaf, S. U.; Cates, M. E. Kinetics of the Micelle-to-Vesicle Transition: Aqueous Lecithin-Bile Salt Mixtures. *Biophysical Journal* **2003**, *85* (3), 1624-1646.
17. Lasic, D. D. Novel applications of liposomes. *Trends in Biotechnology* **1998**, *16* (7), 307-321.
18. Lewis, R. N. A. H.; Mannock, D. A.; McElhaney, R. N.; Turner, D. C.; Gruner, S. M. Effect of fatty acyl chain length and structure on the lamellar gel to liquid-crystalline and lamellar to reversed hexagonal phase transitions of aqueous phosphatidylethanolamine dispersions. *Biochemistry* **1989**, *28* (2), 541-548.
19. Cevc, G. How membrane chain-melting phase-transition temperature is affected by the lipid chain asymmetry and degree of unsaturation: an effective chain-length model. *Biochemistry* **1991**, *30* (29), 7186-7193.
20. Cevc, G. How membrane chain melting properties are regulated by the polar surface of the lipid bilayer. *Biochemistry* **1987**, *26* (20), 6305-6310.
21. Seddon, J. M. Structure of the inverted hexagonal (HII) phase, and non-lamellar phase transitions of lipids. *Biochimica et Biophysica Acta (BBA) - Reviews on Biomembranes* **1990**, *1031* (1), 1-69.

22. Blok, M. C.; Van Der Neut-Kok, E. C. M.; Van Deenen, L. L. M.; De Gier, J. The effect of chain length and lipid phase transitions on the selective permeability properties of liposomes. *Biochimica et Biophysica Acta (BBA) - Biomembranes* **1975**, *406* (2), 187-196.
23. Papahadjopoulos, D.; Jacobson, K.; Nir, S.; Isac, I. Phase transitions in phospholipid vesicles Fluorescence polarization and permeability measurements concerning the effect of temperature and cholesterol. *Biochimica et Biophysica Acta (BBA) - Biomembranes* **1973**, *311* (3), 330-348.
24. Balazs, D. A.; Godbey, W. T. Liposomes for Use in Gene Delivery. *Journal of Drug Delivery* **2011**, *2011*, 1-12.
25. Jølck, R.; Feldborg, L.; Andersen, S.; Moghimi, S. M.; Andresen, T. Engineering Liposomes and Nanoparticles for Biological Targeting. In *Biofunctionalization of Polymers and their Applications*, Nyanhongo, G. S.; Steiner, W.; Gübitz, G., Eds. Springer Berlin Heidelberg: 2011; Vol. 125, pp 251-280.
26. Iden, D. L.; Allen, T. M. In vitro and in vivo comparison of immunoliposomes made by conventional coupling techniques with those made by a new post-insertion approach. *Biochim Biophys Acta* **2001**, *1513* (2), 207-16.
27. Bourel-Bonnet, L.; Pecheur, E. I.; Grandjean, C.; Blanpain, A.; Baust, T.; Melnyk, O.; Hoflack, B.; Gras-Masse, H. Anchorage of synthetic peptides onto liposomes via hydrazone and alpha-oxo hydrazone bonds. preliminary functional investigations. *Bioconjug Chem* **2005**, *16* (2), 450-7.
28. Cavalli, S.; Tipton, A. R.; Overhand, M.; Kros, A. The chemical modification of liposome surfaces via a copper-mediated [3 + 2] azide-alkyne cycloaddition monitored by a colorimetric assay. *Chemical Communications* **2006**, (30), 3193-3195.
29. Said Hassane, F.; Frisch, B.; Schuber, F. Targeted Liposomes: Convenient Coupling of Ligands to Preformed Vesicles Using "Click Chemistry". *Bioconjugate Chemistry* **2006**, *17* (3), 849-854.
30. Torchilin, V. P.; Goldmacher, V. S.; Smirnov, V. N. Comparative studies on covalent and noncovalent immobilization of protein molecules on the surface of liposomes. *Biochemical and Biophysical Research Communications* **1978**, *85* (3), 983-990.
31. Torchilin, V. P.; Khaw, B. A.; Smirnov, V. N.; Haber, E. Preservation of antimyosin antibody activity after covalent coupling to liposomes. *Biochemical and Biophysical Research Communications* **1979**, *89* (4), 1114-1119.
32. Frisch, B.; Boeckler, C.; Schuber, F. Synthesis of short polyoxyethylene-based heterobifunctional cross-linking reagents. Application to the coupling of peptides to liposomes. *Bioconjug Chem* **1996**, *7* (2), 180-6.
33. Schelté, P.; Boeckler, C.; Frisch, B.; Schuber, F. Differential Reactivity of Maleimide and Bromoacetyl Functions with Thiols: Application to the Preparation of Liposomal Diepitope Constructs. *Bioconjugate Chemistry* **1999**, *11* (1), 118-123.
34. Kung, V. T.; Redemann, C. T. Synthesis of carboxyacyl derivatives of phosphatidylethanolamine and use as an efficient method for conjugation of protein to liposomes. *Biochim Biophys Acta* **1986**, *862* (2), 435-9.
35. Maruyama, K.; Takizawa, T.; Iwatsuru, M. Novel Immunoliposomes Modified with Amphipathic Polyethyleneglycols Conjugated at their Distal Terminals to Monoclonal Antibodies. In *Advanced Biomaterials in Biomedical Engineering and Drug Delivery Systems*, Ogata, N.; Kim, S.; Feijen, J.; Okano, T., Eds. Springer Japan: 1996; pp 351-352.
36. Bendas, G.; Krause, A.; Bakowsky, U.; Vogel, J.; Rothe, U. Targetability of novel immunoliposomes prepared by a new antibody conjugation technique. *International Journal of Pharmaceutics* **1999**, *181* (1), 79-93.
37. Reulen, S. W.; Brusselaars, W. W.; Langereis, S.; Mulder, W. J.; Breurken, M.; Merckx, M. Protein-liposome conjugates using cysteine-lipids and native chemical ligation. *Bioconjug Chem* **2007**, *18* (2), 590-6.



38. Zalipsky, S. Synthesis of an end-group functionalized polyethylene glycol-lipid conjugate for preparation of polymer-grafted liposomes. *Bioconjugate Chemistry* **1993**, *4* (4), 296-299.
39. Hansen, C. B.; Kao, G. Y.; Moase, E. H.; Zalipsky, S.; Allen, T. M. Attachment of antibodies to sterically stabilized liposomes: evaluation, comparison and optimization of coupling procedures. *Biochimica et Biophysica Acta (BBA) - Biomembranes* **1995**, *1239* (2), 133-144.
40. Beduneau, A.; Saulnier, P.; Hindre, F.; Clavreul, A.; Leroux, J. C.; Benoit, J. P. Design of targeted lipid nanocapsules by conjugation of whole antibodies and antibody Fab' fragments. *Biomaterials* **2007**, *28* (33), 4978-90.
41. Garnier, B.; Bouter, A.; Gounou, C.; Petry, K. G.; Brisson, A. R. Annexin A5-functionalized liposomes for targeting phosphatidylserine-exposing membranes. *Bioconjug Chem* **2009**, *20* (11), 2114-22.
42. Torchilin, V. P.; Levchenko, T. S.; Lukyanov, A. N.; Khaw, B. A.; Klibanov, A. L.; Rammohan, R.; Samokhin, G. P.; Whiteman, K. R. p-Nitrophenylcarbonyl-PEG-PE-liposomes: fast and simple attachment of specific ligands, including monoclonal antibodies, to distal ends of PEG chains via p-nitrophenylcarbonyl groups. *Biochim Biophys Acta* **2001**, *1511* (2), 397-411.
43. Allen, T. M.; Brandeis, E.; Hansen, C. B.; Kao, G. Y.; Zalipsky, S. A new strategy for attachment of antibodies to sterically stabilized liposomes resulting in efficient targeting to cancer cells. *Biochim Biophys Acta* **1995**, *1237* (2), 99-108.
44. Munoz, M.; Garcia, M.; Reig, F.; Alsina, M. A.; Haro, I. Physico-chemical characterization of liposomes with covalently attached hepatitis A VP3(101-121) synthetic peptide. *Analyst* **1998**, *123* (11), 2223-8.
45. Zhang, H.; Ma, Y.; Sun, X.-L. Chemically-selective surface glyco-functionalization of liposomes through Staudinger ligation. *Chemical Communications* **2009**, (21), 3032-3034.
46. Klibanov, A. L.; Maruyama, K.; Torchilin, V. P.; Huang, L. Amphipathic polyethyleneglycols effectively prolong the circulation time of liposomes. *FEBS Letters* **1990**, *268* (1), 235-237.
47. (a) Chatterjee, S.; Banerjee, D. Preparation, Isolation, and Characterization of Liposomes Containing Natural and Synthetic Lipids. In *Liposome Methods and Protocols*, Basu, S.; Basu, M., Eds. Humana Press: 2002; Vol. 199, pp 3-16; (b) Laouini, A.; Jaafar-Maalej, C.; Limayem-Blouza, I.; Sfar, S.; Charcosset, C.; Fessi, H. Preparation, Characterization and Applications of Liposomes: State of the Art. *Journal of Colloid Science and Biotechnology* **2012**, *1* (2), 147-168.
48. Bangham, A. D. PROPERTIES AND USES OF LIPID VESICLES: AN OVERVIEW. *Annals of the New York Academy of Sciences* **1978**, *308* (1), 2-7.
49. Saunders, L.; Perrin, J.; Gammack, D. Ultrasonic irradiation of some phospholipid sols. *The Journal of pharmacy and pharmacology* **1962**, *14*, 567-72.
50. Olson, F.; Hunt, C. A.; Szoka, F. C.; Vail, W. J.; Papahadjopoulos, D. Preparation of liposomes of defined size distribution by extrusion through polycarbonate membranes. *Biochimica et Biophysica Acta (BBA) - Biomembranes* **1979**, *557* (1), 9-23.
51. Hauser, H.; Gains, N. Spontaneous vesiculation of phospholipids: a simple and quick method of forming unilamellar vesicles. *Proceedings of the National Academy of Sciences of the United States of America* **1982**, *79* (6), 1683-7.
52. Batzri, S.; Korn, E. D. Single bilayer liposomes prepared without sonication. *Biochimica et Biophysica Acta (BBA) - Biomembranes* **1973**, *298* (4), 1015-1019.
53. Zumbuehl, O.; Weder, H. G. Liposomes of controllable size in the range of 40 to 180 nm by defined dialysis of lipid/detergent mixed micelles. *Biochimica et Biophysica Acta (BBA) - Biomembranes* **1981**, *640* (1), 252-262.
54. Szoka, F., Jr.; Papahadjopoulos, D. Procedure for preparation of liposomes with large internal aqueous space and high capture by reverse-phase evaporation. *Proceedings of the National Academy of Sciences of the United States of America* **1978**, *75* (9), 4194-8.



55. Angelova, M. I.; Dimitrov, D. S. Liposome electroformation. *Faraday Discussions of the Chemical Society* **1986**, *81* (0), 303-311.
56. Mozafari, M. R. Liposomes: an overview of manufacturing techniques. *Cell Mol Biol Lett* **2005**, *10* (4), 711-9.
57. Yu, B.; Lee, R. J.; Lee, L. J. Chapter 7 - Microfluidic Methods for Production of Liposomes. In *Methods in Enzymology*, Nejat, D., Ed. Academic Press: 2009; Vol. Volume 465, pp 129-141.
58. Otake, K.; Imura, T.; Sakai, H.; Abe, M. Development of a New Preparation Method of Liposomes Using Supercritical Carbon Dioxide. *Langmuir* **2001**, *17* (13), 3898-3901.
59. Hirsch, M.; Zirolì, V.; Helm, M.; Massing, U. Preparation of small amounts of sterile siRNA-liposomes with high entrapping efficiency by dual asymmetric centrifugation (DAC). *Journal of Controlled Release* **2009**, *135* (1), 80-88.
60. Jaafar-Maalej, C.; Charcosset, C.; Fessi, H. A new method for liposome preparation using a membrane contactor. *Journal of Liposome Research* **2010**, *21* (3), 213-220.
61. Wang, T.; Deng, Y.; Geng, Y.; Gao, Z.; Zou, J.; Wang, Z. Preparation of submicron unilamellar liposomes by freeze-drying double emulsions. *Biochimica et Biophysica Acta (BBA) - Biomembranes* **2006**, *1758* (2), 222-231.
62. Genç, R. k.; Ortiz, M.; O'Sullivan, C. K. Curvature-Tuned Preparation of Nanoliposomes. *Langmuir* **2009**, *25* (21), 12604-12613.
63. Hope, M. J.; Bally, M. B.; Webb, G.; Cullis, P. R. Production of large unilamellar vesicles by a rapid extrusion procedure. Characterization of size distribution, trapped volume and ability to maintain a membrane potential. *Biochimica et Biophysica Acta (BBA) - Biomembranes* **1985**, *812* (1), 55-65.
64. Goll, J. H.; Stock, G. B. Determination by photon correlation spectroscopy of particle size distributions in lipid vesicle suspensions. *Biophys J* **1977**, *19* (3), 265-73.
65. Bibi, S.; Kaur, R.; Henriksen-Lacey, M.; McNeil, S. E.; Wilkhu, J.; Lattmann, E.; Christensen, D.; Mohammed, A. R.; Perrie, Y. Microscopy imaging of liposomes: From coverslips to environmental SEM. *International Journal of Pharmaceutics* **2011**, *417* (1-2), 138-150.
66. Grabielle-Madelmont, C.; Lesieur, S.; Ollivon, M. Characterization of loaded liposomes by size exclusion chromatography. *Journal of Biochemical and Biophysical Methods* **2003**, *56* (1-3), 189-217.
67. Moon, M. H.; Giddings, J. C. Size distribution of liposomes by flow field-flow fractionation. *Journal of Pharmaceutical and Biomedical Analysis* **1993**, *11* (10), 911-920.
68. Güven, A.; Ortiz, M.; Constanti, M.; O'Sullivan, C. K. Rapid and efficient method for the size separation of homogeneous fluorescein-encapsulating liposomes. *Journal of Liposome Research* **2009**, *19* (2), 148-154.
69. Vorauer-Uhl, K.; Wagner, A.; Borth, N.; Katinger, H. Determination of liposome size distribution by flow cytometry. *Cytometry* **2000**, *39* (2), 166-71.
70. Radko, S. P.; Stastna, M.; Chrambach, A. Size-dependent electrophoretic migration and separation of liposomes by capillary zone electrophoresis in electrolyte solutions of various ionic strengths. *Anal Chem* **2000**, *72* (24), 5955-60.
71. Matsuzaki, K.; Murase, O.; Sugishita, K. i.; Yoneyama, S.; Akada, K. y.; Ueha, M.; Nakamura, A.; Kobayashi, S. Optical characterization of liposomes by right angle light scattering and turbidity measurement. *Biochimica et Biophysica Acta (BBA) - Biomembranes* **2000**, *1467* (1), 219-226.
72. Ruozi, B.; Belletti, D.; Tombesi, A.; Tosi, G.; Bondioli, L.; Forni, F.; Vandelli, M. A. AFM, ESEM, TEM, and CLSM in liposomal characterization: a comparative study. *International Journal of Nanomedicine* **2011**, *6*, 557-563.
73. Egelhaaf, S. U.; Wehrli, E.; Müller, M.; Adrian, M.; Schurtenberger, P. Determination of the size distribution of lecithin liposomes: a comparative study using freeze fracture,

- cryoelectron microscopy and dynamic light scattering. *Journal of Microscopy* **1996**, *184* (3), 214-228.
74. Almgren, M.; Edwards, K.; Karlsson, G. Cryo transmission electron microscopy of liposomes and related structures. *Colloids and Surfaces A: Physicochemical and Engineering Aspects* **2000**, *174* (1-2), 3-21.
75. Perrie, Y.; Ali, H.; Kirby, D. J.; Mohammed, A. U.; McNeil, S. E.; Vangala, A. Environmental Scanning Electron Microscope Imaging of Vesicle Systems. 2010; Vol. 606, pp 319-331.
76. Ruozi, B.; Tosi, G.; Leo, E.; Vandelli, M. A. Application of atomic force microscopy to characterize liposomes as drug and gene carriers. *Talanta* **2007**, *73* (1), 12-22.
77. Fröhlich, M.; Brecht, V.; Peschka-Süss, R. Parameters influencing the determination of liposome lamellarity by <sup>31</sup>P-NMR. *Chemistry and Physics of Lipids* **2001**, *109* (1), 103-112.
78. Schwartz, M. A.; McConnell, H. M. Surface areas of lipid membranes. *Biochemistry* **1978**, *17* (5), 837-840.
79. Traïkia, M.; Warschawski, D. E.; Recouvreur, M.; Cartaud, J.; Devaux, P. F. Formation of unilamellar vesicles by repetitive freeze-thaw cycles: characterization by electron microscopy and <sup>31</sup>P-nuclear magnetic resonance. *Eur Biophys J* **2000**, *29* (3), 184-195.
80. Mui, B. L.; Cullis, P. R.; Evans, E. A.; Madden, T. D. Osmotic properties of large unilamellar vesicles prepared by extrusion. *Biophysical Journal* **1993**, *64* (2), 443-453.
81. Tilcock, C. P. S.; Cullis, P. R.; Hope, M. J.; Gruner, S. M. Polymorphic phase behavior of unsaturated lysophosphatidylethanolamines: A phosphorus-31 NMR and x-ray diffraction study. *Biochemistry* **1986**, *25* (4), 816-822.
82. Talsma, H.; Jousma, H.; Nicolay, K.; Crommelin, D. J. A. Multilamellar or multivesicular vesicles? *International Journal of Pharmaceutics* **1987**, *37* (1-2), 171-173.
83. Bartlett, G. R. Phosphorus Assay in Column Chromatography. *Journal of Biological Chemistry* **1959**, *234* (3), 466-468.
84. Stewart, J. C. M. Colorimetric determination of phospholipids with ammonium ferrotiocyanate. *Analytical Biochemistry* **1980**, *104* (1), 10-14.
85. Zhong, Z.; Ji, Q.; Zhang, J. A. Analysis of cationic liposomes by reversed-phase HPLC with evaporative light-scattering detection. *Journal of Pharmaceutical and Biomedical Analysis* **2010**, *51* (4), 947-951.
86. Nguyen, T. T.; Ostergaard, J.; Sturup, S.; Gammelgaard, B. Metallomics in drug development: characterization of a liposomal cisplatin drug formulation in human plasma by CE-ICP-MS. *Anal Bioanal Chem* **2013**, *405* (6), 1845-54.
87. Becart, J.; Chevalier, C.; Biesse, J. QUANTITATIVE-ANALYSIS OF PHOSPHOLIPIDS BY HPLC WITH A LIGHT-SCATTERING EVAPORATING DETECTOR - APPLICATION TO RAW-MATERIALS FOR COSMETIC USE. *Hrc-Journal of High Resolution Chromatography* **1990**, *13* (2), 126-129.
88. Schwiering, M.; Hellmann, N. Validation of liposomal lipid composition by thin-layer chromatography. *Journal of Liposome Research* **2012**, *22* (4), 279-284.
89. Shim, G.; Kim, M.-G.; Park, J. Y.; Oh, Y.-K. Application of cationic liposomes for delivery of nucleic acids. *Asian Journal of Pharmaceutical Sciences* **2013**, *8* (2), 72-80.
90. (a) Fatouros, D. G.; Antimisiaris, S. G. Effect of Amphiphilic Drugs on the Stability and Zeta-Potential of Their Liposome Formulations: A Study with Prednisolone, Diazepam, and Griseofulvin. *Journal of Colloid and Interface Science* **2002**, *251* (2), 271-277; (b) Brgles, M.; Jurašin, D.; Sikirić, M. D.; Frkanec, R.; Tomašić, J. Entrapment of Ovalbumin into Liposomes—Factors Affecting Entrapment Efficiency, Liposome Size, and Zeta Potential. *Journal of Liposome Research* **2008**, *18* (3), 235-248.
91. Carrión, F. J.; De La Maza, A.; Parra, J. L. The Influence of Ionic Strength and Lipid Bilayer Charge on the Stability of Liposomes. *Journal of Colloid and Interface Science* **1994**, *164* (1), 78-87.

92. Taylor, K. M. G.; Morris, R. M. Thermal analysis of phase transition behaviour in liposomes. *Thermochimica Acta* **1995**, *248* (0), 289-301.
93. Sezer, A. D.; Bas, A. L.; Akbuga, J. Encapsulation of enrofloxacin in liposomes I: preparation and in vitro characterization of LUV. *J Liposome Res* **2004**, *14* (1-2), 77-86.
94. Guo, W.; Ahmad, A.; Khan, S.; Dahhani, F.; Wang, Y. F.; Ahmad, I. Determination by liquid chromatography with fluorescence detection of total 7-ethyl-10-hydroxy-camptothecin (SN-38) in beagle dog plasma after intravenous administration of liposome-based SN-38 (LE-SN38). *Journal of Chromatography B* **2003**, *791* (1-2), 85-92.
95. Ramaldes, G. A.; Deverre, J. R.; Grognet, J. M.; Puisieux, F.; Fattal, E. Use of an enzyme immunoassay for the evaluation of entrapment efficiency and in vitro stability in intestinal fluids of liposomal bovine serum albumin. *International Journal of Pharmaceutics* **1996**, *143* (1), 1-11.
96. Kensova, R.; Blazkova, I.; Konecna, M.; Kopel, P.; Chudobova, D.; Zitka, O.; Vaculovicova, M.; Hynek, D.; Adam, V.; Beklova, M.; Kizek, R. Lead ions encapsulated in liposomes and their effect on *Staphylococcus aureus*. *Int J Environ Res Public Health* **2013**, *10* (12), 6687-700.
97. Zhang, X.-M.; Patel, A. B.; de Graaf, R. A.; Behar, K. L. Determination of liposomal encapsulation efficiency using proton NMR spectroscopy. *Chemistry and Physics of Lipids* **2004**, *127* (1), 113-120.
98. Nguyen, T. T. N.; Østergaard, J.; Stürup, S.; Gammelgaard, B. Determination of platinum drug release and liposome stability in human plasma by CE-ICP-MS. *International Journal of Pharmaceutics* **2013**, *449* (1-2), 95-102.
99. Fritze, A.; Hens, F.; Kimpfler, A.; Schubert, R.; Peschka-Süss, R. Remote loading of doxorubicin into liposomes driven by a transmembrane phosphate gradient. *Biochimica et Biophysica Acta (BBA) - Biomembranes* **2006**, *1758* (10), 1633-1640.
100. Gregoriadis, G.; Ryman, B. E. Liposomes as carriers of enzymes or drugs: a new approach to the treatment of storage diseases. *Biochem J* **1971**, *124* (5), 58P.
101. Drummond, D. C.; Meyer, O.; Hong, K. L.; Kirpotin, D. B.; Papahadjopoulos, D. Optimizing liposomes for delivery of chemotherapeutic agents to solid tumors. *Pharmacological Reviews* **1999**, *51* (4), 691-743.
102. Jones, M. N. Use of Liposomes to Deliver Bactericides to Bacterial Biofilms. In *Methods in Enzymology*, Nejat, D., Ed. Academic Press: 2005; Vol. Volume 391, pp 211-228.
103. El-Badry, M.; Fetih, G.; Shakeel, F. Comparative topical delivery of antifungal drug croconazole using liposome and micro-emulsion-based gel formulations. *Drug delivery* **2014**, *21* (1), 34-43.
104. Agrawal, A. K.; Harde, H.; Thanki, K.; Jain, S. Improved Stability and Antidiabetic Potential of Insulin Containing Folic Acid Functionalized Polymer Stabilized Multilayered Liposomes Following Oral Administration. *Biomacromolecules* **2013**, *15* (1), 350-360.
105. Chaize, B.; Colletier, J. P.; Winterhalter, M.; Fournier, D. Encapsulation of enzymes in liposomes: high encapsulation efficiency and control of substrate permeability. *Artificial cells, blood substitutes, and immobilization biotechnology* **2004**, *32* (1), 67-75.
106. Monnard, P.-A.; Oberholzer, T.; Luisi, P. Entrapment of nucleic acids in liposomes. *Biochimica et Biophysica Acta (BBA) - Biomembranes* **1997**, *1329* (1), 39-50.
107. Allen, T. M.; Cullis, P. R. Liposomal drug delivery systems: From concept to clinical applications. *Advanced Drug Delivery Reviews* **2013**, *65* (1), 36-48.
108. Kraft, J. C.; Freeling, J. P.; Wang, Z.; Ho, R. J. Y. Emerging Research and Clinical Development Trends of Liposome and Lipid Nanoparticle Drug Delivery Systems. *Journal of Pharmaceutical Sciences* **2014**, *103* (1), 29-52.
109. Schwendener, R.; Ludewig, B.; Cerny, A.; Engler, O. Liposome-Based Vaccines. In *Liposomes*, Weissig, V., Ed. Humana Press: 2010; Vol. 605, pp 163-175.

110. Watson, D. S.; Endsley, A. N.; Huang, L. Design considerations for liposomal vaccines: influence of formulation parameters on antibody and cell-mediated immune responses to liposome associated antigens. *Vaccine* **2012**, *30* (13), 2256-72.
111. Haensler, J. Liposomal adjuvants: preparation and formulation with antigens. *Methods Mol Biol* **2010**, *626*, 73-90.
112. Kikuchi, H.; Suzuki, N.; Ebihara, K.; Morita, H.; Ishii, Y.; Kikuchi, A.; Sugaya, S.; Serikawa, T.; Tanaka, K. Gene delivery using liposome technology. *Journal of controlled release : official journal of the Controlled Release Society* **1999**, *62* (1-2), 269-77.
113. Bhavsar, D.; Subramanian, K.; Sethuraman, S.; Krishnan, U. M. Translational siRNA therapeutics using liposomal carriers: prospects & challenges. *Current gene therapy* **2012**, *12* (4), 315-32.
114. Wasungu, L.; Hoekstra, D. Cationic lipids, lipoplexes and intracellular delivery of genes. *Journal of controlled release : official journal of the Controlled Release Society* **2006**, *116* (2), 255-64.
115. Murray, K. D.; McQuillin, A.; Stewart, L.; Etheridge, C. J.; Cooper, R. G.; Miller, A. D.; Gurling, H. M. Cationic liposome-mediated DNA transfection in organotypic explant cultures of the ventral mesencephalon. *Gene therapy* **1999**, *6* (2), 190-7.
116. Mezei, M.; Gulasekharan, V. Liposomes - a selective drug delivery system for the topical route of administration I. Lotion dosage form. *Life Sciences* **1980**, *26* (18), 1473-1477.
117. Bouwstra, J. A.; Honeywell-Nguyen, P. L. Skin structure and mode of action of vesicles. *Advanced Drug Delivery Reviews* **2002**, *54*, Supplement (0), S41-S55.
118. Honeywell-Nguyen, P. L.; Bouwstra, J. A. Vesicles as a tool for transdermal and dermal delivery. *Drug Discovery Today: Technologies* **2005**, *2* (1), 67-74.
119. Elsayed, M. M. A.; Abdallah, O. Y.; Naggar, V. F.; Khalafallah, N. M. Lipid vesicles for skin delivery of drugs: Reviewing three decades of research. *International Journal of Pharmaceutics* **2007**, *332* (1-2), 1-16.
120. Cevc, G. Lipid vesicles and other colloids as drug carriers on the skin. *Advanced Drug Delivery Reviews* **2004**, *56* (5), 675-711.
121. Silindir, M.; Erdoğan, S.; Özer, A. Y.; Doğan, A. L.; Tuncel, M.; Uğur, Ö.; Torchilin, V. P. Nanosized multifunctional liposomes for tumor diagnosis and molecular imaging by SPECT/CT. *Journal of Liposome Research* **2013**, *23* (1), 20-27.
122. Petersen, A. L.; Hansen, A. E.; Gabizon, A.; Andresen, T. L. Liposome imaging agents in personalized medicine. *Advanced Drug Delivery Reviews* **2012**, *64* (13), 1417-1435.
123. Béalle, G.; Di Corato, R.; Kolosnjaj-Tabi, J.; Dupuis, V.; Clément, O.; Gazeau, F.; Wilhelm, C.; Ménager, C. Ultra Magnetic Liposomes for MR Imaging, Targeting, and Hyperthermia. *Langmuir* **2012**, *28* (32), 11834-11842.
124. Li, S.; Goins, B.; Zhang, L.; Bao, A. Novel Multifunctional Theranostic Liposome Drug Delivery System: Construction, Characterization, and Multimodality MR, Near-Infrared Fluorescent, and Nuclear Imaging. *Bioconjugate Chemistry* **2012**, *23* (6), 1322-1332.
125. Zhang, L.-W.; Wen, C.-J.; Al-Suwayeh, S.; Yen, T.-C.; Fang, J.-Y. Cisplatin and quantum dots encapsulated in liposomes as multifunctional nanocarriers for theranostic use in brain and skin. *Journal of Nanoparticle Research* **2012**, *14* (7), 1-18.
126. Taruttis, A.; Lozano, N.; Nunes, A.; Jasim, D.; Beziere, N.; Herzog, E.; Kostarelos, K.; Ntziachristos, V. siRNA Liposome-Gold-Nanorod Vectors for Multispectral Optoacoustic Tomography Theranostics. *Nanoscale* **2014**.
127. Hendriks, B. S.; Reynolds, J. G.; Klinz, S. G.; Geretti, E.; Lee, H.; Leonard, S. C.; Gaddy, D. F.; Espelin, C. W.; Nielsen, U. B.; Wickham, T. J. Multiscale Kinetic Modeling of Liposomal Doxorubicin Delivery Quantifies the Role of Tumor and Drug-Specific Parameters in Local Delivery to Tumors. *CPT: pharmacomet. syst. pharmacol.* **2012**, *1*, e15.
128. Murrell, M. P.; Voituriez, R.; Joanny, J.-F.; Nassoy, P.; Sykes, C.; Gardel, M. L. Liposome adhesion generates traction stress. *Nat Phys* **2014**, advance online publication.

129. Sabín, J.; Prieto, G.; Sarmiento, F. Studying Colloidal Aggregation Using Liposomes. In *Liposomes*, Weissig, V., Ed. Humana Press: 2010; Vol. 606, pp 189-198.
130. Yoshimoto, M.; Miyazaki, Y.; Kudo, Y.; Fukunaga, K.; Nakao, K. Glucose oxidation catalyzed by liposomal glucose oxidase in the presence of catalase-containing liposomes. *Biotechnology progress* **2006**, *22* (3), 704-9.
131. Steinberg-Yfrach, G.; Liddell, P. A.; Hung, S.-C.; Moore, A. L.; Gust, D.; Moore, T. A. Conversion of light energy to proton potential in liposomes by artificial photosynthetic reaction centres. *Nature* **1997**, *385* (6613), 239-241.
132. Matsumoto, R.; Kakuta, M.; Sugiyama, T.; Goto, Y.; Sakai, H.; Tokita, Y.; Hatazawa, T.; Tsujimura, S.; Shirai, O.; Kano, K. A liposome-based energy conversion system for accelerating the multi-enzyme reactions. *Physical Chemistry Chemical Physics* **2010**, *12* (42), 13904-13906.
133. Graff, A.; Winterhalter, M.; Meier, W. Nanoreactors from Polymer-Stabilized Liposomes. *Langmuir* **2001**, *17* (3), 919-923.
134. Kazakov, S.; Kaholek, M.; Teraoka, I.; Levon, K. UV-Induced Gelation on Nanometer Scale Using Liposome Reactor. *Macromolecules* **2002**, *35* (5), 1911-1920.
135. Bangham, A. D.; Hill, M. W.; Miller, N. G. A. Preparation and Use of Liposomes as Models of Biological Membranes. In *Methods in Membrane Biology*, Korn, E., Ed. Springer US: 1974; pp 1-68.
136. Nakane, Y.; Ito, M. M.; Kubo, I. Novel Detection Method of Endocrine Disrupting Chemicals Utilizing Liposomes as Cell Membrane Model. *Analytical Letters* **2008**, *41* (16), 2923-2932.
137. Taylor, T. M.; Davidson, P. M.; Bruce, B. D.; Weiss, J. Liposomal nanocapsules in food science and agriculture. *Critical reviews in food science and nutrition* **2005**, *45* (7-8), 587-605.
138. Barani, H.; Montazer, M. A Review on Applications of Liposomes in Textile Processing. *Journal of Liposome Research* **2008**, *18* (3), 249-262.
139. Kim, C.-K.; Lim, S.-J. Liposome immunoassay (LIA) with antigen-coupled liposomes containing alkaline phosphatase. *Journal of Immunological Methods* **1993**, *159* (1-2), 101-106.
140. Ishimori, Y.; Yasuda, T.; Tsumita, T.; Notsuki, M.; Koyama, M.; Tadakuma, T. Liposome immune lysis assay (LILA): a simple method to measure anti-protein antibody using protein antigen-bearing liposomes. *J Immunol Methods* **1984**, *75* (2), 351-60.
141. Rongen, H. A. H.; van der Horst, H. M.; Hugenholtz, G. W. K.; Bult, A.; van Bennekom, W. P.; van der Meide, P. H. Development of a liposome immunosorbent assay for human interferon- $\gamma$ . *Analytica Chimica Acta* **1994**, *287* (3), 191-199.
142. Edwards, A. J.; Durst, R. A. Flow-injection liposome immunoanalysis (FILIA) with electrochemical detection. *Electroanalysis* **1995**, *7* (9), 838-845.
143. Liu, Q.; Boyd, B. J. Liposomes in biosensors. *Analyst* **2013**, *138* (2), 391-409.
144. Tao, A. R.; Habas, S.; Yang, P. Shape control of colloidal metal nanocrystals. *Small* **2008**, *4* (3), 310-325.
145. Roldan Cuenya, B. Metal Nanoparticle Catalysts Beginning to Shape-up. *Accounts of Chemical Research* **2012**, *46* (8), 1682-1691.
146. Shipway, A. N.; Katz, E.; Willner, I. Nanoparticle arrays on surfaces for electronic, optical, and sensor applications. *Chemphyschem : a European journal of chemical physics and physical chemistry* **2000**, *1* (1), 18-52.
147. Garcia, M. A. Surface plasmons in metallic nanoparticles: fundamentals and applications. *Journal of Physics D: Applied Physics* **2011**, *44* (28), 283001.
148. Doria, G.; Conde, J.; Veigas, B.; Giestas, L.; Almeida, C.; Assuncao, M.; Rosa, J.; Baptista, P. V. Noble metal nanoparticles for biosensing applications. *Sensors (Basel, Switzerland)* **2012**, *12* (2), 1657-87.
149. Hao, R.; Xing, R.; Xu, Z.; Hou, Y.; Gao, S.; Sun, S. Synthesis, Functionalization, and Biomedical Applications of Multifunctional Magnetic Nanoparticles. *Advanced Materials* **2010**, *22* (25), 2729-2742.



150. Tobiška, P.; Hugon, O.; Trouillet, A.; Gagnaire, H. An integrated optic hydrogen sensor based on SPR on palladium. *Sensors and Actuators B: Chemical* **2001**, *74* (1–3), 168-172.
151. Kim, S. W.; Park, J.; Jang, Y.; Chung, Y.; Hwang, S.; Hyeon, T.; Kim, Y. W. Synthesis of monodisperse palladium nanoparticles. *Nano Letters* **2003**, *3* (9), 1289-1291.
152. Arul Dhas, N.; Gedanken, A. Sonochemical preparation and properties of nanostructured palladium metallic clusters. *Journal of Materials Chemistry* **1998**, *8* (2), 445-450.
153. Schmid, G.; Harms, M.; Malm, J. O.; Bovin, J. O.; Van Ruitenbeck, J.; Zandbergen, H. W.; Fu, W. T. Ligand-stabilized giant palladium clusters: promising candidates in heterogeneous catalysis. *Journal of the American Chemical Society* **1993**, *115* (5), 2046-2048.
154. Reetz, M. T.; Helbig, W. Size-Selective Synthesis of Nanostructured Transition Metal Clusters. *Journal of the American Chemical Society* **1994**, *116* (16), 7401-7402.
155. Yee, C. K.; Jordan, R.; Ulman, A.; White, H.; King, A.; Rafailovich, M.; Sokolov, J. Novel one-phase synthesis of thiol-functionalized gold, palladium, and iridium nanoparticles using superhydride. *Langmuir* **1999**, *15* (10), 3486-3491.
156. Brust, M.; Walker, M.; Bethell, D.; Schiffrin, D. J.; Whyman, R. Synthesis of thiol-derivatised gold nanoparticles in a two-phase Liquid-Liquid system. *Journal of the Chemical Society, Chemical Communications* **1994**, *0* (7), 801-802.
157. Srivastava, S.; Constanti, M. Room temperature biogenic synthesis of multiple nanoparticles (Ag, Pd, Fe, Rh, Ni, Ru, Pt, Co, and Li) by *Pseudomonas aeruginosa* SM1. *Journal of Nanoparticle Research* **2012**, *14* (4), 1-10.
158. Bilecka, I.; Elser, P.; Niederberger, M. Kinetic and Thermodynamic Aspects in the Microwave-Assisted Synthesis of ZnO Nanoparticles in Benzyl Alcohol. *Acs Nano* **2009**, *3* (2), 467-477.
159. Zhao, P.; Li, N.; Astruc, D. State of the art in gold nanoparticle synthesis. *Coordination Chemistry Reviews* **2013**, *257* (3–4), 638-665.
160. Moon, S. Y.; Kusunose, T.; Sekino, T. CTAB-Assisted Synthesis of Size- and Shape-Controlled Gold Nanoparticles in SDS Aqueous Solution. *Materials Letters* **2009**, *63* (23), 2038-2040.
161. Wang, C.-C.; Chen, D.-H.; Huang, T.-C. Synthesis of palladium nanoparticles in water-in-oil microemulsions. *Colloids and Surfaces A: Physicochemical and Engineering Aspects* **2001**, *189* (1–3), 145-154.
162. Heshmatpour, F.; Abazari, R.; Balalaie, S. Preparation of monometallic (Pd, Ag) and bimetallic (Pd/Ag, Pd/Ni, Pd/Cu) nanoparticles via reversed micelles and their use in the Heck reaction. *Tetrahedron* **2012**, *68* (14), 3001-3011.
163. Coulter, M. M.; Dinglasan, J. A.; Goh, J. B.; Nair, S.; Anderson, D. J.; Dong, V. M. Preparing water-dispersed palladium nanoparticles via polyelectrolyte nanoreactors. *Chemical Science* **2010**, *1* (6), 772-775.
164. Grace, A. N.; Pandian, K. One pot synthesis of polymer protected gold nanoparticles and nanoprisms in glycerol. *Colloids and Surfaces A: Physicochemical and Engineering Aspects* **2006**, *290* (1–3), 138-142.
165. Leong, W. L.; Lee, P. S.; Lohani, A.; Lam, Y. M.; Chen, T.; Zhang, S.; Dodabalapur, A.; G. Mhaisalkar, S. Non-Volatile Organic Memory Applications Enabled by In Situ Synthesis of Gold Nanoparticles in a Self-Assembled Block Copolymer. *Advanced Materials* **2008**, *20* (12), 2325-2331.
166. Nemancha, A.; Moumeni, H.; Rehspringer, J. L. PVP Protective mechanism of palladium nanoparticles obtained by sonochemical process. In *Proceedings of the Jmsm 2008 Conference*, Cheikhrouhou, A., Ed. 2009; Vol. 2, pp 713-717.
167. He, P.; Urban, M. W. Phospholipid-stabilized Au-nanoparticles. *Biomacromolecules* **2005**, *6* (3), 1224-5.

168. Chow, G. M.; Markowitz, M. A.; Rayne, R.; Dunn, D. N.; Singh, A. Phospholipid Mediated Synthesis and Characterization of Gold Nanoparticles. *Journal of Colloid and Interface Science* **1996**, *183* (1), 135-142.
169. Song, Y.; Yang, Y.; Medforth, C. J.; Pereira, E.; Singh, A. K.; Xu, H.; Jiang, Y.; Brinker, C. J.; van Swol, F.; Shelnett, J. A. Controlled Synthesis of 2-D and 3-D Dendritic Platinum Nanostructures. *Journal of the American Chemical Society* **2003**, *126* (2), 635-645.
170. Song, Y.; Garcia, R. M.; Dorin, R. M.; Wang, H.; Qiu, Y.; Shelnett, J. A. Synthesis of platinum nanocages by using liposomes containing photocatalyst molecules. *Angewandte Chemie-International Edition* **2006**, *45* (48), 8126-8130.
171. Sau, T. K.; Urban, A. S.; Dondapati, S. K.; Fedoruk, M.; Horton, M. R.; Rogach, A. L.; Stefani, F. D.; Rädler, J. O.; Feldmann, J. Controlling loading and optical properties of gold nanoparticles on liposome membranes. *Colloids and Surfaces A: Physicochemical and Engineering Aspects* **2009**, *342* (1-3), 92-96.
172. Bakshi, M. S.; Possmayer, F.; Petersen, N. O. Simultaneous Synthesis of Au and Cu Nanoparticles in Pseudo-Core-Shell Type Arrangement Facilitated by DMPG and 12-6-12 Capping Agents. *Chemistry of Materials* **2007**, *19* (6), 1257-1266.
173. Bakshi, M. S.; Possmayer, F.; Petersen, N. O. Role of Different Phospholipids in the Synthesis of Pearl-Necklace-Type Gold-Silver Bimetallic Nanoparticles as Bioconjugate Materials. *The Journal of Physical Chemistry C* **2007**, *111* (38), 14113-14124.
174. Sackmann, E.; Smith, A.-S. Physics of cell adhesion: some lessons from cell-mimetic systems. *Soft Matter* **2014**, *10* (11), 1644-1659.
175. Ding, W.-Q.; Lind, S. E. Metal ionophores – An emerging class of anticancer drugs. *IUBMB Life* **2009**, *61* (11), 1013-1018.
176. Fukada, T.; Yamasaki, S.; Nishida, K.; Murakami, M.; Hirano, T. Zinc homeostasis and signaling in health and diseases. *J Biol Inorg Chem* **2011**, *16* (7), 1123-1134.
177. Maret, W. Metals on the move: zinc ions in cellular regulation and in the coordination dynamics of zinc proteins. *Biometals* **2011**, *24* (3), 411-418.
178. Egert, S.; Rimbach, G. Which Sources of Flavonoids: Complex Diets or Dietary Supplements? *Advances in Nutrition: An International Review Journal* **2011**, *2* (1), 8-14.
179. Ramos, S. Cancer chemoprevention and chemotherapy: Dietary polyphenols and signalling pathways. *Molecular Nutrition & Food Research* **2008**, *52* (5), 507-526.
180. Anê, F. F.; Desjardins, Y.; Pilon, G.; Dudonné, S.; Genovese, M. I.; Lajolo, F. M.; Marette, A. Polyphenols and type 2 diabetes: A prospective review. *PharmaNutrition* **2013**, *1* (4), 105-114.
181. Jagtap, S.; Meganathan, K.; Wagh, V.; Winkler, J.; Hescheler, J.; Sachinidis, A. Chemoprotective Mechanism of the Natural Compounds, Epigallocatechin-3-O-Gallate, Quercetin and Curcumin Against Cancer and Cardiovascular Diseases. *Current Medicinal Chemistry* **2009**, *16* (12), 1451-1462.
182. Williams, R. J.; Spencer, J. P. E. Flavonoids, cognition, and dementia: Actions, mechanisms, and potential therapeutic utility for Alzheimer disease. *Free Radical Biology and Medicine* **2012**, *52* (1), 35-45.
183. Sankaram, M. B.; Shastri, B. P.; Easwaran, K. R. K. Interaction of carrier ionophores with phospholipid vesicles. *Biochemistry* **1987**, *26* (16), 4936-4941.
184. Weissmann, G.; Anderson, P.; Serhan, C.; Samuelsson, E.; Goodman, E. A general method, employing arsenazo III in liposomes, for study of calcium ionophores: results with A23187 and prostaglandins. *Proceedings of the National Academy of Sciences* **1980**, *77* (3), 1506-1510.
185. Kolber, M. A.; Haynes, D. H. FLUORESCENCE STUDY OF THE DIVALENT CATION-TRANSPORT MECHANISM OF IONOPHORE A23187 IN PHOSPHOLIPID-MEMBRANES. *Biophysical Journal* **1981**, *36* (2), 369-391.
186. Mathew, M. K.; Nagaraj, R.; Balaram, P. Ionophore-mediated transmembrane movement of divalent cations in small unilamellar liposomes: An evaluation of the

chlortetracycline fluorescence technique and correlations with black lipid membrane studies. *J. Membr. Biol.* **1982**, *65* (1-2), 13-17.

187. Barenholz, Y. Doxil® — The first FDA-approved nano-drug: Lessons learned. *Journal of Controlled Release* **2012**, *160* (2), 117-134.

188. Immordino, M. L.; Dosio, F.; Cattel, L. Stealth liposomes: review of the basic science, rationale, and clinical applications, existing and potential. *Int J Nanomedicine* **2006**, *1* (3), 297-315.

189. Maeda, H.; Sawa, T.; Konno, T. Mechanism of tumor-targeted delivery of macromolecular drugs, including the EPR effect in solid tumor and clinical overview of the prototype polymeric drug SMANCS. *Journal of Controlled Release* **2001**, *74* (1-3), 47-61.

190. Noble, G. T.; Stefanick, J. F.; Ashley, J. D.; Kiziltepe, T.; Bilgicer, B. Ligand-targeted liposome design: challenges and fundamental considerations. *Trends in Biotechnology* *32* (1), 32-45.

191. Lu, Y.; Low, P. S. Folate-mediated delivery of macromolecular anticancer therapeutic agents. *Advanced Drug Delivery Reviews* **2002**, *54* (5), 675-693.

192. Sawant, R. R.; Torchilin, V. P. Challenges in Development of Targeted Liposomal Therapeutics. *The AAPS Journal* **2012**, *14* (2), 303-315.

193. Shin, J.; Shum, P.; Grey, J.; Fujiwara, S.; Malhotra, G. S.; Gonzalez-Bonet, A.; Hyun, S. H.; Moase, E.; Allen, T. M.; Thompson, D. H. Acid-labile mPEG-vinyl ether-1,2-dioleoylglycerol lipids with tunable pH sensitivity: synthesis and structural effects on hydrolysis rates, DOPE liposome release performance, and pharmacokinetics. *Mol Pharm* **2012**, *9* (11), 3266-76.

194. Ta, T.; Porter, T. M. Thermosensitive liposomes for localized delivery and triggered release of chemotherapy. *Journal of Controlled Release* *169* (1-2), 112-125.

195. Yavlovich, A.; Smith, B.; Gupta, K.; Blumenthal, R.; Puri, A. Light-sensitive lipid-based nanoparticles for drug delivery: design principles and future considerations for biological applications. *Molecular membrane biology* **2010**, *27* (7), 364-81.

196. Andresen, T. L.; Thompson, D. H.; Kaasgaard, T. Enzyme-triggered nanomedicine: drug release strategies in cancer therapy. *Molecular membrane biology* **2010**, *27* (7), 353-63.

197. Davidsen, J.; Jørgensen, K.; Andresen, T. L.; Mouritsen, O. G. Secreted phospholipase A2 as a new enzymatic trigger mechanism for localised liposomal drug release and absorption in diseased tissue. *Biochimica et Biophysica Acta (BBA) - Biomembranes* **2003**, *1609* (1), 95-101.

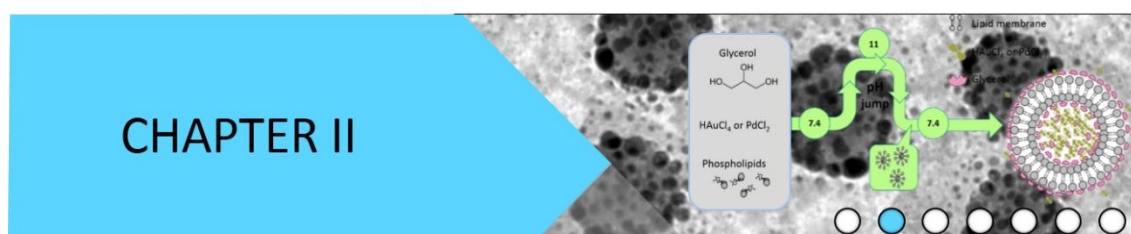
198. Davis, S. C.; Szoka, F. C. Cholesterol Phosphate Derivatives: Synthesis and Incorporation into a Phosphatase and Calcium-Sensitive Triggered Release Liposome. *Bioconjugate Chemistry* **1998**, *9* (6), 783-792.

199. Pak, C. C.; Erukulla, R. K.; Ahl, P. L.; Janoff, A. S.; Meers, P. Elastase activated liposomal delivery to nucleated cells. *Biochimica et Biophysica Acta (BBA) - Biomembranes* **1999**, *1419* (2), 111-126.

200. Sarkar, N.; Banerjee, J.; Hanson, A. J.; Elegbede, A. I.; Rosendahl, T.; Krueger, A. B.; Banerjee, A. L.; Tobwala, S.; Wang, R.; Lu, X.; Mallik, S.; Srivastava, D. K. Matrix Metalloproteinase-Assisted Triggered Release of Liposomal Contents. *Bioconjugate Chemistry* **2007**, *19* (1), 57-64.







# Green synthesis of gold nanoparticles using glycerol-incorporated nanosized liposomes



## Green synthesis of gold nanoparticles using glycerol-incorporated nanosized liposomes

*Langmuir* **2011**, *27*, 10894–10900

Rükan Genç,<sup>†</sup> Gael Clergeaud,<sup>†</sup> Mayreli Ortiz,<sup>\*,†</sup> and Ciara K. O'Sullivan<sup>\*,†,§</sup>

<sup>†</sup> Nanobiotechnology & Bioanalysis Group, Department d'Enginyeria Química, Universitat Rovira i Virgili, Tarragona 43007, Spain

<sup>§</sup> Institució Catalana de Recerca i Estudis Avancats, Barcelona 08010, Spain



## 2.1. Abstract

There has been enormous interest in the last decade in development methods for the inorganic synthesis of metallic nanoparticles of desired sizes and shapes because of their unique properties and extensive applications in catalysis, electronics, plasmonics, and sensing. Here we report on an environmentally friendly, one-pot synthesis of metallic nanoparticles, which avoids the use of organic solvents and requires mild experimental conditions. The developed method uses liposomes as nanoreactors, where the liposomes were prepared by encapsulating chloroauric acid and exploited the use of glycerol, incorporated within the lipid bilayer as well as in its hydrophilic core, as a reducing agent for the controlled preparation of highly homogeneous populations of gold nanoparticles. The effects of temperature, the presence of a capping agent, and the concentration of glycerol on the size and homogeneity of the nanoparticles formed were investigated and compared with solution-based glycerol-mediated nanoparticle synthesis. Well-distributed gold nanoparticle populations in the range of 2-8 nm were prepared in the designed liposomal nanoreactor with a clear dependence of the size on the concentration of glycerol, the temperature, and the presence of a capping agent whereas large, heterogeneous populations of nanoparticles with amorphous shapes were obtained in the absence of liposomes. The particle morphology and sizes were analysed using transmission electron microscopy imaging, and the liposome size was measured using photon correlation spectroscopy.

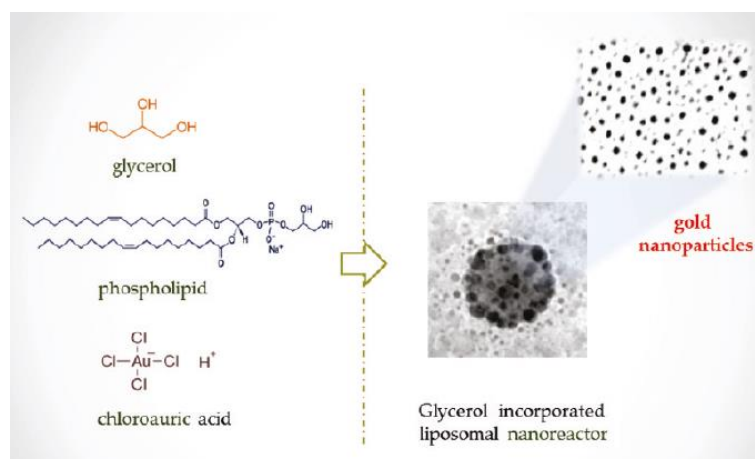


Figure 2.1. Table of contents figure

## 2.2. Introduction

Metal nanoparticles with diverse sizes and shapes have garnered great interest in the past decade because of their exceptional unique optical, electronic, and chemical properties, which are not displayed in the bulk state of the metal.<sup>1,2</sup> Among those metals, gold (Au)-based nanoparticles (NPs) have been of particular interest because of their widespread applications in catalysis, plasmonics, sensors, and biomedical technologies (e.g., drug delivery) as well as electronics.<sup>3,4</sup> The development of synthesis methods to obtain homogeneous size- and shape-tunable nanoparticles for specific application requirements is a priority in nanoparticle-based technology development.<sup>1</sup> In the majority of the reported chemical synthesis methods of gold NPs, the basic principle is the reduction of Au(III) to Au(0), often exploiting sodium citrate and sodium borohydride as reducing agents in aqueous solutions. Subsequently, reduced gold atoms

assemble in small clusters, and finally these clusters provide nucleation sites for other molecules to adhere to and grow nanoparticles.<sup>5</sup> To avoid uncontrolled aggregation into larger particles, stabilizing or capping agents are usually added to the mixture.<sup>6</sup> By addressing environmentally friendly methods of producing nanoparticles, renewable reagent sources such as alcohols,<sup>6</sup> bacteria,<sup>7</sup> plant extracts,<sup>5</sup> and polyols<sup>8</sup> have been demonstrated as successful reducing agents and/or capping agents.

Glycerol is a known polyol used as a moistening agent and a preservative to extend shelf life, as well as a sweetener in food technology and in the manufacture of many drugs. Oxidation products of glycerol are also of great interest, and the development of new cost-effective methodologies for their production, using gold or palladium nanoparticles as catalysts, have been reported.<sup>9-12</sup> However, there have been very few attempts to exploit the reverse reaction, where the metals are reduced by glycerol, thus forming nanoparticles. To date, the synthesis of nanoparticles with polyols (most often ethylene glycol) is based on heating a polyol-inorganic salt mixture typically to high temperatures of over 100 °C depending on the melting temperature of the polyol under continuous stirring conditions.<sup>13</sup> In their recent study, Grace and Pandian reported on the synthesis of gold nanoparticles and nanoprisms using glycerol as a reducing agent under both reflux and microwave conditions, where the glycerol HAuCl<sub>4</sub> mixture was heated to its boiling point, resulting in the synthesis of spherical or prism-shaped nanoparticles depending on the reaction time.<sup>14</sup> Nisaratanaporn and Wongsuwan prepared silver powders with particle sizes of larger than 63 nm from silver alkoxide using glycerol as a reducing agent, again heating the metal and undiluted glycerol solution to high temperatures (150-180 °C),<sup>15</sup> and Sarkar et al. achieved the glycerol-mediated reduction of silver to form nanoparticles of 25 nm at room temperature but the reduction required the addition of NaOH.<sup>16</sup> To the best of our knowledge, there is no report to date demonstrating the formation of extremely small nanoparticles using glycerol as a reducing agent at low temperatures and not requiring any additional reactants.

A widely reported method for the preparation of nanoparticles is the reverse micelle method, which exploits water-in-oil droplets stabilized by a surfactant (most often AOT (aerosol OT, sodium bis(2-ethylhexyl) sulfosuccinate)).<sup>17,18</sup> They have been used as nanoreactors for the synthesis of structures having the same shapes as the micelle nuclei such as metal nanoparticles<sup>19</sup> or metal hybrids,<sup>20</sup> ceramic materials,<sup>21</sup> and quantum dots<sup>22</sup> as well as polymer composites.<sup>23</sup> Reverse micelles tend to fuse and disperse randomly because of Brownian motion, and the content exchange between two fused reverse micelles results in the formation of nanosized particles, with their size being defined by the micelle volume.<sup>24</sup>

As an alternative to reverse micelles as nanoreactors, liposomes are promising candidates for the synthesis of metal nanoparticles because they provide a controllable environment, not only in the core but also within the lipid bilayer.<sup>25</sup> However, the preparation of nanosized liposomes is labor-intensive. In a previous study carried out in our group, nanosized liposomes have been prepared using a one-step preparation method based on a pH jump<sup>26</sup> that was not only environmentally friendly because it avoids the use of organic solvents but also extremely rapid because it requires no homogenization steps such as extrusion and sonication, with the preparation of a highly uniform population of nanosized liposomes being achieved in less than an hour.

In this work, we report a new environmentally friendly, low temperature method to obtain a homogeneous population of ultrasmall gold nanoparticles using liposomes incorporating glycerol. Glycerol, which is incorporated on both the external and internal polar surfaces of

liposomes encapsulating chloroauric acid,  $\text{HAuCl}_4$ , facilitates the reduction of Au(III) to form Au(0) atoms and subsequent nanoparticles. The effect of parameters such as the temperature, the use of a capping agent, and the glycerol concentration was investigated in terms of the particle size and monodispersity. The resulting nanoparticles were characterized by transmission electron microscopy (TEM). Highly monodisperse Au NPs in a size range of 2-8 nm were obtained after 1 day of incubation at room temperature depending on the conditions used.

## 2.3. Experimental section

### 2.3.1. Materials

PBS buffer (10 mM, pH 7.4) supplied as a sachet of prepared lyophilized buffer, glycerol,  $\text{HAuCl}_4$ , and 6-mercapto-1-hexanol (MCH) was purchased from Sigma. Liposomes were prepared using phospholipids supplied by Avanti Polar Lipids Inc. All lipids were supplied as powders and were used without further purification. Sodium hydroxide and hydrochloric acid (ACS reagent grade) were also purchased from Scharlau Chemie SA.

### 2.3.2. Preparation of encapsulating nanoliposomes

Twenty milligrams of  $\text{HAuCl}_4$  or MCH/ $\text{HAuCl}_4$  encapsulating liposomes were prepared via the curvature-tuned preparation (CTP) method as reported previously.<sup>26</sup> Briefly, 50 mg of a phospholipid formulation of 1, 2-dioleoyl-sn-glycero-3-[phosphor-rac-(1-glycerol)] (DOPG) and 1-palmitoyl-2-hydroxy-sn-glycero-3-phosphocholine (lyso-PPC) in an 88:12 molar ratio was dissolved in 10 mL of a previously prepared  $\text{HAuCl}_4$  solution (2 mg/mL) in the presence or absence of 6-mercapto-1-hexanol (MCH, 1:50  $\text{HAuCl}_4$ /MCH molar ratio) in PBS buffer (10 mM, pH 7.4) at various concentrations of glycerol. The solution was stirred at room temperature under argon. The mixture was then treated with a rapid pH jump (pH 7.4  $\rightarrow$  pH 11  $\rightarrow$  pH 7.4) followed by an equilibration period of 25 min, where lipid clusters curl into encapsulating liposomes of 20 nm diameter. The resulting liposomes were purified using a Sephadex G-25 column and used freshly prepared.

### 2.3.3. Synthesis of Gold Nanoparticles in the Presence of Liposomes

Solutions of nanoliposomes prepared as explained in section 2.2 were incubated at predetermined temperatures under shaking conditions. Following incubation, nanoparticles were purified by centrifuging at 1000 rpm for 5 min and three times with a methanol/ethanol mixture (1:4 v/v), and the collected pellet was resuspended in toluene and stored at 4 °C for further characterization studies.

### 2.3.4. Synthesis of Gold Nanoparticles in the Absence of Liposomes

(I) Twenty milligrams of  $\text{HAuCl}_4$  was resuspended in a constant-concentration of glycerol solution (3-15 % v/v) in PBS (10 mM, pH 7.4) and incubated at predetermined temperatures for 24 h. (II) Twenty milligrams of  $\text{HAuCl}_4$  was resuspended in a constant concentration of glycerol solution in PBS (10 mM, pH 7.4), and the mixture was exposed to a rapid pH jump from pH 7.4 to pH 11 and a subsequent decrease to pH 7.4. The solution was again incubated at predetermined temperatures. (III)  $\text{HAuCl}_4$  and capping agent 6-mercapto-1-hexanol (MCH) were mixed with a constant-concentration of glycerol solution (3-15 % v/v) in PBS (10 mM, pH 7.4),



and the mixture was exposed to a rapid pH jump from pH 7.4 to pH 11 and a subsequent decrease to pH 7.4 and further incubated at predetermined temperatures. Solutions were continuously shaken in a temperature-controlled shaker, and nanoparticles were purified by centrifuging at 1000 rpm for 5 min and three times with a methanol/ethanol mixture (1:4 v/v). The collected pellet was resuspended in toluene and kept at 4 °C for further characterization studies.

### 2.3.5. Photon Correlation Spectroscopy (PCS)

The mean diameter of nanoreactor liposomes was measured using Zeta Sizer 3000H from Malvern Instruments, Inc., (He-Ne laser (633 nm), detector angle of 90°), which measures the rate of fluctuation of the light scattered from the particles using photon correlation spectroscopy (PCS). Standard deviations were calculated from the mean of the data of a series of experiments ( $n \geq 3$ ).

### 2.3.6. Transmission Electron Microscopy (TEM) Imaging

Using a glass pipette we added a drop of sample to a 200 mesh copper grid with a thin film of Formvar polymer and carefully dried it using filter paper. The sample was left at room temperature until a dried film was obtained. Transmission electron microscopy (TEM) analyses were performed using a JEOL 1011 transmission electron microscope operated at 80 keV with an ultrahigh resolution pole piece providing a point resolution of 2 Å. Micrographs (1024 pixels x 1024 pixels) were acquired using a Megaview III multiscan CCD camera. Images were analysed with an iTEM image analysis platform, and the mean diameter was calculated by measuring at least 100 particles from the series of experiments ( $n \geq 3$ ).

## 2.4. Results and discussion

### 2.4.1. Solution-based synthesis of gold nanoparticles in glycerol

We have previously reported on an environmentally friendly method for the rapid (< 1 h) preparation of highly homogeneous spherical liposome populations, the size of which can be carefully controlled via a combination of lipid composition and temperature applied during an equilibration stage following a rapid pH jump from pH 7.4 to pH 11 and back to pH 7.4, which we term the curvature-tuned liposome preparation (CTLP).<sup>26</sup> To demonstrate the concept of producing gold nanoparticles by the use of the glycerol-mediated reduction of chloroauric acid (HAuCl<sub>4</sub>), the solution-based synthesis of nanoparticles was primarily studied under the same conditions as in the absence of lipids. Briefly, 20 mg of chloroauric acid was mixed with glycerol in solution (15 % v/v) at 25 °C in PBS (pH 7.4, 10 mM) in the absence of liposomes. As illustrated in Figure 2.2, after 1 day of incubation at room temperature, relatively large, heterogeneous particles (10-50 nm or more) with an amorphous shape were obtained.

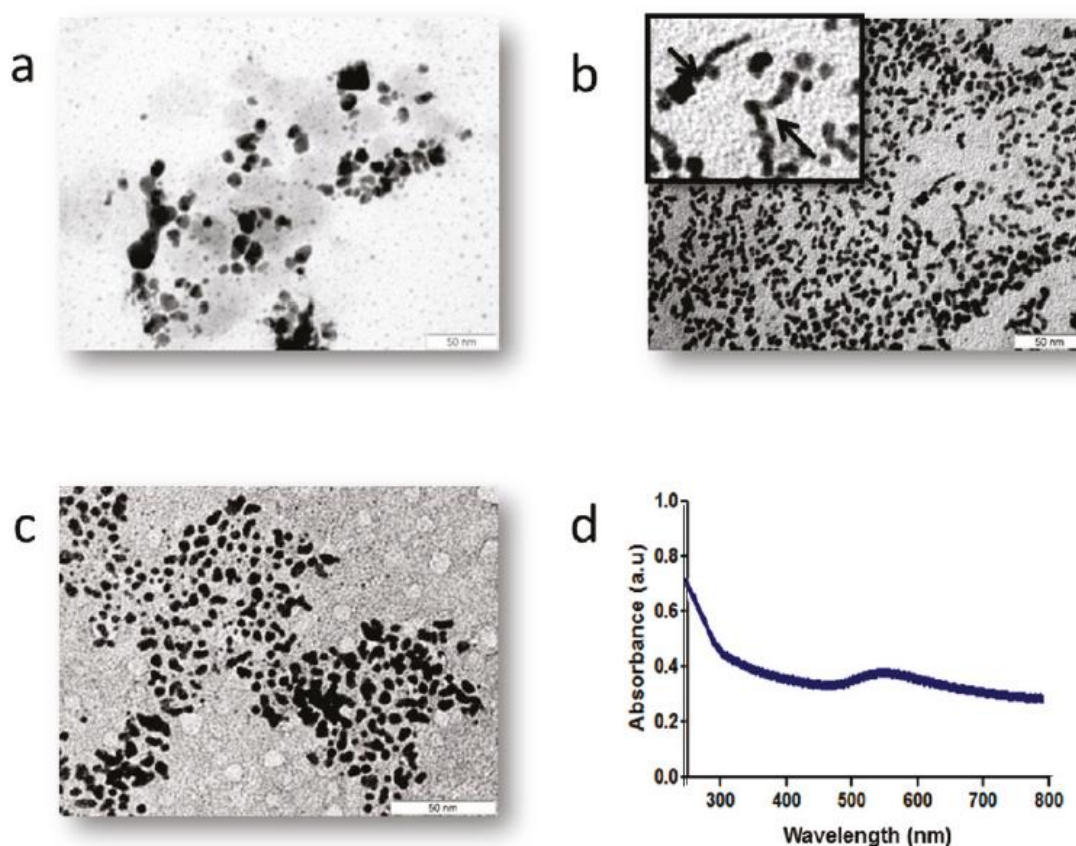


Figure 2.2. TEM images of the particles synthesized using the direct synthesis of gold nanoparticles using glycerol in PBS after 24 h of incubation: (a) glycerol- $\text{HAuCl}_4$  mixture in PBS (10 mM, pH 7.4) incubated at 25 °C without a capping agent, (b) glycerol- $\text{HAuCl}_4$  mixture in PBS (10 mM, pH 7.4) incubated at 25 °C without a capping agent after an instant pH jump (arrows indicate the particle chains), and (c) glycerol- $\text{HAuCl}_4$  mixture in PBS (10 mM, pH 7.4) incubated at 25 °C at a constant concentration of the capping agent after an instant pH jump. Insets are magnified images of corresponding particles. (d) UV-vis spectra of the sample in part c, with the band observed at 546 nm.

Polyol-based reduction-oxidation reactions mainly depend on the reaction pH, thus one of the important parameters of the curvature-tuned liposome preparation method, which exploits a pH jump, will have an impact on the reaction kinetics.<sup>27,28</sup> Thus, solution-based synthesis was also carried out at a constant concentration of glycerol (15 % v/v) after an instant pH jump to pH 11 and a subsequent drop back to pH 7.4, followed by incubation at room temperature for 24 h. TEM images of the nanoparticle population following the elimination of excess glycerol by centrifugation with a methanol:ethanol solution (1:4 v/v, Figure 2.2b) demonstrated that there was a decrease in the particle size and an increase in the number of particles (Figure 2.2b). However, the particles were still amorphous and mainly aligned as chains of several particles (inset of Figure 2.2b) with a length of around 20 nm.

Further studies on the effect of a capping agent at a glycerol concentration of 15 % v/v in the absence of liposomes resulted in smaller particles (5-10 nm) compared to those obtained without MCH (around 20 nm). These results clearly show that the reduction of Au(III) to Au(0) at room temperature using glycerol produces relatively small nanoparticles when they are exposed to an instant pH change compared to those formed directly in PBS solution (10 mM, pH 7.4) in the absence of a capping agent.

#### 2.4.2. Liposomal nanoreactor design

As an alternative to the well-established technique of the reverse micelle method for the preparation of nanoparticles, liposomes were exploited as a nanoreactor for nanoparticle synthesis. It was expected that in the presence of liposomes the nanoenvironment of the interior core would provide a semisolid reaction environment by keeping glycerol semimobile, thus facilitating the formation of nanoparticles in a more controlled manner than their synthesis in solution, and we thus incorporated glycerol into the nanoliposomes formulation. Glycerol is commonly used in liposomal formulations because it increases the solubility of lipids and encapsulated materials in water and enhances the stability of formed liposomes via interaction with the polar head groups of the phospholipids.<sup>29</sup> Furthermore, glycerol can be used to reduce chloroauric acid to form gold nanoparticles. There are many reports on the polyol-mediated synthesis of metal nanoparticles, but there is not extensive information available on the underlying mechanism. Leiva et al. postulated that although the exact mechanism is not fully understood the gold reduction reaction in the presence of alcohols most likely occurs because of the OH groups of the reducing agent.<sup>30</sup> Like all other redox reactions, the reduction of the metal is driven by the difference between the redox potentials ( $\Delta E$ ) of the oxidation capacity of the metal salt and the reductivity of the polyol.

The preparation of nanoliposomes encapsulating chloroauric acid, while also incorporating glycerol in the lipid bilayer as a reducing agent, to produce gold nanoparticles both in the lipid bilayer and in the liposome core was explored.

In the designed nanoreactor, hydrophilic Au(III) would be expected to be encapsulated in the aquatic core of the membrane and glycerol would be located on the internal and external surfaces of the liposomes as well as within the aquatic core, providing nucleation sites for gold nanoparticle formation (Figure 2.3).

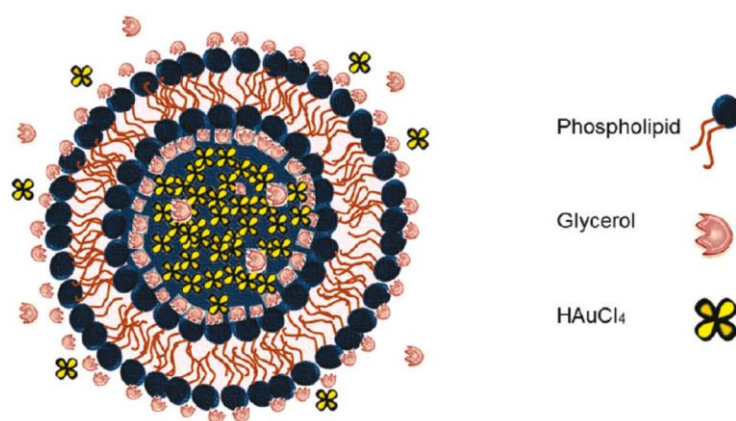


Figure 2.3. Schematic of the designed liposomal nanoreactor.

Liposomal nanoreactors of  $24 \pm 1$  nm radius, as measured by photon correlation spectroscopy (PCS), were prepared using a formulation of 1,2-dioleoyl-*sn*-glycero-3-phospho-(10-*rac*-glycerol) (DOPG) and 1-palmitoyl-2-hydroxy-*sn*-glycero-3-phosphocholine (lyso-PPC) in an 88:12 molar ratio using our previously reported CTP method<sup>18</sup> at 25 °C in the presence of a constant concentration of HAuCl<sub>4</sub> and at varying concentrations of glycerol (0-15 % (v/v)). Figure 3.4

depicts the TEM images showing the stages of the reduction reaction in the presence of glycerol-incorporated liposomal nanoreactors before reduction and during the reaction with a clear appearance of nanoparticles within the nanoreactor as well as the homogeneous nanoparticle population observed following the elimination of the lipidic membrane by centrifugation with a methanol:ethanol mixture.

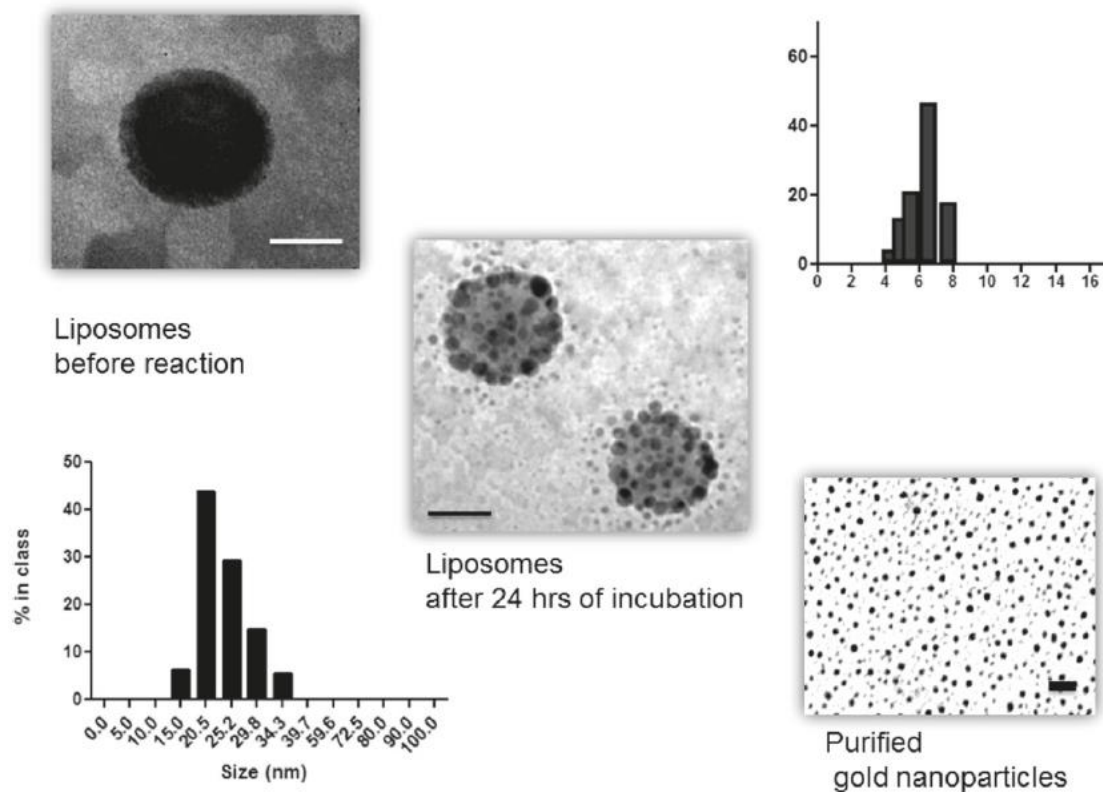


Figure 2.4. Formation stages of gold nanoparticles inside the glycerol-incorporated (15 % v/v) liposomes: liposomes before reaction (top left), liposomes during the reaction (middle) (scale bars = 10 nm), and purified gold nanoparticle synthesized in the nanoreactor (bottom right, scale bar 20 nm). Photon correlation spectroscopy graph of the liposome size distribution before the reaction,  $PI = 0.232$  (bottom left corner) and graph of the calculated nanoparticle size distribution using *iTEM* (top right corner).

Particle formation occurs mostly throughout the liposome membrane, where the glycerol molecules are less mobile, as well as inside the liposome core, as was expected. Although liposomes were purified using gel chromatography, because the system is dynamic trace amounts of gold and/or glycerol could diffuse into the bulk solution. As can be seen from the TEM image of liposomal nanoreactors after 24 h of incubation (Figure 2.4), some particles are located close to the liposomal membrane. Thus, it is likely that this small number of gold nanoparticles have grown from some free gold impurities remaining after the purification. Moreover, no particle formation was observed in control experiments carried out with  $H AuCl_4$  encapsulating liposomes in the absence of glycerol under the same conditions studied.

### 2.4.3. Evaluation of the effect of the reducing agent concentration and capping agent

In previous reports, 3 % v/v glycerol was found to be optimum for the long-term storage of liposomes.<sup>26,29</sup> However, because the reducing agent concentration is an important parameter for a well-defined method of metal nanoparticle synthesis, the effect of glycerol concentration in the range from 3 to 15 % v/v was studied. (Note that at higher concentrations of glycerol no liposomes were formed.) In addition to the glycerol concentration, the influence of the presence of a capping agent was also evaluated using a short-chain alkanethiol, 6-mercapto-1-hexanol (MCH), as a model; this was encapsulated in liposomes with HAuCl<sub>4</sub> in an excess of 1:50 HAuCl<sub>4</sub>:MCH (mol/mol). The formed liposomes were incubated in sealed glass bottles at room temperature under stirring. In the absence of MCH, the solution color changed from pale yellow to green-brown, with the color intensity proportional to the glycerol concentration, which over time deepened to a very dark brown, indicative of the oxidation by-product of glycerol formed from the reaction between Au(III) and glycerol. As can be seen in Table 2.1, no significant change in size was observed (from 7.7 ± 1.7 to 6.4 ± 1.3 nm) with increasing glycerol concentrations of 3 and 15 % v/v (Figure 2.5, first line). However, the presence of the MCH capping agent encapsulated in the liposomes together with the HAuCl<sub>4</sub> lead to a sharp decrease in the particle size, with particles of 2.9 to 4.9 nm obtained using MCH with glycerol concentrations of 15 and 3 % v/v, respectively (Figure 3.5, second line).

Table 2.1. Particle size after 24 h of incubation at different glycerol concentrations in the presence and absence of a capping agent at 25 °C<sup>a</sup>.

Glycerol concentration (v/v %)	Absence of capping agent (nm)	Presence of capping agent (nm)
15	6.4 ± 1.3	2.9 ± 0.2
10	7.3 ± 1.5	3.5 ± 0.3
3	7.7 ± 1.7	4.9 ± 1.4

<sup>a</sup> Standard deviations were calculated from the mean of the data of a series of experiments (n ≥ 3).

This decrease in particle size in the presence of MCH can also be attributed to the fact that MCH can, to a minor extent, act as a reducing agent because of the presence of the alcohol group. Similar correlations between the particle size and the stabilizer and/or the reducing agent have been reported elsewhere.<sup>33</sup> In a recent study on the use of poly(ε-caprolactone)/poly(N-vinyl-2-pyrrolidone) triblock copolymer as a stabilizer and reducing agent for the Au NPs, a decrease in the particle size with an increased ratio of copolymer to gold salt was reported.<sup>31</sup> In another study on the effect of the Au/thiol ratio by Frenkel et al. where they used X-ray absorption fine-structure EXAFS spectroscopy, they concluded that the mean cluster size strongly depends on the Au/thiol ratio, with the lower the Au/thiol ratio, the smaller the nanoparticles formed.<sup>32</sup>



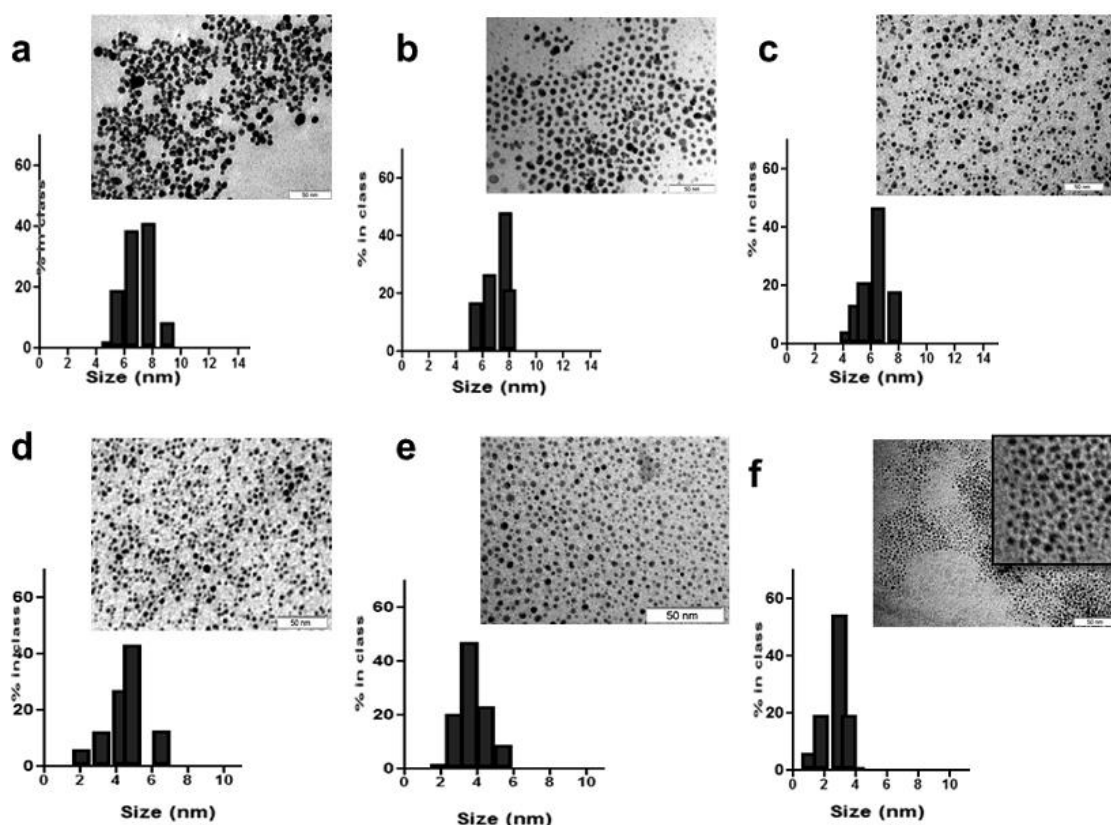


Figure 2.5. Effect of capping agent and glycerol concentration. Calculated particle size distribution and corresponding TEM images of particles prepared (a-c) in liposomes in the absence of a capping agent (MCH) and (d-f) in the presence of MCH using changing concentrations of glycerol: (a, d) 3 %, (b, e) 10 %, and (c, f) 15 % after 24 h of incubation at 25 °C. Scale bars are 50 nm.

#### 2.4.4. Influence of temperature

In addition to the reactant concentration, the reaction kinetics are also governed by temperature and pH.<sup>30</sup> Thus, polyol-driven synthesis reactions are more efficient at high temperatures, although at optimized concentrations of metal salt slow reduction might occur at low temperatures.<sup>33</sup> Therefore, it is crucial to study the effect of temperature on the particle properties because the parameters influencing the reaction will control the shape and size of the particles formed. Here, we investigated the effect of temperature (in the range of 4-50 °C) on the particles formed. MCH/HAuCl<sub>4</sub>-encapsulating liposome solutions (15 % v/v glycerol) were incubated for 24 h under constant stirring conditions at a defined constant temperature. As shown in Figure 2.6, decreasing particle sizes were obtained with increasing temperature over the range of 4-50 °C, with a significantly larger nanoparticle size observed at 4 °C compared to the particles obtained at 50 °C (6.3 and 1.9 nm, respectively). As the temperature increases, the reaction rate increases as a result of rapid nucleation, and thus the amount of metal consumed in the nucleation increases, resulting in a decrease in the number of molecules available for the further growth of nanoparticles, thus producing smaller nanoparticles (Figure 2.6e).<sup>32,33</sup>

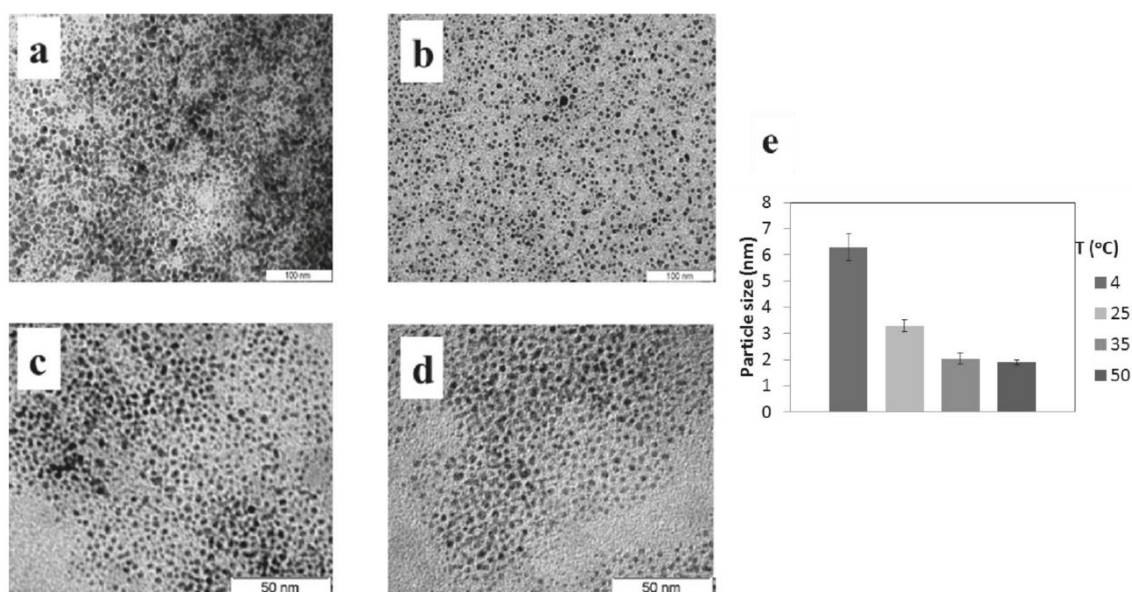


Figure 2.6. Effect of temperature on the particle size and shape synthesized in glycerol (15% v/v)-incorporated liposomes in the presence of capping agent MCH at changing temperatures: (a) 4, (b) 25, (c) 35, and (d) 50 C after 24 h of incubation and (e) a graph presenting the calculated mean diameter of the particles ( $n = 3$ , scale bars = 20 nm).

## 2.5. Conclusions

The synthesis of metal nanoparticles using polyols is an environmentally friendly method that often proceeds both under reflux and microwave conditions, where the undiluted polyol-metal mixture is heated to temperatures higher than the boiling point of the polyol used, achieving nanoparticles of 10-100 nm depending on the operational conditions. In this report, glycerol, a renewable and natural polyol, was studied as a green catalyst for the reduction of gold to assemble in nanoparticles without the use of any harsh chemicals. Moreover, by exploiting the ability of glycerol to be incorporated within a liposomal membrane, here we report a functional, nanosized liposomal nanoreactor exploiting glycerol incorporated in both the external and internal surfaces of the lipid bilayer. The liposomal membrane keeps the reducing agent semimobile in its nanoenvironment, exposing nucleation sites for subsequent particle growth in a controlled manner. Reaction parameters such as the temperature, the glycerol concentration, and the effect of the capping agent were studied in terms of their effect on the size and the homogeneity of nanoparticles formed and were compared to solution-based synthesis under the same conditions studied. Increased concentrations of glycerol resulted in a slightly decreased size of the nanoparticles; furthermore, nanoparticles synthesized in the presence of a capping agent showed an almost 2-fold decrease in the particle size leading to ultrasmall gold nanoparticles of around 2 nm. Moreover, a decrease in the nanoparticle size at constant concentrations of capping agent and glycerol was observed when the temperature was increased in the range of 4 to 50 °C. Comparison studies of gold nanoparticle synthesis in solution under the same conditions without the use of nanoliposome reactors resulted in highly heterogeneous nanoparticles with an amorphous shape, where in the presence of a capping agent and a pH jump step relatively finer results were obtained. These results indicate that with the designed liposomal nanoreactors, with glycerol integrated into the membrane as a reducing

agent, a one-pot synthesis of highly homogeneous nanoparticles was successfully achieved as a result of the semisolid reaction environment provided by the liposome. The functional nanoreactors presented here could provide inspiration for the development of new and greener synthesis methodologies in order to produce metallic nanoparticles in a safer and more efficient way.

## 2.6. Associated content

Supporting Information. Size distribution of the particles synthesized using a liposome-free solution-based method and a TEM image representing gold aggregates obtained in the presence of MCH alone. This material is available free of charge via the Internet at <http://pubs.acs.org>.

## 2.7. Acknowledgements

R.G. acknowledges the support from a FI predoctoral scholarship of the Generalitat de Catalunya. M.O. thanks the Marie Curie Program (grant PIIF-GA 2009-237011 ECLOBIOSENS).

## 2.8. References

1. Daniel, M. C.; Astruc D.; Gold nanoparticles: assembly, supramolecular chemistry, quantum-size-related properties, and applications toward biology, catalysis, and nanotechnology. *Chem. Rev.* **2004**, *104*, 293–346.
2. Grzelczak, M.; Perez-Juste, J.; Mulvaney, P.; Liz-Marzan, L. M.; Shape control in gold nanoparticle synthesis. *Chem. Soc. Rev.* **2008**, *37*, 1783–1791.
3. Eustis, S.; El-Sayed, M. A. Why gold nanoparticles are more precious than pretty gold: noble metal surface plasmon resonance and its enhancement of the radiative and nonradiative properties of nanocrystals of different shapes. *Chem. Soc. Rev.* **2006**, *35*, 209–217.
4. Shipway, A. N.; Katz, E.; Willner, I. Nanoparticle arrays on surfaces for electronic, optical, and sensor applications. *ChemPhysChem* **2000**, *1*, 18–52.
5. Nadagouda, M. N.; Hoag, G.; Collins, J.; Varma, R. S. Green Synthesis of Au Nanostructures at Room Temperature Using Biodegradable Plant Surfactants *Cryst. Growth Des.* **2009**, *9*, 4979–4983.
6. Bilecka, I.; Elser, P.; Niederberger, M. Kinetic and thermodynamic aspects in the microwave-assisted synthesis of ZnO nanoparticles in benzyl alcohol. *ACS Nano* **2009**, *3*, 467–477.
7. He, S.; Guo, Z.; Zhang, Y.; Zhang, S.; Wang, J.; Gu, N. Biosynthesis of gold nanoparticles using the bacteria *Rhodospseudomonas*. *Mater. Lett.* **2007**, *61*, 3984–3987.
8. Herricks, T.; Chen, J.; Xia, Y. Polyol Synthesis of Platinum Nanoparticles: Control of Morphology with Sodium Nitrate. *Nano Lett.* **2004**, *4*, 2367–2371.
9. Adhikari, S.; Fernando, S. D.; Haryanto, A. Hydrogen production from glycerol: An update. *Energy Convers. Manage.* **2009**, *50*, 2600–2604.



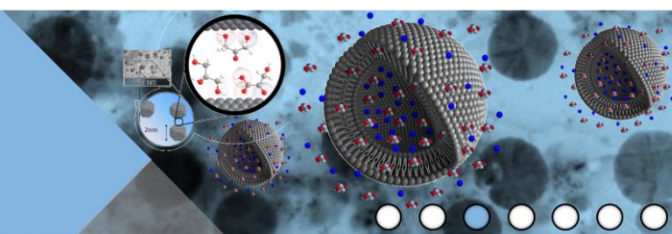
10. Porta, F.; Prati, L. Selective oxidation of glycerol to sodium glycerate with gold-on-carbon catalyst: an insight into reaction selectivity. *J. Catal.* **2004**, *224*, 397–403.
11. Demirel, S.; Lucas, M.; W€arna, J.; Salmi, T.; Murzin, D.; Claus, P. Reaction kinetics and modelling of the gold catalysed glycerol oxidation. *Top. Catal.* **2007**, *44*(1-2), 299-305.
12. Villa, A.; Wang, D.; Su, D. S.; Prati, L. Gold Sols as Catalysts for Glycerol Oxidation: The Role of Stabilizer. *ChemCatChem* **2009**, *1*, 510–514.
13. Kamarudin, K. S. N.; Mohamad, M. F. Synthesis of Gold (Au) Nanoparticles for Mercury Adsorption. *Am. J. Appl. Sci.* **2010**, *7*, 835–839.
14. Grace, N.; Pandian, K. One pot synthesis of polymer protected gold nanoparticles and nanoprisms in glycerol. *Colloids Surf. A* **2006**, *290*, 138–142.
15. Nisaratanaporn, E.; Wongsuwan, K. Preparation of ultrafine silver powder using glycerol as reducing agent. *J. Miner. Met. Mater. Soc.* **2008**, *18*, 1–5.
16. Sarkar, A.; Kapoor, S.; Mukherjee, T. Synthesis and characterisation of silver nanoparticles in viscous solvents and its transfer into non-polar solvents. *Res. Chem. Intermed.* **2010**, *36*, 411–421.
17. Meyre, M. E.; Lambert, O.; Desbat, B.; Faure, C. Synthesis of stable, gold-particle-containing onion-type multilamellar vesicles. Influence of particle size on the onions' internal structure. *Nanotechnology* **2006**, *17*, 1193–1201.
18. D€oker, O.; Bayraktar, E.; Mehmetoglu, ˘.; ˘alimli, A. Production of Iron-Cobalt Compound Nanoparticles Using Reverse Micellar System. *Rev. Adv. Mater. Sci* **2003**, *5*, 498–500.
19. Chen, M.; Feng, Y.-G.; Wang, L.-Y.; Zhang, L.; Zhang, J.-Y. Study of palladium nanoparticles prepared from water-in-oil microemulsion. *Colloids Surf. A* **2006**, *281*, 119–124.
20. Naoe, K.; Kataoka, M.; Kawagoe, M. Preparation of water-soluble palladium nanocrystals by reverse micelle method: Digestive ripening behavior of mercaptocarboxylic acids as stabilizing agent. *Colloids Surf. A* **2010**, *364*, 116–122.
21. Lin, W.-C.; Chen, C.-N.; Tseng, T.-T.; Wei, M.-H.; Hsieh, J. H.; Tseng, W. J. Micellar layer-by-layer synthesis of TiO<sub>2</sub>/Ag hybrid particles for bactericidal and photocatalytic activities. *J. Eur. Ceram. Soc.* **2010**, *30*, 2849–2857.
22. Bae, D. S.; Han, K. S.; Adair, J. H. Synthesis of Platinum/Silica Nanocomposite Particles by Reverse Micelle and Sol–Gel Processing. *J. Am. Ceram. Soc.* **2002**, *85*, 1321–1223.
23. Ward, A. J. I.; O'Sullivan, E. C.; Rang, J. C.; Nedeljkovic, J.; Patel, R.C. The Synthesis of Quantum Size Lead Sulfide Particles in Surfactant-Based Complex Fluid Media. *J. Colloid Interface Sci.* **1993**, *161*, 316–320.
24. Uskokovic, V.; Drogenik, M. Synthesis of Materials within Reverse Micelles. *Surf. Rev. Lett.* **2005**, *12*, 239–277.
25. Eastoe, J.; Hollamby, M. J.; Hudson, L. Recent advances in nanoparticle synthesis with reversed micelles. *Adv. Colloid Interface Sci.* **2006**, *128-130*, 5–15.
26. Genç, R.; Ortiz, M.; O'Sullivan, C. K. Curvature-tuned preparation of nanoliposomes. *Langmuir* **2009**, *25*, 12604–12613.
27. Yong, S.-J.; Hyeon-Kyeong, J.; Soo, K. B. Biological synthesis of gold nanoparticles using *Magnolia kobus* and *Diopyros kaki* leaf extracts. *Process Biochem.* **2009**, *44*, 1133–1138.

28. Bock, C.; Paquet, C.; Couillard, M.; Botton, G. A.; MacDougall, B. R. Size-Selected Synthesis of PtRu Nano-Catalysts: Reaction and Size Control Mechanism. *J. Am. Chem. Soc.* **2004**, *126*, 8028–8037.
29. Mozafari, M. R.; Reed, C. J.; Rostron, C. Development of non-toxic liposomal formulations for gene and drug delivery to the lung. *Tech. Health Care* **2002**, *10*, 342-344.
30. Leiva, A.; Saldías, C.; Quezada, C.; Toro-Labbe, A.; Espinoza-Beltran, F. J.; Urzua, M.; Gargallo, L.; Radic, D. Gold-copolymer nanoparticles: Poly( $\epsilon$ -caprolactone)/poly(N-vinyl-2-pyrrolidone) Biodegradable triblock copolymer as stabilizer and reductant. *Eur. Polym. J.* **2009**, *45*, 3035–3042.
31. Young-ho, L.; Dae-wook, K.; Seung-il, S.; Seong-geun, O. Preparation of Au colloids by polyol process using NaHCO<sub>3</sub> as a buffering agent. *Mater. Chem. Phys.* **2006**, *100*, 85–91.
32. Frenkel, A. I.; Nemzer, S.; Pister, I.; Soussan, L.; Harris, T. Size-controlled synthesis and characterization of thiol-stabilized gold nanoparticles. *J. Chem. Phys.* **2005**, *123*, 184701–184707.
33. Goia, D. V.; Matijevic, E. Preparation of monodispersed metal particles. *New J. Chem.* **1998**, *22*, 1203–1215.



---

## CHAPTER III



# Liposomal Nanoreactors for the Synthesis of Monodisperse Palladium Nanoparticles Using Glycerol

---



## Liposomal Nanoreactors for the Synthesis of Monodisperse Palladium Nanoparticles Using Glycerol

*Langmuir* **2013**, *29*, 15405–15413

Gael Clergeaud,<sup>†</sup> Rükân Genç,<sup>‡</sup> Mayreli Ortiz,<sup>\*,†</sup> and Ciara K. O'Sullivan<sup>\*,†,§</sup>

<sup>†</sup> Nanobiotechnology & Bioanalysis Group, Department d'Enginyeria Química, Universitat Rovira i Virgili, Tarragona 43007, Spain

<sup>‡</sup> Department of Chemistry, Middle East Technical University, 06800 Cankaya, Ankara, Turkey

<sup>§</sup> Institució Catalana de Recerca i Estudis Avancats, Barcelona 08010, Spain



### 3.1. Abstract

The synthesis of highly stable ultrasmall monodisperse populations of palladium nanoparticles in the range of 1–3 nm in size was achieved via polyol reduction within 1,2-dioleoyl-*sn*-glycero-3-phosphor-*rac*-(1-glycerol) liposomal nanoreactors exploiting glycerol as both reducing and stabilizing agent. The liposome-based green method was compared with synthesis in solution, and the reducing agent concentration and the lipidic composition of the liposomal nanoreactors were demonstrated to have a strong effect on the final size and homogeneity of the palladium nanoparticles. Glycerol molecules acting as capping agent demonstrated the ability to stabilize the palladium nanoparticles over a long period of time, maintaining their homogeneity in size and shape. The obtained palladium nanoparticles were characterized using transmission electron microscopy, selected area electron diffraction, Fourier transform infrared and Raman spectroscopies, X-ray diffraction, and dynamic light scattering to determine their morphology, size, charge, surface chemistry, and crystal structure. The catalytic activity of the palladium nanoparticles was also tested for a reduction reaction.

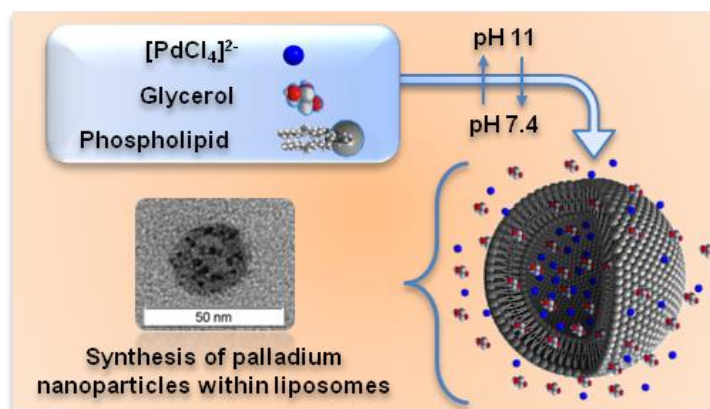


Figure 3.13. Table of contents figure

### 3.2. Introduction

The past decade has witnessed an increased interest in the development of uniform metallic nanosized particles due to their unusual size dependent chemical, electronic, magnetic, and optical properties, which are not achievable in their bulk state.<sup>1–3</sup> Among other noble metals, palladium (Pd) nanoparticles (NPs) have been exploited in an extensive number of applications including catalysis, electronics, plasmonics, and sensors.<sup>4–6</sup>

The development of synthesis methods to obtain homogeneous size- and shape-tunable Pd nanoparticles is a grand challenge, and different techniques, including photolytic<sup>6</sup> and thermal decomposition,<sup>7</sup> sonochemical<sup>8</sup> and hydrogen reduction,<sup>9</sup> electrochemical deposition,<sup>10</sup> one-phase<sup>11</sup> and twophase<sup>12</sup> reduction methods, and biogenic methods<sup>13,14</sup> have been reported. The most common methods utilize reducing agents such as citrates, ascorbic acid, or borohydrides, often in combination with capping agents such as surfactants, polymers, or organic ligands to mediate the reduction reaction and avoid aggregation.<sup>15</sup>

The synthesis of nanoparticles using the so-called polyol process is one of the most widely used methods to produce colloidal nanoparticles, in which a boiling polyalcohol acts as both solvent



and mild reducing agent as well as a stabilizer, for the reduction of a suitable metal salt precursor.<sup>16-20</sup> The most commonly used polyols for nanoparticles preparation are ethylene glycol,<sup>21</sup> diethylene glycol,<sup>22</sup> ethanol,<sup>23</sup> and glycerol,<sup>24</sup> with glycerol being particularly attractive. Glycerol, a nontoxic, nonhazardous, nonvolatile, biodegradable, recyclable, and cheap liquid, has been reported as a solvent and reducing agent for the synthesis of many different nanoparticles including Au,<sup>24,25</sup> Ru,<sup>26</sup> Ag,<sup>25-28</sup> Pd,<sup>26,29,30</sup> Pt,<sup>26,31</sup> Pt-Ru,<sup>31</sup> Pt-Pd,<sup>32</sup> TiO<sub>2</sub>,<sup>33</sup> Mn(OH)<sub>2</sub>, and MnCO<sub>3</sub>.<sup>34</sup>

Regarding the production of Pd nanoparticles, Lee et al. have demonstrated the ability of glycerol, together with PVP as a capping agent, to form Pd NPs at 100 °C with an average size of ~60 nm.<sup>29</sup> Grace et al. reported the synthesis of 7 nm Pd nanoparticles employing glycerol at its boiling point (290 °C) as a solvent and reducing agent also combined with PVP to stabilize and avoid particle aggregation.<sup>26</sup> In addition, Marquardt et al. achieved the synthesis of 1.5 nm sized Pt nanocrystals in glycerol without any additional stabilizer.<sup>35</sup>

There are several reports detailing the utilization of nanoreactors to control the reduction reaction and synthesize small homogeneous nanoparticles. An environmentally friendly report presented by Puvvada et al. uses mild experimental conditions to produce Pd nanoparticles of 3.3 nm in size at room temperature using a controlled sponge like structure of bicontinuous cubic phase of glycerol monooleate.<sup>30</sup> It has been reported that glycerol can act as a soft capping agent, and Bakshi et al. have demonstrated that phosphoglycerol lipids act as stabilizers for Au and Cu nanoparticles<sup>36</sup> and Au-Cu bimetallic nanoparticles.<sup>37</sup> In another example, dendrimer mediated synthesis of nanoparticles has been reported for monometallic<sup>38</sup> and bimetallic<sup>39,40</sup> Pd nanostructures. In addition, Coulter et al. reported the use of functional polyelectrolytes as nanoreactors to produce Pd nanoparticles using NaBH<sub>4</sub> with an average size of 5 ± 1.5 nm.<sup>41</sup>

A wide number of reports using reverse micelles for the synthesis of palladium nanoparticles inside the reverse micelle cores, exploiting the water-in-oil microemulsions stabilized by surfactant molecules, most frequently cetyltrimethylammonium bromide (CTAB)<sup>42-44</sup> or dioctylsulfosuccinate sodium salt (AOT),<sup>45-47</sup> have been reported. In a novel approach, Sanchez-Dominguez described the synthesis of Pd nanoparticles of 6 nm using NaBH<sub>4</sub> within oil-in-water microemulsions.<sup>48</sup>

As detailed in Table 3.1, most of the previously reported methodologies to produce Pd nanoparticles require the use of harsh reducing agents, lengthy preparation time, or high reaction temperatures under stringent process control. There is thus a need for a straightforward method for the synthesis of highly homogeneous small Pd nanoparticles using a simple green system obviating the need for additional reactants and omitting harsh procedures with extreme temperatures or utilizing no environmentally friendly chemicals.

In our recently reported work, liposomes were used as nanoreactors for the preparation of homogeneous small gold nanoparticles<sup>49</sup> and were demonstrated to provide an excellent control over the nanoparticle synthesis process within their internal core. Moreover, the lipidic membrane of the liposomes can act as permeable nanoreactor walls offering both an enhanced and restricted mobility for different reactants of the synthesis reaction. Glycerol-incorporating liposomes are promising candidates for the synthesis of nanoparticles via glycerol reduction, as they provide a specific space inside their internal hydrophilic cavity, as well as a hydrophobic environment within the lipid bilayer, where the polyol reduction reaction can occur in a more controlled manner.

Table 3.1. Methodologies to produce palladium nanoparticles.

Reducing agent (reaction conditions)	Stabilizing/capping agent	Pd NPs diameter (nm)	References
NaBH <sub>4</sub> (RT)	TOAB	~1-4	3
Glycerol (290°C)	PVP	7	26
Glycerol (100°C)	PVP	~60	29
Glycerol monooleate (RT)	-	~3	30
Dendrimer amino groups (50°C)	Dendrimer	~6	38
NaBH <sub>4</sub> (RT)	Dendrimer	~2	40
NaBH <sub>4</sub> (RT, UV-light)	Poly (acrylic acid)	~5	41
Hydrazine (RT)	CTAB	~4	42
Ascorbic acid (UV-light)	CTAB	~7-50	43
Hydrazine (RT)	AOT	~10	45
Hydrazine (RT)	AOT	~6-13	47
NaBH <sub>4</sub> (RT)	Oil-in-water	~6	48

Herein, we exploit our previously reported method for the rapid preparation of highly homogeneous nanosized liposomes<sup>50</sup> to introduce an environmentally friendly, solvent free, one-pot method for the synthesis of Pd nanoparticles using glycerol as both reducing and capping agent under mild experimental conditions. The method involves the encapsulation of [PdCl<sub>4</sub>]<sup>2-</sup> with glycerol molecules within nanosized liposomes for the controlled production of highly homogeneous populations of ultrasmall glycerol-stabilized Pd nanoparticles. Furthermore, we have systematically investigated the effect of the experimental conditions, including the type and concentration of reducing agent, the membrane lipid composition, and the effect of the addition of a capping agent on the homogeneity and size evolution of the Pd nanoparticles.

### 3.3. Experimental section

#### 3.3.1. Materials

All the chemicals were used without further purification. The phospholipids 1,2-dipalmitoyl-sn-glycero-3-phosphorac-(1-glycerol) (DPPG), 1,2-dioleoyl-sn-glycero-3-phosphoethanolamine (DOPE), and 1,2-dioleoyl-sn-glycero-3-phosphor-rac-(1-glycerol) (DOPG) were purchased as powders (Figure 3.2) from Avanti Polar Lipids. The phospholipid 1,2-dipalmitoyl-sn-glycero-3-phosphocholine (DPPC) as well as the palladium(II) chloride (PdCl<sub>2</sub>), sodium borohydride (NaBH<sub>4</sub>), p-nitrophenol, sodium citrate, and phosphate buffer saline (PBS: 10 mM prepared lyophilized buffer with NaCl 0.138 M, KCl 0.0027 M, pH 7.4) were purchased from Sigma-Aldrich. Glycerol, toluene, ethanol, and methanol were supplied by Scharlau. A Simplicity 185 Millipore-Water System was used to obtain Milli-Q water (1.82 MΩ cm<sup>-1</sup>) for the preparation of buffers and liposomes.

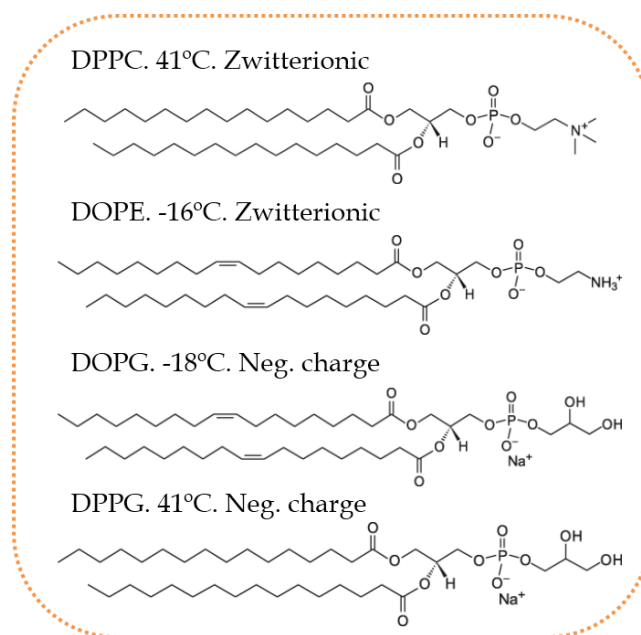


Figure 3.2. Structure of the lipid molecules used for the liposomal nanoreactor study.

### 3.3.2. Synthesis of Pd NPs

#### 3.3.2.1 Synthesis within liposomal nanoreactors

The liposomal nanoreactors were prepared employing the method previously reported by our group to produce homogeneous populations of liposomes.<sup>50</sup> Briefly, 20 mg of PdCl<sub>2</sub> was dissolved in 10 mL of PBS with 10 % (v/v) glycerol under continuous stirring conditions and in the presence of bubbling argon gas. Because of the presence of NaCl, the suspension of non-water soluble PdCl<sub>2</sub> changed to a reddish-brown solution of [PdCl<sub>4</sub>]<sup>2-</sup> after 15 min. Then 50 mg of different lipid formulations (DPPC, DPPG, DOPE or DOPG) was added and maintained under stirring conditions and argon at 25 °C for another 15 min. The well homogenized mixture was then subjected to a rapid pH jump from pH 7.4 to pH 11 and then back to pH 7.4 within a 3 s time frame, followed by an equilibration step of 25 min where lipids curl into [PdCl<sub>4</sub>]<sup>2-</sup> encapsulating liposomes. Large lipid aggregates that do not assemble into liposomes were discarded by centrifuging at 2000 rpm for 5 min, and the nanoliposomes present in the supernatant were then incubated for 24 h in a temperature-controlled shaker (25 °C, 400 rpm). Following incubation, the nanoparticles formed inside the liposomal nanoreactors were purified by centrifuging 3 times at 5000 rpm for 5 min with a methanol/ethanol solution (1:4 v/v) to break up the liposomes and recover the pellet that contains the Pd NPs. The pellet was resuspended in toluene and stored at 4 °C for further characterization studies.

#### 3.3.2.2. Solution-Based Synthesis.

Pd NPs were synthesized via reduction, in the absence of liposomal nanoreactors, in the presence of three different reducing agents, sodium citrate (1.4 M), NaBH<sub>4</sub> (0.1 M), and glycerol, which was used at different concentrations (5%, 10%, and 20% v/v). In all cases, 20 mg of PdCl<sub>2</sub> was mixed with each of the reducing agents in 10 mL of 10 mM PBS (pH 7.4) and then incubated for 24 h in a temperature-controlled shaker (25 °C, 400 rpm). The nanoparticles formed were purified by centrifuging first at 2000 rpm for 5 min, and the collected supernatant was then centrifuged three times at 5000 rpm for 5 min, as described in the previous section. Following

the first centrifugation, the pellet formed was resuspended in a methanol:ethanol solution (1:4 v/v), and after the final centrifugation, the pellet was resuspended in toluene and stored at 4 °C.

### 3.3.3. Characterization studies

#### 3.3.3.1. Dynamic light scattering and Zeta potential analysis

The Zeta Sizer 3000H (Malvern Instruments Inc. He-Ne laser of 635 nm, detector angle of 90°) was used to measure the mean diameter of the liposome nanoreactors via dynamic light scattering (DLS). The zeta potential was used to determine the surface charge of the liposomes and the Pd NPs. The standards deviations were calculated from the mean data of experiments ( $n \geq 3$ ).

#### 3.3.3.2. Transmission electron microscopy studies

The morphology characterization and measurement of the mean diameter of the Pd NPs and liposome nanoreactors were performed using a transmission electron microscope (TEM) JEOL 1011 operated at 100 keV with an ultrahigh-resolution pole piece providing 2 Å of point resolution. A drop of each sample was placed using a glass pipet onto a 200 mesh copper grid with a Formvar polymer thin film and left at room temperature to dry. The TEM images or micrographs (1024 pixels × 1024 pixels) were acquired using a CCD camera (Megaview III multiscan) and analysed with the iTEM image analysis software. The mean diameter of the nanoparticles was calculated measuring at least 100 particles from multiple experiments ( $n \pm 3$ ).

In addition, the crystal structure of the Pd NPs was elucidated using the selected area electron diffraction technique (SAED) by observing the diffracted patterns of the electrons scattered from the Pd NPs.

#### 3.3.3.3. X-ray diffraction investigation

X-ray diffraction (XRD) was used to reveal the crystal structure of the Pd NPs. The XRD measurements were made using a Siemens D5000 diffractometer (Bragg-Brentano parafocusing geometry and vertical goniometer) fitted with a curved graphite diffracted-beam monochromator and diffracted-beam Soller slits, a 0.06° receiving slit, and scintillation counter as a detector. The angular  $2\theta$  diffraction range was between 35° and 90°. The sample was dusted on to a low background Si(510) sample holder. The data were collected with an angular step of 0.05° at 20 s per step and sample rotation. Cu K radiation was obtained from a copper X-ray tube operated at 40 kV and 30 mA.

#### 3.3.3.4. Ultraviolet-Visible spectroscopy

The formation of the Pd NPs was monitored measuring the ultraviolet-visible (UV-vis) absorbance at 450 nm recorded in a Cary 100 Bio spectrophotometer (Varian) in 1 cm quartz cells.

#### 3.3.3.5. Study of the catalytic properties

The UV-vis spectrum of a  $6 \times 10^{-5}$  M p-nitrophenolate solution in 0.1 M NaOH was recorded in 1 cm quartz cell. An aliquot of a concentrated solution of  $\text{NaBH}_4$  (prepared immediately before use) was added to a final concentration of 0.2 M, and the spectrum was recorded again. Finally, 10 µL of Pd NPs suspension was added, and the spectra were recorded until the band at 400 nm disappeared. A similar experiment in the absence of Pd NPs was used as a control.

### 3.3.3.6. Fourier transform infrared spectroscopy

Fourier transform infrared (FTIR) spectra was recorded on a Jasco FT/IR- 600 PlusATR Specac Golden Gate spectrometer. 128 scans at  $2\text{ cm}^{-1}$  resolution were recorded.

### 3.3.3.7. Raman spectroscopy

Raman spectra were recorded using a Renishaw 2003 spectrometer operating at wavelength of 633 nm of HeNe laser and using CCD camera as detector. The spectra were analysed using Wire 3.2 version software (Renishawplc, New Mills, Wotton-underEdge, and Gloucestershire, GL12 8JR, United Kingdom).

## 3.4. Results and discussion

### 3.4.1. Synthesis of Pd NPs in solution

As mentioned previously, glycerol was used as a component in the liposomal nanoreactor formulation as well as for the synthesis of Pd NPs. To date, the reported methods that employ glycerol to reduce Pd(II) to form Pd nanoparticles are usually based on the use of elevated working temperatures and additional capping agent molecules.<sup>26,29</sup> We have previously reported that glycerol can act as a reducing agent to produce extremely small Au NPs at low temperatures without requiring additional reagents.<sup>49</sup> In order to demonstrate that glycerol can reduce Pd(II) to Pd(0), palladium chloride ( $\text{PdCl}_2$ ) was mixed with 10 % (v/v) glycerol at  $25\text{ }^\circ\text{C}$  in 10 mL of PBS (10 mM + 0.138 M NaCl, pH 7.4) and left for 24 h. The presence of NaCl in the buffer solution facilitates the solubilization of Pd(II) salt by forming the complex anion  $[\text{PdCl}_4]^{2-}$ . The formation of Pd NPs was monitored using UV-vis (Figure 3.3). The spectrum of  $[\text{PdCl}_4]^{2-}$  in solution exhibited an absorption band at 425 nm, and when the Pd(II) was reduced to Pd(0), the absorption band disappeared and a broad spectrum was observed, in agreement with that reported in the literature indicating the formation of nanoparticles.<sup>26</sup>

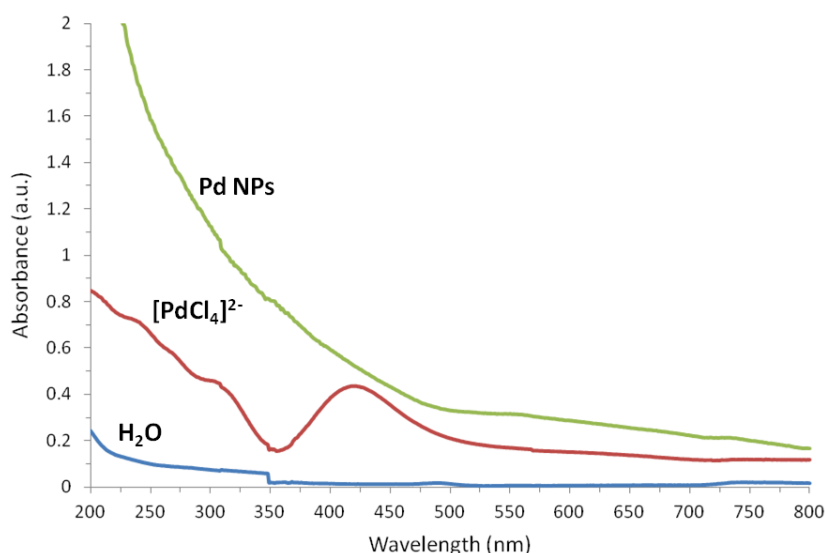


Figure 3.3. UV-vis spectra of  $[\text{PdCl}_4]^{2-}$  and Pd NPs produced by glycerol in solution.

The TEM characterization studies (Figure 3.4) clearly confirm that glycerol is able to reduce Pd(II) to Pd(0), producing small Pd NPs under mild conditions.

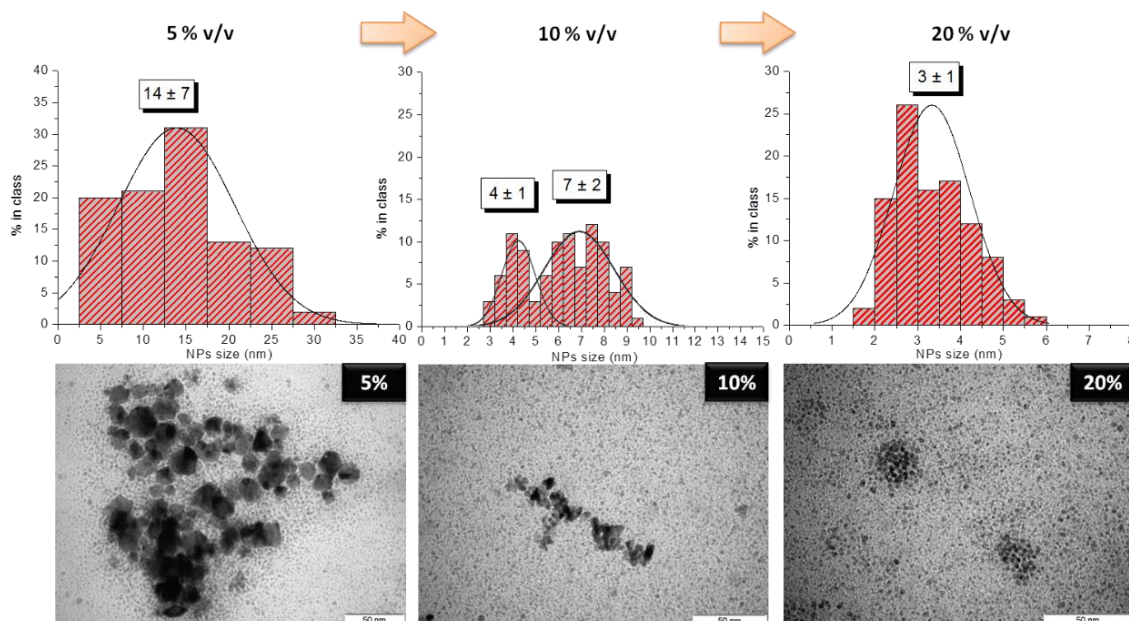


Figure 3.4. Effect of the concentration of glycerol on the solution-based synthesis of Pd nanoparticles. Effect of the concentration of glycerol on the solution-based synthesis of Pd nanoparticles. TEM images show the Pd nanoparticles produced in PBS solution containing 5 %, 10 %, and 20 % (v/v) glycerol at 25 °C and their correspondent size distribution graphs calculated using iTEM ( $n = 100$ ). Scale bars are 50 nm

Once it had been demonstrated that Pd NPs can be produced using glycerol as a reducing agent, the effect of using a lower and higher concentration of glycerol (5 % and 20 % v/v) was investigated to observe how the ratio between glycerol/Pd(II) affects the formation of the Pd NPs. At higher glycerol/Pd(II) ratios the number of particles obtained increased, and their mean size was smaller and more homogeneous (5 % =  $14 \pm 7$ ; 10 % =  $4 \pm 1$ ,  $7 \pm 2$  and 20 % =  $3 \pm 1$ ). However, the particles were amorphous without a well-defined shape. A 10 % (v/v) concentration was selected as optimal as while a marked effect on the size was observed changing the glycerol concentration from 5 % to 10 %, no considerable change was seen at higher concentrations, and above 15 % (v/v), the liposomes were not formed properly.

### 3.4.2. Synthesis of Pd NPs inside liposomes

The described method for the preparation of homogeneous liposomal nanoreactors was used to provide nanoenvironments in the internal core where glycerol molecules are maintained semimobile and the reduction kinetics are less governed by random processes, thus facilitating the formation of Pd nanoparticles in a more controlled manner than their synthesis in solution.

The formation of nanoparticles in solution is often irreproducible as well as difficulties in restricting the freedom of components that can interact and govern the reduction kinetics in a bulky state reaction. As described in the Introduction, reduction kinetics plays a key role in controlling the nucleation and growth of nanocrystals, and in the work reported here, we addressed this by providing a confined nanoenvironment in the liposomal internal core where the formation of nanoparticles can take place in a more controlled manner than in solution.

Taking advantage of the use of glycerol in liposomal formulations as a stabilizer, it was also exploited for the polyol mediated reduction of Pd(II) to Pd(0) within the liposomal nanoreactors. The small glycerol molecule adsorbed on the surface of the liposome could assist in increasing



the solubility of the vesicle. Typically, the  $[\text{PdCl}_4]^{2-}$  ions are encapsulated inside the hydrophilic core while glycerol molecules are distributed, in the external and internal part of the lipid membrane, as well as in the aqueous core forming small clusters from Pd atoms in the encapsulated solution (Figure 3.5).

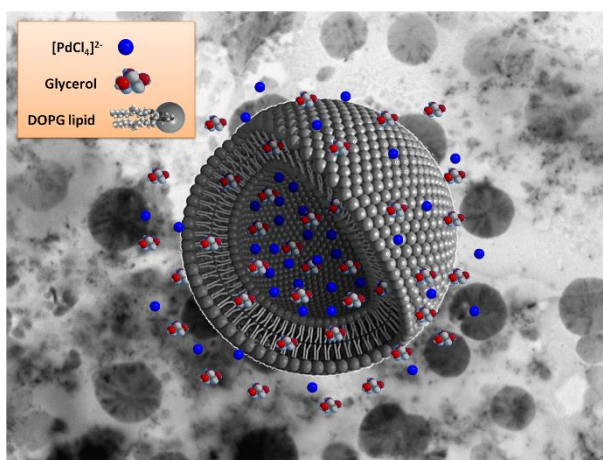


Figure 3.5. Schematic design of the glycerol-incorporated DOPG liposomal nanoreactor for the synthesis of Pd NPs.

As a proof of concept, the Pd NPs produced via glycerol reduction inside DOPG liposomes were compared in terms of size, shape, and homogeneity with those prepared in solution (i.e., in the absence of the liposome nanoreactors) using the same concentration of glycerol.

As can be seen in Figure 3.6, the Pd NPs obtained in solution were bigger in size compared with those obtained within the liposomes. Both systems were able to produce Pd NPs. But in the case of those prepared within the liposomes, the Pd NPs were highly homogeneous, while in the solution-based reaction the NPs appear to have a tendency to aggregate, resulting in more dispersive populations of NPs with amorphous shapeless structures.

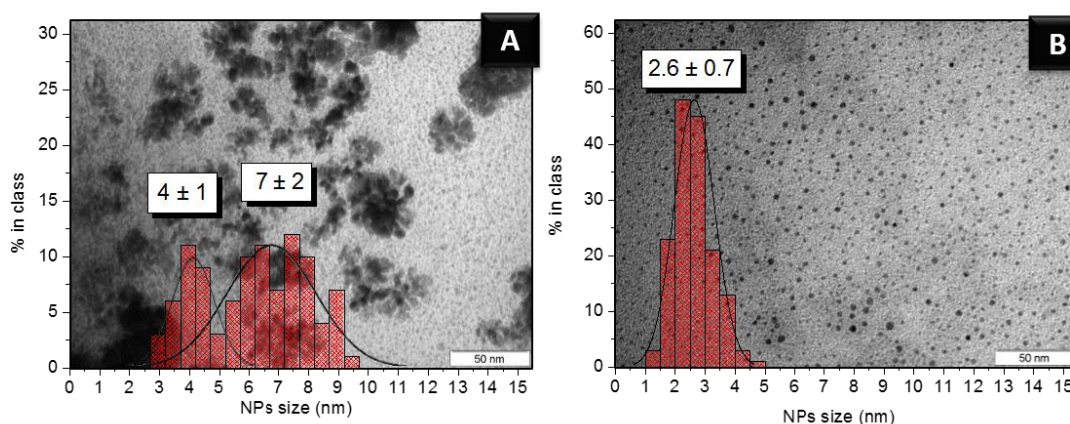


Figure 3.6. TEM images of Pd NPs obtained in solution (A) and within DOPG liposomes (B) using 10 % (v/v) glycerol and their corresponding size distribution graphs calculated using *i*TEM ( $n = 100$ ). Scale bars are 50 nm.

In addition, the results obtained within glycerol-incorporated DOPG liposomes were compared with standard reducing agents used for NP synthesis under the same experimental conditions. The same 10 % (v/v) concentration was used with monosodium citrate (1.4 M) while a lower concentration of  $\text{NaBH}_4$  (0.1 M) was employed as it is a much more powerful reducing agent. As

expected, both reducing agents were able to form Pd NPs. Citrate-encapsulated DOPG liposomes produced highly dispersive populations of Pd NPs with heterogeneous sizes and shapes ( $11 \pm 4$  nm), and triangular- and decahedron-shaped Pd NPs were also observed which can be attributed to the citrate preferred binding sites to the (111) facets of Pd and, therefore, giving different growth rates to each of the facets.<sup>51</sup>

When sodium borohydride was used as reducing agent in the DOPG liposomal nanoreactors, the Pd particle size synthesized was reduced ( $5 \pm 2$  nm), but dispersive and heterogeneous populations were present. However, homogeneous populations of monodisperse Pd nanoparticles of 0.9–3.5 nm in size produced with NaBH<sub>4</sub> in solution have been reported, but TOAB was required to act as capping agent and control reaction kinetics to avoid nanoparticle aggregation.<sup>3</sup>

Control experiments were carried out in the absence of glycerol. PdCl<sub>2</sub> was mixed with different lipids (DPPC, DPPG, DOPE or DOPG) at 25 °C in PBS (pH 7.4) under stirring conditions and argon, followed by a pH jump from pH 7.4 to 11 and back to 7.4 and left for 24 h of incubation. It is believed that the presence of the strong acid and base reagents required for the pH jump (NaOH and HCl), even at very low concentrations, could be responsible for the presence of the small amounts of Pd NPs observed when DOPG was used (data not shown). In order to investigate if the pH jump can produce Pd NPs, control experiments were carried out mixing PdCl<sub>2</sub> with DPPC or glycerol-coated DOPG lipids in PBS (pH 7.4) at 25 °C. TEM characterization confirmed that in the absence of the pH jump step no liposomes are formed as expected, and furthermore, no Pd NPs were produced in the case of DPPC lipids, while with DOPG lipids an extremely low number of NPs were formed, which can be attributed to the polyol reduction of the Pd(II) by the glycerol head groups present in DOPG lipids.

### 3.4.3. Lipid composition effect

The membrane of the liposome plays a very important role in nanoparticle synthesis, acting as route for the precursors to enter the nanoreactor. The membrane properties, such as permeability, surface charge, and functional group, can be modulated by changing the lipidic composition.<sup>52</sup>

The membrane permeability is a decisive parameter for the enhancement of the mobility of glycerol molecules through the lipid bilayer, providing a semimobile nanoenvironment for glycerol and facilitating access to the encapsulated palladium ions for the formation of nanoparticles in a highly controlled manner. The fluidic characteristics of the membrane are a result of the lipid melting temperature (T<sub>m</sub>), where the lipids undergo a transition from a gel phase to a liquid phase, rendering a phase behaviour to the entire bilayered system. Taking advantage of this membrane permeability given by the phase behaviour, different lipidic formulations were tested with transition temperatures above and below the working temperature (25 °C).

Liposomes prepared with DPPC and DPPG lipids (T<sub>m</sub> 41 °C) have a gel phase behaviour that provides highly ordered and dense bilayers reducing the capacity of glycerol to flow inside the liposome core, leading to a lower OH/Pd ratio and thus producing larger Pd NPs. As can be seen from the TEM images in Figure 3.7, the fixed number of glycerol molecules encapsulated within DPPC liposomes produces a narrow particle size distribution due to the rigid ratio of OH/Pd ( $16 \pm 2$  nm), whereas in the case of DPPG lipids, the higher OH/Pd ratio given by the glycerol-capped



lipids leads to high, but irregular, reductive conditions within the liposome core producing smaller but randomly dispersed Pd NPs with irregular shapes ( $4 \pm 2$  and  $16 \pm 6$  nm).

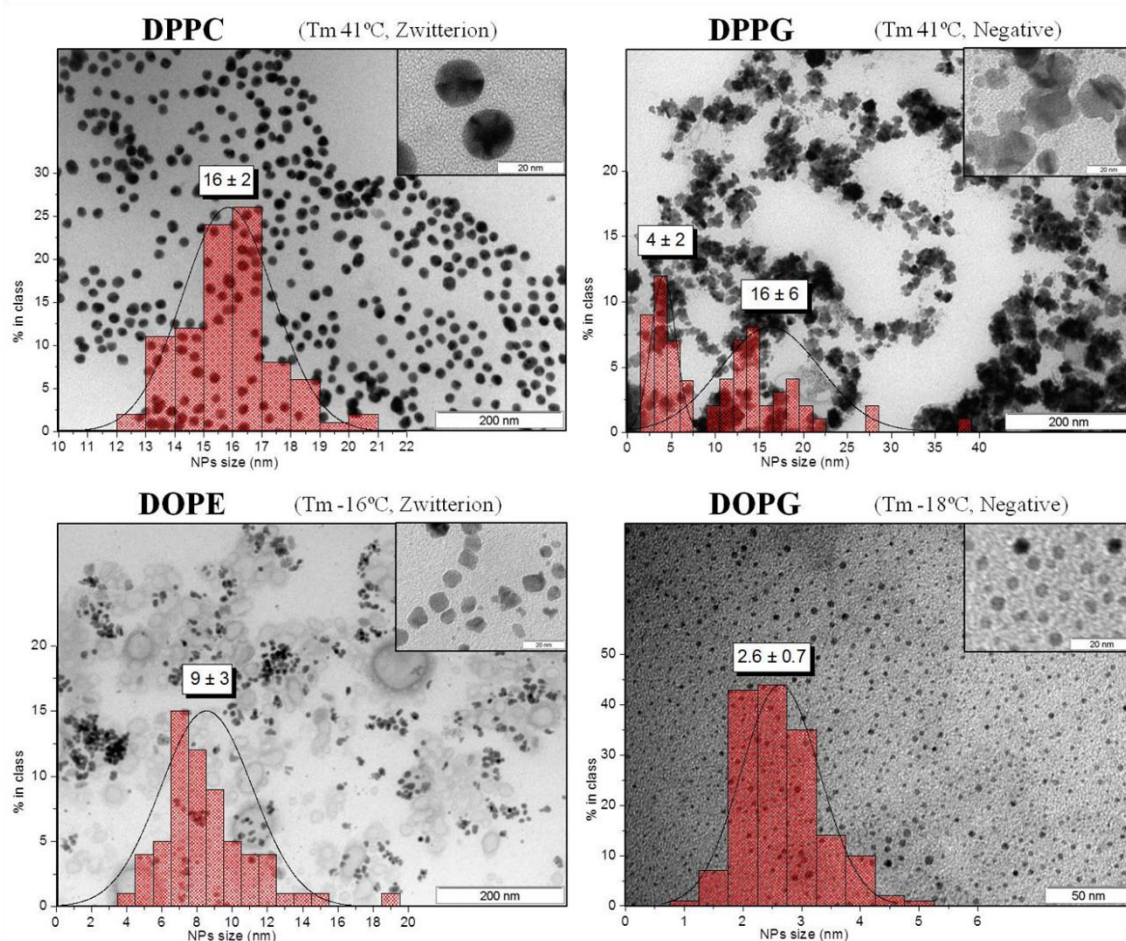


Figure 3.7. Lipid composition effect on the synthesis of Pd nanoparticles. TEM images show the Pd NPs synthesized inside different liposomes and their correspondent size distribution graphs calculated using iTEM. Scale bars are 200 nm in top and bottom-left images and 50 nm in bottom-right (insets scale bars are 20 nm). In the case of DPPG there are clearly two populations of NPs.

On the other hand, DOPE and DOPG liposomes have lower melting temperatures of  $-16$  and  $-18$  °C, respectively, and a higher degree of disorder induced by the carbon-carbon double bond in their oleic fatty acid chain. These properties confer flexible membranes where glycerol molecules can easily diffuse into the nanoreactor, producing Pd NPs smaller in size (Figure 3.7). The Pd NPs produced within DOPE liposomes are bigger and shapeless compared to the ones synthesized within DOPG,  $9 \pm 3$  and  $2.6 \pm 0.7$  nm, respectively, and that can be explained due to the instability that ethanolamine head groups confer to the liposome system, promoting liposome fusion or membrane disruption.

As seen in Table 3.2, DOPG liposomes were optimal for the generation of small and homogeneous populations of Pd NPs. The presence of phosphoglycerol DOPG lipid provides an internal core coated with glycerol groups providing a confined reducing environment for the reaction and a semipermeable membrane for glycerol to diffuse inside the nanoreactor core, thus forming notably smaller Pd NPs with a narrow particle size distribution. This suggests that reduction kinetics can be modulated by an optimal selection of the lipid composition of liposomal nanoreactor.

*Table 3.2. Effect of the lipidic composition of the liposomal nanoreactor on the size and distribution of the palladium nanoparticles produced.*

Lipid	T <sub>m</sub> (°C)	Charge	Size of Pd NPs (nm)
DPPC	41	Zwitterion	16 ± 2
DPPG	41	Negative	4 ± 2 ; 16 ± 6
DOPE	-16	Zwitterion	9 ± 3
DOPG	-18	Negative	2.6 ± 0.7

The head charge of the lipids gives both the internal and external regions a specific charge. These electrostatic forces not only prevent the fusion of liposomes into larger reactors but could also contribute to the synthesis of smaller sized NPs if the NPs are negatively charged as the repulsive forces between the lipids and the NPs will facilitate a tighter size control. Zeta potential experiments were carried out to measure the charge of the synthesized Pd NPs, and they were observed to be negatively charged with a Z-Pot of  $-23.8 \pm 0.9$  (n = 3). This repulsive interaction can also help in avoiding aggregations between lipids and nanoparticles, particularly in the final separation process where the liposomes are broken and the purified nanoparticles are obtained. TEM images of the produced nanoparticles clearly show the smallest Pd NPs in size with the narrowest dispersive distribution ( $2.6 \pm 0.7$  nm) when the liposome nanoreactor is composed with glycerol head groups at the inner and outer part of the membrane, as in the case of DOPG liposomes. This can be explained by the presence of a higher number of glycerol molecules in the lipid headgroup which gives a higher number of available hydroxyl groups to reduce the palladium ions and stabilize the synthesized Pd NPs inside the nanoreactors. Moreover, stability studies from those nanoparticles demonstrated that were highly stable over time, maintaining homogeneity in size and shape as was observed in the TEM images from 3 months after the Pd NPs preparation (data not shown).

Since DOPG liposomes provide the most monodisperse Pd nanoparticle populations, XRD tests were carried out to confirm their crystal structure. The synthesized Pd NPs were observed to have a single-crystalline face-centered-cubic (fcc) structure which was confirmed by the XRD results shown in Figure 3.8. The XRD peaks correlated with the electron diffraction pattern obtained in TEM (SAED) confirmed that the nanoparticles show a cuboctahedron predominant structure with (100), (200), (220), (310) and (222) planes present in the FTT pattern.

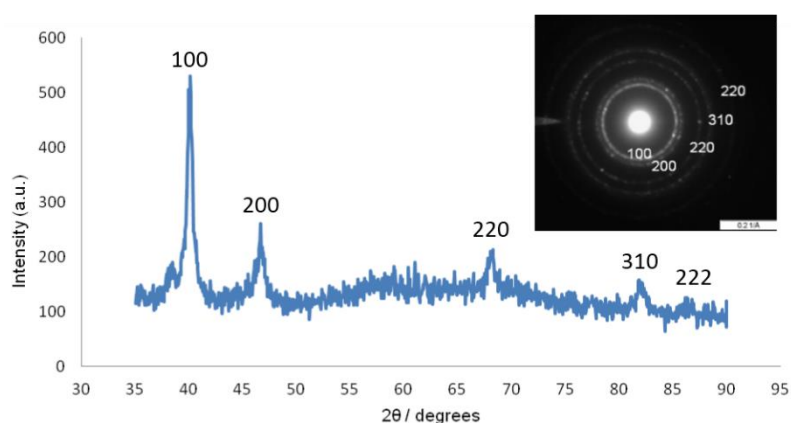


*Figure 3.8. XRD pattern and SAED of the prepared Pd nanoparticles from glycerol-incorporated DOPG liposomes.*

### 3.4.4. Effect of glycerol

Since the catalytic activity of nanoparticles is clearly modulated by their surface properties, we explored the role of the capping or stabilizing agent.<sup>53,54</sup> As previously reported, glycerol has been shown to reduce Pd(II) to form Pd(0) through the oxidation of the free hydroxyl groups. This oxidation might occur in all or in part of the alcohol groups in the glycerol molecules, and if any hydroxyl group remains in its oxidized form, they could therefore be participating in the stabilization of the Pd(0) atoms avoiding nanoparticle aggregation. We believe that glycerol-stabilized Pd nanoparticles occurs via one hydroxyl-end group or via the two hydroxyls from the ends or with the middle one, as we illustrate in Figure 3.9.

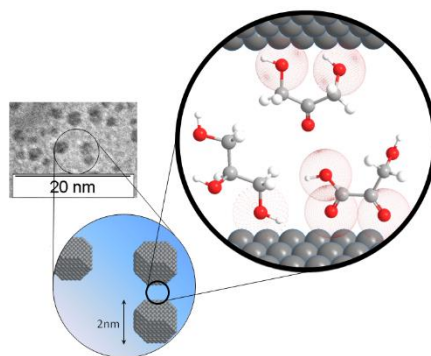


Figure 3.9. Schematic illustration of glycerol acting as a capping agent for nanoparticle stabilization.

To address our hypothesis, Pd NPs obtained in the absence of lipids were analysed using FTIR (Figure 3.10). The FTIR spectrum demonstrated the presence of glycerol on the surface of the formed nanoparticles, as reflected by the bands corresponding to the asymmetric and symmetric C-H vibration between 2970 and 2845  $\text{cm}^{-1}$ , as well as the bands corresponding to alcohol groups such as -OH band centered in 3300  $\text{cm}^{-1}$  and C-O at 1035  $\text{cm}^{-1}$ . The presence of weak bands at 1749/1724  $\text{cm}^{-1}$  was of particular interest as it indicates the presence of C-O groups resulting from the oxidation of glycerol during the formation of nanoparticles. The low intensity of this band suggests that glycerol in a reduced form acts as a capping agent.

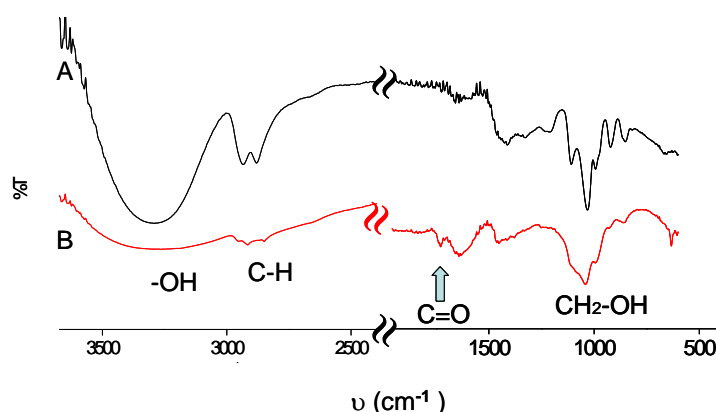


Figure 3.10. FTIR spectra of (A) glycerol and (B) Pd NPs.

The Pd nanoparticle surface was also analysed by Raman spectroscopy, taking the advantage of the already surface enhanced Raman scattering (SERS) properties of these particles.<sup>55</sup> Figure 3.11 shows the Raman spectra of glycerol, DOPG, and Pd NPs prepared in the liposomal

nanoreactor. As can be observed, the prepared nanoparticles show several bands in the region where the bands of glycerol and lipid appear, making a careful assignation difficult, although the presence of both reducing agent and phospholipid is clear. These bands are not observed when the nanoparticles were prepared in the absence of liposomes, perhaps due to a lower concentration of organic layer on the surface. This can also explain the higher stability of the particles obtained with the liposome method and the importance of the selection of lipids for the nanoreactor synthesis.

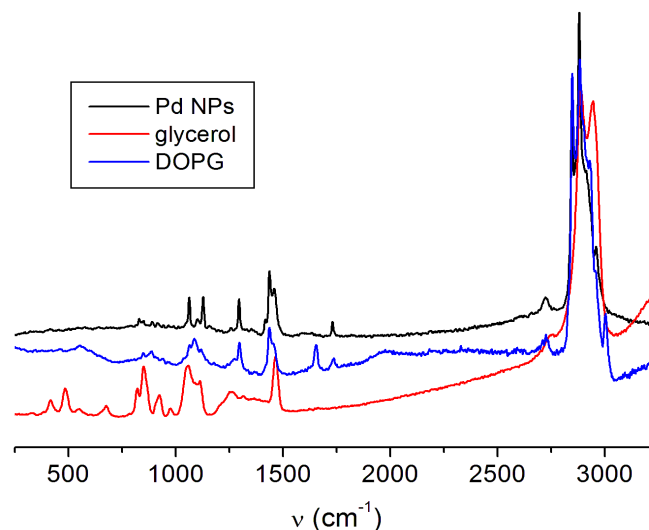


Figure 3.11. Raman spectra of glycerol, DOPG, and Pd nanoparticles.

After preparation, Pd NPs were reconstituted in toluene. From that solution, they could be precipitated with ethanol and reconstituted again in toluene or in water. In the case of the reconstitution in water, some aggregation was observed. The reconstitution in water affects the stabilizing layer of Pd NPs, probably by breaking the interactions between Pd and OH groups, at least at levels no detectable by Raman. It can be a method for removing the capping agent from the particles in case the presence of glycerol is not desirable, but these nanoparticles will not be as stable as those reconstituted in toluene and should be used as soon as possible.

#### 3.4.5. Catalytic activity of Pd NPs

Stevenson<sup>56</sup> has recently reported the reduction of p-nitrophenol to p-aminophenol in the presence of sodium borohydride catalysed by bimetallic nanoparticles, demonstrating that the reaction takes place on the surface of the particles and not in the solution phase, even in the presence of an excess of reducer. We have preliminarily evaluated the catalytic activity of the ultrasmall Pd NPs obtained with the liposome nanoreactor using this model reaction.

Figure 3.12 shows the UV-vis spectra for the reaction of p-nitrophenolate with sodium borohydride in the presence and absence of Pd NPs. The absorption band at 400 nm decreased rapidly when Pd NPs were added due to the reduction of p-aminophenolate and, at the same time, an absorption band at 315 nm corresponding to p-aminophenolate appeared and increased in intensity. As can be observed in the inset of Figure 3.12, no reaction took place in the absence of Pd NPs, demonstrating the catalytic properties of the nanoparticles. Further applications of the catalytic properties of Pd NPs are under study.

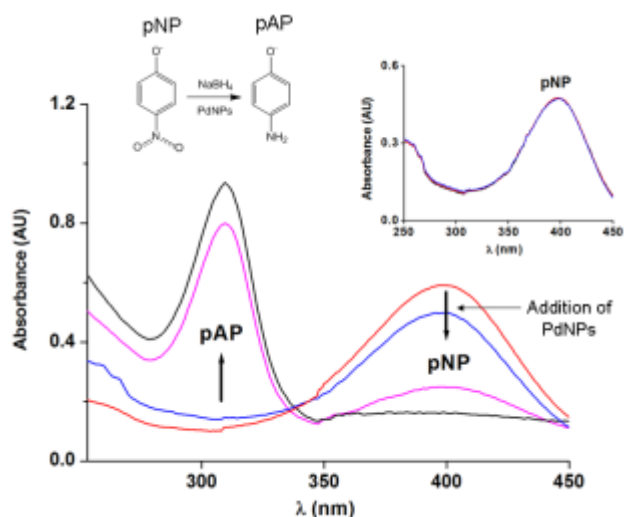


Figure 3.12. Reduction of *p*-nitrophenolate (pNP) catalysed by palladium nanoparticles (Pd NPs) studied by UV-vis. Inset: UV-vis spectra of *p*-nitrophenolate (pNP) +  $\text{NaBH}_4$  in the absence of palladium nanoparticles (Pd NPs).

### 3.5. Conclusions

A liposomal nanoreactor system was demonstrated to provide a confined nanoenvironment in which the synthesis of palladium nanoparticles proceeds in a controlled manner. The method uses environmentally friendly conditions, such as low temperature, avoiding the use of organic solvents or harsh chemicals, only exploiting glycerol, a renewable and natural polyol as reducing agent, as well as capping agent, to produce small homogeneous palladium nanoparticles.

Moreover, the importance of critical parameters in the procedure was evaluated, including type and/or concentration of reducing agent, lipid composition of the liposomes, and presence of glycerol as capping agent to elucidate their effect on the homogeneity and size of the palladium nanoparticles produced in the absence and presence of nanosized liposomal reactors. In addition, we have demonstrated for the first time the use of glycerol as both reducing and stabilizer agent to produce palladium nanoparticles.

Homogeneous highly stable palladium nanoparticles of  $\sim 2$  nm in size inside DOPG liposomes were obtained without additional capping agents due to their contribution to form bilayers that allow glycerol to move semi-freely through the liposome membrane. The contribution of more glycerol molecules present in the DOPG formulation gives the entire system the best conditions to form extremely small monodisperse Pd NPs. The glycerol group of DOPG also participates in the stabilization of the nanoparticles.

The functional liposomal nanoreactors reported herein demonstrate that the controlled conditions created in the liposome core provide a greener, safer, and more efficient system for the production of monodisperse ultrasmall palladium nanoparticles with catalytic properties for organic reaction.



### 3.6. References

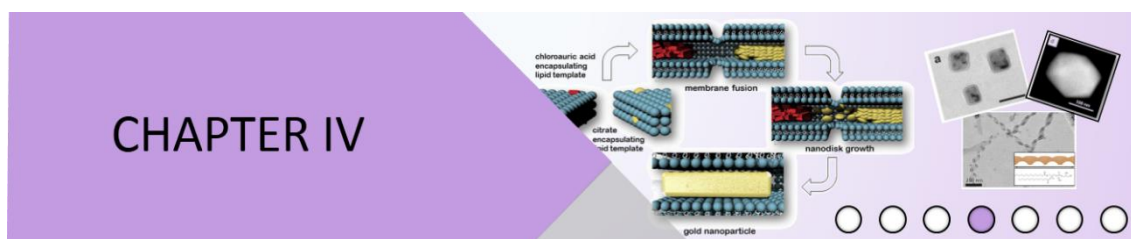
1. Daniel, M.-C.; Astruc, D., Gold Nanoparticles: Assembly, Supramolecular Chemistry, Quantum-Size-Related Properties, and Applications toward Biology, Catalysis, and Nanotechnology. *Chem. Rev.* **2003**, *104*, 293-346.
2. Grzelczak, M.; Perez-Juste, J.; Mulvaney, P.; Liz-Marzan, L. M., Shape control in gold nanoparticle synthesis. *Chem. Soc. Rev.* **2008**, *37*, 1783-1791.
3. Coronado, E.; Ribera, A.; Garcia-Martinez, J.; Linares, N.; Liz-Marzan, L. M., Synthesis, characterization and magnetism of monodispersed water soluble palladium nanoparticles. *J. Mater. Chem.* **2008**, *18*, 5682-5688.
4. Kim, S.-W.; Kim, M.; Lee, W. Y.; Hyeon, T., Fabrication of Hollow Palladium Spheres and Their Successful Application to the Recyclable Heterogeneous Catalyst for Suzuki Coupling Reactions. *J. Am. Chem. Soc.* **2002**, *124*, 7642-7643.
5. Xiong, Y. J.; McLellan, J. M.; Chen, J. Y.; Yin, Y. D.; Li, Z. Y.; Xia, Y. N., Kinetically controlled synthesis of triangular and hexagonal nanoplates of palladium and their SPR/SERS properties. *J. Am. Chem. Soc.* **2005**, *127*, 17118-17127.
6. Tobiška, P.; Hugon, O.; Trouillet, A.; Gagnaire, H., An integrated optic hydrogen sensor based on SPR on palladium. *Sens. Actuators, B* **2001**, *74*, 168-172.
7. Kim, S. W.; Park, J.; Jang, Y.; Chung, Y.; Hwang, S.; Hyeon, T.; Kim, Y. W., Synthesis of monodisperse palladium nanoparticles. *Nano Lett.* **2003**, *3*, 1289-1291.
8. Arul Dhas, N.; Gedanken, A., Sonochemical preparation and properties of nanostructured palladium metallic clusters. *J. Mater. Chem.* **1998**, *8*, 445-450.
9. Schmid, G.; Harms, M.; Malm, J. O.; Bovin, J. O.; Van Ruitenbeck, J.; Zandbergen, H. W.; Fu, W. T., Ligand-stabilized giant palladium clusters: promising candidates in heterogeneous catalysis. *J. Am. Chem. Soc.* **1993**, *115*, 2046-2048.
10. Reetz, M. T.; Helbig, W., Size-Selective Synthesis of Nanostructured Transition Metal Clusters. *J. Am. Chem. Soc.* **1994**, *116*, 7401-7402.
11. Yee, C. K.; Jordan, R.; Ulman, A.; White, H.; King, A.; Rafailovich, M.; Sokolov, J., Novel one-phase synthesis of thiol-functionalized gold, palladium, and iridium nanoparticles using superhydride. *Langmuir* **1999**, *15*, 3486-3491.
12. Brust, M.; Walker, M.; Bethell, D.; Schiffrin, D. J.; Whyman, R., Synthesis of thiol-derivatised gold nanoparticles in a two-phase Liquid-Liquid system. *J. Chem. Soc., Chem. Comm.* **1994**, 801-802.
13. Srivastava, S. K.; Yamada, R.; Ogino, C.; Kondo, A., Biogenic synthesis and characterization of gold nanoparticles by Escherichia coli K12 and its heterogeneous catalysis in degradation of 4-nitrophenol. *Nanoscale Res. Lett.* **2013**, *8*, 70-73.
14. Srivastava, S.; Constanti, M., Room temperature biogenic synthesis of multiple nanoparticles (Ag, Pd, Fe, Rh, Ni, Ru, Pt, Co, and Li) by Pseudomonas aeruginosa SM1. *J. Nanopart. Res.* **2012**, *14*, 1-10.

15. Bilecka, I.; Elser, P.; Niederberger, M., Kinetic and Thermodynamic Aspects in the Microwave-Assisted Synthesis of ZnO Nanoparticles in Benzyl Alcohol. *ACS Nano* **2009**, *3*, 467-477.
16. Biacchi, A. J.; Schaak, R. E., The Solvent Matters: Kinetic versus Thermodynamic Shape Control in the Polyol Synthesis of Rhodium Nanoparticles. *ACS Nano* **2011**, *5*, 8089-8099.
17. Carroll, K. J.; Reveles, J. U.; Shultz, M. D.; Khanna, S. N.; Carpenter, E. E., Preparation of Elemental Cu and Ni Nanoparticles by the Polyol Method: An Experimental and Theoretical Approach. *J. Phys. Chem. C* **2011**, *115*, 2656-2664.
18. Park, K. H.; Im, S. H.; Park, O. O., The size control of silver nanocrystals with different polyols and its application to low-reflection coating materials. *Nanotechnology* **2011**, *22*, 045602.
19. Cai, W.; Wan, J., Facile synthesis of superparamagnetic magnetite nanoparticles in liquid polyols. *J. Colloid Interface Sci.* **2007**, *305*, 366-370.
20. Yan, X.; Liu, H.; Liew, K. Y., Size control of polymer-stabilized ruthenium nanoparticles by polyol reduction. *J. Mater. Chem.* **2001**, *11*, 3387-3391.
21. Wiley, B.; Herricks, T.; Sun, Y. G.; Xia, Y. N., Polyol synthesis of silver nanoparticles: Use of chloride and oxygen to promote the formation of single-crystal, truncated cubes and tetrahedrons. *Nano Lett.* **2004**, *4*, 1733-1739.
22. Feldmann, C., Polyol-mediated synthesis of nanoscale functional materials. *Solid State Sci.* **2005**, *7*, 868-873.
23. Ayyappan, S.; Gopalan, R. S.; Subbanna, G. N.; Rao, C. N. R., Nanoparticles of Ag, Au, Pd, and Cu produced by alcohol reduction of the salts. *J. Mater. Res.* **1997**, *12*, 398-401.
24. Grace, A. N.; Pandian, K., One pot synthesis of polymer protected gold nanoparticles and nanoprisms in glycerol. *Colloids Surf., A* **2006**, *290*, 138-142.
25. Siegel, J.; Kvítek, O.; Ulbrich, P.; Kolská, Z.; Slepíčka, P.; Švorčík, V., Progressive approach for metal nanoparticle synthesis. *Mater. Lett.* **2012**, *89*, 47-50.
26. Nirmala Grace, A.; Pandian, K., One pot synthesis of polymer protected Pt, Pd, Ag and Ru nanoparticles and nanoprisms under reflux and microwave mode of heating in glycerol—A comparative study. *Mater. Chem. Phys.* **2007**, *104*, 191-198.
27. Ullah, M. H.; Il, K.; Ha, C.-S., Preparation and optical properties of colloidal silver nanoparticles at a high Ag<sup>+</sup> concentration. *Mater. Lett.* **2006**, *60*, 1496-1501.
28. Dzido, G.; Jarzębski, A., Fabrication of silver nanoparticles in a continuous flow, low temperature microwave-assisted polyol process. *J. Nanopart. Res.* **2011**, *13*, 2533-2541.
29. Lee, Y.-W.; Han, S.-B.; Ko, A. R.; Kim, H.-S.; Park, K.-W., Glycerol-mediated synthesis of Pd nanostructures with dominant {111} facets for enhanced electrocatalytic activity. *Catal. Comm.* **2011**, *15*, 137-140.
30. Puvvada, S.; Baral, S.; Chow, G. M.; Qadri, S. B.; Ratna, B. R., Synthesis of palladium metal nanoparticles in the bicontinuous cubic phase of glycerol monooleate. *J. Am. Chem. Soc.* **1994**, *116*, 2135-2136.

31. Selvaraj, V.; Vinoba, M.; Alagar, M., Electrocatalytic oxidation of ethylene glycol on Pt and Pt–Ru nanoparticles modified multi-walled carbon nanotubes. *J. Colloid Interface Sci.* **2008**, *322*, 537-544.
32. Lee, Y.-W.; Ko, A. R.; Han, S.-B.; Kim, H.-S.; Park, K.-W., Synthesis of octahedral Pt-Pd alloy nanoparticles for improved catalytic activity and stability in methanol electrooxidation. *Phys. Chem. Chem. Phys.* **2011**, *13*, 5569-5572.
33. Trung, T.; Cho, W.-J.; Ha, C.-S., Preparation of TiO<sub>2</sub> nanoparticles in glycerol-containing solutions. *Mater. Lett.* **2003**, *57*, 2746-2750.
34. Wang, X.; Li, Y., Hydrothermal reduction route to Mn(OH)<sub>2</sub> and MnCO<sub>3</sub> nanocrystals. *Mater. Chem. Phys.* **2003**, *82*, 419-422.
35. Marquardt, D.; Barthel, J.; Braun, M.; Ganter, C.; Janiak, C., Weakly-coordinated stable platinum nanocrystals. *CrystEngComm* **2012**, *14*, 7607-7615.
36. Bakshi, M. S.; Possmayer, F.; Petersen, N. O., Simultaneous Synthesis of Au and Cu Nanoparticles in Pseudo-Core-Shell Type Arrangement Facilitated by DMPG and 12-6-12 Capping Agents. *Chem. Mater.* **2007**, *19*, 1257-1266.
37. Bakshi, M. S.; Possmayer, F.; Petersen, N. O., Role of Different Phospholipids in the Synthesis of Pearl-Necklace-Type Gold-Silver Bimetallic Nanoparticles as Bioconjugate Materials. *J. Phys. Chem. C* **2007**, *111*, 14113-14124.
38. Naka, K.; Sato, M.; Chujo, Y., Stabilized spherical aggregate of palladium nanoparticles prepared by reduction of palladium acetate in octa(3-aminopropyl)octasilsesquioxane as a rigid template. *Langmuir* **2008**, *24*, 2719-2726.
39. Scott, R. W. J.; Datye, A. K.; Crooks, R. M., Bimetallic Palladium–Platinum Dendrimer-Encapsulated Catalysts. *J. Am. Chem. Soc.* **2003**, *125*, 3708-3709.
40. Scott, R. W. J.; Wilson, O. M.; Oh, S.-K.; Kenik, E. A.; Crooks, R. M., Bimetallic Palladium–Gold Dendrimer-Encapsulated Catalysts. *J. Am. Chem. Soc.* **2004**, *126*, 15583-15591.
41. Coulter, M. M.; Dinglasan, J. A.; Goh, J. B.; Nair, S.; Anderson, D. J.; Dong, V. M., Preparing water-dispersed palladium nanoparticles via polyelectrolyte nanoreactors. *Chem. Sci.* **2010**, *1*, 772-775.
42. Wang, C.-C.; Chen, D.-H.; Huang, T.-C., Synthesis of palladium nanoparticles in water-in-oil microemulsions. *Colloids Surf. A* **2001**, *189*, 145-154.
43. Kundu, S.; Wang, K.; Lau, S.; Liang, H., Photochemical synthesis of shape-selective palladium nanocubes in aqueous solution. *J. Nanopart. Res.* **2010**, *12*, 2799-2811.
44. Fan, F.-R.; Attia, A.; Sur, U. K.; Chen, J.-B.; Xie, Z.-X.; Li, J.-F.; Ren, B.; Tian, Z.-Q., An Effective Strategy for Room-Temperature Synthesis of Single-Crystalline Palladium Nanocubes and Nanodendrites in Aqueous Solution. *Cryst. Growth Des.* **2009**, *9*, 2335-2340.
45. Heshmatpour, F.; Abazari, R.; Balalaie, S., Preparation of monometallic (Pd, Ag) and bimetallic (Pd/Ag, Pd/Ni, Pd/Cu) nanoparticles via reversed micelles and their use in the Heck reaction. *Tetrahedron* **2012**, *68*, 3001-3011.
46. Chen, D.-H.; Wang, C.-C.; Huang, T.-C., Preparation of Palladium Ultrafine Particles in Reverse Micelles. *J. Colloid Interface Sci.* **1999**, *210*, 123-129.



47. Semagina, N.; Renken, A.; Laub, D.; Kiwi-Minsker, L., Synthesis of monodispersed palladium nanoparticles to study structure sensitivity of solvent-free selective hydrogenation of 2-methyl-3-butyn-2-ol. *J. Catal.* **2007**, *246*, 308-314.
48. Sanchez-Dominguez, M.; Boutonnet, M.; Solans, C., A novel approach to metal and metal oxide nanoparticle synthesis: the oil-in-water microemulsion reaction method. *J. Nanopart. Res.* **2009**, *11*, 1823-1829.
49. Genc, R.; Clergeaud, G.; Ortiz, M.; O'Sullivan, C. K., Green Synthesis of Gold Nanoparticles Using Glycerol-Incorporated Nanosized Liposomes. *Langmuir* **2011**, *27*, 10894-10900.
50. Genç, R. ; Ortiz, M.; O'Sullivan, C. K., Curvature-Tuned Preparation of Nanoliposomes. *Langmuir* **2009**, *25*, 12604-12613.
51. Lim, B.; Jiang, M.; Tao, J.; Camargo, P. H. C.; Zhu, Y.; Xia, Y., Shape-Controlled Synthesis of Pd Nanocrystals in Aqueous Solutions. *Adv. Funct. Mater.* **2009**, *19*, 189-200.
52. Drummond, D. C.; Meyer, O.; Hong, K. L.; Kirpotin, D. B.; Papahadjopoulos, D., Optimizing liposomes for delivery of chemotherapeutic agents to solid tumors. *Pharmacol. Rev.* **1999**, *51*, 691-743.
53. Pérez-Lorenzo, M., Palladium nanoparticles as efficient catalysts for suzuki cross-coupling reactions *J. Phys. Chem. Lett.* **2012**, *3*, 167-174.
54. Nalawade, P., Mukherjee, T., Kapoor, S. Green synthesis of gold nanoparticles using glycerol as a reducing agent. *Advances in Nanoparticles* **2013**, *2*, 78-86.
55. Chen, H., Wei G., Ispas, A., Hickey A. H., Eychmüller A. Synthesis of palladium nanoparticles and their applications for Surface-Enhanced Raman Scattering and electrocatalysis. *J. Phys. Chem. C* **2010**, *114*, 21976-21981.
56. Pozun, Z. D., Rodenbusch, S. E., Keller, E., Tran, K., Tang, W., Stevenson, K. J. Henkelman, G. A systematic investigation of p-nitrophenol reduction by bimetallic dendrimer encapsulated nanoparticles. *J. Phys. Chem. C* **2013**, *117*, 7598-7604.



# Shape directed biomineralization of gold nanoparticles using self- assembled lipid structures



## Shape directed biomineralization of gold nanoparticles using self-assembled lipid structures

*Biomater. Sci.* **2014**, *2*, 1128–1134

Rükan Genç,<sup>¥</sup> Gael Clergeaud,<sup>†</sup> Mayreli Ortiz,<sup>†</sup> and Ciara K. O’Sullivan<sup>†,§</sup>

<sup>¥</sup> Department of Chemical Engineering, University of Mersin, 33343 Ciftlikkoy, Mersin, Turkey.

<sup>†</sup> Nanobiotechnology & Bioanalysis Group, Department d’Enginyeria Quimica, Universitat Rovira i Virgili, Tarragona 43007, Spain

<sup>§</sup> Institució Catalana de Recerca i Estudis Avancats, Barcelona 08010, Spain



## 4.1. Abstract

As one of the building blocks of the cell membrane, lipids and their interaction with neighbouring lipids and other molecules, as well as their ability to form different kinds of structures, have garnered immense interest. By exploiting the effective shape and thermal-phase behaviour of lipids, we have prepared lipid superstructures such as twisted ribbons and rectangular and hexagonal shaped lipidic nanostructures using the curvature tuned preparation method. These lipidic superstructures were then used as nanoreactor templates for the inorganic synthesis of diversely shaped and sized gold nanostructures exploring different administration routes of reducing agents, citrate, and tetrachloroauric acid, which as a result formed different organizations of gold nanoparticles aligned and guided by the template structure. Tailor-designed metallic nanostructures can be obtained through a careful selection of lipids and conditions for lipid superstructure preparation and their consequent use as template nanoreactors. The diversely sized and shaped gold nanostructures obtained have great potential for catalysis and plasmonics.

## 4.2. Introduction

As one of the building blocks of cell membranes, lipids and their interaction with neighbouring lipids and other molecules, as well as their ability to form different kinds of structures, have garnered immense interest.<sup>1</sup> There are several structural factors and environmental conditions that affect the self-assembly of lipids into nano-sized structures, influencing the phase behaviour and the curvature of the lipid. Lipid superstructures have been studied intensively over the last 30 years<sup>2</sup> with the recent increasing interest in these nanostructured materials formed by self-organisation.<sup>3</sup> Vesicles, or liposomes, are the most widely known lipid based structures; however, lipids are also known to be able to self-assemble into several other structures, such as lipid tubes and rods,<sup>4</sup> lipid ribbons,<sup>5,6</sup> hexasomes<sup>7</sup> as well as cubosomes<sup>8</sup> and non-lamellar mesophase lipid aggregations.<sup>9</sup> Aside from being used as model systems to understand the cell membrane nature,<sup>6</sup> these nano- and micro-structures are attractive as substrates for protein crystallization,<sup>10</sup> as templates for the synthesis of one-dimensional inorganic materials,<sup>11,12</sup> and as vectors for drug delivery.<sup>4,13</sup>

In parallel, there is enormous interest in the development of methods for the preparation of metallic nanoparticles of diverse sizes and shapes, particularly for application in catalysis, where structures such as cubes,<sup>14</sup> disks,<sup>15</sup> tubes,<sup>16</sup> stars,<sup>17</sup> and nanocages<sup>18</sup> provide crystal plane architectures that can be tailor-designed according to the specific application. Spherical nanoparticles are, to a large extent, synthesized by wet-state preparation methods such as the Turkevich method (1951)<sup>19</sup> or the Schmidt method (1981),<sup>20</sup> which are based on reduction/oxidation reactions. However, further control of the one and two-dimensional shapes of nanoparticles is still largely unaddressed. The seed mediated synthesis of rod-like structures exploiting the use of a growth-directing agent (hexadecyltrimethylammonium bromide (CTAB)),<sup>21</sup> as well as vapour phase synthesis,<sup>22</sup> vapour-solid-liquid synthesis methods,<sup>23</sup> or patterning on a solid surface by etching or lithography methods<sup>24</sup> are some of the methods reported to achieve particle growth of specific shapes.<sup>25</sup> However, those methods often reveal nanoparticle populations with different sizes and shapes and require strong reaction conditions, e.g. high temperature, high pressure, extreme pH or organic solvents.<sup>26,27</sup> As an alternative, template directed synthesis using self-assembled structures offers several advantages in

comparison, not only because of the relative inexpensiveness of the technique and its simplicity and inherent applicability to scale-up, but also due to the unlimited potential combinations of biomaterials to form diverse template structures.<sup>4,11,28-30</sup>

A highly reported method that has been used for the preparation of nanoparticles is the so-called reverse micelle method. In this method, the inner core of the reverse micelles is considered as a nanoreactor,<sup>25</sup> within which controlled reactions leading to the formation of nanosized metallic and metal halide particles are carried out,<sup>31</sup> where the size of the micelle core is controlled by the molar ratio of water to surfactant/lipid molecules in solution. Typically, individual reverse micelle populations are prepared containing metallic precursors e.g. metallic salts and reducing agents. An exchange process occurs when the micelles collide due to both Brownian motion and attractive forces between the micelles, resulting in a fusion of the reverse micelles, an exchange of the contents within the cores, followed by a re-dispersion of the micelles.<sup>32,33</sup> As a result the reduction of the metal salt results in the growth of metallic nanoparticles within the core of the micelle. This method has found widespread applications and has been used, for example, for the synthesis of semi-conductor materials,<sup>34</sup> metallic nanoparticles<sup>35</sup> and nanoalloys.<sup>36</sup>

Phospholipids are naturally occurring amphipathic molecules that can form bilayer structures with a high aqueous interior volume. Their capacity to encapsulate a wide range of molecules makes lipid based structures efficient nanoreactors for inorganic synthesis of metal nanostructures under milder and greener reaction conditions.<sup>37,38</sup> Moreover, the use of lipid based templates could overcome the problems faced with soft-template strategies, such as poor stability of the template during the synthesis and removal following particle synthesis, since they can be formulated to be stable in aqueous media and easily dissolved in organic solvents.<sup>39</sup> However, unlike micelle forming surfactants (e.g. CTAB), lipids often prefer to self-assemble in spherical vesicles which limits their use in the synthesis of differently shaped inorganic nanoparticles.<sup>40</sup> Recently, we reported on an ultra-rapid and environmentally friendly method for the preparation of highly stable liposomes using both charged and zwitterionic lipids, with different phase transition melting ( $T_m$ ), exploiting a combination of a rapid pH change followed by a defined period of equilibration, resulting in monodisperse and stable liposome populations and also differently shaped lipid mesostructures depending on the properties of lipids used.<sup>41</sup> In previous studies, those nanoliposomes were used to synthesize tiny gold and palladium nanoparticles with catalytic properties.<sup>39,42</sup> In the work described here, we exploit the curvature-tuned liposome preparation method for the formation of several lipidic nanostructures using different formulations of phospholipids leading to the self-assembly of the lipids into structures different from liposomes, such as twisted ribbons, rectangular and hexagonal shaped lipid nanostructures. Inspired from reverse-micelles, we proposed to use these nanostructures for the production of metallic nanoparticles with the size and shape of the resulting nanoparticle dictated by the lipid templates. Analysis of the lipid nanostructures and the metallic nanostructures formed was carried out by biological transmission electron microscopy (TEM), scanning electron microscopy (SEM), and X-ray diffraction analysis and the feasibility of the approach for the preparation of ribbons, hexagonal and cubical metallic nanostructures was clearly demonstrated.

## 4.2. Experimental section

### 4.2.1. Materials

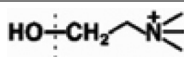
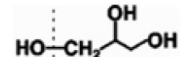
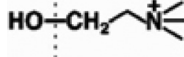
Phospholipids were supplied as a powder by Avanti Polar Lipids, Inc. and used without further purification. Sodium hydroxide, hydrochloric acid, di-sodium hydrogen phosphate (anhydrous, reagent grade,  $\text{Na}_2\text{HPO}_4$ ), sodium dihydrogen phosphate (anhydrous), extra pure, ( $\text{NaH}_2\text{PO}_4$ ) and glycerol 99.5 %, reagent grade, were purchased from Scharlau Chemie SA. Sodium chloride was provided by Riedel-de Haën. Milli-Q water ( $1.82 \text{ M}\Omega \text{ cm}^{-1}$ ) used to prepare buffers and liposomes was obtained using a Simplicity 185 Millipore-Water System.

### 4.2.2. Preparation of lipid based nanostructures and template directed synthesis

#### 4.2.2.1. Preparation of lipid nanostructures using the curvature tuned preparation method<sup>41</sup>

Different lipid mixtures (50 mg) were directly hydrated in 4 mL of buffer (0.1 M PBS, pH 7.4), which had previously been heated to a pre-determined temperature,  $T_0$  (Table 4.1). The temperature was kept constant by placing a glass flask (15 mL) in a water jacket connected to an UltraTerm 200 Model (P-Selecta) thermocycler. The mixture was vortexed in a 10 mL falcon tube (with glass beads) for 1-3 min and added to 6 mL of preheated and degassed buffer solution (0.1 M PBS, pH 7.4) in order to prepare empty lipid templates. In the case of the encapsulating lipid nanostructures, the lipid mixture was mixed with 6 mL of preheated and degassed buffer solution (0.1 M PBS, pH 7.4) including either  $\text{HAuCl}_4$  (20 mg) or sodium citrate (115 mg) and was left to stir for 15 min while the temperature was kept constant at  $T_0$ . As used in the nanoliposome preparation, lipid nanotemplates were prepared by the use of an immediate “pH jump” to produce a fast protonation and deprotonation induced lipid self-assembly.<sup>41</sup> For this, the pH was subsequently increased to pH 11 using NaOH and immediately readjusted to pH 7.4 using HCl. The resulting mixture was left to mix for a 25 min equilibration period under the same conditions. Finally, the stirring and heating process was stopped, and the solution was left to cool to room temperature for 25 min, and, subsequently, samples were stored at 4 °C before use. All steps were conducted under argon. Unless otherwise described, all lipid formulations consisted of phospholipid and lyso-PPC (88:12 molar ratio). The final lipid mass concentration was kept constant for all lipid formulations at 0.5 % (w/v) (see the ESI† for the formation of lipid nanotemplates).

Table 4.1. Properties of the phospholipids studied and conditions for the preparation of differently shaped lipid templates.

Lipid (tail length)	Head group	Molecule charge	Final shape (operation $T_0$ <sup>a</sup> )
DPPC (18C) (1,2-dipalmitoyl-sn-glycero-3-phosphocholine)	 -Choline-	Neutral	Hexagonal (25 °C) Rectangular (45 °C)
DMPG (14C) (1,2-dimyristoyl-sn-glycero-3-phospho-(1'-rac-glycerol))	 -Glycerol-	Negative	Twisted ribbon (25 °C)
Lyso-PC (16C) (1-palmitoyl-2-hydroxy-sn-glycero-3-phosphocholine)	 -Choline-	Neutral	

<sup>a</sup> It should be noted that the sample preparation method includes a cooling step to room temperature afterwards and all analyses were carried out at room temperature.



#### 4.2.2.2. Gold nanostructure synthesis patterned by lipid structures

In the case of the hexagonal and square shaped lipid structures, two individual populations of the lipid template either encapsulating citrate or tetrachloroauric acid were mixed, or, as a control, tetrachloroauric acid encapsulating lipid structures were immersed in PBS. In the case of the twisted ribbon shaped lipid templates, tetrachloroauric acid encapsulating lipids were immersed in PBS or citrate solution in PBS, or, alternatively were mixed with citrate encapsulating ribbons. In addition, citrate encapsulating lipid ribbons were immersed in tetrachloroauric acid solution in PBS. Mixtures were incubated at room temperature and samples were taken every 24 hours and purified by centrifugation with methanol:ethanol (1:4 v/v) and kept in toluene at 4 °C until analysed.

#### 4.2.3. Characterization of structural changes and determination of size

##### 4.2.3.1. Transmission electron microscopy (TEM) imaging via phosphotungstic acid hydrate staining

Encapsulating and empty lipid templates were analysed structurally using a transmission electron microscope. Using a glass pipette, a drop of sample was added to a 200 mesh copper grid with a thin film of Formvar polymer and was kept at room temperature for 1 min, followed by addition of a drop of 2 % v/v phosphotungstic acid hydrate (PA) (Panreac) solution (pH 7.2) in distilled water for 2 min. Subsequently, excess liquid was carefully dried using filter paper and the sample was left at room temperature until a dried film was obtained. Transmission electron microscopy (TEM) analyses were performed using a JEOL 1011 transmission electron microscope operated at 80 keV with an ultrahigh-resolution pole piece providing a point resolution of 2 Å. Micrographs (1024 pixels × 1024 pixels) were acquired using a Megaview III multiscan-CCD camera. Images were analysed with an iTEM image analysis platform, measuring the dimensions of particles from the photos captured at different parts of the grid and calculating the mean diameter from the series of experiments ( $n \pm 3$ ) conducted using the same parameters.

##### 4.2.3.2. Determination of the reaction yield of the gold nanoparticle synthesis

An ICP-OES instrument Spectro Arcos FHS16 was used to measure the mass fractions of Au in the nanostructures using calibration curves generated from standard solutions (0-40 ppm dilutions of transition metal mix 3 which was purchased from Sigma-Aldrich) with an R value of 0.999. The samples and standards were dissolved in 1 % aqua regia (3HCl:1HNO<sub>3</sub>). The analytical line used for the determination of Au was 242.795 nm. The synthetic yield for the different Au nanostructures was calculated as the difference between the Au mass determined by ICP-OES and the starting Au mass, corrected with the dilution factors and expressed in percentage ( $n = 3$ ). The formula used was  $X \% = (C/C_i) \times 100$  where C is the Au concentration (mg L<sup>-1</sup>) measured by ICP in the samples containing the nanostructures and C<sub>i</sub> is the starting concentration of Au (mg L<sup>-1</sup>).

##### 4.2.3.3. Scanning electron microscope (SEM)

Scanning electron microscopy studies were carried out using a scanning electron microscope, SEM (Jeol JSM 6400, 40 kV). Spectrometric measurements were performed by the spectrophotometer UV-Vis-NIR, Cary 500-Varian.

##### 4.2.3.4. X-ray diffraction measurements

X-ray diffraction measurements were performed with a Rigaku X-ray diffractometer.

### 4.3. Results and discussion

There have been a plethora of reports detailing the reverse micelle method,<sup>25,31–35</sup> where a clear correlation between the template size and the resulting nanoparticles formed has been established. Reverse micelles are dynamic lipid clusters where they continuously fuse and re-disperse due to Brownian motion, exchanging their contents.<sup>43</sup> However, in the case of lipid bilayers, fusion is a more complex process where the membrane fluidity and hydrophobic interactions have been reported to be important factors for liposome membrane fusion, and is mostly an irreversible process.<sup>44</sup> Zwitterionic lipids fuse at temperatures below their critical melting temperature while fusion of charged lipids occurs at higher temperatures.<sup>45</sup> The mechanism of the 2D growth of rigid particles is proposed to be due to a shape patterned by a single template due to fusion of the two lipid structures encapsulating H<sub>2</sub>AuCl<sub>4</sub> and citrate in their aqueous core, respectively. In the proposed model depicted in Figure 4.1, the electrostatic interaction occurring between AuCl<sub>4</sub><sup>-</sup> with a net negative charge and the zwitterionic-PC head with mobile positive charge (Table 1) provides nucleation sites for the synthesis. Subsequent to the fusion of two lipid structures, citrate molecules slowly diffuse into the bilayer and reduce the Au(III) to Au(0) resulting in the formation of solid gold hexagonal and rectangular nanoparticles. However, possible transport of tetrachloroauric acid in the reverse direction should be taken into account as this would possibly result in amorphous aggregates as the reaction will occur faster in that direction.

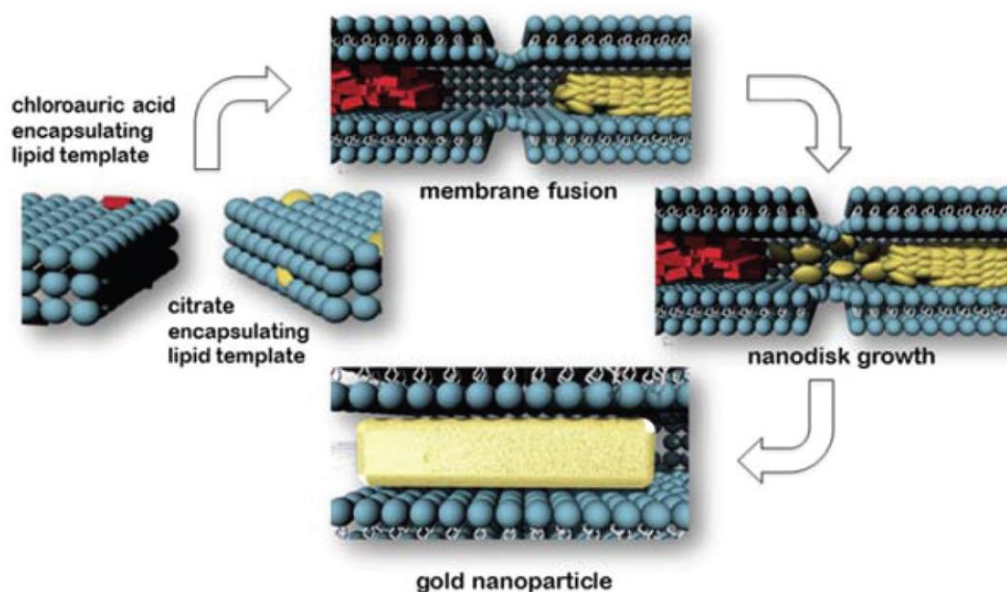


Figure 4.1. Proposed growth path of nanoparticle formation through membrane fusion of reactant encapsulating lipid structures.

To explore the proposed usage of the prepared lipid superstructures as templates and nanoreactors for the preparation of metallic nanostructures of controlled size and shape, the aforementioned lipid nanostructures were prepared from DPPC and DMPG lipids (Table 1) as described above, to form rectangular, hexagonal as well as ribbon shaped nano-architectures.

Rectangular-shaped lipid templates were prepared at an operating temperature of 45 °C from DPPC lipids and cooled down to RT before purification and analysis. The formed lipid structures were then used as templates (Figure 4.2a) afterwards, and nanoparticle synthesis was carried out by mixing H<sub>2</sub>AuCl<sub>4</sub> encapsulating and citrate encapsulating lipid nano-templates in a 1:1 ratio,

and particle formation was monitored over 72 h at room temperature. For control experiments, the citrate was replaced by PBS. Figure 4.2b shows the metallic nanoparticles formed within the lipid template and obtained following the lipid removal via centrifugation in a methanol:ethanol mixture. The metallic nanostructures prepared were disk-like with  $200 \pm 11$  nm length and  $80 \pm 7$  nm width (aspect ratio between 1 and 1.5), which is 10-20 nm smaller (both length and width) than the average template size. As depicted in Figure 4.2c, a large proportion of the nanoparticles is oriented in the (111) crystal plane ( $2\theta$ ) at  $38^\circ$  with a relatively poor signal in (200) and (220) which is coherent with the crystal structure of the disk-like metal nanoparticles.<sup>46</sup>

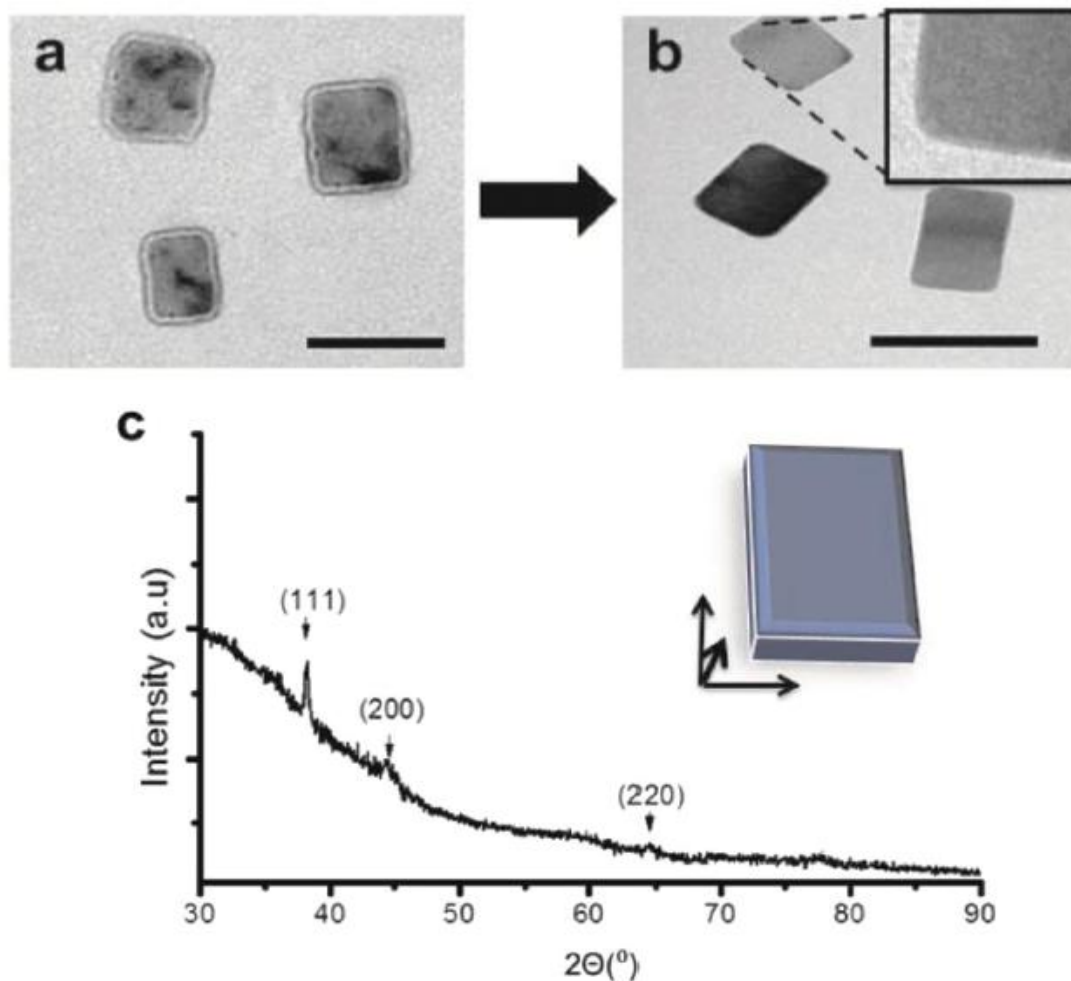


Figure 4.2. TEM images representing the square shaped templates, the purified gold nanoparticles and their XRD pattern: (a) the square shaped DPPC based lipid templates encapsulating AuCl<sub>4</sub><sup>-</sup> prepared at an operating temperature of 45 °C, (b) purified gold nanoparticles in toluene which were prepared after 72 h of incubation at room temperature. Inset: a magnified image highlighting the smooth edges of the gold nano-rectangle, and (c) their XRD pattern. Scale bars are 200 nm.

The reaction yield of the gold nanoparticle synthesis was measured by inductively coupled plasma optical emission spectrometry (ICP-OES). After the sample was subjected to centrifugation, the Au NPs were effectively separated from the unreacted Au(III). Results showed a moderate turn-over with a calculated yield of 25.6 %. As with the rectangular shaped lipids, lipidic hexagonal structures encapsulating tetrachloroauric acid and sodium citrate were prepared, respectively, from the DPPC lipid at 25 °C. Again, a 1:1 molar ratio of each was mixed and monitored for over 72 h and analysed by transmission electron microscopy (TEM) and

scanning electron microscopy (SEM) before synthesis, during synthesis and following separation of the lipids from the formed gold nanostructures by centrifugation. Even though the yield was not very high (18.9 %), a heterogeneous population, mostly of rectangular and hexagonal shaped gold nanoparticles, was obtained after 24 h where the number of particles increased after 72 h (Supp. Fig. ESI1 and Fig. ESI2<sup>†</sup>). A better control over the template shape could reveal more homogeneous distribution in the particle shape and size. In the absence of sodium citrate encapsulating liposomes, no nanoparticle structures were observed. The template size was measured as ca. 250 nm (Figure 4.3a), and the resulting particles were approximately 200-250 nm (Figure 2c and Supp. Fig. ESI1<sup>†</sup>). As can be seen from the inset of Figure 4.3b, a lipid bilayer surrounding the produced nanoparticles can be observed prior to purification. The particles produced had a tendency to grow in the (111) crystal plane (Figure 4.3c) and with the (111), (200), (220), (311) and (222) planes, equal to that of a typical XRD pattern of the face-centered cubic (fcc) structure was obtained.<sup>47,48</sup> A SEM image of a single hexagon is depicted in Figure 4.3d.

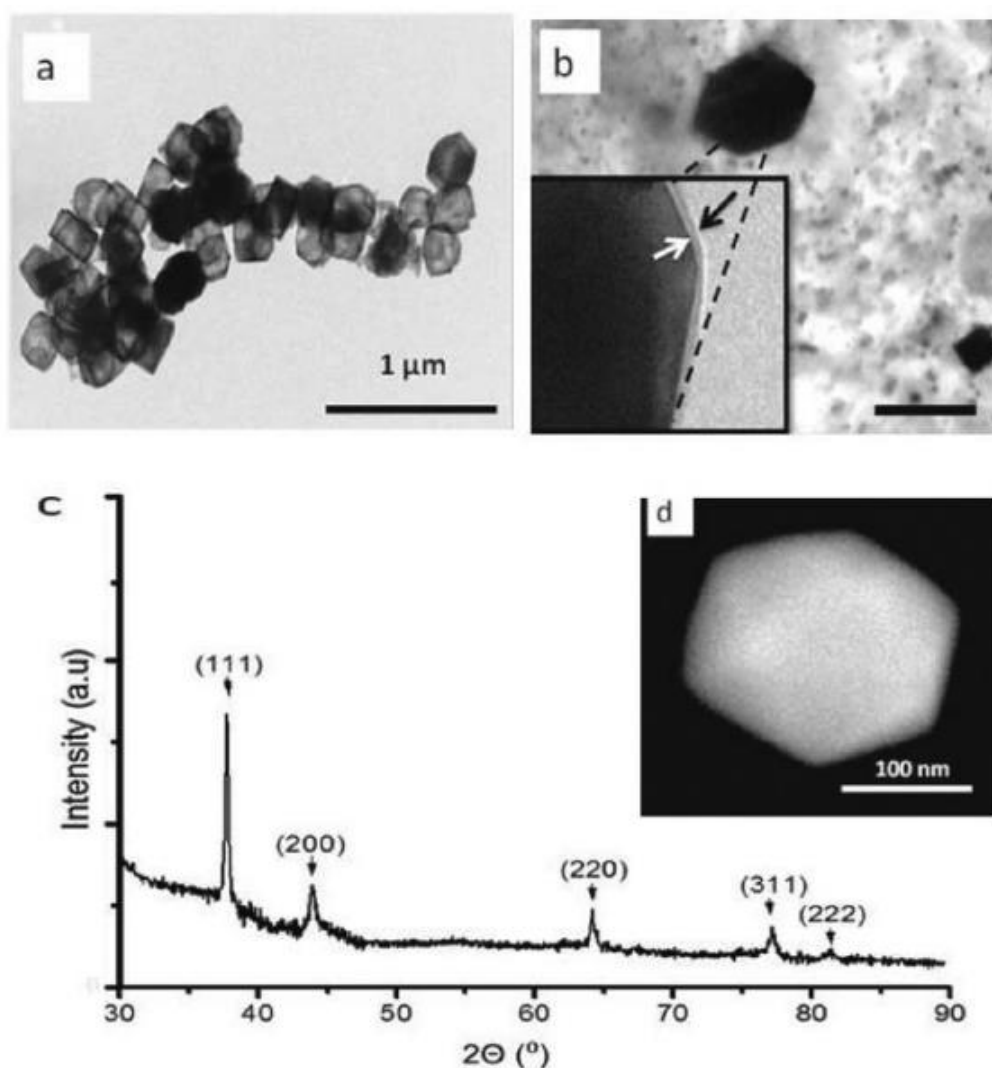


Figure 4.3. TEM images representing the hexagonal shaped templates, the purified gold nanoparticles and their XRD pattern: (a) the hexagonal shaped lipid templates formed from DPPC:LysoPPC prepared at an operating temperature of 25 °C, (b) a single hexagonal shaped gold nanoparticle before purification from lipids (inset shows a magnified TEM image in which the lipid layer on the particle is highlighted by the arrows), (c) XRD pattern and (d) SEM image of a purified gold nanostructure demonstrating the (111) face of a single hexagonal gold nanoparticle.

Whilst there are many studies on the use of nanotubes<sup>28,49</sup> as templates for inorganic particle synthesis, there are very few studies on the use of ribbons as templates for ribbon shaped metal nanostructures. Jung et al., reported self-assembled helical lipid ribbons as templates for the synthesis of palladium nanoparticles using ascorbic acid as a reducing agent, where they observed either tiny nanoparticles embedded on the template surface or solid nanostructures depending on the patterning method used.<sup>50</sup> Jin et al., in another study, reported the preparation of silica nanostructures patterned from lipid structures including ribbons, hollow spheres and other chiral materials.<sup>5</sup>

In this study, we analysed the template capacity of twisted ribbon-like lipid nanowires prepared from the DMPG lipid (Figure 4.4, Table 4.1) for the biomineralization of metal salts as demonstrated with the rectangular and hexagonal lipid templates. However, due to the multiple fusion sites available on the ribbons, which could lead to aggregation and collapse of the template, alternative routes were also considered and compared since the exchange of the lipidic contents would not occur by membrane fusion, but rather diffusion of the respective reagents across the lipid bilayer into the interior core of the ribbon-like structure would occur.

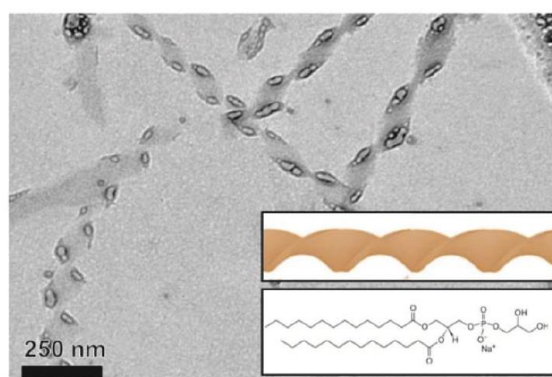


Figure 4.4. TEM images of twisted ribbon-shaped DMPG lipid self-assembly prepared at an operating temperature of 25 °C. Inset images are representative drawings of the twisted ribbon shape and chemical structure of the DMPG lipid.

Of the four different approaches used, in Method I, tetrachloroauric acid encapsulating lipid templates were directly immersed in PBS buffer and monitored for over 72 h of incubation at 25 °C as a control. Ribbon-like thin rods with slight appearance were spontaneously formed, even in the absence of a reducing agent (Figure 4.5a) with no apparent signal in XRD measurements (data not shown). This is attributed to the ability of the DMPG to act as a capping agent on gold nanoparticles and –OH groups present on the glycerol head of the lipid might act as initiators of the slow reduction of gold ions (Table 1) which took 72 h to complete.<sup>29,51</sup>

However, when HAuCl<sub>4</sub> encapsulating twisted lipid ribbons were immersed in a solution containing sodium citrate (Method II), ribbon shaped nanostructures with a more solid appearance and a stronger resemblance to the template were obtained (Figure 4.5b). The reaction yield of gold nanoribbons synthesized with this approach was calculated to be 30.5 %. In the third approach (Method III), tetrachloroauric acid and citrate encapsulating lipid structures were mixed and small nanoparticles of 2 to 5 nm, arranged in a one-dimensional ribbon shape (Figure 4.5b inset), were observed after 24 h of incubation at 25 °C. As depicted in the scheme represented in Figure 4.5-III, when two twisted encapsulating lipid ribbons are mixed, the tetrachloroauric acid and citrate interact at the contact points, and particles form at



these points due to the reduction of the Au(III) to Au(0), resulting in a nanoparticle chain which resembles the template.

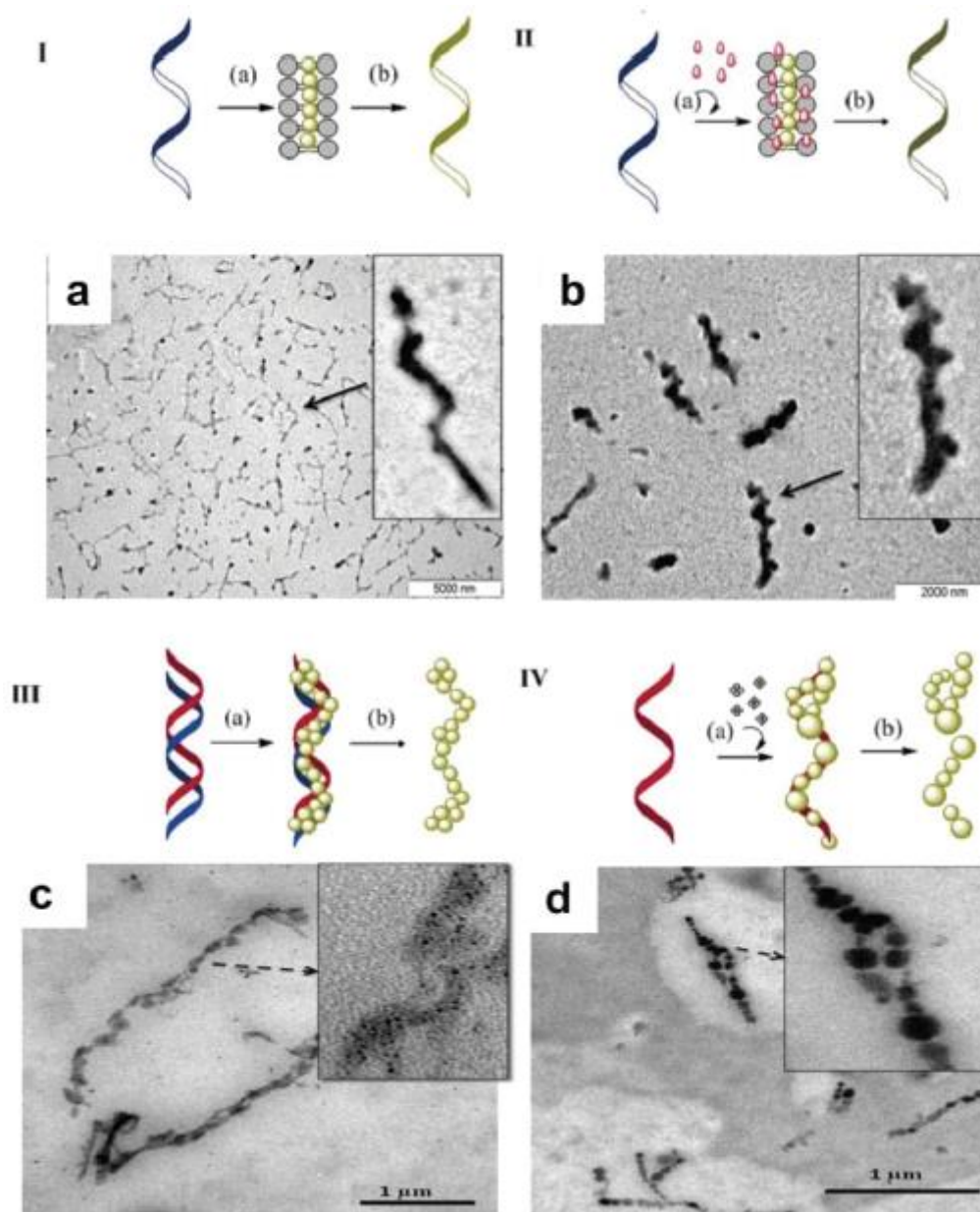


*Figure 4.5. Schemes outlining the different strategies for the use of twisted ribbon shaped lipid templates for the preparation of ribbon-like gold nanostructures and TEM images of gold nanostructures formed as a result of the methodology used. (a) Method I: tetrachloroauric acid encapsulating the lipid template alone after 72 h, (b) Method II: tetrachloroauric acid encapsulating the lipid template immersed in citrate solution, (c) Method III: the tetrachloroauric acid encapsulating and citrate encapsulating lipid template were mixed and left for 24 h at room temperature, and (d) Method IV: the citrate encapsulating lipid template was immersed directly into the tetrachloroauric acid solution.*

The same type of one-dimensional particle alignment as obtained in Method III was observed when the citrate encapsulating lipid template was immersed in chloroauric acid solution in PBS (pH 7.4, 10 mM, 25 °C) (Method IV). The particles were around 15 nm (Figure 4.5d), and were arranged in a nanoparticle chain type structure guided by the dimensions of the lipid template. These structures were formed due to the interaction between the tetrachloroauric acid and the citrate diffusing from the bilayer core. This facilitated rapid nucleation of particles on the

diffusion sites of the template where they further aggregated to form chains aligned one after the other (Figure 4.5d). Both chain shaped and ribbon shaped gold nanostructures were stored at room temperature for a month. TEM studies showed no apparent aggregation during that period of time, demonstrating the stability of the resulting nanostructures.

When we analysed the crystal properties of the metallic nanostructures obtained using the different methods, nanostructures obtained in the presence of a lipid template (Method I) and by mixing lipid structures encapsulating citrate and tetrachloroauric acid (Method III) showed no apparent signal. On the other hand, the ribbon-like structures obtained in Method II and nanochains obtained in Method IV showed a typical pattern of the face centered cubic structure with higher and distinctive signal dominated at a  $2\theta$  of  $38^\circ$  assigned to the (111) face and also a distinctive peak at a  $2\theta$  of  $44.5^\circ$  assigned to the (200) face (Figure 4.6). Twisted Au nanoribbons demonstrated a pattern of a two-fold symmetry with an additional lattice spacing at (222). These results suggest that both samples mostly consist of one dimensional arrangement that were preferentially oriented with their (111) planes, therefore attributing to a significantly high (111) reflection intensity.

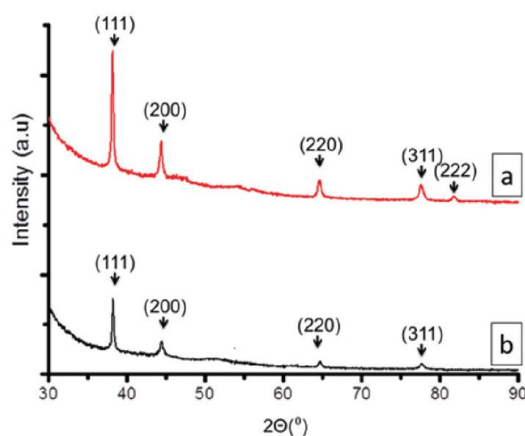


Figure 4.6. XRD pattern of nanostructures synthesized. Both ribbon shaped gold nanostructures (a) and nanochains (b), prepared via Method II and Method IV, respectively, positioned dominantly in the (111) crystal plane with a more distinctive intensity at (111) and (200) faces in the case of gold nanoribbons.

#### 4.4. Conclusions

The work reported here examines the potential of the lipid nanostructures as soft matter templates for metal biomineralization. Unusual lipid nanostructures including rectangular, hexagonal and twisted ribbons were formed via the curvature tuned preparation method and used as templates for gold nanostructures. The resulting nanostructures' shape was mostly patterned by the template and the homogeneity of the particles formed was directly dependent on the homogeneity of the template shape. Ribbon shaped lipidic nanostructures resulted in diverse types of nanostructures where atomic alignment was strongly dependent on the biomineralization approach chosen and the direction was driven by the template shape (e.g. ribbon and chain-like alignments). Resulting twisted gold nanoribbons showed a typical face centered cubic structure primarily dominated by (111) facets. In conclusion, self-assembled lipid based nanostructures were demonstrated to be promising tools for the synthesis of metal nanoparticles of controlled morphology and size. The possibility to prepare diversely shaped and

sized nanoparticles under mild conditions should find a plethora of potential applications in catalysis, plasmonics and electronics.

#### 4.5. Acknowledgements

Authors would like to thank H. U. Genc for his contribution to the design and drawing of 2D illustrations used in Figure 4.1.

#### 4.6. References

- 1 A. Zidovska, K. K. Ewert, J. Quispe, B. Carragher, C. S. Potter and C. R. Safinya, *Langmuir*, **2009**, 25, 2979–2985.
- 2 D. J. Keller, H. M. McConnell and V. T. Moy, *J. Phys. Chem.*, **1986**, 90, 2311–2315.
- 3 A. Wenzel and M. Antonietti, *Adv. Mater.*, **1997**, 9, 487–490.
- 4 Y. Zhou, *Crit. Rev. Solid State Mater. Sci.*, **2008**, 33, 183–196.
- 5 H. Jin, H. Qiu, Y. Sakamoto, P. Shu, O. Terasaki and S. Che, *Chemistry*, **2008**, 14, 6413–6420.
- 6 M. S. Spector, A. Singh, P. B. Messersmith and J. M. Schnur, *Nano Lett.*, **2001**, 1, 375–378.
- 7 B. J. Boyd, S. B. Rizwan, Y.-D. Dong, S. Hook and T. Rades, *Langmuir*, **2007**, 23, 12461–12464.
- 8 M. Qiao, D. Chen, X. Ma and Y. Liu, *Int. J. Pharm.*, **2003**, 260, 239–247.
- 9 J. Barauskas, M. Johnsson and F. Tiberg, *Nano Lett.*, **2005**, 5, 1615–1619.
- 10 J. Fang, *J. Mater. Chem.*, **2007**, 17, 3479.
- 11 E. M. Wilson-Kubalek, R. E. Brown, H. Celia and R. A. Milligan, *Proc. Natl. Acad. Sci. U. S. A.*, **1998**, 95, 8040–8045.
- 12 Q. Ji and T. Shimizu, *Chem. Commun.*, **2005**, 4411–4413.
- 13 X. Pan, K. Han, X. Peng, Z. Yang, L. Qin, C. Zhu, X. Huang, X. Shi, L. Dian, M. Lu and C. Wu, *Curr. Pharm. Des.*, **2013**, 19(35), 6290–6297.
- 14 Y. Xia, Y. Xiong, B. Lim and S. E. Skrabalak, *Angew. Chem. Int. Ed.*, **2009**, 48(1), 60–103.
- 15 W. L. Johnson, S. A. Kim, Z. N. Utegulov, J. M. Shaw and B. T. Draine, *J. Phys. Chem. C*, **2009**, 113, 14651–14657.
- 16 C. J. Johnson, E. Dujardin, S. A. Davis, C. J. Murphy and S. Mann, *J. Mater. Chem.*, **2002**, 12, 1765–1770.
- 17 W. Jia, J. Li and L. Jiang, *ACS Appl. Mater. Interfaces*, **2013**, 5, 6886–6892.
- 18 S. E. Skrabalak, J. Chen, Y. Sun, X. Lu, L. Au, C. M. Cobley and Y. Xia, *Acc. Chem. Res.*, **2008**, 41, 1587–1595.
- 19 P. C. Stevenson, *Discuss. Faraday Soc.*, **1951**, 55, 55.
- 20 G. Schmid, R. Pfeil, R. Boese, F. Bandermann, S. Meyer, G. H. M. Calis and J. W. A. van der Velden, *Chem. Ber.*, **1981**, 114, 3634–3642.



- 21 B. Nikoobakht and M. A. El-Sayed, *Chem. Mater.*, **2003**, 15, 1957–1962.
- 22 W. Lu, B. Wang, K. Wang, X. Wang and J. G. Hou, *Langmuir*, **2003**, 19, 5887–5891.
- 23 G. Sears, *Acta Metall.*, **1955**, 3, 367–369.
- 24 H. H. Song, K. M. Jones and A. A. Baski, *J. Vac. Sci. Technol., A*, **1999**, 17, 1696.
- 25 K. Naoe, M. Kataoka and M. Kawagoe, *Colloids Surf., A: Physicochemical and Engineering Aspects*, **2010**, 364, 116–122.
- 26 N. R. Jana, L. Gearheart and C. J. Murphy, *J. Phys. Chem. B*, **2001**, 105, 4065–4067.
- 27 H. Yan, S. Cingarapu, K. J. Klabunde, A. Chakrabarti and C. M. Sorensen, *Phys. Rev. Lett.*, **2009**, 095501, 1–4.
- 28 H. Acar, R. Garifullin and M. O. Guler, *Langmuir*, **2011**, 27, 1079–1084.
- 29 R. Genç, G. Clergeaud, M. Ortiz and C. K. O’Sullivan, *Langmuir*, **2011**, 27, 10894–10900.
- 30 M. A. Khalily, O. Ustahuseyin, R. Garifullin, R. Genc and M. O. Guler, *Chem. Commun.*, **2012**, 48, 11358–11360.
- 31 J. P. Cason, M. E. Miller, J. B. Thompson and C. B. Roberts, *J. Phys. Chem. B*, **2001**, 105, 2297–2302.
- 32 H. Sato, T. Hirai and I. Komasa, *Ind. Eng. Chem. Res.*, **1995**, 34, 2493–2498.
- 33 R. P. Bagwe and K. C. Khilar, *Langmuir*, **2000**, 16, 905–910.
- 34 J. Eastoe and A. R. Cox, *Colloids Surf., A: Physicochemical and Engineering Aspects*, **1995**, 101, 63–76.
- 35 A. B. Smetana, J. S. Wang, J. Boeckl, G. J. Brown and C. M. Wai, *Langmuir*, **2007**, 23, 10429–10432.
- 36 S.-J. Cho, J.-C. Idrobo, J. Olamit, K. Liu, N. D. Browning and S. M. Kauzlarich, *Chem. Mater.*, **2005**, 17, 3181–3186.
- 37 Y. Zhou and T. Shimizu, *Chem. Mater.*, **2007**, 625–633.
- 38 S. Schuerle, S. Pané, E. Pellicer, J. Sort, M. D. Baró and B. J. Nelson, *Small*, **2012**, 8, 1498–1502.
- 39 G. Clergeaud, R. Genç, M. Ortiz and C. K. O’Sullivan, *Langmuir*, **2013**, 29(49), 15405–15413.
- 40 P. O. G. Mouritsen, *Life - As a Matter of Fat*, Springer-Verlag, Berlin/Heidelberg, **2005**.
- 41 R. Genç, M. Ortiz and C. K. O’Sullivan, *Langmuir*, **2009**, 25, 12604–12613.
- 42 R. Genç, G. Clergeaud, M. Ortiz and C. K. O’Sullivan, *Langmuir*, **2011**, 27, 10894–10900.
- 43 M.-P. Pileni, *Nat. Mater.*, **2003**, 2, 145–150.
- 44 M. M. Félix, H. Umakoshi, T. Shimanouchi, M. Yoshimoto and R. Kuboi, *Biochem. Eng. J.*, **2002**, 12, 7–19.
- 45 S. Nir, J. Bentz, J. Wilschut and N. Duzgunes, *Prog. Surf. Sci.*, **1983**, 13, 1–124.
- 46 W. Niu and G. Xu, *Nano Today*, **2011**, 6, 265–285.

47 Y. Chen, X. Gu, C.-G. Nie, Z.-Y. Jiang, Z.-X. Xie and C.-J. Lin, *Chem. Commun.*, **2005**, 1, 4181–4183.

48 J. Chai, F. Li, Y. Hu, Q. Zhang, D. Han and L. Niu, *J. Mater. Chem.*, **2011**, 21, 17922.

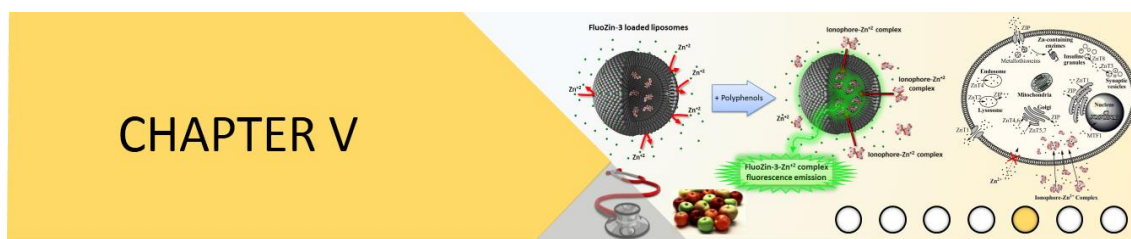
49 H. Ma, H. Chi, J. Wu, M. Wang, J. Li, H. Hoshina, S. Saiki and N. Seko, *ACS Appl. Mater. Interfaces*, **2013**, 5(17), 8761–8765.

50 J. H. Jung, J. A. Rim, S. J. Lee and S. S. Lee, *Chem. Commun.*, **2005**, 468–470.

51 M. S. Bakshi, F. Possmayer and N. O. Petersen, *J. Phys. Chem. C*, **2007**, 111, 14113–14124.



## CHAPTER V



Zinc ionophore activity of quercetin  
and epigallocatechin-gallate: From  
Hepa1-6 cells to a liposome model



## Zinc ionophore activity of quercetin and epigallocatechin-gallate: From Hepa1-6 cells to a liposome model

*J. Agric. Food Chem.* **2014**, *62*, 8085–8093

Husam Dabbagh-Bazarbachi,<sup>†,‡</sup> Gael Clergeaud,<sup>‡,‡</sup> Isabel M. Quesada,<sup>§</sup> Mayreli Ortiz,<sup>‡</sup>  
Ciara K. O’Sullivan,<sup>\*,‡,||</sup> and Juan B. Fernández-Larrea<sup>\*,†</sup>

<sup>†</sup> Nutrigenomics Research Group, Department of Biochemistry and Biotechnology, and

<sup>‡</sup> Nanobiotechnology & Bioanalysis Group, Department of Chemical Engineering, Universitat Rovira i Virgili, 43007 Tarragona, Spain

<sup>§</sup> Vascular Biology Laboratory, IMBECU-CONICET, Facultad de Ciencias Médicas, Universidad Nacional de Cuyo, 5500 Mendoza, Argentina

<sup>||</sup> Institució Catalana de Recerca i Estudis Avançats, 08010 Barcelona, Spain

<sup>‡</sup> Husam Dabbagh-Bazarbachi and Gael Clergeaud contributed equally to this work.



## 5.1. Abstract

Labile zinc, a tiny fraction of total intracellular zinc that is loosely bound to proteins and easily interchangeable, modulates the activity of numerous signaling and metabolic pathways. Dietary plant polyphenols such as the flavonoids quercetin and epigallocatechin-gallate act as antioxidants and as signaling molecules. Remarkably, the activities of numerous enzymes that are targeted by polyphenols are dependent on zinc. We have previously shown that these polyphenols chelate zinc cations and hypothesized that these flavonoids might be also acting as zinc ionophores, transporting zinc cations through the plasma membrane. To prove this hypothesis, herein, we have demonstrated the capacity of quercetin and epigallocatechin-gallate to rapidly increase labile zinc in mouse hepatocarcinoma Hepa 1-6 cells as well as, for the first time, in liposomes. In order to confirm that the polyphenols transport zinc cations across the plasma membrane independently of plasma membrane zinc transporters, quercetin, epigallocatechin-gallate, or clioquinol, alone and combined with zinc, were added to unilamellar dipalmitoylphosphocholine:cholesterol liposomes loaded with membrane-impermeant FluoZin-3. Only the combinations of the chelators with zinc triggered a rapid increase of FluoZin-3 fluorescence within the liposomes, thus demonstrating the ionophore action of quercetin, epigallocatechin-gallate, and clioquinol on lipid membrane systems. The ionophore activity of dietary polyphenols may underlay the raising of labile zinc levels triggered in cells by polyphenols and thus many of their biological actions.

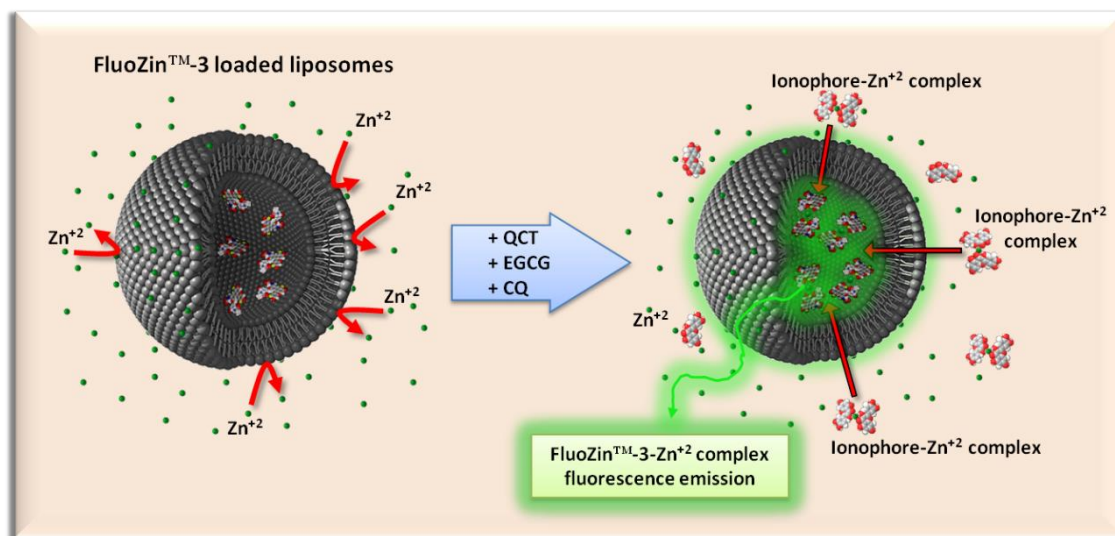


Figure 5.1. Table of contents figure

## 5.2. Introduction

Quercetin (QCT), a water-insoluble flavonoid present in onions, nuts, and many other vegetables, and epigallocatechin-3-gallate (EGCG), a water-soluble flavonoid present in green tea, are among the most consumed and most studied polyphenols present in the human diet.<sup>1</sup> Flavonoids are considered bioactive micronutrients whose regular consumption, either as food components, or as dietary supplements and nutraceuticals,<sup>2</sup> entails benefits for human health, including prevention and amelioration of cancers,<sup>3</sup> diabetes, and cardiovascular<sup>4</sup> and neurodegenerative<sup>5</sup> diseases. Many of the health benefits of flavonoids have historically been ascribed to their antioxidant activity, which they exert directly by scavenging reactive oxygen



species (ROS) and by chelating the redox-active transition metals iron and copper, which may act as ROS generators in biological systems.<sup>6</sup> Flavonoids also act as antioxidants indirectly by inhibiting redox-sensitive transcription factors and pro-oxidant enzymes as well as through induction of phase II and antioxidant enzymes.<sup>7</sup> However, it is currently believed that the levels of polyphenols achieved through ingestion are not enough to justify their wide array of biological actions. Beyond their antioxidant actions, flavonoids are also known to act as signaling molecules that, either directly or indirectly, interact with proteins and nucleic acids, thus modulating multiple cell signaling pathways, gene transcription, metabolic fluxes, and cell fate including apoptosis.<sup>8,9</sup>

Diverse polyphenols have been shown able to form complexes with the redox-inactive transition metal zinc.<sup>10</sup> Zinc is an essential micronutrient for humans, the deficiency of which causes multiple dysfunctions, including alterations of glucidic and lipidic metabolisms.<sup>11</sup> Within cells, the vast majority of zinc cations (in concentrations usually ranging from 100 to 300  $\mu\text{M}$  for most cells) are tightly bound to proteins, functioning as a catalytic or structural component of an estimated 3000 mammalian proteins involved in virtually all cellular processes.<sup>12</sup> A minor fraction of intracellular zinc, termed labile zinc, exists in its free ionic form (picomolar concentrations) or loosely bound to proteins (in nanomolar concentrations). This pool of zinc is detectable by specific fluorophores with very high affinities for zinc cations at neutral pH such as Zinquin and FluoZin-3. Zinc ionophores such as pyrithione and clioquinol (CQ) have been used to increment labile zinc within cells and determine the fundamental roles that this zinc pool plays in cellular biology. Thus, free and labile zinc acts as second messenger molecule, which modulates the activity of many enzymes and thus signaling and metabolic pathways and cellular processes, including cell fate and apoptosis.<sup>13,14</sup> While many enzymes are inhibited by small elevations of zinc concentrations, others are activated.<sup>15,16</sup> Mammalian cells tightly control the subcellular distribution of zinc cations and the levels of labile zinc through the coordinated action of dedicated transmembrane zinc transporters and zinc-chelating metallothioneins.

Zinc from the extracellular milieu and from intracellular compartments enters the cytoplasm through 14 specialized transmembrane proteins of the ZIP/SLC39 family, whereas cytoplasmic extrusion of zinc toward organelles or the extracellular environment is performed by 10 transporters of the ZnT/SLC30 family, being ZnT1, located at the plasma membrane, the main regulator of cellular zinc efflux and export of excess zinc in most cells.<sup>17</sup> Within the cytoplasm, zinc may bind to metal free apo-metallothionein (apo-MT) to generate Zn-MT complexes. The apo-MT/Zn-MT ratio controls free and labile zinc concentrations. MT also serves as a ROS scavenger and heavy metal chelator, and the transcription of MT responds, in addition to zinc, to stress stimuli such as ROS, heavy metals, and pro-inflammatory cytokines.<sup>18</sup> In response to elevations of intracellular zinc, the zinc-sensor transcription factor MTF1 coordinately up-regulates the expression of MT and ZnT1,<sup>19</sup> thus keeping zinc levels within a functional range. Excessively high levels of labile zinc are associated with cellular death through apoptosis.<sup>20</sup> Dysfunctions of MT and zinc transporters are promoting factors in cardiovascular diseases,<sup>21</sup> diabetes,<sup>22</sup> Alzheimer's disease,<sup>23</sup> and cancer.<sup>24</sup>

Several studies have shown that flavonoids affect zinc metabolism. For instance, rats fed during long periods with bicalain and rutin showed reduced hepatic levels of total zinc, as well as iron and copper, implying that flavonoids may sequester these metals and render them unavailable for absorption in a similar way as phytate.<sup>25</sup> Consistent with this, feeding obese rats with proanthocyanidins reverse dyslipidemia and lower protein levels of ZnT1 in the liver, reflecting lower levels of hepatic zinc.<sup>26</sup> Early in vitro studies showed that, in human intestinal Caco-2 cells,

genistein enhanced the expression of MT, here regarded as an antioxidant enzyme,<sup>27</sup> while QCT increased the copper-induced expression of MT.<sup>28</sup> More recently, QCT was shown to enhance zinc uptake by Caco-2 cells, increasing total zinc accumulation and MT expression.<sup>29</sup> In contrast, grape seed flavonoids, produced a reduction in apical zinc uptake in Caco-2 cells, similar to that produced by phytate, whereas EGCG did not alter zinc absorption.<sup>30</sup> In prostate cancer cells, EGCG accelerated the accumulation of total zinc in the cytosol and mitochondria.<sup>31</sup> Two reports have shown that polyphenols may produce an increase of intracellular labile zinc. A water-soluble glycoside of the isoflavone genistin enhanced MT expression in human hepatocarcinoma HepG2 cells concomitantly increasing labile zinc and cellular death.<sup>32</sup> Furthermore, the stilbene resveratrol was shown to enhance total and labile zinc in normal human prostate epithelial cells, while not significantly affecting MT expression, and this was accompanied by increased cellular death. These authors suggested that the increment of labile zinc elicited by resveratrol might be due to the uptake of resveratrol-zinc complexes, followed by the dissociation of the complexes in the cytoplasm.<sup>33</sup>

Conversely, zinc may affect the bioactivity of flavonoids, as detailed in a few reports, including one that outlines the stimulating effect of zinc on the apoptotic effect of genistein in osteoclastic cells.<sup>34</sup> Zinc also yields EGCG effective in protecting cultured rat hepatocytes against hepatotoxin-induced cell injury<sup>35</sup> and enhances the antiproliferative, proapoptotic effects of EGCG on various lines of prostate cancer cells.<sup>36</sup> Zinc was also shown to affect the uptake of EGCG by prostate carcinoma cells, where Zn-EGCG chelates were less internalized by cells than EGCG alone, while mixtures of EGCG with zinc enhanced the transport of EGCG into the cells. These authors also showed that zinc enhances the incorporation of EGCG into liposomes.<sup>37</sup>

We have previously reported that the water-soluble flavonoid EGCG and the water-insoluble flavonoid QCT profoundly alter zinc homeostasis in cultured human and mouse hepatocarcinoma cells. Whereas EGCG reduced the levels of total intracellular zinc and the expression of MT and ZnT1,<sup>38</sup> QCT enhanced total zinc accumulation as well as MT and ZnT1 expression (M. Bustos, personal communication, 2011, Universitat Rovira i Virgili). However, both QCT and EGCG dose-dependently prevented zinc-induced toxicity, suggesting that most zinc cations in the culture medium are rendered unavailable to cells due to their chelation by flavonoids and the formation of flavonoid-zinc concatemers, as shown for iron and copper complexed with diverse polyphenols.<sup>39</sup> In addition, both polyphenols enhanced cytoplasmic levels of Zinquin-detectable labile zinc, suggesting that a fraction of the flavonoid molecules in the culture medium formed complexes with zinc that cross the plasma membrane; that is, the flavonoids may also act as zinc ionophores, transporting zinc cations across the plasma membrane independently from zinc transporters.

The aim of this work was to evaluate the capacity of QCT and EGCG to act as zinc ionophores. CQ was also tested in this study as it is a synthetic antitumor drug recently reported to induce apoptosis in diverse cells lines by enhancing intracellular labile zinc and therefore inferred to act as a water-soluble zinc ionophore.<sup>40</sup> We evaluated the ability of QCT, EGCG, and CQ to chelate zinc cations and the subsequent formation of a complex with FluoZin-3, a fluorophore that displays a very high affinity for zinc cations ( $K_d = 15$  nM).<sup>41</sup> The uptake of zinc by mouse hepatocarcinoma cells was measured fluorescently using FluoZin-3 in the presence and absence of QCT, EGCG, and CQ. This study was repeated using unilamellar liposomes with encapsulated FluoZin-3 to investigate whether the transport of the zinc cations across the cytoplasmic membrane to form a complex with FluoZin-3 was indeed enhanced by the presence of QCT, EGCG, or CQ or was simply due to the activity of cellular zinc transporters.

## 5.3. Materials and methods

### 5.3.1. Chemicals

The lipid 1,2-dipalmitoyl-sn-glycero-3-phosphocholine (DPPC), cholesterol, zinc chloride ( $\text{ZnCl}_2$ ), QCT, EGCG, CQ, dimethyl sulfoxide (DMSO), ethanol, and phosphate-buffered saline (0.01 M PBS, pH 7.4) were bought from Sigma-Aldrich. Cell-impermeant FluoZin-3 tetrapotassium salt and cell permeant FluoZin-3 AM were bought from Molecular Probes. A Simplicity 185 Millipore water system was used to obtain Milli-Q water ( $18.2 \text{ m}\Omega\text{-cm}^{-1}$ ) for the preparation of buffers and liposomes. The compounds QCT, EGCG, and CQ were dissolved as 100  $\mu\text{M}$  solutions in 100% DMSO, aliquoted, and stored at  $-20 \text{ }^\circ\text{C}$ .  $\text{ZnCl}_2$  was stored as 1 M solution in ethanol/PBS (50%/50% v/v). FluoZin-3 indicators were used at 10  $\mu\text{M}$  in 100% DMSO.

### 5.3.2. Cell culture and treatments

The mouse hepatoma cell line Hepa 1-6 was obtained from the European Collection of Cell Cultures (BW7756 ECACC) and propagated in Dulbecco's Modified Eagle medium (DMEM; BioWittaker) supplemented with 10% fetal bovine serum (BioWittaker), 2 mM glutamine in 0.85% NaCl, 1000 U/mL penicillin/streptomycin, and 1.25 M HEPES. This medium contains  $4.9 \pm 0.2 \text{ }\mu\text{M}$  zinc, as determined by flame atomic absorption spectroscopy (FAAS). Cells were cultured at  $37 \text{ }^\circ\text{C}$  in a humidified, 5%  $\text{CO}_2$ -enriched atmosphere and routinely split every 3-4 days at a 1:5 ratio upon reaching approximately 80% confluence. For treatments, cells at 80% confluence were detached with Accutase (Sigma-Aldrich) and resuspended at a density of  $5 \times 10^5$  cells/mL; 500  $\mu\text{L}$  of this cell suspension ( $25 \times 10^4$  cells) was then seeded per well in 24-well plates (Orange Scientific). Twenty four hours after plating, medium was removed, and the cells were treated by adding 100  $\mu\text{L}$  of fresh medium containing either 50  $\mu\text{M}$   $\text{ZnCl}_2$ , 100  $\mu\text{M}$  QCT, 100  $\mu\text{M}$  EGCG, 100  $\mu\text{M}$  CQ, or the combination of 50  $\mu\text{M}$   $\text{ZnCl}_2$  with each chelator for 1 and 4 h, respectively. As a control experiment, untreated cells were incubated just with medium and vehicle (final 0.1% DMSO and 0.05% ethanol).

### 5.3.3. Measurements of cytoplasmic labile zinc in Hepa 1-6 cells

The intracellular levels of free and labile zinc cations were measured as the fluorescence emission of cells upon loading them with the membrane-permeant zinc specific detector FluoZin-3, using fluorescence microscopy as described.<sup>42</sup> Briefly, following cell treatment (Section 2.2), culture media were replaced with a fresh one containing 1.5  $\mu\text{M}$  FluoZin-3 (AM, cell permeant) and incubated for 30 min at  $37 \text{ }^\circ\text{C}$ . This medium was then removed, and the cells were washed three times with PBS, and the zinc-dependent FluoZin-3 fluorescence within cells was measured using a Nikon Eclipse TE2000-S microscope, with excitation set at 494 nm and emission at 516 nm. Fluorescent intensities were quantified using the NIS-Elements AR software (Nikon Instruments) and the software ImageJ, a Java-based image processing program developed at the NIH (National Institutes of Health).<sup>43</sup>

### 5.3.4. Liposomes as cell membrane models

Homogeneous populations of liposomes were prepared using a previously reported method.<sup>44</sup> FluoZin-3 in a final concentration of 3  $\mu\text{M}$  was mixed with 5 mL of PBS (0.01 M, pH 7.4) in a glass reactor protected from light induced degradation, under stirring conditions and a blanket of argon gas. After 15 min, a mixture of DPPC and cholesterol (9:1 molar ratio) was added and maintained under stirring conditions and argon at  $25 \text{ }^\circ\text{C}$  for another 15 min. The homogeneous

mixture was then treated with a rapid pH jump from pH 7.4 to pH 11 and then back to pH 7.4 within a 3 s frame, followed by an equilibration step of 25 min where lipid clusters curl into FluoZin-3 encapsulating liposomes. The resulting FluoZin-3 loaded liposomes were purified using a Sephadex G-100 size-separation column and used immediately. Liposomes with encapsulated FluoZin-3 were separately incubated with 10  $\mu\text{M}$  QCT, EGCG or CQ, in the presence and absence of 10  $\mu\text{M}$   $\text{ZnCl}_2$ . All the solutions were allowed to incubate at 25  $^\circ\text{C}$  for 30 min before measuring their fluorescence. For the kinetic experiment, liposomes loaded with FluoZin-3 were added to three different cuvettes, the fluorescence was measured for 15 min, followed by addition of  $\text{ZnCl}_2$  (final 10  $\mu\text{M}$ ) to each cuvette, and the fluorescence emission was measured for another 15 min. Finally, QCT, EGCG, or CQ was added (final 10  $\mu\text{M}$ ) to each sample, and fluorescence emission was monitored over the duration of 1 h until the fluorescent intensity reached a plateau.

## 5.4. Results

### 5.4.1. QCT, EGCG, and CQ increase the cytoplasmic labile zinc in Hepa 1-6 cells

The increase of cytoplasmic labile zinc is modulated by the cellular zinc transporters, where the zinc ions are transported to the cytoplasm through specific channels of the ZIP family, bound to ionophore molecules that independently cross the lipid bilayer, or liberated from zinc binding proteins such as metallothioneins (Figure 5.2).

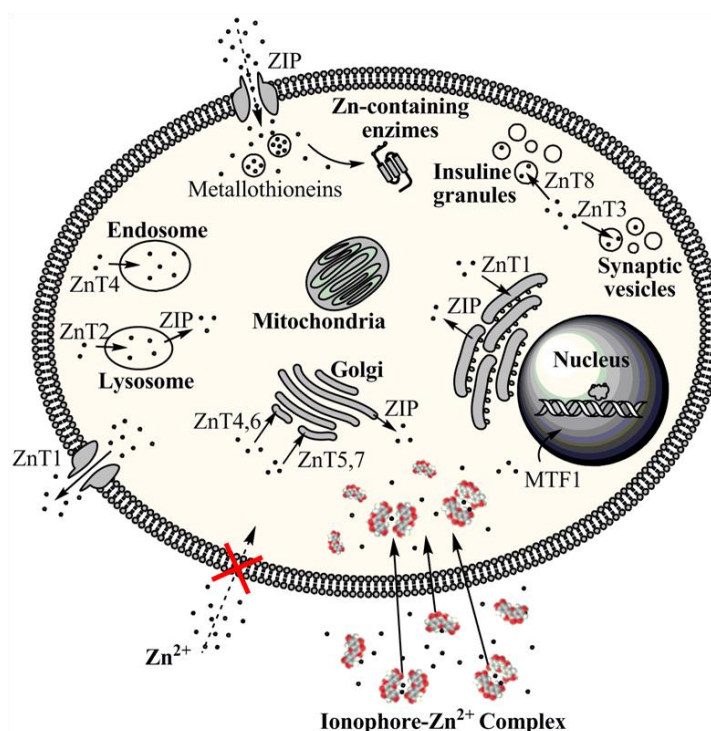


Figure 5.2. Schematic representation of zinc homeostasis. Intracellular labile zinc is modulated by the coordinated activity of a large family of zinc transporters (ZnT and ZIP) and zinc-binding proteins, such as metallothionein or ionophore molecules.

In order to assess the effect of QCT, EGCG, CQ and zinc on cytoplasmic labile zinc, Hepa 1-6 cells were treated for 1 and 4 h with the chelators and supplemental zinc, and variations in the intracellular levels of labile zinc were measured as changes in the FluoZin-3 fluorescence intensity as described in Section 2.3. Figure 5.3 shows the fluorescent images of the Hepa 1-6

cells after 1 and 4 h of treatment. No significant increase in fluorescence was obtained when QCT or EGCG were added to the culture medium without additional zinc. Only CQ insignificantly enhanced the fluorescence in these conditions, that is, with basal zinc concentration in the culture medium, which is roughly 5  $\mu\text{M}$ .

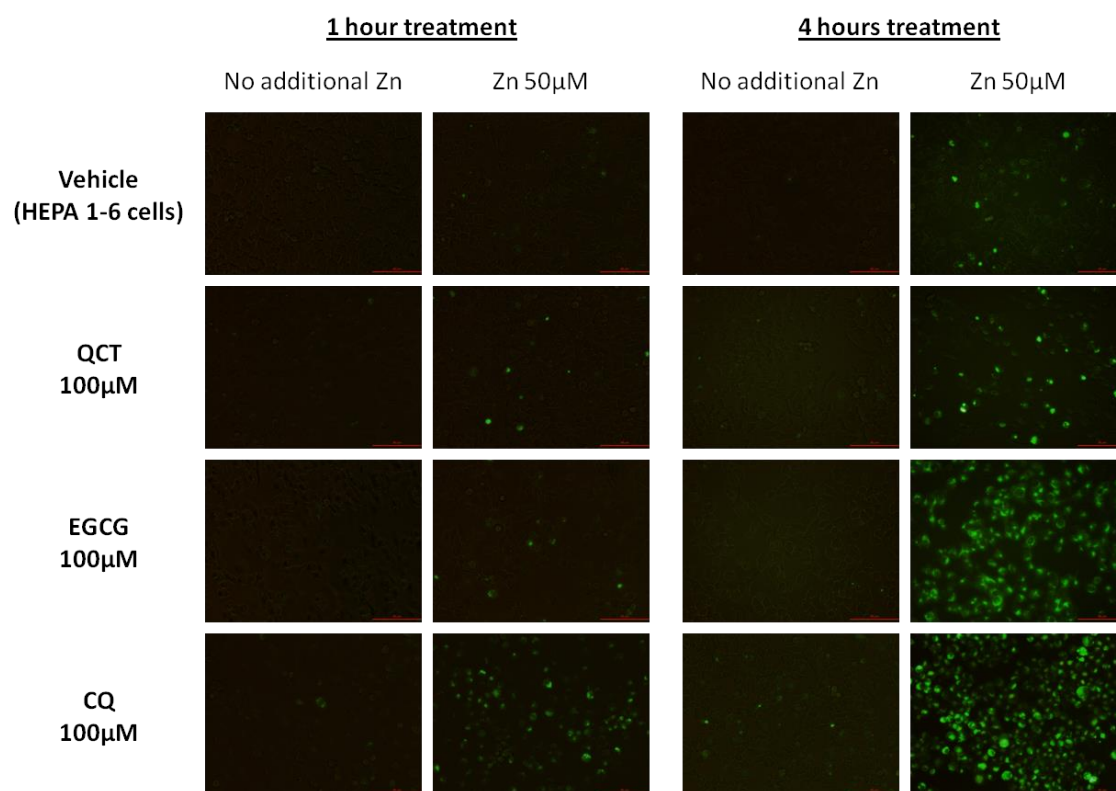


Figure 5.3. Effect of QCT, EGCG, and CQ on the cytoplasmic pool of labile zinc in Hepa 1-6 cells. Hepa 1-6 cells were first treated with 100  $\mu\text{M}$  QCT, EGCG, or CQ, in the presence or absence of 50  $\mu\text{M}$   $\text{ZnCl}_2$  for 1 and 4 h. The medium was then removed, and 3  $\mu\text{M}$  FluoZin-3 (AM, cell permeant) was added. After 30 min incubation, cells were washed and examined using a confocal fluorescence microscope. Control cells were treated with vehicle (final 0.05% ethanol, 0.1% DMSO). Scale bars are 50  $\mu\text{m}$ .

However, when 50  $\mu\text{M}$   $\text{ZnCl}_2$  was added, both QCT and EGCG doubled the amount of FluoZin-3-detectable zinc after 1 h, and CQ increased this pool of zinc 10-fold with respect to the control (50  $\mu\text{M}$   $\text{ZnCl}_2$  in the absence of any of QCT, EGCG or CQ) (Figure 5.4), suggesting a slower ionophore action of the flavonoids as compared to CQ. After 4 h treatment with additional 50  $\mu\text{M}$   $\text{ZnCl}_2$ , all treatments triggered a significant increase in fluorescence intensity. In the case of the control, the increase of the cytoplasmic labile zinc is associated with the plasma membrane ZIP transporters, whereby zinc ions are transported into the cell. QCT doubled the amount of labile zinc attained with only 50  $\mu\text{M}$  zinc, EGCG quadrupled this value, and CQ increased it 7-fold.

A closer view of intracellular distribution of FluoZin-3 fluorescence (Figure 5.5) after 4 h of treatment shows a similar punctuated pattern of labile zinc for CQ, EGCG and QCT, suggesting similar ways of action for the three compounds.



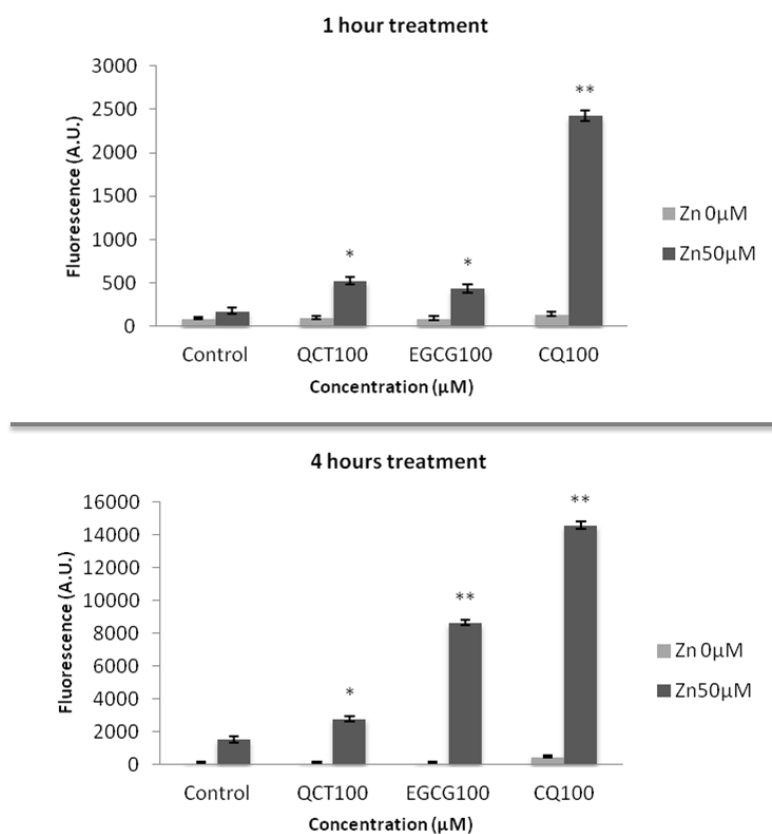


Figure 5.4. Intensity of FluoZin-3 fluorescence signal from images in Figure 5.3 was quantified using quanta program and considering an equal number of cells in each field. All values are mean  $\pm$  SEM of three independent experiments. Significant differences between treatments were determined using one-way ANOVA (Tukey test). \* $P \leq 0.05$ ; \*\* $P \leq 0.01$ .

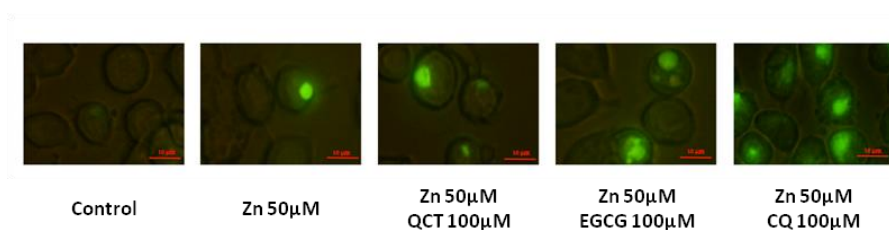


Figure 5.5. Subcellular localization of FluoZin-3 detectable zinc in Hepa 1-6 cells after 4 h treatment in the same samples as in Figure 5.3 showed at a greater magnification. Scale bars are 10  $\mu$ m.

#### 5.4.2. Zinc ionophore activity of QCT, EGCG, and CQ using liposomes as membrane models

Increases of cytoplasmic labile zinc levels triggered by CQ and pyrithione in a variety of cell lines have been attributed to their ionophore activity, that is, to the capacity of CQ-zinc and pyrithione-zinc complexes to cross the plasma membrane. To our knowledge, however, the classification of CQ and pyrithione as zinc ionophores is based on their functional effect in cells, that is, the rapid increase in Zinquin-detectable or FluoZin-3-detectable intracellular zinc, but no direct biochemical assay has been performed to discard the involvement of plasma membrane zinc importers or the origin of labile zinc from intracellular components on this effect. Furthermore, there is no report confirming that polyphenols are able to transport zinc across

the plasma membrane independently of cell transport mechanisms, such as zinc transporters or endocytosis. To directly prove the ionophore action of the flavonoids and CQ, we tested their capacity to transport zinc cations across the lipid bilayer of protein-free liposomes as a model system that mimics a cell membrane devoid of protein and polysaccharide fractions. Taking advantage of our previously reported method for the rapid preparation of liposomes,<sup>44</sup> 3  $\mu\text{M}$  concentration of cell impermeant FluoZin-3 was encapsulated within unilamellar liposomes composed of DPPC:cholesterol in a 9:1 molar ratio. The resulting FluoZin-3-loaded liposomes were purified by passing the sample through a Sephadex G-100 size-separation column to remove the unencapsulated FluoZin-3 molecules. Dynamic light scattering (DLS) and  $\zeta$  potential analysis were performed to clearly confirm the presence of stable liposomes within a size range 1–2  $\mu\text{m}$  and surface charge around zero (Table 5.1).

Table 5.1. Dynamic light scattering and  $\zeta$  Potential Measurements of liposomes loaded with FluoZin-3 before and after treatments with 10  $\mu\text{M}$  quercetin (QCT10), 10  $\mu\text{M}$  epigallocatechin-3-gallate (EGCG10) or 10  $\mu\text{M}$  clioquinol (CQ10) in the presence and absence of 10  $\mu\text{M}$  quercetin (QCT10), 10  $\mu\text{M}$  epigallocatechin-3-gallate (EGCG10) or 10  $\mu\text{M}$  clioquinol (CQ10) in the presence and absence of 10  $\mu\text{M}$  zinc chloride (Zn10)<sup>a</sup>

Sample	Size average ( $\mu\text{m}$ )	$\zeta$ potential (mV)
FluoZin-3 loaded liposomes	1.4 $\pm$ 0.3	-4.7 $\pm$ 2.5
FluoZin-3 loaded liposomes + Zn10	1.1 $\pm$ 0.7	-5.0 $\pm$ 5.9
FluoZin-3 loaded liposomes + QCT10	1.2 $\pm$ 0.5	-1.9 $\pm$ 4.1
FluoZin-3 loaded liposomes + EGCG10	1.5 $\pm$ 0.4	-6.9 $\pm$ 7.6
FluoZin-3 loaded liposomes + CQ10	1.4 $\pm$ 0.2	-3.0 $\pm$ 3.7
FluoZin-3 loaded liposomes + Zn10 + QCT10	1.8 $\pm$ 0.2	-1.2 $\pm$ 2.5
FluoZin-3 loaded liposomes + Zn10 + EGCG10	1.6 $\pm$ 0.3	-3.5 $\pm$ 3.2
FluoZin-3 loaded liposomes + Zn10 + CQ10	1.4 $\pm$ 0.2	-9.0 $\pm$ 2.7

<sup>a</sup> Final concentrations of solvents in the samples were 0.05 % ethanol and 0.1 % DMSO. Standard deviations were calculated from the mean data of a series of experiments ( $n \geq 3$ ).

The zinc ionophore activity of polyphenols was then tested as their capacity to transport zinc cations into the liposome cavity, interacting with the encapsulated zinc-dependent FluoZin-3 and consequently increasing the fluorescence signal within the liposomes (Figure 5.6).  $\text{ZnCl}_2$  (10  $\mu\text{M}$ ) was added to the liposomal suspension in the absence and presence of 10  $\mu\text{M}$  QCT, EGCG and CQ, respectively, and zinc-dependent fluorescence intensity was measured over time.

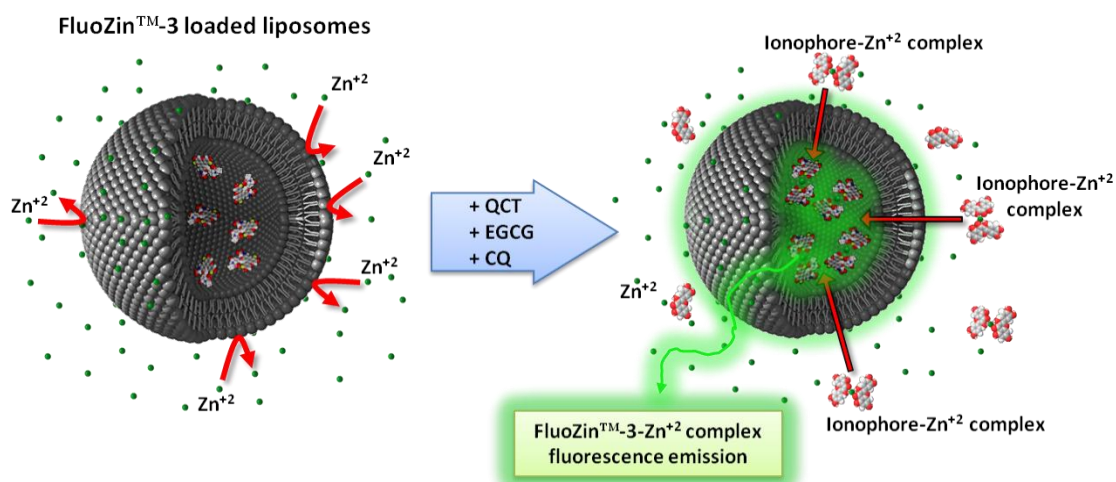
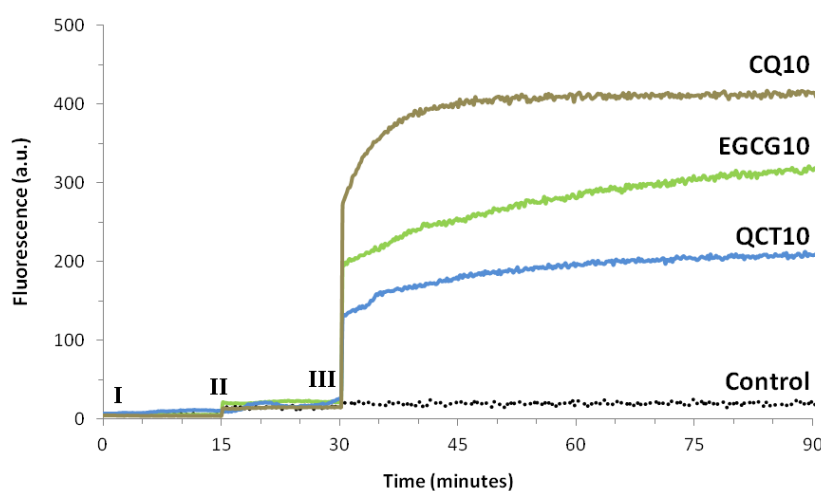


Figure 5.6. Schematic design of the FluoZin-3 loaded liposomes and the ionophore-like effect interpretation.

Following the addition of QCT, EGCG or CQ, the Zn-polyphenol chelation complex is formed and transported across the bilayer, followed by interaction with the encapsulated FluoZin-3 probe, resulting in a significant and immediate increase in the fluorescence intensity. Following the addition of 10  $\mu\text{M}$   $\text{ZnCl}_2$  to the liposomes, a very small increase in the fluorescence appears due to the presence of a few free FluoZin-3 molecules that were not removed during the purification process and represent the background fluorescent signal. Even so, the fluorescent signal remains very low as zinc ions alone cannot cross the liposome membrane. The results from the kinetic experiment demonstrate that QCT, EGCG and CQ present different ionophore properties. CQ showed the strongest ionophore activity, producing a 35-fold increase in the zinc-dependent FluoZin-3 fluorescence intensity. Moreover, the maximum fluorescence is achieved rapidly after reaching the equilibrium in less than 15 min. QCT and EGCG also display a high ionophore activity in the system, although to a lesser extent as compared to the strong ionophore CQ, with 8- and 16-fold increases in fluorescence signal observed for QCT and EGCG, respectively. It can also be observed that both QCT and EGCG required more time (> 60 min) to achieve the plateau phase, displaying slower chelation and transport kinetics (Figure 5.7).



*Figure 5.7. Effect of QCT, EGCG and CQ on the uptake of zinc cations by liposomes. Zinc-dependent fluorescence emission of FluoZin-3 encapsulated within liposomes treated with zinc cations, polyphenols, and CQ. The fluorescence emission ( $\lambda_{\text{ex}} = 494 \text{ nm}$ ;  $\lambda_{\text{em}} = 516 \text{ nm}$ ) of purified FluoZin-3-loaded liposomes was recorded continuously. Background fluorescence (0-15 min) was negligible (I). Upon the addition of 10  $\mu\text{M}$   $\text{ZnCl}_2$  to the liposomal suspensions (II), a small fluorescence signal was detected, presumably due to the presence of trace amounts of unencapsulated FluoZin-3 in the liposomal solutions. At time point 30 min, 10  $\mu\text{M}$  quercetin (QCT10), epigallocatechin-3-gallate (EGCG10), clioquinol (CQ10), or vehicle (control, final 0.1% DMSO) were added to the liposomal solutions, and the fluorescence was monitored for one additional hour (III).*

Confocal microscopy analysis was also performed in order to visualize and corroborate that the fluorescence produced by the interaction between zinc and FluoZin-3 was attributable to fluorescence in the inner part of the liposomes. As can be seen in Figure 5.8, fluorescence is only observed when the combination of  $\text{ZnCl}_2$  with QCT, EGCG or CQ is present, and the fluorescent signal comes from the inside part of the liposomes and not from the lipid membrane or the background solution. To further support this, stability studies were carried out in order to check whether the QCT, EGCG or CQ can destabilize and break the lipid vesicles. All the liposomes were characterized using TEM, DLS and  $\zeta$  potential to check that their stability was maintained following exposure.



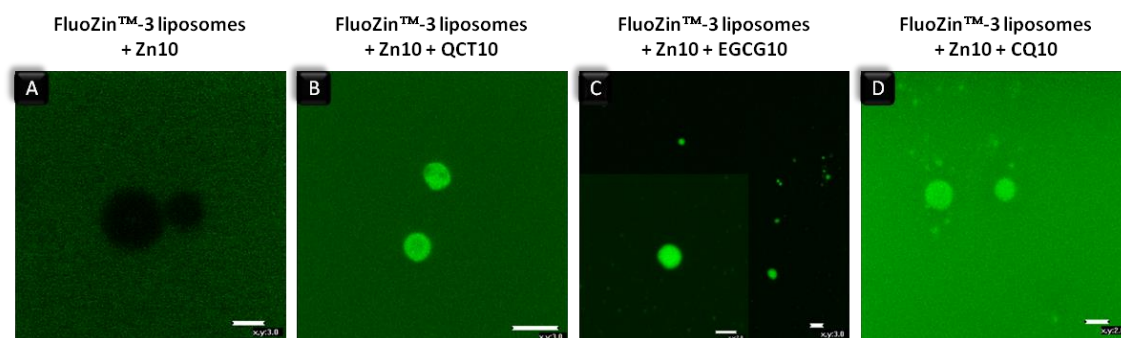


Figure 5.8. Three-dimensional confocal microscopy images of zinc dependent fluorescence emission of FluoZin-3 loaded within liposomes treated with zinc cations, polyphenols and CQ.

As shown in Figure 5.9, TEM images of the liposomes before and after treatments clearly demonstrate that liposome stability was not affected with the morphology and mean size (1-2  $\mu\text{m}$ ) being maintained. Moreover, the DLS and  $\zeta$  potential results presented in Table 5.1, confirmed that the size of the liposomes and their surface charge were not significantly affected by the addition of zinc and/or the ionophores, thus demonstrating that FluoZin-3-loaded liposomes were not destabilized and their around-zero charge, due to the zwitterionic nature of main lipid component DPPC, was maintained, thus confirming that the fluorescence signal is due to transport of the Zn-QCT/EGCG/CQ complex across the lipid membrane.

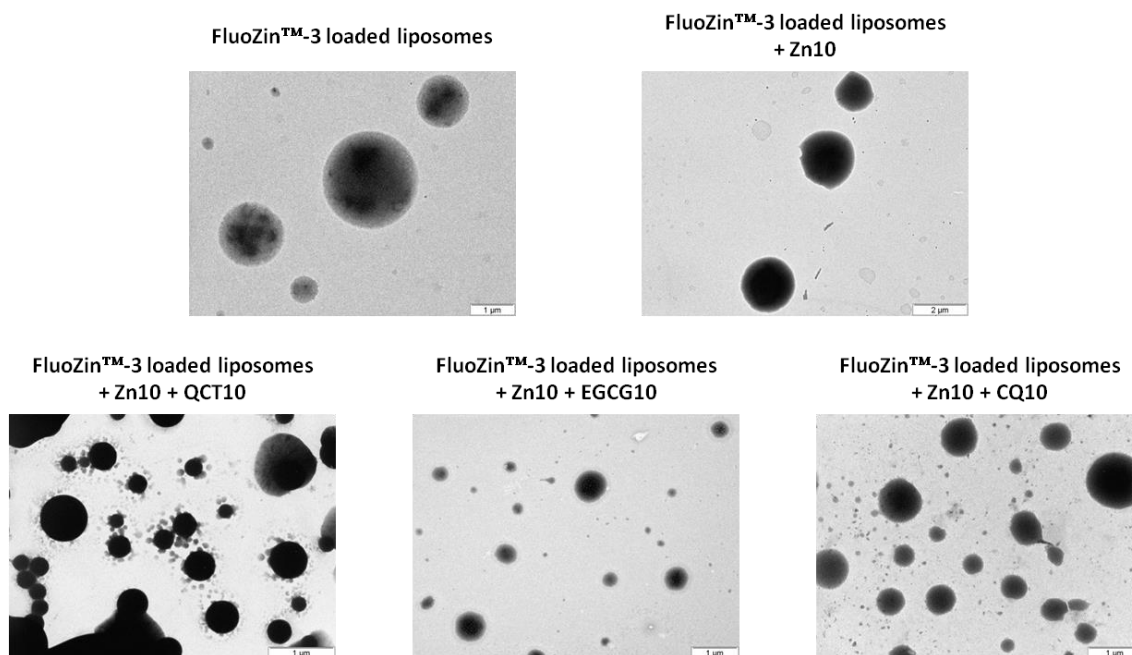


Figure 5.9. Transmission electron micrographs of liposomes with encapsulated FluoZin-3 after treatment with  $\text{ZnCl}_2$ , QCT, EGCG and CQ.

## 5.5. Discussion

The consequences that zinc chelation by flavonoids may have on zinc availability to the cells may in principle be dual: sequestering or ionophore, as shown for other well-characterized zinc-binding compounds.<sup>45</sup> On the one hand, the formation of zinc-flavonoid complexes may render zinc unavailable for cells, as do other dietary phytochemicals such as phytates<sup>46</sup> and zinc-

chelator drugs such as TPEN that induce zinc deficiency *in vitro* and *in vivo*.<sup>47</sup> Metal chelating therapy using CQ has been proposed for neurodegenerative disorders that course with high levels of metal accumulation such as Alzheimer's and Parkinson.<sup>48</sup> On the other hand, flavonoids may form water-insoluble membrane-permeant complexes with zinc that cross the plasma membrane, and thereby act as zinc ionophores. The ionophore effect of zinc binding compounds has been characterized for pyrithione and CQ. Both drugs chelate zinc cations and, when applied to cells, trigger a rapid increase of the intracellular pool of zinc that is detectable with different fluorophores such as Zinquin or FluoZin-3. Thereafter, it is assumed that these chelators form membrane-permeable complexes that are transported into the cell and that, once within the cell, chelator-zinc complexes dissociate into the single compounds due to the low concentration of intracellular free and labile zinc, thus providing labile zinc cations. Although FluoZin-3 has been widely accepted as a fluorophore that specifically interacts with zinc,<sup>49-52</sup> a recent report has indicated that this marker may in fact suffer from a lack of specificity.<sup>53</sup> However, this has no impact on the proof-of-concept study reported here as zinc is the only ion present and studied and thus no interfering effect from other ions will occur. We have shown here that treatment of Hepa 1-6 cells with zinc together with QCT, EGCG or CQ elicits a rapid and drastic increase in FluoZin-3-detectable intracellular zinc. The same effect was previously observed using Zinquin upon treatments of HepG2 cells with combinations of zinc and EGCG or zinc and QCT.<sup>38</sup> In these cells, the upregulation of MT and ZnT1 by zinc was enhanced by QCT. In contrast, EGCG decreased the intracellular zinc accumulation. Similar to QCT, the stilbene resveratrol efficiently chelates zinc in solution and enhances total and Zinquin-detectable cytoplasmic zinc in cultured human prostate epithelial cells, and this correlated with the antiproliferative action of resveratrol on cells.<sup>33</sup>

While an increasing effort has been made to understand the interaction of flavonoids with lipid bilayers,<sup>54</sup> no report has been published reporting the use of liposomes to demonstrate the zinc ionophore activity of polyphenols. Liposomes have been widely used as the simplest cell membrane systems in order to study the ionophore activity of molecules across the lipidic bilayer.<sup>55</sup> We have herein used a liposomal system to prove that zinc can transverse lipid bilayers when combined with flavonoids. It is not necessary to evoke the intervention of zinc transporters in the plasma membrane or the mobilization of zinc from intracellular compartments to account for the elevation of intracellular zinc levels in cells treated with flavonoids. The flavonoid-dependent transport of zinc cations into the liposomal cavity also implies that polyphenols may cross biological membranes when conjugated with metal cations. The mechanisms by which polyphenols enter the cells are largely unknown, but our results imply that complexation with metals may increase the bioavailability of polyphenols to cells.

There are several reports that strongly suggest that the demonstrated zinc ionophore effect on polyphenols will be observed in real physiological conditions if studied *in vivo*. Lee et al.<sup>56</sup> in 2002 has reported that a minor part of the EGCG found in plasma conserved its native form, and it has also been reported that the polyphenol metabolites still maintain their ability to chelate and form complexes with metal ions<sup>30</sup> and furthermore that nanomolar concentrations of polyphenols or their metabolites are able to modulate some metabolic pathways,<sup>5,57,58</sup> as does labile zinc in a picomolar to nanomolar concentration range.<sup>14</sup> While all these reports point toward the same ionophore effect being observed under physiological conditions, in a recent report by Oyama et al.,<sup>59</sup> the authors suggest the dual effect of CQ depending on the extracellular zinc concentration, where the known ionophore effect of CQ was only observed when extracellular zinc was available, and when zinc was not available in the extracellular environment, CQ could cross the membrane and chelate the intracellular zinc ions. To this end,

ongoing work is looking at extending the proof-of-concept reported and demonstrated here with both liposomes and cellular models to true physiological conditions exploring the interactions between a range of polyphenols and polyphenol metabolites and zinc in a lower concentration range of picomolar to micromolar.

In conclusion, we have demonstrated that QCT, EGCG and CQ rapidly increase intracellular labile zinc in Hepa 1-6 cells and that they function as ionophores for zinc in a liposomal system. Thus, natural flavonoids can be added to an arsenal of drugs that may be used to modulate zinc homeostasis and regulate zinc-dependent biological pathways.

## 5.6. Acknowledgements

This work was supported by grant AGL2008-00387 from the Spanish Ministry of Education and Science. H.D. was granted a predoctoral grant from the University Rovira i Virgili.

## 5.6. References

- (1) Aron, P. M.; Kennedy, J. A. Flavan-3-ols: Nature, occurrence and biological activity. *Mol. Nutr. Food Res.* **2008**, *52*, 79–104.
- (2) Egert, S.; Rimbach, G. Which sources of flavonoids: Complex diets or dietary supplements? *Adv. Nutr.* **2011**, *2*, 8–14.
- (3) Ramos, S. Cancer chemoprevention and chemotherapy: Dietary polyphenols and signalling pathways. *Mol. Nutr. Food Res.* **2008**, *52*, 507–526.
- (4) Jagtap, S.; Meganathan, K.; Wagh, V.; Winkler, J.; Hescheler, J.; Sachinidis, A. Chemoprotective mechanism of the natural compounds, epigallocatechin-3-O-gallate, quercetin and curcumin against cancer and cardiovascular diseases. *Curr. Med. Chem.* **2009**, *16*, 1451–1462.
- (5) Williams, R. J.; Spencer, J. P. E. Flavonoids, cognition, and dementia: Actions, mechanisms, and potential therapeutic utility for Alzheimer disease. *Free Radical Biol. Med.* **2012**, *52*, 35–45.
- (6) Selvaraj, S.; Krishnaswamy, S.; Devashya, V.; Sethuraman, S.; Krishnan, U. M. Flavonoid–metal ion complexes: A novel class of therapeutic agents. *Med. Res. Rev.* **2014**, *34*, 677–702.
- (7) Na, H.-K.; Surh, Y.-J. Modulation of Nrf2-mediated antioxidant and detoxifying enzyme induction by the green tea polyphenol EGCG. *Food Chem. Toxicol.* **2008**, *46*, 1271–1278.
- (8) Williams, R. J.; Spencer, J. P. E.; Rice-Evans, C. Flavonoids: Antioxidants or signalling molecules? *Free Radical Biol. Med.* **2004**, *36*, 838–849.
- (9) Ramos, S. Effects of dietary flavonoids on apoptotic pathways related to cancer chemoprevention. *J. Nutr. Biochem.* **2007**, *18*, 427–442.
- (10) Le Nest, G.; Caille, O.; Woudstra, M.; Roche, S.; Burlat, B.; Belle, V.; Guigliarelli, B.; Lexa, D. Zn–polyphenol chelation: Complexes with quercetin, (+)-catechin, and derivatives: II Electrochemical and EPR studies. *Inorg. Chim. Acta* **2004**, *357*, 2027–2037.

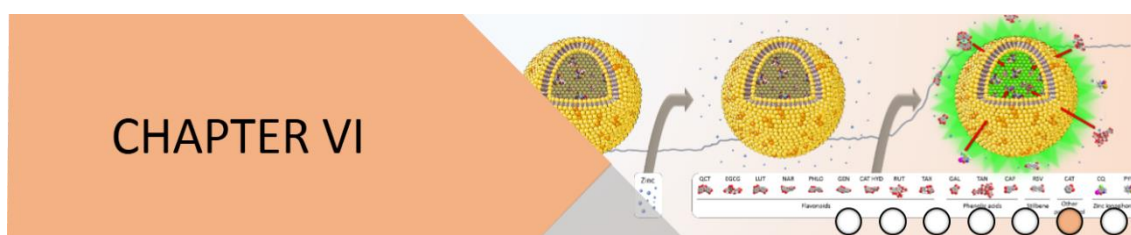
- (11) Prasad, A. S. Discovery of human zinc deficiency: 50 years later. *J. Trace Elem. Med. Biol.* **2012**, *26*, 66–69.
- (12) Maret, W. Zinc biochemistry: From a single zinc enzyme to a key element of life. *Adv. Nutr.* **2013**, *4*, 82–91.
- (13) Fukada, T.; Yamasaki, S.; Nishida, K.; Murakami, M.; Hirano, T. Zinc homeostasis and signaling in health and diseases. *J. Biol. Inorg. Chem.* **2011**, *16*, 1123–1134.
- (14) Maret, W. Metals on the move: Zinc ions in cellular regulation and in the coordination dynamics of zinc proteins. *Biometals* **2011**, *24*, 411–418.
- (15) Wilson, M.; Hogstrand, C.; Maret, W. Picomolar concentrations of free zinc(II) ions regulate receptor protein-tyrosine phosphatase  $\beta$  activity. *J. Biol. Chem.* **2012**, *287*, 9322–9326.
- (16) Maret, W. Inhibitory zinc sites in enzymes. *Biometals* **2013**, *26*, 197–204.
- (17) Cousins, R. J.; Liuzzi, J. P.; Lichten, L. A. Mammalian zinc transport, trafficking, and signals. *J. Biol. Chem.* **2006**, *281*, 24085–24089.
- (18) Krężel, A.; Maret, W. Thionein/metallothionein control Zn(II) availability and the activity of enzymes. *J. Biol. Inorg. Chem.* **2008**, *13*, 401–409.
- (19) Laity, J. H.; Andrews, G. K. Understanding the mechanisms of zinc-sensing by metal-response element binding transcription factor-1 (MTF-1). *Arch. Biochem. Biophys.* **2007**, *463*, 201–210.
- (20) Truong-Tran, A. Q.; Ho, L. H.; Chai, F.; Zalewski, P. D. Cellular zinc fluxes and the regulation of apoptosis/gene-directed cell death. *J. Nutr.* **2000**, *130*, 1459S–1466S.
- (21) Little, P. J.; Bhattacharya, R.; Moreyra, A. E.; Korichneva, I. L. Zinc and cardiovascular disease. *Nutrition* **2010**, *26*, 1050–1057.
- (22) Myers, S. A.; Nield, A.; Myers, M. Zinc transporters, mechanisms of action and therapeutic utility: Implications for type 2 diabetes mellitus. *J. Nutr. Metab.* **2012**, *2012*, 173712.
- (23) Watt, N. T.; Whitehouse, I. J.; Hooper, N. M. The role of zinc in Alzheimer's disease. *Int. J. Alzheimer's Dis.* **2010**, *2011*, 971021.
- (24) Hogstrand, C.; Kille, P.; Nicholson, R. I.; Taylor, K. M. Zinc transporters and cancer: A potential role for ZIP7 as a hub for tyrosine kinase activation. *Trends Mol. Med.* **2009**, *15*, 101–111.
- (25) Gao, Z.; Xu, H.; Chen, X.; Chen, H. Antioxidant status and mineral contents in tissues of rutin and baicalin fed rats. *Life Sci.* **2003**, *73*, 1599–1607.
- (26) Baiges, I.; Palmfeldt, J.; Blade, C.; Gregersen, N.; Arola, L. Lipogenesis is decreased by grape seed proanthocyanidins according to liver proteomics of rats fed a high fat diet. *Mol. Cell Proteomics* **2010**, *9*, 1499–513.
- (27) Kuo, S.-M.; Leavitt, P. S. Genistein increases metallothionein expression in human intestinal cells, Caco-2. *Biochem. Cell Biol.* **1999**, *77*, 79–88.
- (28) Kuo, S.-M.; Huang, C.-T.; Blum, P.; Chang, C. Quercetin cumulatively enhances copper induction of metallothionein in intestinal cells. *Biol. Trace Elem. Res.* **2001**, *84*, 1–10.

- (29) Sreenivasulu, K.; Raghu, P.; Nair, K. M. Polyphenol-rich beverages enhance zinc uptake and metallothionein expression in Caco-2 cells. *J. Food Sci.* **2010**, *75*, H123–H128.
- (30) Kim, E.-Y.; Pai, T.-K.; Han, O. Effect of bioactive dietary polyphenols on zinc transport across the intestinal Caco-2 cell monolayers. *J. Agric. Food Chem.* **2011**, *59*, 3606–3612.
- (31) Yang, J.; Yu, H.; Sun, S.; Zhang, L.; Das, U.; Ruan, H.; He, G.; Shen, S. Mechanism of free Zn(2+) enhancing inhibitory effects of EGCG on the growth of PC-3 cells: Interactions with mitochondria. *Biol. Trace Elem. Res.* **2009**, *131*, 298–310.
- (32) Chung, M. J.; Kang, A.-Y.; Lee, K. M.; Oh, E.; Jun, H.-J.; Kim, S.-Y.; Auh, J. H.; Moon, T.-W.; Lee, S.-J.; Park, K.-H. Water-soluble genistin glycoside isoflavones Up-regulate antioxidant metallothionein expression and scavenge free radicals. *J. Agric. Food Chem.* **2006**, *54*, 3819–3826.
- (33) Zhang, J. J.; Wu, M.; Schoene, N. W.; Cheng, W.-H.; Wang, T. T. Y.; Alshatwi, A. A.; Alsaif, M.; Lei, K. Y. Effect of resveratrol and zinc on intracellular zinc status in normal human prostate epithelial cells. *Am. J. Physiol.: Cell Physiol.* **2009**, *297*, C632–C644.
- (34) Uchiyama, S.; Yamaguchi, M. Genistein and zinc synergistically stimulate apoptotic cell death and suppress RANKL signaling-related gene expression in osteoclastic cells. *J. Cell. Biochem.* **2007**, *101*, 529–542.
- (35) Kagaya, N.; Kawase, M.; Maeda, H.; Tagawa, Y.-i.; Nagashima, H.; Ohmori, H.; Yagi, K. Enhancing effect of zinc on hepatoprotectivity of epigallocatechin gallate in isolated rat hepatocytes. *Biol. Pharm. Bull.* **2002**, *25*, 1156–1160.
- (36) Sun, S.-l.; He, G.-q.; Yu, H.-n.; Yang, J.-g.; Borthakur, D.; Zhang, L.-c.; Shen, S.-r.; Das, U. N. Free Zn<sup>2+</sup> enhances inhibitory effects of EGCG on the growth of PC-3 cells. *Mol. Nutr. Food Res.* **2008**, *52*, 465–471.
- (37) Yang, J. G.; Yu, H. N.; Sun, S. L.; Zhang, L. C.; He, G. Q.; Das, U. N.; Ruan, H.; Shen, S. R. Epigallocatechin-3-gallate affects the growth of LNCaP cells via membrane fluidity and distribution of cellular zinc. *J. Zhejiang Univ., Sci., B* **2009**, *10*, 411–21.
- (38) Quesada, I. M.; Bustos, M.; Blay, M.; Pujadas, G.; Ardèvol, A.; Salvadó, M. J.; Bladé, C.; Arola, L.; Fernández-Larrea, J. Dietary catechins and procyanidins modulate zinc homeostasis in human HepG2 cells. *J. Nutr. Biochem.* **2011**, *22*, 153–163.
- (39) Hider, R. C.; Liu, Z. D.; Khodr, H. H. Metal chelation of polyphenols. In *Methods in Enzymology*; Lester, P., Ed.; Academic Press: Waltham, MA, **2001**; Vol. 335, pp 190–203.
- (40) Ding, W.-Q.; Liu, B.; Vaught, J. L.; Yamauchi, H.; Lind, S. E. Anticancer activity of the antibiotic clioquinol. *Cancer Res.* **2005**, *65*, 3389–3395.
- (41) Li, Y.-M.; Shi, J.; Wu, X.; Luo, Z.-F.; Wang, F.-L.; Guo, Q.-X. Tracing of intracellular zinc(II) fluorescence flux to monitor cell apoptosis by using FluoZin-3AM. *Cell Biochem. Funct.* **2009**, *27*, 417–423.
- (42) Yu, H.; Zhou, Y.; Lind, S. E.; Ding, W.-Q. Clioquinol targets zinc to lysosomes in human cancer cells. *Biochem. J.* **2009**, *417*, 133–139.
- (43) Collins, T. J. ImageJ for microscopy. *Biotechniques* **2007**, *43*, 25–30.



- (44) Genç, R. k.; Ortiz, M.; O'Sullivan, C. K. Curvature-tuned preparation of nanoliposomes. *Langmuir* **2009**, *25*, 12604–12613.
- (45) Ding, W.-Q.; Yu, H.-J.; Lind, S. E. Zinc-binding compounds induce cancer cell death via distinct modes of action. *Cancer Lett.* **2008**, *271*, 251–259.
- (46) Wise, A. Phytate and zinc bioavailability. *Int. J. Food Sci. Nutr.* **1995**, *46*, 53–63.
- (47) Li, B.; Tan, Y.; Sun, W.; Fu, Y.; Miao, L.; Cai, L. The role of zinc in the prevention of diabetic cardiomyopathy and nephropathy. *Toxicol. Mech. Methods* **2013**, *23*, 27–33.
- (48) Bareggi, S. R.; Cornelli, U. Clioquinol: Review of its mechanisms of action and clinical uses in neurodegenerative disorders. *CNS Neurosci. Ther.* **2012**, *18*, 41–46.
- (49) Muylle, F. R.; Adriaensen, D.; Coen, W.; Timmermans, J.-P.; Blust, R. Tracing of labile zinc in live fish hepatocytes using FluoZin-3. *Biometals* **2006**, *19*, 437–450.
- (50) Wessels, I.; Haase, H.; Engelhardt, G.; Rink, L.; Uciechowski, P. Zinc deficiency induces production of the proinflammatory cytokines IL-1 $\beta$  and TNF $\alpha$  in promyeloid cells via epigenetic and redoxdependent mechanisms. *J. Nutr. Biochem.* **2013**, *24*, 289–297.
- (51) Kim, J.-H.; Jeon, J.; Shin, M.; Won, Y.; Lee, M.; Kwak, J.-S.; Lee, G.; Rhee, J.; Ryu, J.-H.; Chun, C.-H.; Chun, J.-S. Regulation of the catabolic cascade in osteoarthritis by the zinc-ZIP8-MTF1 axis. *Cell* **2014**, *156*, 730–743.
- (52) Chevallet, M.; Jarvis, L.; Harel, A.; Luche, S.; Degot, S.; Chapuis, V.; Boulay, G.; Rabilloud, T.; Bouron, A. Functional consequences of the over-expression of TRPC6 channels in HEK cells: Impact on the homeostasis of zinc. *Metallomics* **2014**, *6*, 1269–1276.
- (53) Landero Figueroa, J. A.; Subramanian Vignesh, K.; Deepe, G. S., Jr.; Caruso, J. Selectivity and specificity of small molecule fluorescent dyes/probes used for the detection of Zn<sup>2+</sup> and Ca<sup>2+</sup> in cells. *Metallomics* **2014**, *6*, 301–315.
- (54) Efimova, S. S.; Ostroumova, O. S. Effect of dipole modifiers on the magnitude of the dipole potential of sterol-containing bilayers. *Langmuir* **2012**, *28*, 9908–9914.
- (55) Sankaram, M. B.; Shastri, B. P.; Easwaran, K. R. K. Interaction of carrier ionophores with phospholipid vesicles. *Biochemistry* **1987**, *26*, 4936–4941.
- (56) Lee, M.-J.; Maliakal, P.; Chen, L.; Meng, X.; Bondoc, F. Y.; Prabhu, S.; Lambert, G.; Mohr, S.; Yang, C. S. Pharmacokinetics of tea catechins after ingestion of green tea and (–)-epigallocatechin-3-gallate by humans: Formation of different metabolites and individual variability. *Cancer Epidemiol., Biomarkers Prev.* **2002**, *11*, 1025–1032.
- (57) Schroeter, H.; Bahia, P.; Spencer, J. P. E.; Sheppard, O.; Rattray, M.; Cadenas, E.; Rice-Evans, C.; Williams, R. J. (–)Epicatechin stimulates ERK-dependent cyclic AMP response element activity and up-regulates GluR2 in cortical neurons. *J. Neurochem.* **2007**, *101*, 1596–1606.
- (58) Vauzour, D.; Vafeiadou, K.; Rice-Evans, C.; Williams, R. J.; Spencer, J. P. E. Activation of pro-survival Akt and ERK1/2 signalling pathways underlie the anti-apoptotic effects of flavanones in cortical neurons. *J. Neurochem.* **2007**, *103*, 1355–1367.
- (59) Oyama, T. M.; Ishida, S.; Okano, Y.; Seo, H.; Oyama, Y. Clioquinol-induced increase and decrease in the intracellular Zn<sup>2+</sup> level in rat thymocytes. *Life Sci.* **2012**, *91*, 1216–1220.





A simple liposome assay for the  
screening of zinc ionophore  
activity of polyphenols





## A simple liposome assay for the screening of zinc ionophore activity of polyphenols

For submission to *RSC Adv.*

Gael Clergeaud,<sup>1,#</sup> Husam Dabbagh-Bazarbachi,<sup>2,#</sup> Mayreli Ortiz,<sup>1</sup> Juan B. Fernández-Larrea<sup>2,\*</sup> and Ciara K. O'Sullivan<sup>1,3,\*</sup>

<sup>1</sup> Nanobiotechnology & Bioanalysis Group, Department of Chemical Engineering and

<sup>2</sup> Nutrigenomics Research Group, Department of Biochemistry and Biotechnology, Universitat Rovira i Virgili, 43007 Tarragona, Spain

<sup>3</sup> Institució Catalana de Recerca i Estudis Avançats, 08010 Barcelona, Spain

# Gael Clergeaud and Husam Dabbagh-Bazarbachi contributed equally to this work.



## 6.1. Abstract

An efficient liposomal system for screening the zinc ionophore activity of a selected library consisting of the most relevant dietary polyphenols is presented. The zinc ionophore activity was demonstrated by exploring the use of zinc-specific fluorophore FluoZin-3 loaded liposomes as simple membrane tools that mimic the cell membrane. The zinc ionophore activity was demonstrated as the capacity of polyphenols to transport zinc cations across the liposome membrane and increase the zinc-specific fluorescence of the encapsulated fluorophore FluoZin-3. In addition, the zinc chelation strength of the polyphenols was also tested in a competition assay based on the fluorescence quenching of zinc-dependent fluorescence emitted by zinc-FluoZin-3 complex. Finally, the correlation between the chelation capacity and ionophore activity is demonstrated, thus underlining the sequestering or ionophoric activity that the phenolic compounds can display, thus, providing better knowledge of the importance of the structural conformation versus their biological activity. Furthermore, the developed assays can be used as tools for rapid, high-throughput screening of families of polyphenols.

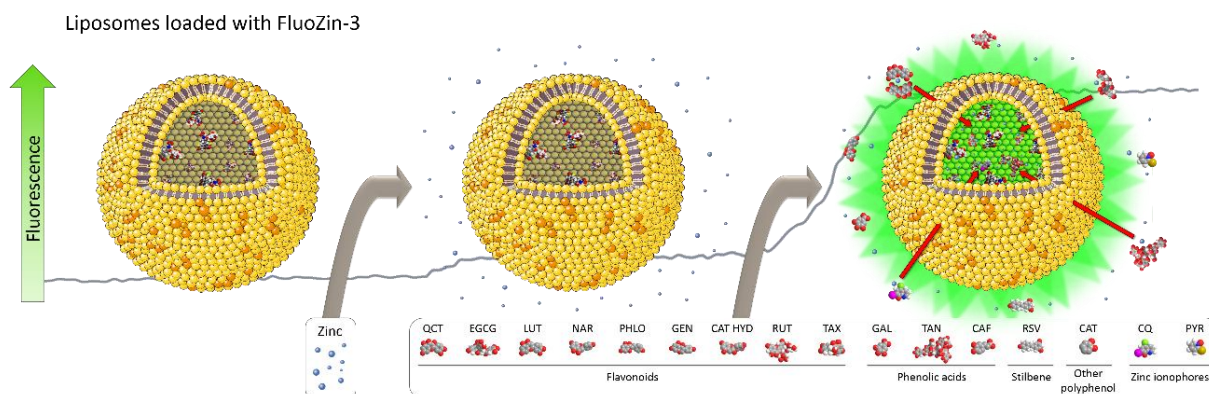


Figure 6.1. Table of contents figure

## 6.2. Introduction

Zinc ions have long been known to mimic the actions of hormones, growth factors, neurotransmitters and cytokines, and it is believed that zinc may act on intracellular signalling molecules.<sup>1-3</sup> In fact, zinc is a known inhibitor of protein tyrosine phosphatases<sup>4</sup> with a constant of inhibition in the nanomolar range.<sup>5</sup> In addition, zinc affects the regulation of transcription factors, and can induce the expression of some genes, including those coding for molecules involved in zinc homeostasis, such as zinc transporters and metallothioneins.<sup>6</sup> The gene expression of metallothioneins by zinc is regulated by metal response element-binding transcription factor-1.<sup>7</sup> The chemical properties of zinc that differentiate it from other transition metals, such as copper and iron, which display several different oxidation states in biological systems, is that zinc exists as a redox inert  $Zn^{2+}$  cation, which does not undergo redox reactions at physiological redox potentials.<sup>8,9</sup> Additionally, zinc can induce the expression and maintain the levels of potentially radical scavenging proteins such as metallothionein (MT), the major zinc binding protein associated with zinc homeostasis,<sup>10</sup> DNA protection, oxidative stress, and apoptosis.<sup>11,12</sup> Furthermore, it can act through stabilization of cell membranes<sup>13</sup> or as a structural component of anti-oxidant enzymes.<sup>14</sup>

On the other hand, recent studies have focused on dietary phenolic compounds as natural improvers of health and more than 8000 dietary polyphenols have been identified.<sup>15</sup> The

growing interest in these compounds resides in the accumulating evidence regarding their ability to trigger several cellular pathways leading to the prevention and/or amelioration of pathological conditions, acting as anti-oxidants,<sup>16</sup> anti-carcinogenics,<sup>17,18</sup> anti-inflammatories,<sup>19</sup> neuroprotectors,<sup>20</sup> anti-lipidemic and vaso-relaxing agents.<sup>15</sup>

In the last decades, it has been demonstrated and understood that phenolic compounds interact with different metals, including zinc, and because of their distinctive chemical structure, they can easily form complexes through metal ion chelation<sup>21</sup> in a manner similar to that of other well-known metal chelators such as the drug clioquinol (CQ) and also exerts a ionophore activity comparable to pyrithione (Pyr).<sup>22,23</sup> The first evidence of polyphenol-metal complexes was reported in 1962 between aluminium ions and flavonoids. Since then, more than 40 metal-flavonoid complexes have been investigated.<sup>24</sup>

One of the mechanisms by which flavonoids exert their anti-oxidant activity is via the chelation of redox-active transition metals,<sup>25</sup> which are known to catalyze many biological processes leading to the production of free radicals.<sup>26</sup> The essential sites for metal chelation are hydroxyl groups, and the most suitable cations for chelation are Fe(II), Fe(III), Cu(II) and Zn(II) as they high charge density, stimulating the interaction with the phenoxide groups that have a high negative charge density.<sup>21</sup> The structure of the formed complexes depends on the type of flavonoid and metal ion involved, which in turn can influence its' biological interactions that may be different from the native flavonoid.<sup>27-31</sup> Depending on the polyphenol and its' potential binding sites, different structures could be formed with different stoichiometries, thus affecting the biological function of the complex.<sup>32</sup> Experimental data has indicated that the chelated compounds are more effective free radical scavengers than flavonoids alone, suggesting that the Zn-Polyphenol complexes not only exert singular biological properties, but can also enhance the effects of both compounds individually.<sup>33</sup>

Further studies have revealed that polyphenols not only interact with metal ions, but also deeply modulate expression of MTs, cellular zinc transporters, extracellular zinc carriers, and intracellular zinc accumulation which are key factors in zinc homeostasis.<sup>10</sup> Zinquin is a fluorescent zinc-specific indicator and an increase in Zinquin-detectable cytoplasmic levels of zinc in a HepG2 cell line has been monitored when treated with phenolic compounds.<sup>10</sup> This increment in intracellular zinc levels have been reported to induce apoptosis of tumour cells,<sup>34,35</sup> suggesting that zinc ionophores may serve as anticancer agents.<sup>36</sup>

Although the ionophore activity of natural occurring compounds has not been well established, there is strong evidence of their interaction and complex formation with zinc ions,<sup>33</sup> suggesting that they could be potential candidates as zinc ionophore molecules. The interaction of quercetin (QCT) and epigallocatechin-3-gallate (EGCG) with zinc, as well as their ionophore activity has been confirmed in a liposome model using the specific zinc indicator FluoZin-3.<sup>37</sup> Luteolin (LUT) and naringenin (NAR) interact with zinc ions, forming complexes and exerting a biological function acting as strong radical scavengers.<sup>38,39</sup> The ability of genistein (GEN) to bind zinc ions has not been well elucidated, although its' ability to bind iron is well known and these complexes exert a strong anti-oxidant role, and this suggests that it could have a similar action with other metals such as zinc.<sup>40</sup> There is also evidence of the ability of catechin hydrate (CAT HYD), which is the one of the main bioactive components in green tea, to interact and form complexes with zinc ions,<sup>41,42</sup> exerting an anti-oxidant activity, but also having an essential role in treatment of different cancers, such as prostate cancer.<sup>43</sup> Several reports have confirmed that rutin (RUT) forms complexes with zinc,<sup>44</sup> also acting as a free radical scavenger in a much more effective way than the free flavonoid.<sup>45</sup> The anti-inflammatory activity of this bioflavonoid is also enhanced when complexed with zinc.<sup>28</sup> Taxifolin (TAX) is also able to interact and form complexes with zinc ions, being an effective radical scavenger too.<sup>46</sup> Most phenolic acids are good metal chelators, due to their structure with several catechol and/or galloyl moieties.<sup>47</sup> To

our knowledge, there are no reports to date on interactions and complex formation with zinc ions with phloretin (PHLO) or the stilbene resveratrol (RSV), although for RSV there are some evidences on complex formation with copper, suggesting that maybe similar structures can be formed with other metal ions.<sup>48</sup> Catechol (CAT) is one of the simplest naturally occurring polyphenols, and also one of the most important moieties in a high variety of polyphenols, responsible for the interaction with metal ions. CAT forms complexes with Ruthenium, a rare transition metal, suggesting that it could have the same behaviour with other transition metals like zinc.<sup>49</sup> Thus, a high proportion of polyphenols present some kind of interaction with zinc or other metal ions, although for the majority of polyphenols the ionophore activity is still undescribed.

The aim of this work was to evaluate the capacity of fourteen different phenolic compounds to bind and chelate zinc ions in solution. We focused on fourteen phenolic compounds grouped according to their chemical structure, including the flavonoids quercetin (QCT), epigallocatechin-3-gallate (EGCG), luteolin (LUT), naringenin (NAR), phloretin (PHLO), genistein (GEN), catechin hydrate (CAT HYD), rutin (RUT) and dihydroquercetin or taxifolin (TAX); the phenolic acids gallic acid (GAL), tannic acid (TAN) and caffeic acid (CAF); the stilbene resveratrol (RSV); and other polyphenols such as catechol (CAT). Two different zinc ionophore agents, clioquinol and pyrithione, were used to compare the ionophore activity of the selected polyphenols, as well as the zinc sequestrant molecule, TPEN (N,N,N',N'-tetrakis (2-pyridylmethyl) ethylenediamine).

Binding/chelation of the zinc ions by the polyphenols was evaluated using a competition assay based on the fluorescence quenching of zinc-dependent fluorescence emitted by FluoZin-3. In this competition assay the zinc chelation strength of each phenolic compound was correlated with the decrease in the fluorescence signal due to the dissociation of the zinc-FluoZin-3 complex as zinc cations are sequestered from the fluorophore complex by the polyphenol. In addition, we present a simple and rapid liposome assay for demonstrating the ionophore activity of common polyphenols and compared them to strong, well-established ionophores, such as clioquinol and pyrithione. The correlation between the chelation capacity and ionophore activity underlines the different behaviours the phenolic compounds can display and the developed assays can be used as tools for rapid, high-throughput screening of families of polyphenols.

## 6.3. Experimental section

### 6.3.1. Materials

All the phenolic compounds, pyrithione (PYR), quercetin (QCT), epigallocatechin-3-gallate (EGCG), genistein (GEN), taxifolin (TAX), luteolin (LUT), phloretin (PHLO), catechol (CAT), naringenin (NAR), rutin (RUT), catechin (CAT HYD), caffeic acid (CAF), tannic acid (TAN), gallic acid (GAL), resveratrol (RSV) and clioquinol (CQ) were purchased from Sigma-Aldrich, as well as the lipid 1,2-dipalmitoyl-sn-glycero-3-phosphocholine (DPPC), cholesterol, dimethyl sulfoxide (DMSO), ethanol, zinc chloride (ZnCl<sub>2</sub>), N,N,N',N'-tetrakis(2-pyridylmethyl)ethylenediamine (TPEN) and the phosphate buffered saline (0.01M PBS, pH 7.4). Cell impermeant FluoZin-3 tetrapotassium salt was obtained from Molecular Probes. A Simplicity 185 Millipore-Water System was used to obtain Milli-Q water (18.2 mΩ.cm<sup>-1</sup>) for the preparation of buffers and liposomes. The phenolic compounds PYR, QCT, EGCG, GEN, TAX, LUT, PHLO, CAT, NAR, RUT, CAT HYD, CAF, TAN, GAL, RSV and CQ were dissolved as 100 μM solutions in 100 % DMSO and aliquoted of at -20 °C. ZnCl<sub>2</sub> was stored as 1 M solution in ethanol/PBS (50/50 % v/v). FluoZin-3 zinc indicator was used at 10 μM in 100 % DMSO.

### 6.3.2. Measurement of the interaction of the polyphenols with zinc cations in solution

A competition assay was carried out to test the ability of the polyphenols PYR, QCT, EGCG, GEN, TAX, LUT, PHLO, CAT, NAR, RUT, CAT HYD, CAF, TAN, GAL, RSV and CQ to chelate zinc cations in solution, thus reverting their binding with the zinc specific fluorophore FluoZin-3. TPEN was also included as a positive control, to compare with a well-recognized zinc chelator.<sup>50</sup> FluoZin-3 tetrapotassium salt was used to demonstrate the capacity of the flavonoids and of clioquinol to form complexes with zinc. First, a fluorescence titration curve was constructed using a range of zinc concentrations (from 0 to 1.25  $\mu\text{M}$ ) to establish where the fluorescence of 3  $\mu\text{M}$  FluoZin-3 is not saturated by zinc cations. The relative capacity of the polyphenols and clioquinol to quench the zinc-dependent fluorescence of FluoZin-3 at 1  $\mu\text{M}$  zinc concentration was then monitored. The final concentration of test substances in the competition reaction with FluoZin-3 was 10  $\mu\text{M}$ .

Briefly, 3  $\mu\text{M}$  FluoZin-3 was mixed with 1  $\mu\text{M}$  zinc in PBS (0.01 M, pH 7.4) and incubated for 15 minutes at room temperature to facilitate formation of the zinc-complex. Subsequently, 10  $\mu\text{M}$  (final concentration) of the test substances (PYR, QCT, EGCG, GEN, TAX, LUT, PHLO, CAT, NAR, RUT, CAT HYD, CAF, TAN, GAL, RSV, CQ or TPEN), were added, mixed vigorously and incubated at 37 °C for 30 minutes under shaking conditions, protected from light. All fluorescence measurements were performed in an Eclipse fluorescence spectrophotometer from Varian coupled with a Cary temperature controller at 25 °C using quartz cuvettes with 1 cm path length and with a maximum volume of 150  $\mu\text{L}$ . The excitation and emission wavelengths used were 494 nm and 516 nm with slits of 5 nm.

### 6.3.3. Preparation of FluoZin-3 loaded liposomes

Liposomes were prepared using the curvature-tuned method previously reported.<sup>51</sup> Briefly, FluoZin-3 (final concentration 3  $\mu\text{M}$ ) was mixed with 2 mL of PBS (0.01 M, pH 7.4) in a glass reactor protected from light-induced degradation, under stirring conditions and bubbling argon gas. After 15 minutes, a previously homogenized mixture of DPPC and cholesterol (9:1 molar ratio) in 3 mL PBS was added and maintained under stirring conditions and argon at 25 °C for another 15 minutes. The homogeneous mixture was then subjected to a rapid pH jump from pH 7.4 to pH 11, and then back to pH 7.4 within a 3 seconds frame, followed by an equilibration step of 25 minutes where lipid clusters curl into liposomes entrapping the buffer containing the FluoZin-3 molecules. The resulting FluoZin-3-loaded liposomes were purified to remove any unencapsulated material by size exclusion chromatography (SEC) using a Sephadex G-100 column and the size and charge of the formed liposomes was determined using dynamic light scattering (DLS) and zeta-potential. Prepared liposomes were used immediately.

### 6.3.4. Liposome assay to assess zinc ionophore activity

The zinc ionophore activity of the different polyphenols and clioquinol was demonstrated by the increase in zinc-dependent fluorescence of FluoZin-3 loaded liposomes. Freshly prepared liposomes loaded with FluoZin-3 were placed in separate vials and their fluorescence measured. Subsequently,  $\text{ZnCl}_2$  was added to each solution to a final concentration of 10  $\mu\text{M}$ , the solution was softly vortexed, incubated at 25 °C for 30 minutes and the fluorescence was measured again. Finally, 50  $\mu\text{M}$  of PYR, QCT, EGCG, GEN, TAX, LUT, PHLO, CAT, NAR, RUT, CAT HYD, CAF, TAN, GAL, RSV or CQ was added to each vial respectively, softly vortexed and allowed to incubate at 25 °C for 30 minutes under shaking conditions before measuring their fluorescence. The evaluation of the ionophore behavior of each polyphenol was tested in a time-dependent assay to further understand the velocity of the zinc transport. The kinetic experiment was carried out by continuously measuring the fluorescence of the FluoZin-3 loaded liposomes over a period of time of 70 minutes, with the addition of  $\text{ZnCl}_2$  (final 10  $\mu\text{M}$ ) after 5 minutes and the addition of the test substances (50  $\mu\text{M}$ ) to each cuvette respectively after 10 minutes. All fluorescence

measurements were performed in an Eclipse fluorescence spectrophotometer from Varian coupled with Cary temperature controller at 25 °C using quartz cuvettes with a 1 cm path length and with a maximum volume of 150  $\mu$ L. The excitation and emission wavelengths used were 494 nm and 516 nm with slits of 5 nm. Control experiments were performed by adding to the cuvette FluoZin-3 loaded liposomes with 10  $\mu$ M ZnCl<sub>2</sub> and the solvent used to dissolve the ionophores (final DMSO concentration 0.1 % v/v) after 10 minutes.

## 6.4. Results and discussion

### 6.4.1. Zinc chelation strength of polyphenols in solution

Several polyphenols have been widely reported to chelate metals through their deprotonated hydroxyl groups, in which the oxygen possesses a high charge density offering a strong ligand for metal-binding. As expected, the chelation strength depends on the number of hydroxyl ligands, but also on their proximity, thus bi- or poly-dentate ligands are stronger scavengers than mono-dentate ligands. A detailed structure of the identified chelating groups of each of the polyphenols tested in this work, as well as their classification and food source, is presented in Table 1.

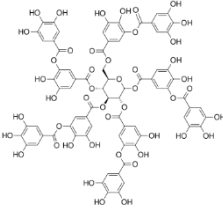
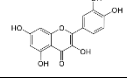
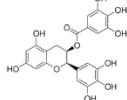
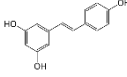
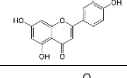
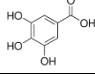
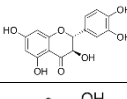
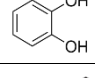
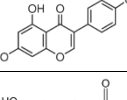
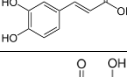
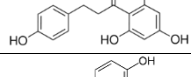
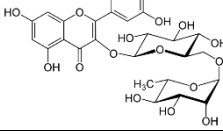
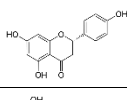
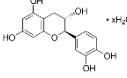
In order to quantify the relative capacity of the phenolic compounds tested in the work reported here (QCT, EGCG, GEN, TAX, LUT, PHLO, CAT, NAR, RUT, CAT HYD, CAF, TAN, GAL and RSV), in addition to the established ionophore (CQ and PYR) and sequestrant (TPEN) agents, to bind zinc cations in aqueous solutions at physiological pH, their capacity to retrieve zinc cations from FluoZin-3-zinc complexes was measured, by monitoring the decrease in zinc-dependent fluorescence emitted by the FluoZin-3-zinc complexes upon addition of the polyphenols to the solution.

Firstly, an assay was carried out showing that the fluorescence of FluoZin-3 (3  $\mu$ M) increments linearly with increasing amounts of zinc cations up to 1.25  $\mu$ M Zn<sup>2+</sup>, where a plateau is reached (Figure 6.2 inset). Therefore, a zinc concentration of 1  $\mu$ M was selected as optimal to demonstrate the decrease in fluorescence of 3  $\mu$ M FluoZin-3-Zn complexes upon addition of the phenolic compounds. As can be seen in Figure 6.2, all 14 polyphenols, together with clioquinol, pyriithione and TPEN, at 10  $\mu$ M concentrations, resulted in a decrease in the zinc-dependent FluoZin-3 fluorescence to some extent, due to sequestering of the zinc ions. The highest zinc-chelating strength was observed to be produced by TPEN, followed by CQ, with an almost complete decrease of the FluoZin-3 fluorescent signal. Similarly, PYR caused an almost 80% reduction of the fluorescence signal. These observations are anticipated, as they are well-known powerful zinc chelators. Regarding the phenolic compounds, TAN surprisingly also quenched 100 % of the fluorescence signal, which can be explained by its' complex molecular structure having 25 hydroxyl groups, most of them positioned in a powerful bi-dentate configuration (Table 6.1), ready to bind and sequester zinc cations from the fluorescent zinc-FluoZin-3 complex. Regarding the rest of the polyphenols, the fluorescence quenching capacity was smaller and similar, within a range from 30 to 15%, and in agreement with the number and position metal-binding sites of present on each compound. For example, the flavonoids having -OH groups positioned together offering a bi-dentate ligand (QCT, EGCG, LUT, GAL, TAX) instead of having the -OH groups positioned on different sides of the molecule (NAR, PHLO, GEN), were observed to have a higher chelating strength. However, containing more hydroxyl groups alone does not result in improved chelation. As it was observed there are other important factors affecting the chelating strength, including the three-dimensional conformation of the potential binding groups, as well as the formed stoichiometry between the polyphenols and the metal. Therefore, the structure of the studied polyphenols does not always correlate with their chelating efficiency. The very low



capacity of some of the studied polyphenols to quench the FluoZin-3 fluorescence despite containing several -OH groups, as well as some compounds being observed to have a high ability to chelate zinc ions, whilst only possessing few hydroxyl groups can thus be attributed to their 3-D conformation and stoichiometry.

Table 6.1. Summary of the phenolic compounds used within this work and divided according to class, food source, chemical structure with the proposed chelating groups highlighted and the number of hydroxyl groups present.

Compound	Class	Dietary source	Structure	# Hydroxyl groups
Tannic acid	Hydroxybenzoic acids	-Grape -Persimmon -Black berry -Myrobalan -Walnut -Maple -Sumac -Tarragon		25
Quercetin	Flavonols	-Cocoa -Onion -Elderberry -Wine -Black plum -Kale		5
(-)-Epigallocatechin gallate (EGCG)	Flavanols (Flavan-3-ols)	-Green tea -Black tea -Apple -Blackberry -Hazelnut -Pecan nut		8
Resveratrol	Stilbenes	-Muscadine grape -Lingonberry -Cranberry -Red wine		3
Luteolin	Flavones	-Olive -Mexican oregano -Globe artichoke -Green pepper		4
Gallic acid	Hydroxybenzoic acids	-Chestnut -Black tea -Blackberry -Green chicory		4
Dihydroquercetin (Taxifolin)	Dihydroflavonols	-Mexican oregano -Acai berry		5
Catechol	Other polyphenols	-Argan oil -Coffee beverage -Cocoa		2
Genistein	Isoflavonoids	-Soy -Red clover		3
Caffeic acid	Hydroxycinnamic acids	-Coffee -Black chokeberry -Plum		3
Phloretin	Dihydrochalcones	-Apple -Apricot		4
Rutin	Flavonol	-Buckwheat -Black olive -Black tea -Plum -Capers -Tomato		11
Naringenin	Flavanones	-Mexican oregano -Grapefruit -Orange -Tomato		3
Catechin hydrate	Flavonol	-Cocoa -Strawberry -Grape -Broad bean		5

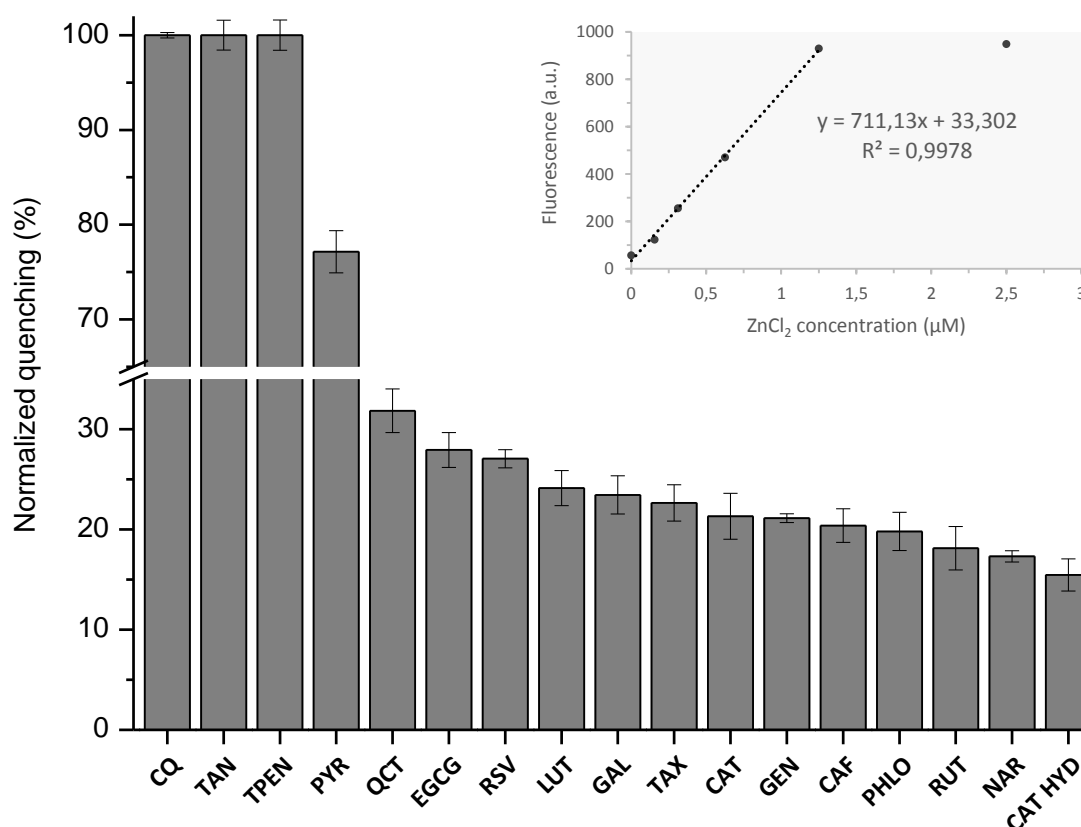


Figure 6.2. Chelation strength of zinc cations by the polyphenols, clioquinol, pyrithione and TPEN in solution. The quenching of the zinc-dependent fluorescence of FluoZin-3 indicates the capacity of the compounds at 10  $\mu\text{M}$  to retrieve zinc cations from the zinc-FluoZin-3 complex formed between 3  $\mu\text{M}$  FluoZin-3 and 1  $\mu\text{M}$   $\text{ZnCl}_2$ . Inset: 3  $\mu\text{M}$  FluoZin-3 calibration plot.  $\lambda_{\text{ex}}$  494nm /  $\lambda_{\text{em}}$  516nm. All values are means  $\pm$  SD of three independent experiments.

#### 6.4.2. Zinc ionophore activity of polyphenols

Polyphenols are known to interact with lipid bilayers and actively modify their membrane fluidity.<sup>52-54</sup> It is believed that the fluidization of the bilayer is due to the intercalation of the lipophilic domains of the molecules within the ordered structure of the lipid membranes. This interaction strongly depends on several characteristics of the polyphenolic molecule, such as its' degree of hydroxylation and their stereochemistry, the polarity and the 3-D structural features. However, the transport phenomena of molecules across lipid membranes is still not fully understood. The permeabilization of the membrane to low-molecular-weight molecules by ionophore molecules has been suggested to also be dependent on the concentration of monovalent ions thus creating a gradient of ions and modifying the membrane potential, thus inducing its' depolarization.<sup>55,56</sup> In addition, other several factors may play an important role and modulate the ionophore strength, such as the type of ion-ionophore complex formed, the different ratios, the kinetic reaction of complexation/decomplexation, the ion-ionophore membrane interaction as well as its' transmembrane diffusion constant.<sup>57</sup> For example, Yang *et al.* reported that the behavior of EGCG was modified due to the formation of zinc-EGCG complexes, resulting in an enhancement of the incorporation of EGCG into the liposome membrane, which could cause the formation of ion passages.<sup>58</sup>

A wide number of publications have reported the use of liposomes as simple membrane systems for the demonstration of ion transport across lipid bilayers.<sup>59-61</sup> However, there is only one previous report of the use of a liposomal system to study the ionophore properties of phenolic compounds to demonstrate the zinc ionophore activity of QCT and EGCG,<sup>37</sup> where they also investigated that the flavonoid compounds did not induce the release of the liposome load, as was also reported by Ollila *et al.*<sup>62</sup>

A simple liposome system with zinc-dependent fluorophore FluoZin-3 encapsulated in the inner cavity was used to determine if the polyphenols can transport zinc across the cell membrane. Using the liposome also limited the transport pathway to be solely due to transmembrane transport as no other transduction mechanisms normally present in cells would contribute to the transport of the zinc cations. The zinc ionophore effect was extrapolated as a function of the increase in fluorescence due to the capacity of the polyphenols to carry zinc cations across the liposome membrane to interact with the encapsulated FluoZin-3. Liposomes with a mean size of  $1.3 \pm 0.2 \mu\text{m}$  and a net charge of  $0.8 \pm 0.2 \text{ mV}$  loaded with FluoZin-3 before and after the addition of  $10 \mu\text{M ZnCl}_2$  showed a negligible fluorescence signal due to the impermeability of the DPPC:Cholesterol liposome membrane at  $25 \text{ }^\circ\text{C}$  to zinc cations. The subsequent addition of the phenolic compounds, caused an increase in the fluorescence signal due to the zinc complexation, transport and consequent interaction with FluoZin-3. The well-reported CQ and PYR zinc ionophores, resulted in a marked increase in the fluorescence signal, as expected, whilst each of the other phenolic compounds studied presented very different ionophore properties (Figure 6.3).

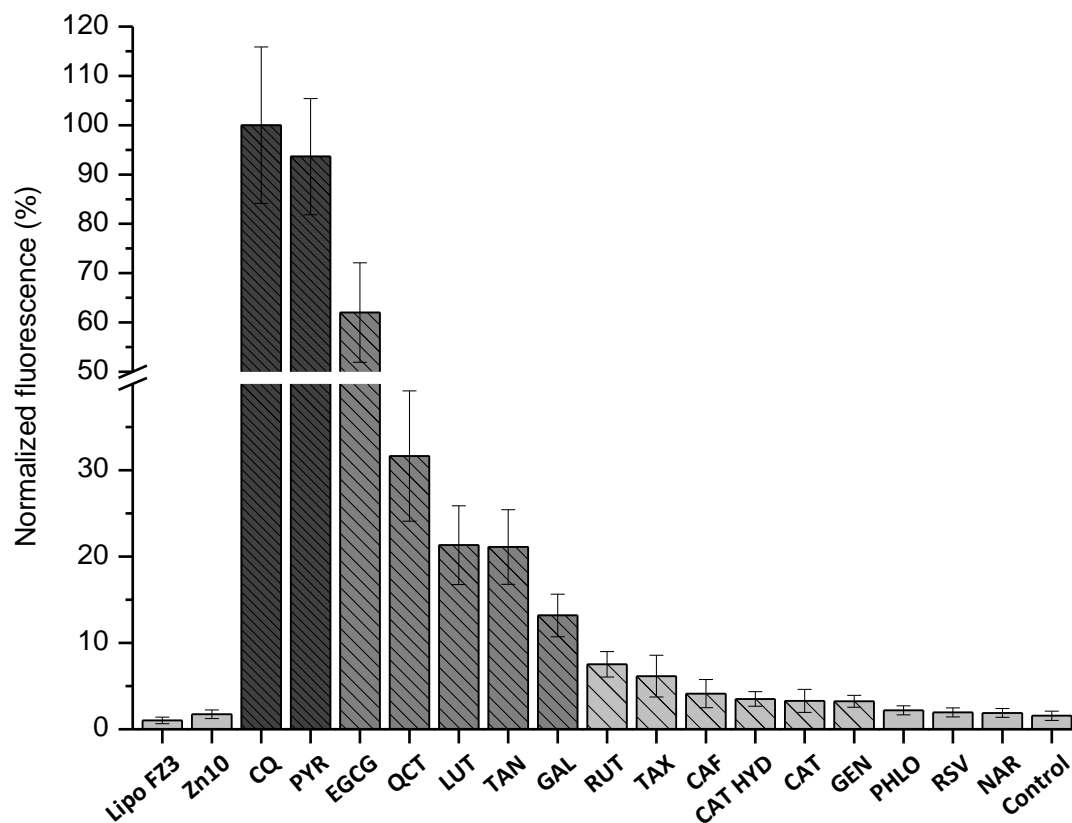


Figure 6.3. Liposome assay for the determination of zinc ionophore activity of polyphenols, clioquinol and pyrithione. The increase in the zinc-dependent fluorescence of FluoZin-3 indicates the capacity of the compounds at  $50 \mu\text{M}$  to interact with  $10 \mu\text{M}$  zinc cations, transport them across the liposome membrane and present them to  $3 \mu\text{M}$  FluoZin-3 in the liposome inner cavity. Control are FluoZin-3 loaded liposomes in the presence of  $10 \mu\text{M}$  zinc cations with 0.1% DMSO. FluoZin-3 loaded liposomes in the absence of zinc (Lipo-FZ3) and in the presence of  $10 \mu\text{M ZnCl}_2$  (Zn10).  $\lambda_{\text{exc}} 494\text{nm} / \lambda_{\text{em}} 516\text{nm}$ . All values are means  $\pm$  SD of three independent experiments.

In the case of EGCG and QCT, both presented a notable zinc ionophore activity, EGCG > QCT, as previously reported.<sup>37</sup> In agreement with the results obtained in the chelation assay, the fluorescence increment ( $\Delta$ ) observed, can be clearly correlated with their chelation strength towards zinc. The polyphenols analyzed can be classified into three groups: strong, soft and no zinc ionophore activity. The polyphenols exhibiting a strong ionophore activity include EGCG (36-fold  $\Delta$ ), QCT (18-fold  $\Delta$ ), LUT (12-fold  $\Delta$ ), TAN (12-fold  $\Delta$ ) and GAL (8-fold  $\Delta$ ); those displaying a soft zinc ionophore activity were RUT (4-fold  $\Delta$ ), TAX (4-fold  $\Delta$ ), CAF (3-fold  $\Delta$ ), CAT HYD (2-fold  $\Delta$ ), CAT (2-fold  $\Delta$ ) and GEN (2-fold  $\Delta$ ), whilst those resulting in no fluorescence were RSV, PHLO and NAR, indicative of a complete lack of zinc ionophore activity. In addition, control experiments demonstrated that the addition of a final concentration of 0.1 % DMSO, as present in the tested samples, did not affect or destabilize the liposomes, thus keeping the FluoZin-3 within the liposomes and not resulting in an increase in fluorescence. Furthermore, TPEN was also tested and displayed a soft zinc ionophore activity as it caused a 10-fold increase in the fluorescent signal (data not shown).

An evaluation of the kinetics of the ionophore behavior of each polyphenol was tested in a time-dependent assay to further understand the zinc transport strength (Figure 6.4). The results showed that the increase of the zinc-FluoZin-3 fluorescence produced by PYR until reaching the maximum fluorescence was instantaneous. CQ also produced a very high increase in the fluorescence and rapidly achieved the maximum fluorescence reaching equilibrium in less than 15 minutes. Regarding the kinetics of the polyphenols studied, almost none of the ionophore active compounds showed a markedly time-dependent increase of the fluorescence. Only in the case of EGCG and QCT a plateau was reached after ca. 40 and 20 minutes respectively, exhibiting a slower, but efficient, chelation and transport kinetics. In addition, control experiments carried out by adding the different compounds to the FluoZin-3 loaded liposomes in the absence of  $ZnCl_2$  did not show any increase in the fluorescence signal (data not shown).

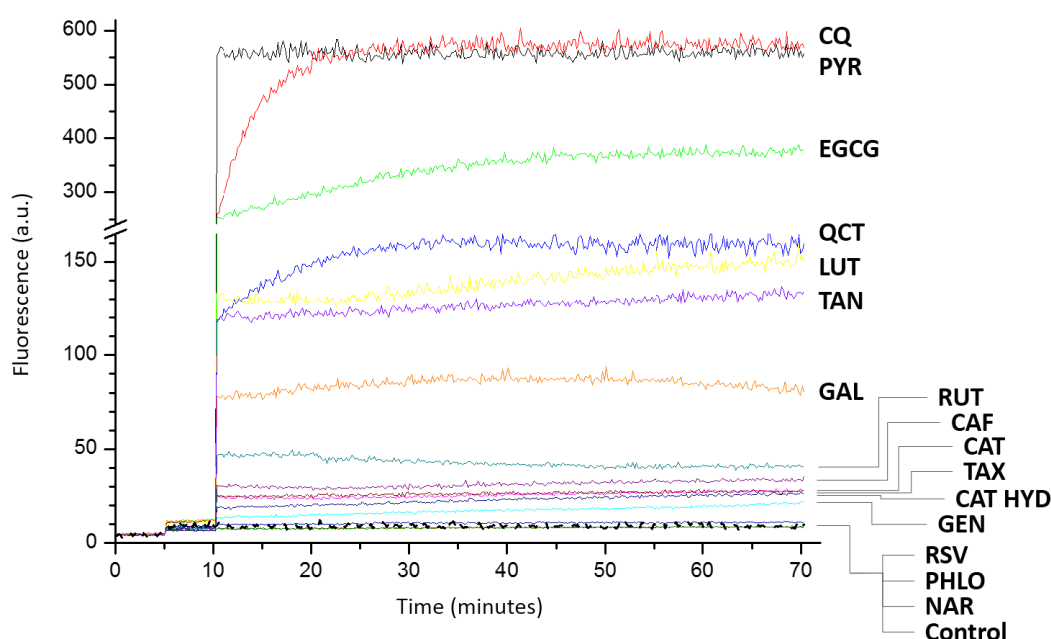


Figure 6.4. Time-dependent fluorescence emission of FluoZin-3 loaded liposomes before (minute 0) and after (minute 5) addition of  $10 \mu M ZnCl_2$ . The fluorescence increased upon the addition of the compounds ( $50 \mu M$ ) at minute 10, and the fluorescence was monitored over the period of an hour.  $\lambda_{exc} 494nm / \lambda_{em} 516nm$ . Results are representative of at least three experiments. In the control sample, only the solvent used to dissolve the ionophores (0.1 % DMSO) was added at minute 10 without showing any fluorescent increase.

In order to confirm the stability of all the liposomes immediately after the fluorescent experiments, DLS and Zeta potential analysis of the vesicles were carried out and the results are presented in Table 6.2. The DLS results confirmed the presence of stable liposomes that had not leaked the fluorophore following exposure to the polyphenols, maintaining roughly the same size as compared with the starting FluoZin-3 loaded liposomes ( $1.3 \pm 0.2 \mu\text{m}$ ) or the control sample (FluoZin-3 loaded liposomes with  $10 \mu\text{M ZnCl}_2$  at final  $0.1 \% \text{ v/v DMSO}$ ) ( $1.1 \pm 0.2 \mu\text{m}$ ) in the absence of the tested compounds. The surface charge of the liposomes following exposure to the polyphenols also demonstrated that the main net charge of the FluoZin-3 loaded liposomes ( $0.8 \pm 2.2 \text{ mV}$ ) was not significantly affected by the zinc-complexes as all measurements indicated approximately a zero charge. Both size and charge results confirmed that the liposome vesicles were maintained intact and the fluorescence signal was solely due to the transport of the zinc-ionophore complex through the lipid bilayer.

Table 6.2. Dynamic light scattering and Zeta-potential measurements of the liposomes loaded with FluoZin-3, as well as the fluorescence increment ( $\Delta$ ) caused by each compound, after the treatment with  $10 \mu\text{M ZnCl}_2$  and polyphenols, clioquinol, pyrithione and TPEN at  $50 \mu\text{M}$  ( $0.1 \% \text{ DMSO}$  final concentration). Standard deviations were calculated from the mean data of a series of experiments ( $n \geq 3$ ).

Compound	$\Delta$ Fluorescence <sup>a</sup>	Liposome parameters	
		Size ( $\mu\text{m}$ )	Charge (mV)
Clioquinol (CQ)	57.2	$1.3 \pm 0.2$	$2.4 \pm 2.9$
Pyrithione (PYR)	53.6	$1.4 \pm 0.1$	$0.8 \pm 1.1$
Epigallocatechin-gallate (EGCG)	35.5	$1.3 \pm 0.1$	$1.6 \pm 2.5$
Quercetin (QCT)	18.1	$1.3 \pm 0.1$	$2.1 \pm 1.8$
Luteolin (LUT)	12.2	$1.4 \pm 0.3$	$1.1 \pm 0.8$
Tannic Ac. (TAN)	12.2	$1.2 \pm 0.1$	$-2.1 \pm 3.6$
TPEN	10.4	$1.1 \pm 0.2$	$0.0 \pm 2.6$
Gallic Ac. (GAL)	7.5	$1.3 \pm 0.3$	$-3.5 \pm 2.8$
Rutin (RUT)	4.3	$1.6 \pm 0.3$	$-2.0 \pm 3.3$
Taxifolin (TAX)	4.3	$1.0 \pm 0.3$	$3.6 \pm 3.0$
Caffeic Ac. (CAF)	2.5	$1.4 \pm 0.4$	$3.6 \pm 1.6$
Catechin (CAT Hyd)	2.4	$1.2 \pm 0.2$	$3.3 \pm 0.6$
Catechol (CAT)	1.9	$1.4 \pm 0.3$	$2.1 \pm 1.3$
Genistein (GEN)	1.8	$1.4 \pm 0.4$	$-2.1 \pm 2.2$
Phloretin (PHLO)	1.3	$1.4 \pm 0.2$	$2.6 \pm 1.1$
Resveratrol (RSV)	1.1	$1.3 \pm 0.2$	$-1.5 \pm 4.1$
Naringenin (NAR)	1.1	$1.3 \pm 0.2$	$4.6 \pm 1.2$
Control <sup>b</sup>	0.9	$1.1 \pm 0.2$	$-2.1 \pm 3.1$

<sup>a</sup> Increment of fluorescence is calculated by the signal obtained from the FluoZin-3 loaded liposomes in the presence of  $10 \mu\text{M ZnCl}_2$  and the respective compound at  $50 \mu\text{M}$  divided by the signal obtained from the FluoZin-3 loaded liposomes with  $10 \mu\text{M ZnCl}_2$ .

<sup>b</sup> Control contains the FluoZin-3 loaded liposomes with  $\text{ZnCl}_2$  ( $10 \mu\text{M}$ ) in the solvent vehicle ( $0.1 \% \text{ DMSO}$ )

The compounds analyzed have been demonstrated to interact to different extents with zinc cations in solution, as well sequestering zinc from fluorescent zinc-FluoZin-3 complexes, forming metal-chelation complexes. In addition, polyphenols were also tested as zinc-carriers across a liposome membrane, and not all compounds were observed to be zinc ionophores. The results from the comparison of both chelating strength capacity and ionophore activity are presented

in figure 6.5, highlighting some interesting observations. Generally, the compounds with a higher chelating capacity, also presented a high ionophore activity. However, some of the polyphenols did not follow this general trend. It is important to note that all the ionophore compounds could chelate the molecule, but not all the chelators have the ability to act as ionophores. The physicochemical properties of each of the polyphenols will directly have an effect on its' ionophore activity, consequently defining the compound as metal sequestering agent or ionophore agent. However a deeper study is still needed to fully understand their mechanism of action.

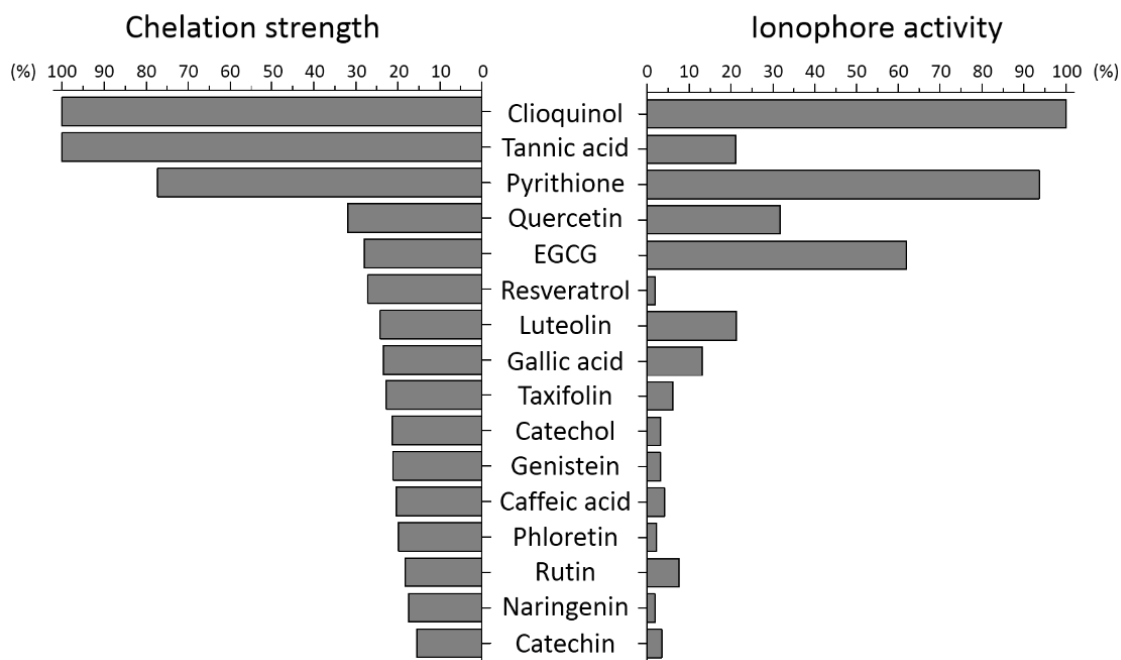


Figure 6.5. Schematic comparison between zinc chelating strength and ionophore activity.

## 6.5. Conclusions

It is confirmed that most of the natural occurring phenolic compounds used in this study have the ability to directly interact and form new structures (complexes) bound with zinc. In many cases these complexes act in a similar way to the control ionophores. We have reported a liposome assay that can be used as a tool for rapid, high-throughput screening of families of polyphenols. In addition, this liposome system can be used to screen the ionophore activity towards other ions such as Ca, Fe or Mg among others. Zinc-specific FluZin-3 loaded liposomes were used to screen the zinc-ionophore activity of a selected library consisting of the most relevant dietary polyphenols, classified according to their zinc-ionophore strength capacity and their chelation efficiency, giving us a better knowledge of the importance of the structural conformation versus biological activity. Synthetic ionophore molecules are currently being used as potential drugs against several chronic diseases including Alzheimer's and different types of cancer, and as demonstrated, one of the mechanisms by which polyphenols exert their beneficial activity is by acting as zinc ionophores. Polyphenol-zinc ion complexes are yet to be investigated and more extensive studies are needed in order to elucidate their possible clinical potential.

## 6.6. References

- [1] Colvin R.A., Fontaine C.P., Laskowski M., Thomas D., Zn<sup>2+</sup> transporters and Zn<sup>2+</sup> homeostasis in neurons. *Eur J Pharmacol* **2003**, 479 (1-3), 171-85.
- [2] Frederickson C., Imaging zinc: old and new tools. *Sci STKE* 2003, **2003** (182), 18.
- [3] Beyersmann D., Haase H., Functions of zinc in signaling, proliferation and differentiation of mammalian cells. *Biometals* **2001**, 14 (3-4), 331-41.
- [4] Brautigan D.L., Bornstein P., Gallis B., Phosphotyrosyl-protein phosphatase. Specific inhibition by Zn. *J Biol Chem* **1981**, 256 (13), 6519-22.
- [5] Maret W., Jacob C., Vallee B.L., Fischer E.H., Inhibitory sites in enzymes: zinc removal and reactivation by thionein. *Proc Natl Acad Sci USA* **1999**, 96 (5), 1936-40.
- [6] Palmiter R.D., Huang L., Efflux and compartmentalization of zinc by members of the SLC30 family of solute carriers. *Pflugers Arch* **2004**, 447 (5), 744-51.
- [7] Lichtlen P., Schaffner W., Putting its fingers on stressful situations: the heavy metal-regulatory transcription factor MTF-1. *Bioessays* **2001**, 23 (11), 1010-7.
- [8] Eide D.J., The oxidative stress of zinc deficiency. *Metallomics* **2011**, 3 (11), 1124-9.
- [9] Laitaoja M., Valjakka J., Jänis J., Zinc coordination spheres in protein structures. *Inorg Chem* **2013**, 52 (19), 10983-91.
- [10] Quesada I.M., Bustos M., Blay M., et al., Dietary catechins and procyanidins modulate zinc homeostasis in human HepG2 cells. *J Nutr Biochem* **2011**, 22 (2), 153-63.
- [11] Higashimoto M., Isoyama N., Ishibashi S., et al., Tissue-dependent preventive effect of metallothionein against DNA damage in dyslipidemic mice under repeated stresses of fasting or restraint. *Life Sci* **2009**, 84 (17-18), 569-75.
- [12] Tapiero H., Tew K.D., Trace elements in human physiology and pathology: zinc and metallothioneins. *Biomed Pharmacother* **2003**, 57 (9), 399-411.
- [13] Powell S.R., The antioxidant properties of zinc. *J Nutr* **2000**, 130 (5S Suppl), 1447S-54S.
- [14] Klotz L.-O., Kröncke K.-D., Buchczyk D.P., Sies H., Role of copper, zinc, selenium and tellurium in the cellular defense against oxidative and nitrosative stress. *J Nutr* **2003**, 133 (5 Suppl 1), 1448S-51S.
- [15] Araújo J.R., Gonçalves P., Martel F., Chemopreventive effect of dietary polyphenols in colorectal cancer cell lines. *Nutr Res* **2011**, 31 (2), 77-87.
- [16] Leopoldini M., Russo N., Toscano M., The molecular basis of working mechanism of natural polyphenolic antioxidants. *Food Chem* **2011**, 125 (2), 288-306.
- [17] Čipák L., Rauko P., Miadoková E., Čipáková I., Novotný L., Effects of flavonoids on cisplatin-induced apoptosis of HL-60 and L1210 leukemia cells. *Leuk Res* **2003**, 27 (1), 65-72.
- [18] Ramos S., Cancer chemoprevention and chemotherapy: dietary polyphenols and signalling pathways. *Mol Nutr Food Res* **2008**, 52 (5), 507-26.
- [19] Bravo L., Polyphenols: chemistry, dietary sources, metabolism, and nutritional significance. *Nutr Rev* **1998**, 56 (11), 317-33.



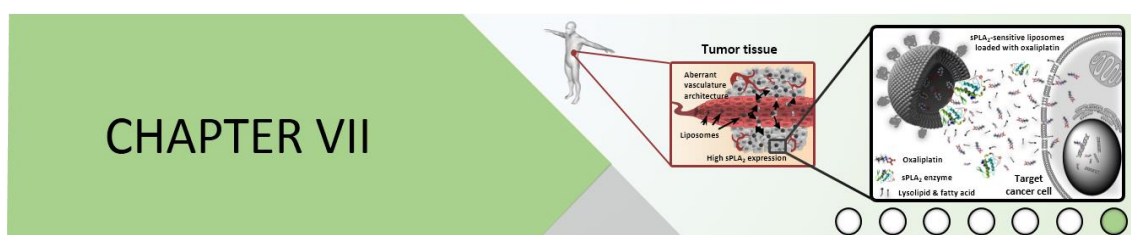
- [20] Russo M., Spagnuolo C., Tedesco I., Bilotto S., Russo G.L., The flavonoid quercetin in disease prevention and therapy: facts and fancies. *Biochem Pharmacol* **2012**, *83* (1), 6-15.
- [21] Hider R.C., Liu Z.D., Khodr H.H., Metal chelation of polyphenols. *Methods Enzymol* **2001**, *335*, 190-203.
- [22] Cao B., Li J., Zhu J., et al., The antiparasitic clioquinol induces apoptosis in leukemia and myeloma cells by inhibiting histone deacetylase activity. *J Biol Chem* **2013**, *288* (47), 34181-9.
- [23] Cao B., Li J., Zhou X., et al., Clioquinol induces pro-death autophagy in leukemia and myeloma cells by disrupting the mTOR signaling pathway. *Sci Rep* **2014**, *4*, 5749.
- [24] Grazul M., Budzisz E., Biological activity of metal ions complexes of chromones, coumarins and flavones. *Coord Chem Rev* **2009**, *253* (21), 2588-2598.
- [25] Thompson M., Williams C.R., Elliot G.E., Stability of flavonoid complexes of copper(II) and flavonoid antioxidant activity. *Anal Chim Acta* **1976**, *85* (2), 375-81.
- [26] Mladenka P., Zatloukalová L., Filipský T., Hrdina R., Cardiovascular effects of flavonoids are not caused only by direct antioxidant activity. *Free Radical Bio Med* **2010**, *49* (6), 963-75.
- [27] Aherne S.A., O'Brien N.M., Mechanism of protection by the flavonoids, quercetin and rutin, against tert-butylhydroperoxide- and menadione-induced DNA single strand breaks in Caco-2 cells. *Free Radical Bio Med* **2000**, *29* (6), 507-14.
- [28] Afanas'eva I.B., Ostrakhovitch E.A., Mikhal'chik E.V., Ibragimova G.A., Korkina L.G., Enhancement of antioxidant and anti-inflammatory activities of bioflavonoid rutin by complexation with transition metals. *Biochem Pharmacol* **2001**, *61* (6), 677-684.
- [29] Fernandez M.T., Mira M.L., Florêncio M.H., Jennings K.R., Iron and copper chelation by flavonoids: an electrospray mass spectrometry study. *J Inorg Biochem* **2002**, *92* (2), 105-11.
- [30] Mira L., Fernandez M.T., Santos M., et al., Interactions of flavonoids with iron and copper ions: a mechanism for their antioxidant activity. *Free Radical Res* **2002**, *36* (11), 1199-208.
- [31] Payán-Gómez S.A., Flores-Holguín N., Pérez-Hernández A., Piñón-Miramontes M., Glossman-Mitnik D., Computational molecular characterization of the flavonoid Morin and its Pt(II), Pd(II) and Zn(II) complexes. *J Mol Model* **2011**, *17* (5), 979-85.
- [32] Wei Y., Guo M., Zinc-Binding Sites on Selected Flavonoids. *Biol Trace Elem Res* **2014**, *161* (2), 223-30.
- [33] Selvaraj S., Krishnaswamy S., Devashya V., Sethuraman S., Krishnan U.M., Flavonoid-Metal Ion Complexes: A Novel Class of Therapeutic Agents. *Med Res Rev* **2013**, *34* (4), 677-702.
- [34] Ding W.-Q., Liu B., Vaught J.L., Yamauchi H., Lind S.E., Anticancer activity of the antibiotic clioquinol. *Cancer Res* **2005**, *65* (8), 3389-95.
- [35] Feng P., Li T., Guan Z., Franklin R.B., Costello L.C., The involvement of Bax in zinc-induced mitochondrial apoptosis in malignant prostate cells. *Mol Cancer* **2008**, *7* (1), 25.
- [36] Liang J.Y., Liu Y.Y., Zou J., et al., Inhibitory effect of zinc on human prostatic carcinoma cell growth. *Prostate* **1999**, *40* (3), 200-7.
- [37] Dabbagh-Bazarbachi H., Clergeaud G., Quesada I.M., et al., Zinc Ionophore Activity of Quercetin and Epigallocatechin-gallate: From Hepa 1-6 Cells to a Liposome Model. *J Agr Food Chem* **2014**, *62* (32), 8085-8093



- [38] Chen L., Wu C., Li J., Study on Scavenging Activities of Free Radical by Luteolin-Zn (II) Complex. *Chem Adhes* **2009**.
- [39] Wang H.-L., Yang Z.-Y., Wang B., Synthesis, Characterization and the Antioxidative Activity of Copper(II), Zinc(II) and Nickel(II) Complexes with Naringenin. *Transit Met Chem* **2006**, *31* (4), 470-474.
- [40] Harper A., Kerr D.J., Gescher A., Chipman J.K., Antioxidant effects of isoflavonoids and lignans, and protection against DNA oxidation. *Free Radical Res* **1999**, *31* (2), 149-160.
- [41] Bodini M.E., del Valle M.A., Tapia R., Leighton F., Berrios P., Zinc catechin complexes in aprotic medium. Redox chemistry and interaction with superoxide radical anion. *Polyhedron* **2001**, *20* (9-10), 1005-1009.
- [42] Le Nest G., Caille O., Woudstra M., et al. Zn-polyphenol chelation: complexes with quercetin, (+)-catechin, and derivatives: II Electrochemical and EPR studies. *Inorganica Chim Acta* **2004**, *357* (7), 2027-2037.
- [43] Yu H.-N., Shen S.-R., Yin J.-J., Effects of metal ions, catechins, and their interactions on prostate cancer. *Crit Rev Food Sci Nutr* **2007**, *47* (8), 711-9.
- [44] Bai Y., Song F., Chen M., et al., Characterization of the rutin-metal complex by electrospray ionization tandem mass spectrometry. *Anal Sci* **2004**, *20* (8), 1147-51.
- [45] De Souza R.F., De Giovanni W.F., Antioxidant properties of complexes of flavonoids with metal ions. *Redox Rep* **2004**, *9* (2), 97-104.
- [46] Donracheva L.G., Mel'nikova N.B., Pegova I.A., et al., Complexes of dihydroquercetin with chromium (III) and zinc (II) asparaginate in water and their effects on the state of lecithin membranes. *Pharm Chem J* **2009**, *42* (10), 564-570.
- [47] Andjelkovic M., Vancamp J., Demeulenaer B., et al., Iron-chelation properties of phenolic acids bearing catechol and galloyl groups. *Food Chem* **2006**, *98* (1), 23-31.
- [48] Chiavarino B., Crestoni M.E., Fornarini S, et al., Infrared spectroscopy of copper-resveratrol complexes: a joint experimental and theoretical study. *J Chem Phys* **2012**, *137* (2), 024307.
- [49] Almeida W.L.C., Vítor D.N., Pereira M.R.G., et al., Redox properties of Ruthenium complex with catechol are involved in toxicity to glial cells. *J Chil Chem Soc* **2007**, *52* (3), 1240-1243.
- [50] Blindauer C.A., Razi M.T., Parsons S., Sadler P.J., Metal complexes of N,N,N',N'-tetrakis(2-pyridylmethyl)ethylenediamine (TPEN): Variable coordination numbers and geometries. *Polyhedron* **2006**, *25* (2), 513-520.
- [51] Genç R., Ortiz M., O'Sullivan C.K., Curvature-Tuned Preparation of Nanoliposomes. *Langmuir* **2009**, *25* (21), 12604-12613.
- [52] Arora A., Byrem T.M., Nair M.G., Strasburg G.M., Modulation of Liposomal Membrane Fluidity by Flavonoids and Isoflavonoids. *Arch Biochem Biophys* **2000**, *373* (1), 102-109.
- [53] Saija A., Scalese M., Lanza M., et al., Flavonoids as antioxidant agents: Importance of their interaction with biomembranes. *Free Radical Bio Med* **1995**, *19* (4), 481-486.
- [54] Yu X., Chu S., Hagerman A.E., Lorigan G.A., Probing the Interaction of Polyphenols with Lipid Bilayers by Solid-State NMR Spectroscopy. *J Agr Food Chem* **2011**, *59* (12), 6783-6789.
- [55] Alonso M.A., Carrasco L., Action of Membrane-Active Compounds on Mammalian Cells. *Eur J Biochem* **1980**, *109* (2), 535-540.

- [56] Alonso M.A., Carrasco L., Molecular basis of the permeabilization of mammalian cells by ionophores. *Eur J Biochem* **1982**, *127* (3), 567-9.
- [57] Erdahl W.L., Chapman C.J., Wang E., Taylor R.W., Pfeiffer D.R., Ionophore 4-BrA23187 Transports  $Zn^{2+}$  and  $Mn^{2+}$  with High Selectivity Over  $Ca^{2+}$ . *Biochemistry* **1996**, *35* (43), 13817-13825.
- [58] Yang J.G., Yu H.N., Sun S.L., et al., Epigallocatechin-3-gallate affects the growth of LNCaP cells via membrane fluidity and distribution of cellular zinc. *J Zhejiang Univ-Sc B* **2009**, *10* (6), 411-21.
- [59] Weissmann G., Anderson P., Serhan C., Samuelsson E., Goodman E., A general method, employing arsenazo III in liposomes, for study of calcium ionophores: results with A23187 and prostaglandins. *P Natl Acad Sci USA* **1980**, *77* (3), 1506-1510.
- [60] Kolber M.A., Haynes D.H., Fluorescence Study of the Divalent Cation-Transport Mechanism of Ionophore A23187 in Phospholipid-Membranes. *Biophys J* **1981**, *36* (2), 369-391.
- [61] Mathew M.K., Nagaraj R., Balaram P., Ionophore-mediated transmembrane movement of divalent cations in small unilamellar liposomes: An evaluation of the chlortetracycline fluorescence technique and correlations with black lipid membrane studies. *J Membrane Biol* **1982**, *65* (1-2), 13-17.
- [62] Ollila F., Halling K., Vuorela P., Vuorela H., Slotte J.P., Characterization of Flavonoid-Biomembrane Interactions. *Arch Biochem Biophys* **2002**, *399* (1), 103-108.





## Activity and tolerability of oxaliplatin formulated in secretory phospholipase A<sub>2</sub>-sensitive liposomes as anticancer drugs



## Activity and tolerability of oxaliplatin formulated in secretory phospholipase A<sub>2</sub>-sensitive liposomes as anticancer drugs

For submission to *ACS Nano*

Houman Pourhassan<sup>†</sup>, Gael Clergeaud<sup>#</sup>, Anders E. Hansen<sup>†‡</sup>, Ragnhild G. Østrem<sup>†</sup>, Frederikke P. Fliedner<sup>†‡</sup>, Ciara K. O'Sullivan<sup>#§</sup>, Andreas Kjær<sup>‡</sup>, Thomas L. Andresen<sup>†</sup>.

<sup>†</sup> Colloids and Biological Interfaces Group, Centre for Nanomedicine and Theranostics, Department of Micro and Nanotechnology, Technical University of Denmark, Produktionstorvet, Building 423, 2800 Kgs. Lyngby, Denmark

<sup>#</sup> Nanobiotechnology & Bioanalysis Group, Department of Chemical Engineering, University of Rovira I Virgili, Avda. Paisos Catalans 26, 43007 Tarragona, Spain

<sup>||</sup> Institució Catalana de Recerca i Estudis Avançats, 08010 Barcelona, Spain

<sup>‡</sup> Cluster for Molecular Imaging, Faculty of Health Sciences, University of Copenhagen, Blegdamsvej 3B, 2200 Copenhagen N, Denmark





## 7.1. Abstract

In this study we investigate the *in vitro* and *in vivo* potential of oxaliplatin formulated in unilamellar phosphatidylcholine/phosphatidylglycerol/PEG2000-phosphatidylethanolamine liposomes with varying degree of sensitivity towards secretory phospholipase A<sub>2</sub> type IIA (sPLA<sub>2</sub>) activation for treating colorectal carcinoma xenografts. From *in vitro* release studies using encapsulated calcein as a drug surrogate, the sensitivity of the formulations towards sPLA<sub>2</sub> activity was tuned by adjusting the fatty acid chain length of the diacyl lipids and the fraction of negatively charged lipid in the liposome lipid bilayer. Treatment of cancer cell lines with these liposomes resulted in efficient *in vitro* growth inhibition compared to non-sensitive liposomes in the presence of sPLA<sub>2</sub>. We demonstrate that membrane perturbation and cytolysis was linked to the sensitivity of the formulation and the ratio between the amount of lysolipids generated and amount of serum proteins present. Using sPLA<sub>2</sub>-secreting human colon cancer xenografts in nude mice as a model, we evaluated the *in vivo* therapeutic potential of sPLA<sub>2</sub>-sensitive liposomes. All of the formulations tested failed to display significant therapeutic efficacy in the evaluated xenografts and the median survival time was not significantly increased. Additionally, sPLA<sub>2</sub>-sensitive liposomes displayed increased toxicity, which at high doses induced diffuse cutaneous hemorrhaging and excessive weight loss.

Despite a clear benefit of including a sPLA<sub>2</sub>-triggered release mechanism *in vitro*, the therapeutic efficacy was not improved compared to conventional liposomes in Colo205 xenografts. In turn, excessive sensitivity of the liposomes can lead to a compromise in their safety making them less tolerogenic and toxic. These findings have implications for the rational design of liposomal drug carriers employing sPLA<sub>2</sub>-triggered drug release.

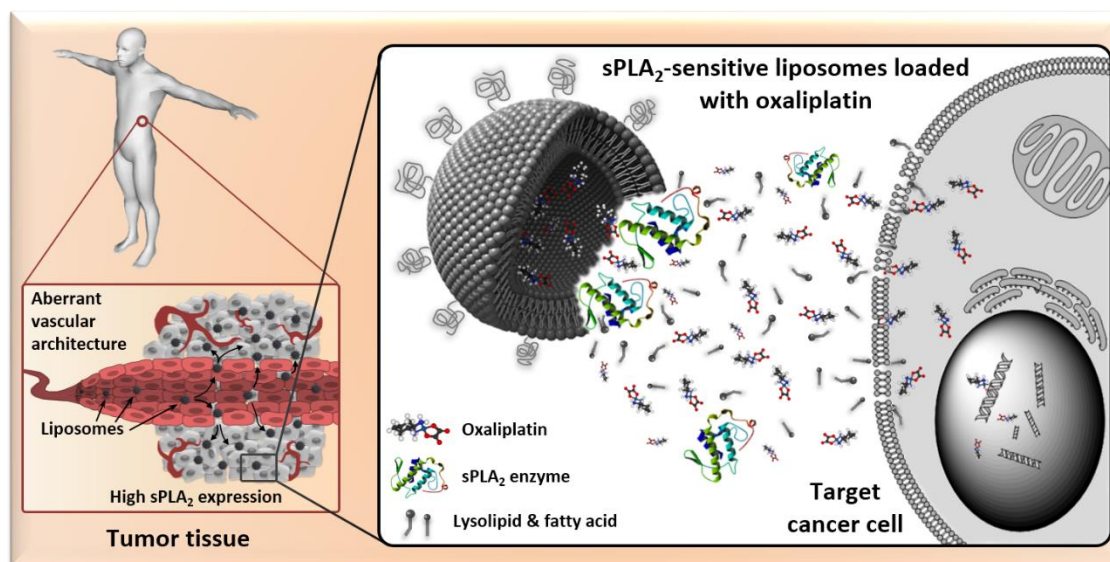


Figure 7.1. Table of contents figure

## 7.2. Introduction

Specific delivery and release of chemotherapeutics within diseased tissue may increase both the therapeutic efficacy and minimize therapy-associated side effects. Delivery strategies that are able to confine and maximize drug exposure specifically to diseased sites are therefore essential

to improve efficacy and tolerability. Long-circulating pegylated liposomes are designed to retain encapsulated drugs, altering drug deposition and improve efficacy and drug toxicity profiles.<sup>1,2</sup> In many cases, insufficient release rates of hydrophilic drugs at the target site limits their therapeutic potential and more advanced liposomal delivery systems are therefore warranted.<sup>3</sup> In general, drugs that benefit from a high peak concentration of bioavailable drug are expected to benefit from triggered release.<sup>4</sup> Several popular approaches exist to trigger drug release by employing environmentally-sensitive liposomes that respond to either external stimuli, e.g. induced hyperthermia,<sup>5,6</sup> or take advantage of pathological changes that arise in the diseased state. The elevated expression of endogenous enzymes in cancerous tissue represents promising strategies to control and obtain a site-specific drug burst release.<sup>7-9</sup> From a therapeutic point of view secretory phospholipase A<sub>2</sub> type IIa (sPLA<sub>2</sub>) is an attractive target, as it is significantly upregulated and highly active in various types of cancer including breast, pancreatic, prostate, and colon.<sup>10-14</sup> Additionally, sPLA<sub>2</sub> exhibits a preferential substrate specificity for organized lipid structures (such as bilayers) over monomeric lipids in solution, thus making it particularly suitable for liposomal drug delivery.<sup>15</sup> Examples of a proof of principle of this concept have been previously reported in both in vitro and in vivo.<sup>9,16,17</sup>

sPLA<sub>2</sub> catalyzes the hydrolysis of the ester linkage in the sn-2-acyl chain of phospholipids, which yields free fatty acids and 1-acyl-lysophospholipids.<sup>3,18</sup> Liposome membrane destabilization by sPLA<sub>2</sub> is thought not only to liberate the encapsulated drug, but also yield high local concentrations of lysolipids and free fatty acids. These can serve as permeability enhancers across biological membranes, or at high amounts, directly induce cellular toxicity by forming aggregated structures with detergent-like properties.<sup>9,16,19</sup>

The sPLA<sub>2</sub> enzyme has a high specificity for anionic lipids, such as phosphatidylglycerol (PG), potentially due to the many positively charged amino acid residues present in the sPLA<sub>2</sub> protein sequence that allows the enzyme to interact with the negatively charged phospholipid head groups.<sup>18</sup> Thus, for controlled delivery purposes the sensitivity of the drug carrier to sPLA<sub>2</sub> and the level of drug release can be modulated by producing liposomes with high amounts of negatively charged lipids.<sup>18</sup>

Encapsulating cisplatin in long-circulating liposomes, similar to the formulation used in Doxil<sup>®</sup>, eliminated the dose-limiting severe nephrotoxicity and peripheral neuropathy commonly associated with cisplatin. However, the liposomal formulation failed to improve therapeutic efficacy, which was believed to be due to inefficient release of the drug (reviewed in Lui et al.).<sup>20</sup> Based on the success from pre-clinical studies, the first liposomal formulation with a sPLA<sub>2</sub>-triggered release mechanism, LiPlaCis<sup>®</sup> entered clinical Phase I trial in patients with advanced or refractory solid tumors to address this issue. The original formulation was, however, reported to be too unstable, with high levels of platinum excreted via urine along with a high incidence of dose-related renal toxicity that is characteristic of free cisplatin. The reason for this stability issue was not clear, but appeared not to be related with a premature activation of the liposomes during circulation, since no correlation was found between serum sPLA<sub>2</sub> levels and the plasma half-life of the particles.<sup>21</sup> Additionally, an unusually high incidence of complement-related acute infusion reactions (39 %) was observed. In comparison, other clinically relevant liposome formulations induce similar symptoms as well, but at a much lower rate of up to 9 %, <sup>21</sup> indicating that the high negative charge of the liposome may have activated the complement system. Despite these obstacles, LiPlaCis has re-entered clinical development after it was temporarily ceased in the clinical Phase I stage in 2009 due to safety issues that required reformulation.

The aim of the present work was to investigate the potential of highly sensitive sPLA<sub>2</sub>-responsive liposomes as drug carriers for the encapsulation of the platinum-based drug oxaliplatin (L-OHP) for treatment of colon cancer. L-OHP has been shown to be particularly effective against colorectal cancers and is not associated with nephrotoxicity.<sup>20</sup> We compare formulations with varying degrees of sensitivity towards sPLA<sub>2</sub> and assess their *in vitro* cytotoxicity against human tumor cell lines, and their efficacy, as well as tolerability *in vivo* using human colorectal tumor xenografts.

## 7.2. Methods

### 7.2.1. Materials

The lipids 1,2-dipalmitoyl-sn-glycero-3-phosphocholine (DPPC), 1,2-dipalmitoyl-sn-glycero-3-phospho-(1'-rac-glycerol) (DPPG), 1,2-distearoyl-sn-glycero-3-phosphocholine (DSPC), 1,2-distearoyl-sn-glycero-3-phospho-(1'-rac-glycerol) (DSPG), 1,2-distearoyl-sn-glycero-3-phosphoethanolamine-N-[methoxy(polyethylene glycol)-2000] (DSPE-PEG2000) were purchased from Avanti Polar Lipids, Inc. (Alabama, USA). Lyophilized mixture of hydrogenated L- $\alpha$ -phosphatidylcholine (HSPC), cholesterol (chol), and DSPE-PEG2000 (57:38:5 mol %) was acquired from Lipoid GmbH (Ludwigshafen, Germany). Oxaliplatin was purchased from Shanghai Yingxuan Chempharm (Shanghai, China).

### 7.2.2. Preparation of liposome vesicles

Liposomes were prepared following a previously reported method.<sup>22</sup> Briefly, accurate amounts of lipids were dissolved in chloroform:methanol (9:1 v/v), followed by solvent evaporation at room temperature (RT) under a gentle stream of nitrogen. To ensure complete solvent removal, the lipid films formed were placed under vacuum overnight. Multilamellar vesicles (MLV) were prepared by hydrating the lipids for 30 minutes with a buffered solution (10 mM HEPES, 5 % glucose, pH = 7.4), containing (if desired) the encapsulate molecule, at a temperature 15 °C above the main phase transition temperature with vortexing every 5-10 minutes. For the preparation of calcein loaded liposomes, calcein was firstly dissolved in water and then the pH was adjusted to pH = 7.4 prior to addition to the hydrating solution to a final calcein concentration of 20 mM. The preparation of oxaliplatin-loaded liposomes was carried out by previously dissolving 15 mg/mL oxaliplatin in the buffered solution at 65 °C for 1 hour under stirring conditions. The MLV suspensions were extruded 21 times through two-stacked 100 nm pore size polycarbonate filters at 55 °C forming homogeneous large unilamellar vesicles (LUV) (< 130nm) with a narrow size distribution (PDI < 0.15). For *in vivo* applications liposomes were extruded using a high-pressure extrusion device (Northern Lipids Inc., Burnaby, Canada) and were sequentially downsized through 400/200/100 nm polycarbonate filters. Calcein containing liposomes were purified by gel filtration through a Sephadex G-50 size exclusion column using HEPES buffer as eluant and liposomes loaded with oxaliplatin were purified by dialysis for 3 days using cassettes of 100 kDa molecular cut-off and HEPES buffer containing 1 mM CaCO<sub>3</sub> (>99% encapsulation). All liposomes were stored at 4 °C.

## 7.2.3. Physicochemical characterization of liposomal drug carriers

### 7.2.3.1 Size and surface charge

Liposome size and size distribution was analyzed using dynamic light scattering (DLS) and the vesicles surface charge was determined by zeta-potential using a ZetaPALS system (Brookhaven Instruments Corporation, New York, USA). Liposome solutions were diluted 100-fold in filtered (0.2  $\mu\text{m}$ ) buffer, placed in plastic cuvettes and degassed for 5 minutes to expel any air in the samples before performing the DLS and zeta-potential analysis. The standard deviations were calculated from the mean data of experiments ( $n \geq 3$ ).

### 7.2.3.2. Lipid and drug concentration

The lipid concentration was determined by measuring the total phosphorous content and the oxaliplatin concentration by determining the amount of platinum present in the liposomes using inductively coupled plasma mass spectrometry (ICP-MS) using a Dionex<sup>TM</sup> ICS-5000<sup>+</sup> system (Thermo Scientific<sup>TM</sup>, Dreieich, Germany). For the phosphorous measurements, samples were analyzed by diluting 5000-fold in 2% v/v HCl containing 10 ppb of Gallium as an internal standard. To accurately measure the platinum-based chemotherapeutic, samples containing oxaliplatin were diluted 500000-fold in 2% v/v HCl containing 0.5 ppb of Iridium as an internal standard.

## 7.2.4. Calcein release assay

Specificity and sensitivity of liposomes toward sPLA<sub>2</sub> was determined by the calcein release assay. Fluorescent calcein was entrapped inside liposomes at a self-quenching concentration following the procedure described above and the time-resolved sPLA<sub>2</sub>-specific release of the fluorophore was recorded as a rise in the fluorescent intensity (FI). Briefly, calcein-loaded liposomes were diluted to 75  $\mu\text{M}$  lipid concentration in Calcein-Release Buffer (CRB, 10 mM Hepes, 110 mM KCl, 30  $\mu\text{M}$  CaCl<sub>2</sub>, 10  $\mu\text{M}$  Na EDTA, pH 7.4) and transferred to a glass quartz cuvette (1 mL) and the fluorescence (Ex. 495 nm, Em. 515 nm) was recorded under magnetic stirring at 37 °C using a SLM8000 spectrophotometer (OLIS Inc., Georgia, USA). Once the signal had stabilized for at least 1000 seconds, the sPLA<sub>2</sub> enzyme was added to the sample (5  $\mu\text{L}$  human tears; 20  $\mu\text{L}$  conditioned cell growth medium (CCM) of Colo205). Triton X-100 (TX-100) was added to obtain maximal fluorescent signal from complete release of calcein. The percentage release was calculated by the formula  $100 \% \times (F_t - F_0)/(F_{\text{TX-100}} - F_0)$ , where  $F_t$  represents the FI at a specific time point,  $F_0$  represents FI at time zero, and  $F_{\text{TX-100}}$  the FI the total FI after addition of TX-100. All studies were done in triplicate.

## 7.2.5. Cell culture and cytotoxicity

The HT-29 human colon carcinoma and Colo205 human colon carcinoma cell lines were purchased from American Type Culture Collection (Virginia, USA). HT-29 cells were maintained in DMEM supplemented with 10 % heat-inactivated FBS, 1 % penicillin/streptomycin (pen/strep) in a humidified 5 % CO<sub>2</sub> atmosphere at 37 °C. Colo205 cells were maintained in RPMI-1640 supplemented with 10 % heat-inactivated FBS, 1 % pen/strep. Both cells were sub-cultured every 2-3 days. Colo205 CCM was prepared under serum-starved conditions using the following procedure: The growth media of the cells, was exchanged after 48 hour incubation of 15-20 $\times 10^6$  cells in a T-75 culture flask with 20 mL fresh RPMI-1640 supplemented only with 1 % pen/strep. Following additional 48 hours of growth, the CCM was collected and stored at -20 °C until needed.

The 3-(4,5-dimethylthiazol-2-yl)-5-(3-carboxymethoxyphenyl)-2-(4-sulfophenyl)-2H-tetrazolium (MTS) assay (Promega Biotech AB, Stockholm, Sweden) was used to determine the *in vitro* anti-proliferative effect. Cells (HT-29 and Colo205) were plated in 96-well plates at a density of  $1 \times 10^4$  cells per well in their respective complete growth media. After overnight incubation to allow cell attachment, the media was removed and replaced with either complete growth media or Colo205 CCM containing varying concentrations of free drug (1.6-100  $\mu$ M) or liposomal samples (1.6-100  $\mu$ M drug, or in the case of empty vesicles, a lipid concentration equivalent to the drug-loaded liposomal sample), and the cells were further incubated for 6 hours at 37 °C. After this co-incubation period, the cell media was exchanged with fresh growth media and the cells were allowed to grow for an additional 66 hours (72 hours in total). Values for cell survival are expressed as the percentage reduction in metabolically active cells relative to the solvent controls. All studies were repeated three times.

#### 7.2.6. Time-lapse micrographs

HT-29 cells (30.000 cells) were seeded in 8-well chamber slides (Sigma-Aldrich) in 0.3 mL of RPMI-1640 medium containing 10% FBS and pre-incubated for 24 h. Hereafter, the media was aspirated and the liposomes (100  $\mu$ L/well) were added to the cells at a final drug concentration of 100  $\mu$ M in Colo205 CCM. The cells were recorded for 4 h and images were captured on a Leica TCS SP5 AOBS confocal microscope with a 20X air-objective (Heidelberg, Germany). The microscope was equipped with an incubator box and CO<sub>2</sub> supply for optimal growth conditions during imaging (Life Imaging Services GmbH, Basel, Switzerland).

#### 7.2.7. *In vivo* antitumor activity of liposomal L-OHP in human colorectal tumor xenografts in nude mice

Colo205 ( $7.5 \times 10^6$ ) cells collected in 100  $\mu$ L culture medium was injected subcutaneous into the right flank of 6-week old female NMRI-nu mice (Taconic, Lille Skensved, Denmark). Once tumor masses reached app. 150 mm<sup>3</sup> (10 days) animals were randomized into 5 groups of 8 mice and received intravenous treatment every 4 days. Treatment groups received a dose of oxaliplatin (5 mg/kg), alone or encapsulated in liposomes, and control mice were injected with isotonic glucose solution at a compatible volume. Tumor size measured by electronic caliper and body weight was monitored two to three times a week. The tumor volume was calculated using the formula: Volume = (length  $\times$  width<sup>2</sup>) / 2, where width was the shortest measurement in millimeter. The animals were sacrificed upon a tumor size of 1000 mm<sup>3</sup>, loss of body weight > 15 % or mice displaying clear signs of mitheriving. Tumor-to-control (T/C) ratios were calculated for all time points and T/C ratios < 0.15 was considered highly effective, T/C ratios 0.15 – 0.45 was considered moderately efficient. Kaplan-Meier plots were constructed based on the above-specified end-points and median survival time determined for all groups and compared log-rank (Mantel-Cox) test, respectively. Differences were considered significant if the *p* value was less than 0.05. Statistical analysis was performed using GraphPad Prism version 6.0 for Mac OS X (California, USA).

### 7.3. Results and discussion

The enzymatic activity of sPLA<sub>2</sub> towards liposomes can be significantly modulated by the composition of the target lipid bilayer and its morphological and physicochemical properties. Thus, it is of great interest to bioengineer liposome carriers that are sufficiently responsive



towards sPLA<sub>2</sub> hydrolysis to cause complete load release within a short period of time. sPLA<sub>2</sub>-sensitive liposomes were composed of 1,2-dipalmitoyl-sn-glycero-3-phosphocholine (DPPC), 1,2-dipalmitoyl-sn-glycero-3-phosphoglycerol (DPPG), 1,2-distearoyl-sn-glycero-3-phosphocholine (DSPC), 1,2-distearoyl-sn-glycero-3-phosphoglycerol (DPPG), N-(carbonyl-methoxypolyethyleneglycol-2000)-1,2-distearoyl-sn-glycero-3-phosphoethanolamine-polyethyleneglycol 2000 (DSPE-PEG2000). As controls, non-hydrolysable liposomes were prepared from hydrogenated soybean phosphocholine (HSPC), cholesterol and DSPE-PEG2000. The liposomes were produced using standard thin film hydration with subsequent downscaling through polycarbonate filters. For in vivo applications we used a high-pressure extruder device to obtain highly homogenous particles (Table 7.1). L-OHP was passively loaded into the liposomes by dispersing the lipid films with a saturated solution of the drug (15 mg/mL) followed by dialysis to remove any excess drug. The size distribution, polydispersity index, and zeta potential of the particles was characterized, along with the lipid and drug concentration and the encapsulation efficiency. Homogenous liposomes were obtained exhibiting particle sizes of ca. 100 nanometers that carried a negative surface charge between -20 to -27 mV. All of the liposomes exhibited drug-loading efficiencies above 99 %, signifying a highly effective intravesicular encapsulation of oxaliplatin in these liposomes. For in vitro release studies calcein was used at self-quenching concentrations as a drug surrogate to produce equivalent calcein-loaded liposomes. This allowed the enzymatically-triggered release to be monitored over time from an increase in calcein fluorescence.

Table 7.1. In vivo evaluated liposomal formulations of oxaliplatin.

	Size (nm)	PDI <sup>a</sup>	Zeta-potential <sup>b</sup> (mV)	L-OHP <sup>c</sup> (mg/mL)	Lipid (mg/mL)	EE <sup>d</sup> (%)	Drug-to-lipid weight ratio
HSPC/Chol/DSPE-PEG2000 (57:38:5) + L-OHP	106 ± 1.0	0.04	-20 ± 1	1.1	17.1	99.7	1:16
DPPC/DPPG/DSPE-PEG2000 (70:25:5) + L-OHP	94 ± 1.0	0.04	-21 ± 1	1.6	16.3	99.6	1:10
DPPC/DPPG/DSPE-PEG2000 (55:40:5) + L-OHP	98 ± 0.1	0.04	-27 ± 1	1.9	22.2	99.9	1:12

<sup>a</sup> Polydispersity index (PDI) determined by dynamic light scattering

<sup>b</sup> Zeta-potential was determined using comparable liposomes without any drug loaded

<sup>c</sup> Oxaliplatin (L-OHP)

<sup>d</sup> Encapsulation efficiency (EE) is the percentage of liposomal to free fraction of L-OHP

The sPLA<sub>2</sub> enzyme has been largely reported to have a moderate and a rapid mode of action separated by a particular lag-time, in which the enzyme accumulate over the lipid membrane and begin to insert within the bilayer.<sup>23</sup> The results presented in figure 7.2 illustrate the differences in lag-time and enzyme activity of sPLA<sub>2</sub> present in human tear fluid from healthy subjects, as well as in the conditioned cell growth medium (CCM) of human Colo205 cancer cells towards calcein-loaded liposomes with different lipidic formulations. The molar ratio of negatively charged lipid present in the liposome membrane played a key role in the enzyme activity and calcein release profiles. In membranes composed of DPPC/DPPG/DSPE-PEG2000, when 25 % of the negatively charged lipid DPPG was present in the bilayer the sPLA<sub>2</sub> was only able to cause partial calcein release irrespective of the enzyme source, whereas increasing the percentage of DPPG lipid to 40 %, the membrane became fully enzyme-degradable and calcein was completely released within 1500 seconds (Fig 7.2). More negatively charged membranes

are also feasible for the sPLA<sub>2</sub>-triggered release concept; however, a compromise exists between the membrane charge and the well-described opsonization by the immune system. In addition, the sensitivity of the liposome towards sPLA<sub>2</sub>-degradation can also be tuned by using membranes composed of phospholipids with different phase transition temperatures ( $T_m$ ). The results showed that liposomes made of 16-carbon chain lipids with an overall  $T_m$  of 41 °C were highly sensitive towards sPLA<sub>2</sub>-degradation, whilst in 18-carbon lipid membranes with a higher  $T_m$  of 55 °C, the enzyme activity was almost suppressed, mainly due to the limited fluidity rendered by the solid-phase behavior of the membrane. This was evident from the time it took to reach 50 % release of calcein with DPPC/DPPG/DSPE-PEG2000 (55:40:5 mol %) liposomes (70.1 sec) being > 10 and > 30 times faster than DPPC/DPPG/DSPE-PEG2000 (70:25:5 mol %) liposomes (857.7 sec) and DSPC/DSPG/DSPE-PEG2000 (55:40:5 mol %) liposomes (>2000 sec), respectively (Fig 7.2). Incorporation of small amounts of pegylated lipids (5 mol % DSPE-PEG2000) into the sPLA<sub>2</sub>-sensitive formulation, which is necessary for intravascular administered liposomes to avoid clearance by the reticulo-endothelial system,<sup>24</sup> did not sterically hinder the enzymatic hydrolysis of the liposome membrane, which is consistent with earlier reports<sup>9,16,25</sup> (Fig. 7.2). It was previously shown using snake PLA<sub>2</sub> that pegylation does in fact facilitate the binding of the enzyme presumably from slightly reducing the zeta potential of the lipid bilayer.<sup>19</sup>

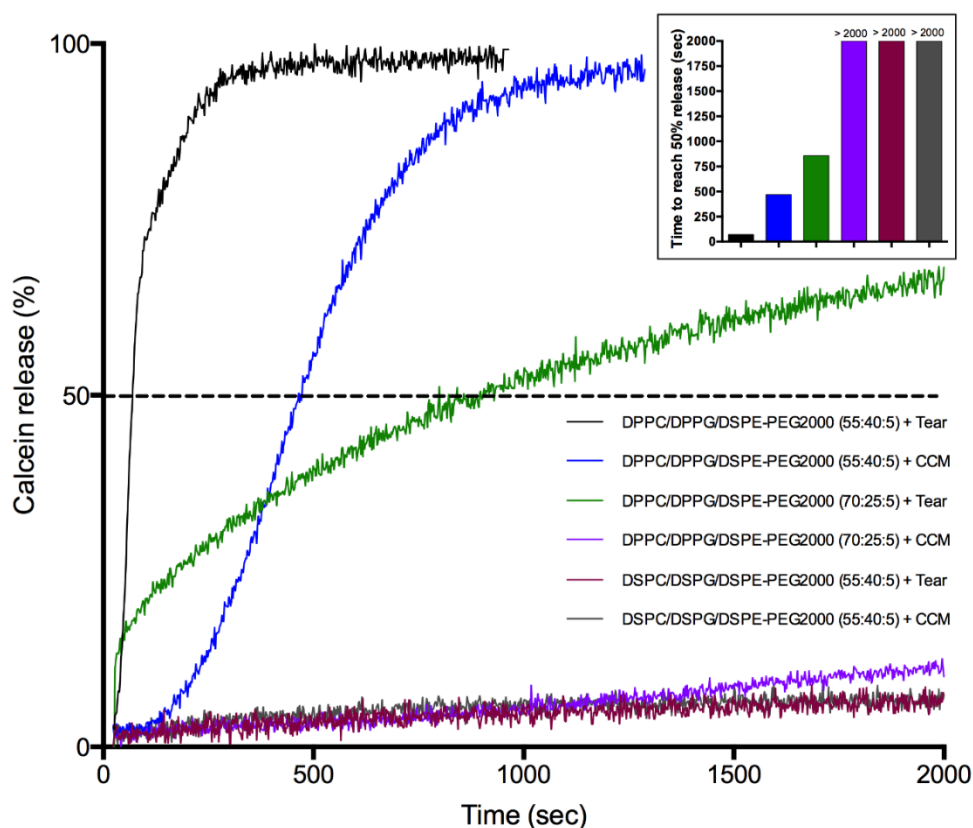


Figure 7.2. *In vitro* sPLA<sub>2</sub>-dependent release kinetic of calcein from liposomal formulations incubated at 37 °C. Human tear fluid and cell conditioned media (CCM) from human Colo205 cancer cells is used as enzyme sources of sPLA<sub>2</sub>. All results are expressed relative to 100 % release observed in the presence of Triton X-100 (TX-100) and are indicative of at least three experiments. Insert shows the time-intersect for the individual formulations reaching 50 % release in seconds.

Levels of sPLA<sub>2</sub> have previously been reported in both tear fluid of healthy subjects ( $55 \pm 34$  µg/mL),<sup>26</sup> and in the CCM of Colo205 cancer cells following 72 hours of *in vitro* culture ( $75 \pm 20$  ng/mL).<sup>16</sup> As sPLA<sub>2</sub> from two different enzyme sources induced comparable leakage behavior, this supports the specificity of the concept towards sPLA<sub>2</sub>-sensitivity. Importantly, the

substantially lower concentration of sPLA<sub>2</sub> present in CCM relative to tear fluid, would explain the differences observed in the release kinetics between the two enzyme sources seen here. However, even though increasing the sensitivity of the formulation would lower the threshold where the liposomes become activated inside the tumor, it also bears a risk of premature activation of the particles before reaching the cancerous tissue. As serum sPLA<sub>2</sub>-levels are frequently seen to be elevated in cancer patients (1-14 ng/mL) compared to cancer-free subjects (1-2 ng/mL),<sup>27-29</sup> an aberrant serum level of sPLA<sub>2</sub> in combination with excessive sensitivity could potentially cause intravascular drug release and result in an undesired redistribution of the drug during circulation.

The in vitro cytotoxicity of L-OHP encapsulated in sPLA<sub>2</sub>-sensitive liposomes shown in figure 7.3 was assessed by MTS staining. The compounds were tested in sPLA<sub>2</sub>-secreting Colo205 cells and non-secreting HT-29 cells with added exogenous sPLA<sub>2</sub> using CCM from Colo205 cells as a source of enzyme. In both colorectal cancer cell lines sPLA<sub>2</sub>-sensitive liposomal L-OHP were highly cytotoxic, with drug concentrations able to inhibit cell growth by 50 % (IC<sub>50</sub>) of around 10 to 12.5 μM (Fig 7.3A and 7.3B). In Colo205 cells, sPLA<sub>2</sub>-sensitive liposomal L-OHP induced a comparable anti-proliferative effect as the free drug (Fig 7.3A), whereas for HT-29 cells the sPLA<sub>2</sub>-degradable liposomes exceeded that of unencapsulated L-OHP at identical drug concentrations (Fig 7.3B). In accordance with the substrate specificity of sPLA<sub>2</sub> shown in figure 7.2, efficient growth inhibition of HT-29 cells was observed only when the liposomes were activated by sPLA<sub>2</sub> (Fig 7.3C). However, increasing the concentration of drug-loaded liposomes, partial growth inhibition was seen even in the absence of enzyme (data not shown).

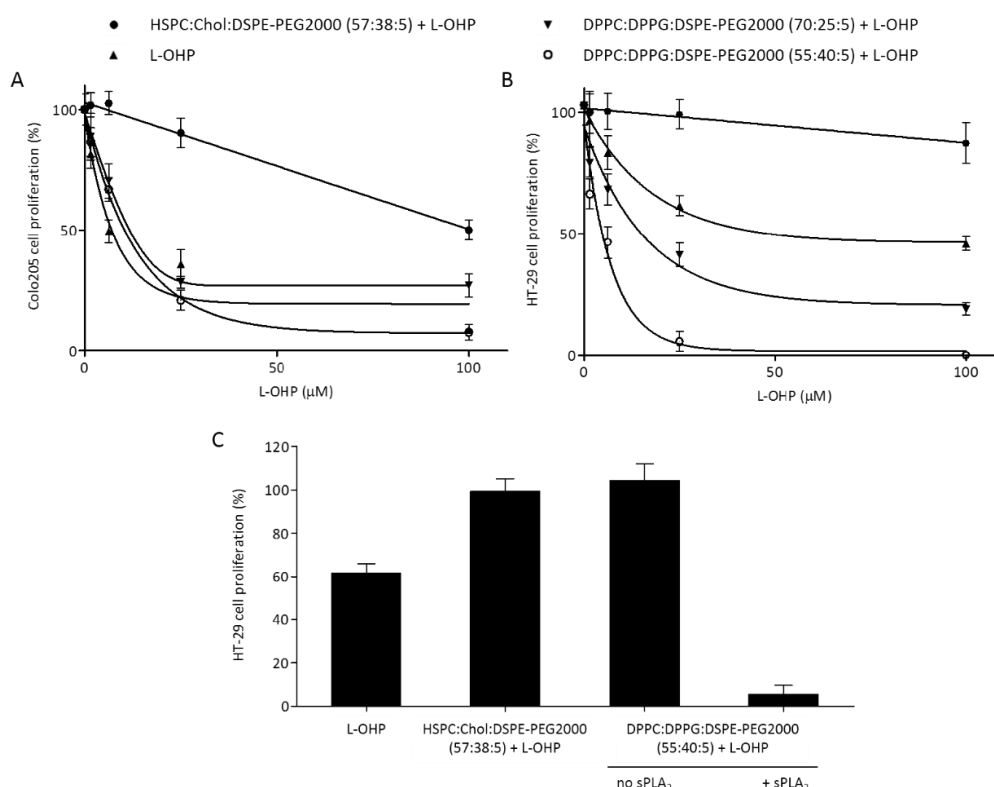
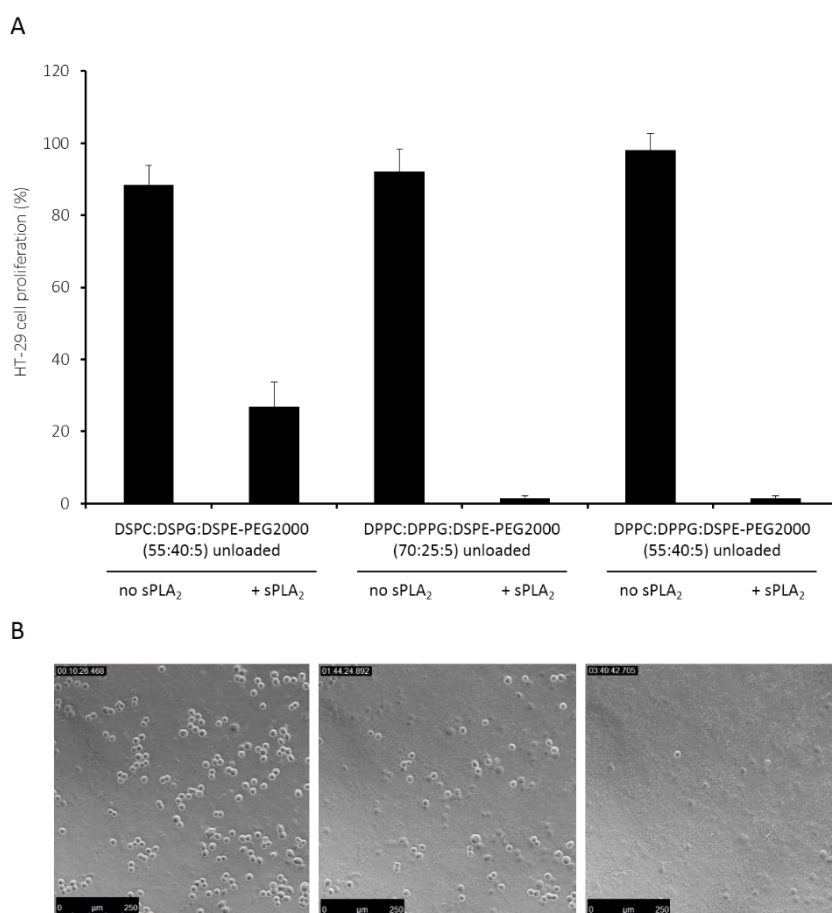


Figure 7.3. In vitro cytotoxicity of sPLA<sub>2</sub>-labile liposomes loaded with L-OHP against sPLA<sub>2</sub>-secreting Colo205 cells (A) and sPLA<sub>2</sub>-deficient HT-29 cells in the presence of Colo205 cell conditioned medium (contain sPLA<sub>2</sub>) (B). L-OHP in free form or encapsulated in non-degradable liposomes are used as controls. Lack of cytotoxicity of sPLA<sub>2</sub>-sensitive liposomes against non-sPLA<sub>2</sub>-secreting HT-29 cells in the absence of exogenous sPLA<sub>2</sub> show the specificity of the concept towards sPLA<sub>2</sub> and dependence of sPLA<sub>2</sub> activation (C). Representative plots of studies done in triplicate. Results are means ± SD of triplicate measurements.



Flow cytometry demonstrated that up to 60 % of the treated cells stained positive for the liposomes labeled with lipid-anchored rhodamine B following 6 h incubation, and exhibited enhanced mean fluorescence intensity upon extended co-incubation times (Supporting information, Section A1). On the other hand, assessing the amount of unspecific drug leakage from the liposomes determined by inductively coupled plasmon mass spectrometry and by use of spin-filtration in order to separate free and liposomal platinum fractions, we found that the liposomes only leaked negligible (<10 % on average) amounts of drug following 24 h in the presence of high amounts of serum, i.e. 50 % fetal bovine serum (Supporting information, Section A2). Taken together, this would imply that the unspecific cytotoxicity was most likely caused by cellular uptake and subsequent intracellular drug release, and not drug leakage from unstable liposomes.

Since a triggered release strategy based on sPLA<sub>2</sub> activity is known to generate permeability enhancing lysolipids and free fatty acids, we investigated the contribution of membrane disruption to the cytotoxic effect, as opposed to the anticancer activity of the released drug. The *in vitro* growth inhibition of sPLA<sub>2</sub>-degradable liposomes was evident to arise predominantly from the carrier upon sPLA<sub>2</sub>-catalyzed hydrolysis. This was demonstrated by measuring the growth inhibition of HT-29 cells treated with unloaded sPLA<sub>2</sub>-sensitive liposomes with and without added sPLA<sub>2</sub> (Fig 7.4A).



*Figure 7.4. In vitro cytotoxicity of unloaded sPLA<sub>2</sub>-sensitive liposomes comes predominantly from cellular lysis following sPLA<sub>2</sub>-driven hydrolysis and formation of permeability enhancing components. In the absence of sPLA<sub>2</sub>, unloaded sPLA<sub>2</sub>-sensitive liposomes are nontoxic, while in presence of sPLA<sub>2</sub>, they effectively inhibit HT-29 cell growth (A). Results are mean ± SD of triplicate measurements. Time-lapse micrographs show complete lysis of HT-29 cells following 3 hours of incubation with DPPC/DPPG/DSPE-PEG2000 (55:40:5 mole %) in the presence of sPLA<sub>2</sub>-proficient Colo205 cell conditioned medium (B).*

Consistent with earlier reports, the empty carriers alone acted as prodrugs that upon enzymatic activation efficiently induced growth inhibition without the presence of an encapsulated drug.<sup>9,16</sup> For HT-29 cells, both of the DPPC/DPPG/DSPE-PEG2000 formulations were able to induce complete growth inhibition of the tumor cells irrespective of the amount of PG present in the membrane (Fig 7.4A). The DSPC/DSPG/DSPE-PEG2000 only induced partial growth inhibition despite the presence of 40 % PG (Fig 7.4A). Thus, based on the evidence from the calcein release experiments and the in vitro cytotoxicity, we found that low enzyme sensitivity of liposomes leads to a more slow generation of membrane permeable products that is related to the slower rate of hydrolysis, however over prolonged periods these can accumulate and lead to release of the encapsulated drug under the investigated conditions. Furthermore, time-lapse micrographs of HT-29 cells during treatment with DPPC/DPPG/DSPE-PEG2000 (55:40:5 mole %) and sPLA<sub>2</sub>-containing cell conditioned media revealed complete disruption of the cellular membranes following 3 hours of incubation with the cells. This supports a dependence of liposome hydrolysis and cytolytic lipid component generation upon sPLA<sub>2</sub> activity and showed the fast temporal onset of the process using highly sensitive liposomes (Fig 7.4B).

Serum albumin has previously been shown to bind up to five lysophospholipids per albumin molecule<sup>30</sup> and therefore the presence of high amounts of plasma proteins can strongly modulate the permeability enhancing properties of sPLA<sub>2</sub>-sensitive liposomes. Even though this can be an advantage during circulation to avoid disruption of blood-borne cells as well as ensure vessel integrity, it may have implications for activating the particles inside tumors. With respect to the intratumoral activation and considering the disrupted nature of the endothelial barrier found in tumor blood vasculature, plasma proteins that under normal circumstances are sterically hindered from crossing the endothelium and extravasate into the surrounding tissues and thereby help to establish the colloidal osmotic pressure of the circulatory system, are likely to be present in abnormally elevated concentrations inside the tumor interstitial space due to the structural defects present in the malignant state.<sup>31</sup> In order to address the effect of serum on the anti-proliferative effect of sPLA<sub>2</sub>-sensitive liposomes, HT-29 cells were treated with sPLA<sub>2</sub>-sensitive liposomal L-OHP, together with Colo205 CCM either without any serum present or spiked with either 10 % (low) or 50 % (high) fetal bovine serum (Fig 7.5). The data demonstrate that a high level of serum proteins can influence the cytotoxic effect of the carrier.

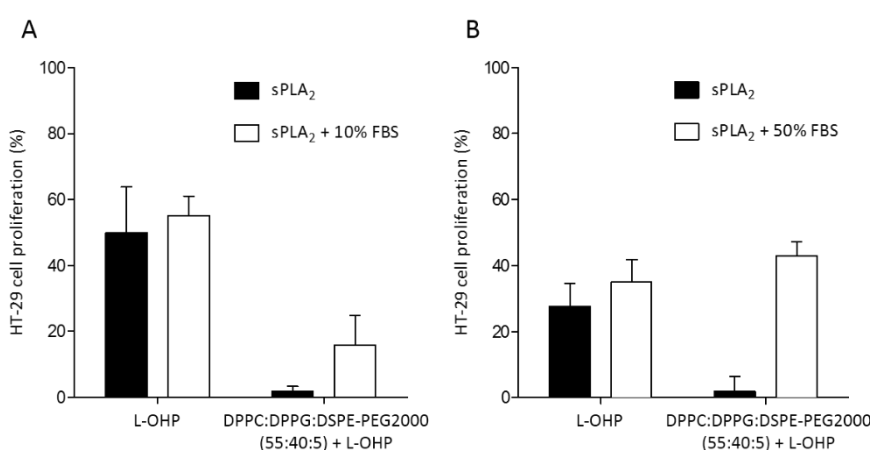
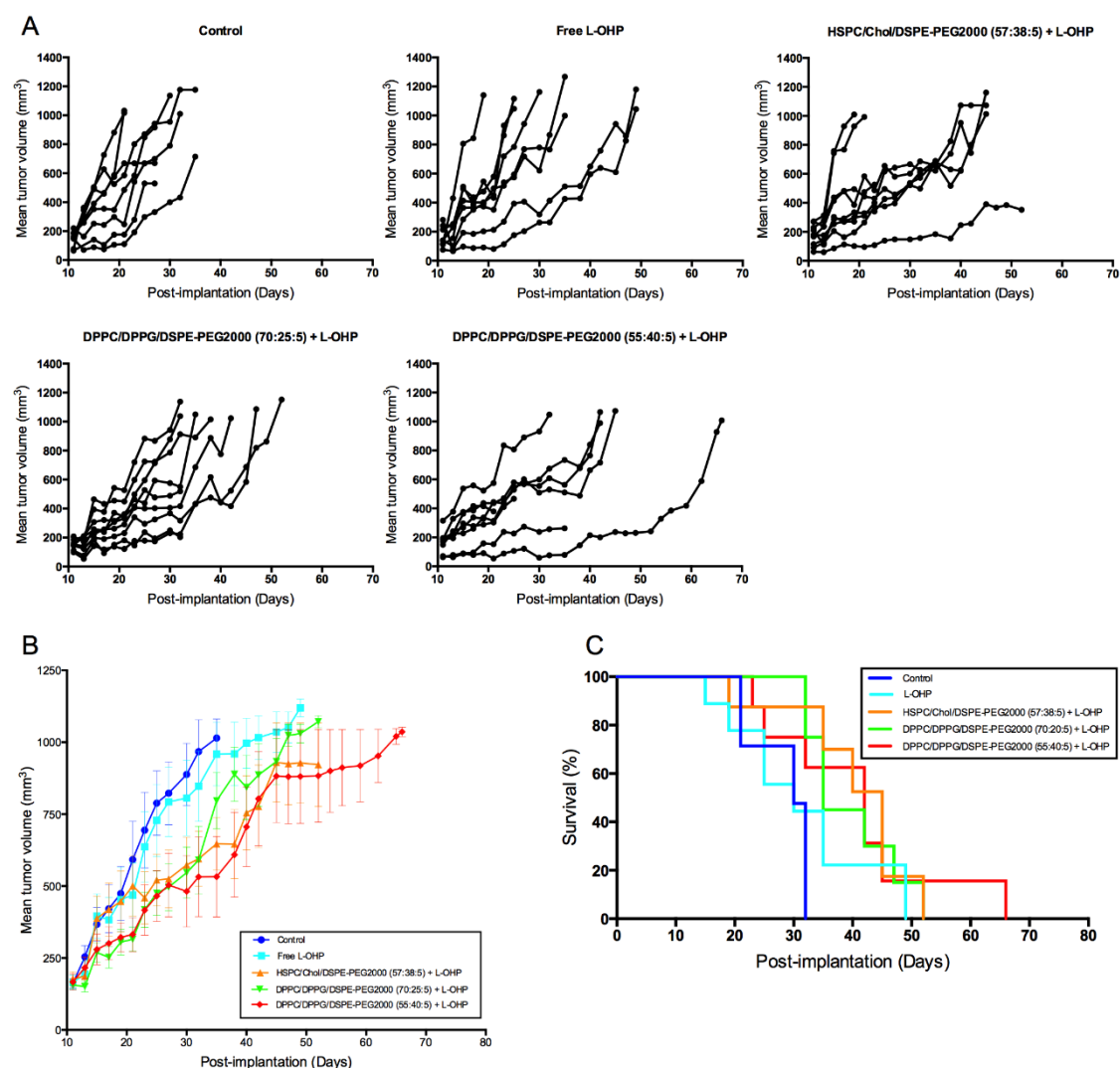


Figure 7.5. Inhibitory effect of sPLA<sub>2</sub>-sensitive liposomes on HT-29 cell proliferation is modulated by presence of serum components. Adding serum to Colo205 cell conditioned medium (A: 10 % FBS; B: 50 % FBS) cytotoxicity induced by sPLA<sub>2</sub>-sensitive liposomal L-OHP falls to same level as free L-OHP. Antiproliferative effect of L-OHP is independent of the presence of serum in the conditioned medium. Colo205 cell conditioned medium (black columns) and with serum (white columns). Results are mean  $\pm$  SD of three experiments.

In addition, for in vivo purposes this would entail that a high intratumoral lipid concentration is necessary to overcome the enzymatically generated membrane permeable products becoming fully sequestered and neutralized by serum albumin. However, leakage of macromolecules such as plasma proteins, and nanoparticulates across the blood endothelium, is not a trivial matter. This is to a large extent influenced by a multitude of factors, such as luminal surface area, blood flow, concentration, hydrostatic and osmotic gradients, which arise from the high fluid escape from blood vessels combined with low lymphatic drainage and high interstitial pressure that limit the movement of large particles by convection.<sup>31,32</sup> Therefore, the in vivo potential of the generated permeability-enhancing enzymatic products of sPLA<sub>2</sub>-catalyzed hydrolysis is closely related to the concentration present of various plasma proteins in the interstitial compartment of the cancer, which can vary enormously and is difficult to predict. Additionally, to rule out that the presence of serum affected the sPLA<sub>2</sub> enzyme activity, we measured the amount of lysolipids generated after treatment of sPLA<sub>2</sub>-sensitive liposomes with enzyme in the presence of serum using mass spectroscopy. We found that the level of lysoPPG generated was unchanged from DPPC/DPPG/DSPE-PEG2000 (55:40:5) liposomes in the presence of serum (Supporting information, Section A3). This demonstrated that even though components in serum can sequester the generated permeability enhancing components from sPLA<sub>2</sub>-sensitive liposomes, the encapsulated drug could become released as the enzyme hydrolyzes the liposomes, irrespective of the presence of serum proteins.

To evaluate the clinical potential of the sPLA<sub>2</sub>-sensitive formulations, we used human Colo205 colon cancer xenografts in nude mice. Earlier studies have confirmed the continued expression of sPLA<sub>2</sub> by Colo205 cells following implantation in mice, which allowed us to use this system as a sPLA<sub>2</sub>-proficient human cancer model.<sup>16</sup> Furthermore, Colo205 xenografts have been shown to be relatively responsive to oxaliplatin following three weekly i.p. injections at a dose of 5 mg/kg.<sup>33</sup> For tumors that express sPLA<sub>2</sub> the expression level is shown to be highest in the tumor periphery. This were the case both in clinical tumors<sup>10,34,35</sup> and also in human cancer xenograft models.<sup>16</sup> To induce triggered-release using liposomal drug delivery, this is of great significance, since the region with highest liposome accumulation tends to be within the tumor periphery. Usually liposomes that extravasate into the tumor parenchyma are restricted to the perivascular region due to poor penetration of the particles that relates to the size of the particles and the high intratumoral pressure build-up.<sup>36</sup> The invasive region of solid tumors is localized in the periphery of the tumor; therefore this region is also the most densely vascularized.<sup>37</sup> For this reason a triggered release strategy based on sPLA<sub>2</sub> is highly feasible as accumulated particles are thought to co-localize with the site of enzyme expression within the tumor.

Despite a clear in vitro anti-proliferative effect of L-OHP against Colo205 cells as shown in figure 7.3, the free drug was not able to significantly improve tumor growth delay of Colo205 xenografts in mice following four i.v. injections of 5 mg/kg at four day intervals (Fig. 7.6). Even though, the antitumor activity was slightly higher for the liposomal formulations of oxaliplatin, it was not possible to show a statistically significant improvement in neither growth inhibition nor median survival relative to the free drug (*p* values > 0.05). In fact, all of the tested formulations exhibited > 40 % treatment-to-control ratios (% T/C) and were therefore classified as therapeutically inactive (Table 7.2; Supporting information, Section A4). Furthermore, the DPPC/DPPG/DSPE-PEG2000 (55:40:5) formulation was observed to be highly toxic with 37.5 % (3 out of 8) of the mice exhibiting excessive weight loss and fatal drug-related toxicity. The cause of this systemic toxicity we suspect is in part related to an excess concentration of permeability enhancing components at high doses is likely to become released into the blood stream.



**Figure 7.6.** Effect of sPLA<sub>2</sub>-degradable liposomal L-OHP against colorectal tumor growth in vivo. Growth inhibition of human Colo205 colorectal carcinoma xenografts subcutaneous in female nude mice after treatment with free L-OHP or sPLA<sub>2</sub>-degradable liposome encapsulated L-OHP (5 mg/kg) intravenous every 4 days for two weeks. Eight or nine mice were included in each group. Tumor volume of individual treatment groups (A), comparison of antitumor activity of treatment groups (B), and survival (C) is shown. Results are presented as mean  $\pm$  SEM. sPLA<sub>2</sub>-degradable liposomal L-OHP did increase tumor growth delay and median survival compared to untreated controls, however were not found to be significantly better than unencapsulated L-OHP or L-OHP formulated in non-sensitive liposomes. Statistical analysis was done by ANOVA test for tumor growth delay and Log-rank test for survival ( $p < 0.05$  is significant).

We found that by increasing the dose of oxaliplatin formulated in DPPC/DPPG/DSPE-PEG2000 (55:40:5) liposomes to 8 mg/kg (equivalent to a lipid dose of 113 mg/kg) in NMRI-nu mice grafted with non-sPLA<sub>2</sub>-secreting FaDu human head and neck squamous cell carcinoma xenografts led to petechial cutaneous hemorrhages in the skin of the mice and concurrent weight loss and dehydration requiring immediate euthanasia (Supporting information, Section A5). Previous findings have shown that several inbred mouse strains have an intact murine group-II sPLA<sub>2</sub> gene, which raises the possibility that sPLA<sub>2</sub> may have been present even though the grafted tumor cells do not secrete the enzyme.<sup>38</sup> In the clinical setting, serum levels of sPLA<sub>2</sub>-IIA are frequently found to be elevated in cancer patients compared to healthy controls.<sup>27-29</sup> Thus, an aberrant serum level of sPLA<sub>2</sub> could potentially lead to premature activation of the particles during circulation, particularly for formulations that are highly sPLA<sub>2</sub>-sensitive. In contrast,

patients treated with LipPlaCis showed no sign of premature activation during systemic circulation, as no correlation was found between serum levels of sPLA<sub>2</sub> and the plasma half life of the liposomes despite plasma sPLA<sub>2</sub> levels were highly variable between the patients.<sup>21</sup> However, as LipPlaCis was comprised of DSPC/DSPG/DSPE-PEG2000 (70:25:5 mol %) the formulation would be expected to be less sensitive towards sPLA<sub>2</sub> than the formulations tested here, with reference to the lower sensitivity of these types of liposomes with up to 40 % PG demonstrated in our in vitro release experiments. This could explain why, despite the high incidence of acute infusion reaction, no compatible side effects were observed in patients that received an escalated dose of 120 mg/m<sup>2</sup> during the course of their treatment.<sup>21</sup> In the case of intravascular activation, we would expect a portion of the drug being released before passive tumor accumulation would be significant. In turn, the drug would reach the tumor as a combination of residual L-OHP still entrapped in liposomes and free drug that has been released from liposomes and has redistributed to tissues including tumor tissue. As we found the antitumor activity of DPPC/DPPG/DSPE-PEG2000 (55:40:5) and HSPC/Chol/DSPE-PEG2000 (57:38:5) to be comparable, it might suggest that only some of the drug was released from the sPLA<sub>2</sub>-sensitive formulation during systemic circulation, while the remaining fraction accumulated in the tumors and became bioavailable following site-specific activation. Yang et al.<sup>39</sup> showed that treating human colorectal carcinoma SW480 xenografts in nude mice with L-OHP formulated in conventional pegylated liposomes achieved a better therapeutic response than the equivalent dose of free L-OHP. Apart from accumulating in tumors the liposomal drug was able to induce apoptosis in the tumor cells associated with the upregulation of proapoptotic Bax and downregulation of antiapoptotic Bcl-2, respectively, as well as induce tumor growth inhibition without having a triggered release mechanism. We believe this effect may be specific for tumor cells with high capacity for taking up the accumulated particles, as other studies using long-circulating liposomes show that most of the accumulated drug remains associated to the liposomes and is not readily released in the tumor interstitium.<sup>40</sup> Also, we show only minor antitumor activity using conventional liposomes against human colorectal carcinoma Colo205 xenografts despite being pegylated.

Table 7.2. Comparison of oxaliplatin and liposomal oxaliplatin against early-stage human Colo205 colorectal carcinoma<sup>a</sup>

Antitumor activity of oxaliplatin									
<i>i.v. agent</i>	Dosage (mg/kg /injection)	Schedule (days)	Drug death (days)	Mean body weight change [g/mouse (day of nadir)]	Median tumor volume [mm <sup>3</sup> on day 19 (range)]	Time for median tumor to reach 500 mm <sup>3</sup>	Time for median tumor to reach 1000 mm <sup>3</sup>	Opt. % T/C (day)	Comments
Free L-OHP <sup>b</sup>	5	11, 15, 19, 23	0/9	-0.11 (25)	398 (91-1140)	23	35	69 (13)	Inactive <sup>c</sup>
HSPC/Chol/DSPE-PEG2000 (57:38:5) + L-OHP	5	11, 15, 19, 23	2/8		334 (101-1010)	30	45	49 (27)	Inactive
DPPC/DPPG/DSPE-PEG2000 (70:25:5) + L-OHP	5	11, 15, 19, 23	2/9	-0.72 (25)	306 (136-542)	32	38	50 (30)	Inactive
DPPC/DPPG/DSPE-PEG2000 (55:40:5) + L-OHP	5	11, 15, 19, 23	3/8	-2.39 (25)	332 (91-522)	25	45	52 (35)	Toxic <sup>d</sup>
Control			0/8	-0,59 (23)	525 (106-881)	19	32		

<sup>a</sup>Colo205 colon carcinoma implanted s.c., 7.5 x 10<sup>6</sup> cells, female NMRI-Nu/Nu; mouse median weight; L-OHP, 25.4 g; HSPC/Chol/DSPE-PEG2000 (57:38:5), 25.8 g; DPPC/DPPG/DSPE-PEG2000 (70:25:5), 26.4 g; DPPC/DPPG/DSPE-PEG2000 (55:40:5), 26.3 g.

<sup>b</sup>Oxaliplatin (L-OHP).

<sup>c</sup>Antitumor activity was based on T/C ratios; < 0.15 is highly efficient; 0.15-0.45 is moderately efficient; > 0.45 is inactive.

<sup>d</sup>Toxicity based on the total body weight loss above 15% over 1 week considered to be excessively toxic according to national ethical standards

In addition to intravascular activation of the particles, a high presence of permeability-enhancing components inside the blood compartment, could possibly also originate from lysolipids and free fatty acids reentering the blood circulation following accumulation and intratumoral activation of the particles. Since sPLA<sub>2</sub> is preferentially localized in the peritumoral tissue of colon cancer,<sup>10,16,34</sup> the site of activation may pose a risk of releasing the components back into the blood stream once generated. Despite reducing the dose to 5 mg/kg (equivalent to a lipid dose of 50 mg/kg for DPPC/DPPG/DSPE-PEG2000 (70:25:5) and 58 mg/kg for DPPC/DPPG/DSPE-PEG2000 (55:40:5), respectively), the DPPC/DPPG/DSPE-PEG2000 (55:40:5 mol %) formulation was still poorly tolerated, with three treatment associated deaths and the group displayed the largest loss in body weight during the treatment period (Fig 7.6, Table 7.2). In contrast, the less sensitive DPPC/DPPG/DSPE-PEG2000 (70:25:5 mol %) formulation was well tolerated with no mice displaying systemic toxicity and very limited weight loss was observed relative to controls (Fig 7.6, Table 7.2). However, despite a lower toxicity this formulation did not improve the therapeutic efficacy, which may signify that the formulation was not sensitive enough to become hydrolyzed in the tumor xenografts. In order to clarify the pharmacokinetics of sPLA<sub>2</sub>-sensitive liposomal L-OHP degradation in the blood circulation and at the target tumor site, further studies with labeled liposomes are required.

#### 7.4. Conclusions

We did not find evidence of an increased sensitivity of liposomal formulations towards sPLA<sub>2</sub>-triggered drug release was able to increase drug efficacy compared to conventional liposomes. In turn, our findings indicate that systemic toxicity of sPLA<sub>2</sub>-sensitive liposomes is a combined effect of both their sensitivity towards the enzyme and the amount of the lipid that is dosed. Increasing the amount of PG to 40 % to render the formulation more sensitive also increases the rate of systemic toxicity and inevitably limit their use in clinical applications, whereas 25 % PG despite no detectable systemic toxicity in our preclinical model, did not induce higher growth inhibition than STEALTH<sup>®</sup> liposomes.

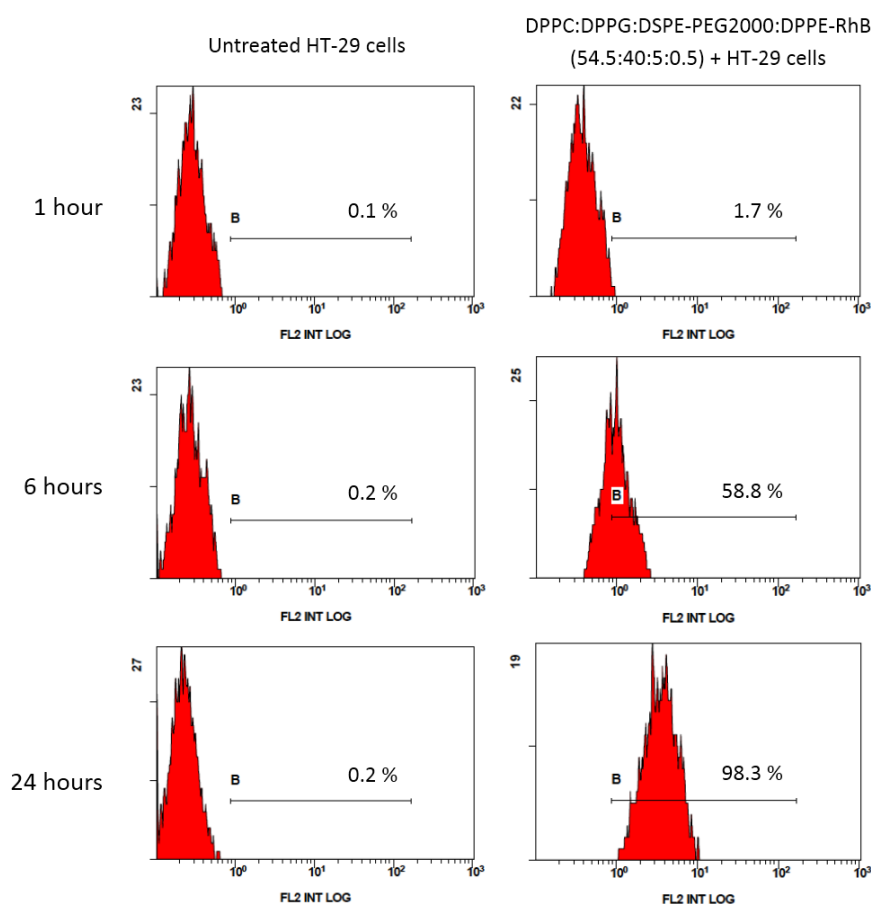
#### 7.5. Supporting information

##### Section A1

###### *Cell uptake study*

HT-29 cells (200.000 cells) were plated in 12-well plates in 2 mL of RPMI-1640 medium containing 10% FBS and pre-incubated for 24 h. After removal of culture medium, 2 mL of fresh medium containing rhodamine B (RhB)-labeled liposomes (300 μM lipid) was added, followed by incubation at 37 °C. At 1, 6 and 24 hours post-incubation, the cells were trypsinized and washed twice with cold phosphate buffered saline (PBS). The cells were resuspended in 0.5 mL of PBS and the cellular uptake of RhB-labeled liposomes was quantified using a Gallios<sup>TM</sup> flow cytometer (Beckman Coulter, California, USA), equipped with an argon-ion (488 nm) laser and 575/30 bandpass filter for emission measurements. A total of 10.000 events were collected based on a large forward and side scatter. The histograms of untreated cells and cells treated with RhB-labeled liposomes are shown after 1, 6 and 24 hours incubation, and the percentage of Rhodamine B-positive cells is included.



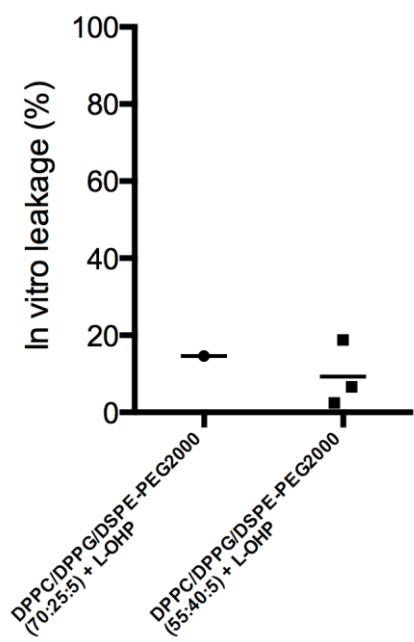


## Section A2

### *In vitro serum leakage*

The *in vitro* leakage of liposome-encapsulated oxaliplatin in serum was assessed following incubation with 50 % (v/v) FBS in 10 mM Hepes, 5 % glucose, pH 7.4 at 37 °C. Briefly, liposomes were diluted in serum-containing solvent to a final lipid concentration of 0.5 mM and incubated for 24 hours at 37 °C. Immediately after drawing aliquots to determine the amount of platinum released using ICP-MS, the samples were diluted 100-fold in Hepes-buffer and fractionated using Amicon spin-filters of 30 kDa molecular cutoff (1000×g, 15 min), which separate the free fraction from the liposome-associated fraction. Hereafter, the total and free fractions were further diluted in 2 % HCL containing 0.5 ppb of Iridium (app. 500000-fold for total platinum, sample before running spin-filtration; app. 100000-fold for free platinum, the run-through sample) before being analyzed by ICP-MS. The percentage of leakage was calculated using the formula  $100 \% \times ([\text{free}] / [\text{total}])$ . Both formulations exhibited low degree of drug leakage (<20 %) in the presence of serum and were therefore considered relatively stable.

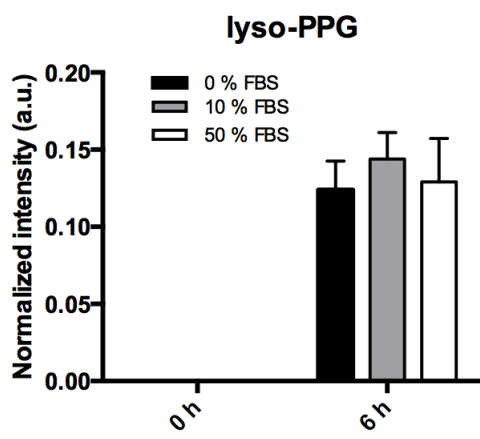




### Section A3

#### Lipid hydrolysis

Liposomes were diluted in cell conditioned growth media (CCM) from Colo205 cells, containing 0, 10 or 50 % FBS, to a final concentration of 4 mM, and incubated at 37 °C for 6 h with gentle magnetic stirring. 0 h samples were prepared by mixing liposomes with heat inactivated CCM. Lipid hydrolysis and consequent formation of lyso-PPG was analyzed by MALDI-TOF MS. Briefly, samples were mixed 1:10 with matrix/POPC (2,5-dihydroxybenzoic acid (DHB) spiked with sodium trifluoroacetate (NaTFA) in methanol as matrix, with 500 μM POPC as internal reference), spotted in triplicates and analyzed by Bruker autoflex speed (Bruker Daltonics, Bremen, Germany). Observed MW: 507.4 (M+H<sup>+</sup>+Na<sup>+</sup>) and 529.4 (M+2Na<sup>+</sup>). Expected MW: 507.3 (M+H<sup>+</sup>+Na<sup>+</sup>) and 529.3 (M+2Na<sup>+</sup>). All peak intensities corresponding to lyso-PPG were normalized to all peak intensities corresponding to POPC. Values are mean of triplicates plus/minus standard deviation. All samples showed formation of lyso-PPG after incubation with sPLA<sub>2</sub> (6 h), and no lyso-PPG was present before incubation (0 h). The formation of lyso-PPG did not seem to be dependent on the presence of serum.



## Section A4

### Overview of T/C ratios of oxaliplatin against Colo205 xenografts

Treatment-to-control (T/C) ratios for free oxaliplatin (5 mg/kg) and liposomal oxaliplatin (5 mg/kg) against human Colo205 colorectal carcinoma xenografts following 4 injections given every 4 days. The median tumor volume and number of mice for each group is presented, along with the calculated T/C ratios using the formula: % T/C = 100 x (median tumor size of treatment group at day x) / (median tumor size of control group at day x). The optimal % T/C for each formulation is highlighted in red and T/C ratios < 0.15 were considered highly effective, T/C ratios 0.15 - 0.45 were considered moderately efficient, and T/C ratios > 0.45 were considered inactive.

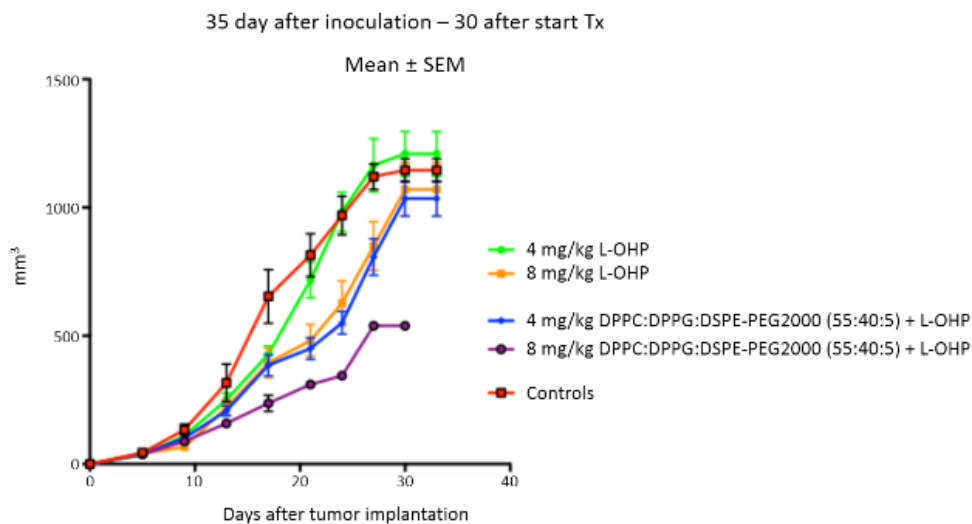
Day	Median tumor volume (mm <sup>3</sup> )												% T/C ratio			
	Control	N	L-OHP	N	HSPC/Chol/DSPE-PEG2000 (57:38:5) + L-OHP	N	DPPC/DPPG/DSPE-PEG2000 (70:25:5) + L-OHP	N	DPPC/DPPG/DSPE-PEG2000 (55:40:5) + L-OHP	N	L-OHP	HSPC/Chol/DSPE-PEG2000 (57:38:5) + L-OHP	DPPC/DPPG/DSPE-PEG2000 (70:25:5) + L-OHP	DPPC/DPPG/DSPE-PEG2000 (55:40:5) + L-OHP		
11	163	7	140	8	180	9	153	9	178	8	86	110	93	109		
13	277	7	192	8	177	9	170	9	225	8	69	64	61	81		
15	390	7	389	8	303	9	251	9	281	8	100	78	64	72		
17	459	7	377	8	293	9	248	9	308	8	82	64	54	67		
19	525	7	398	8	335	9	307	9	333	8	76	64	58	63		
21	585	7	443	8	444	9	331	9	346	8	76	76	57	59		
23	692	6	630	8	416	8	413	9	434	7	91	60	60	63		
25	858	6	689	8	473	8	438	9	528	7	80	55	51	62		
27	929	6	856	8	458	7	477	9	568	6	92	49	51	61		
30	986	6	913	8	537	7	488	9	531	6	93	55	50	54		
32	1024	6	957	8	611	7	519	9	569	6	93	60	51	56		
35	1024	6	1082	8	682	7	800	8	536	6	106	67	78	52		
38			1082	8	685	6	1015	7	677	5						
40			1082	8	789	6	1015	7	765	5						
42			1082	8	801	5	1023	7	989	5						
45			1082	8	1014	5	1023	7	1047	5						
47			1082	8	1014	5	1038	7	1047	5						
49			1128	8	1014	5	1038	7	1047	5						
52					1014	5	1050	7	1047	5						
54									1047	5						
56									1047	5						
59									1047	5						
62									1047	5						
65									1047	5						
66									1047	5						

## Section A5

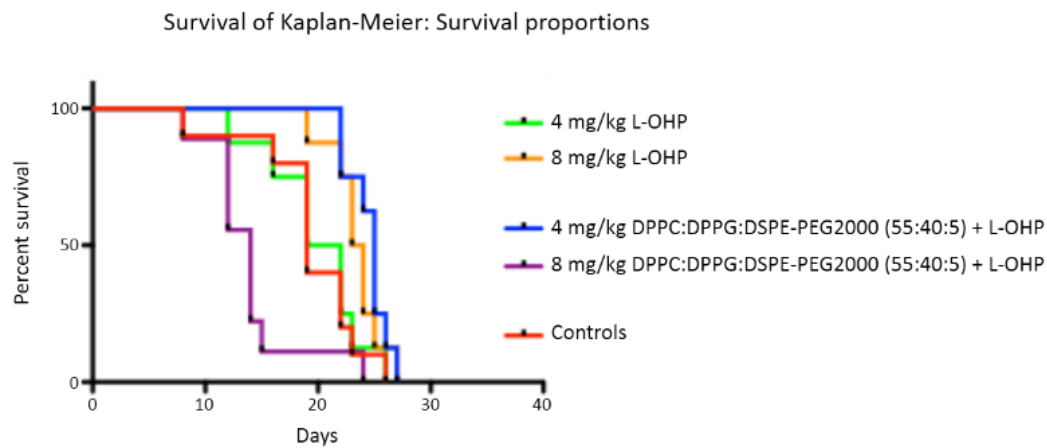
### Antitumor activity of sPLA<sub>2</sub>-degradable liposomal L-OHP against non-sPLA<sub>2</sub>-secreting FaDu human head and neck squamous cell carcinoma xenografts

Growth inhibition of human FaDu tumor xenografts implanted subcutaneous in female nude mice after treatment with free L-OHP or sPLA<sub>2</sub>-degradable DPPC/DPPG/DSPE-PEG2000 (55:40:5 mol %) liposome-encapsulated L-OHP at 4 or 8 mg/kg drug doses (equivalent to 57 and 113 mg/kg lipid dose, respectively) i.v. every 4 days for two weeks. Eight mice were included in each group. Comparison of antitumor activity of treatment groups (A) and survival (B) is shown. Results are presented as means ± SE. sPLA<sub>2</sub>-degradable liposomal L-OHP did not increase tumor growth delay or median survival to a noteworthy degree compared to equivalent doses of free drug. At the high dose tested the sPLA<sub>2</sub>-sensitive liposome formulations became toxic and led to diffuse petechial cutaneous hemorrhages manifested in the skin of the mice that was associated with weight loss, dehydration and required euthanasia when observed (C).

A



B



C



## 7.6. References

- (1) Kraft, J. C.; Freeling, J. P.; Wang, Z.; Ho, R. J. Y. Emerging Research and Clinical Development Trends of Liposome and Lipid Nanoparticle Drug Delivery Systems. *J. Pharm. Sci.* **2014**, *103*, 29–52.
- (2) Knop, K.; Hoogenboom, R.; Fischer, D.; Schubert, U. S. Poly(ethylene Glycol) in Drug Delivery: Pros and Cons as Well as Potential Alternatives. *Angew. Chem. Int. Ed. Engl.* **2010**, *49*, 6288–6308.
- (3) Andresen, T. L.; Jensen, S. S.; Jørgensen, K. Advanced Strategies in Liposomal Cancer Therapy: Problems and Prospects of Active and Tumor Specific Drug Release. *Progress in Lipid Research*, **2005**, *44*, 68–97.
- (4) Drummond, D.; Noble, C. Pharmacokinetics and in Vivo Drug Release Rates in Liposomal Nanocarrier Development. *J. Pharm. Sci.* **2008**, *97*, 4696–4740.
- (5) Ponce, A. M.; Vujaskovic, Z.; Yuan, F.; Needham, D.; Dewhirst, M. W. Hyperthermia Mediated Liposomal Drug Delivery. *Int. J. Hyperthermia* **2006**, *22*, 205–213.
- (6) Yatvin, M.; Weinstein, J.; Dennis, W.; Blumenthal, R. Design of Liposomes for Enhanced Local Release of Drugs by Hyperthermia. *Science*. **1978**, *202*, 1290–1293.
- (7) Satchi, R.; Connors, T. A.; Duncan, R. *Br J Cancer* **2001**, *81*, 1070–1076.
- (8) Basel, M. T.; Shrestha, T. B.; Troyer, D. L.; Bossmann, S. H. Protease-Sensitive, Polymer-Caged Liposomes: A Method for Making Highly Targeted Liposomes Using Triggered Release. *ACS Nano* **2011**, *5*, 2162–2175.
- (9) Andresen, T. L.; Davidsen, J.; Begtrup, M.; Mouritsen, O. G.; Jørgensen, K. Enzymatic Release of Antitumor Ether Lipids by Specific Phospholipase A2 Activation of Liposome-Forming Prodrugs. *J. Med. Chem.* **2004**, *47*, 1694–1703.
- (10) Tribler, L. Increased Expression and Activity of Group IIA and X Secretory Phospholipase A2 in Peritumoral versus Central Colon Carcinoma Tissue. *Anticancer Res.* **2007**, *27*, 3179–3185.
- (11) Yamashita, S.-I.; Yamashita, J.-I.; Sakamoto, K.; Inada, K.; Nakashima, Y.; Murata, K.; Saishoji, T.; Nomura, K.; Ogawa, M. Increased Expression of Membrane-Associated Phospholipase A2 Shows Malignant Potential of Human Breast Cancer Cells. *Cancer* **1993**, *71*, 3058–3064.
- (12) Abe, T.; Sakamoto, K.; Kamohara, H.; Hirano, Y.; Kuwahara, N.; Ogawa, M. Group II Phospholipase A2 Is Increased in Peritoneal and Pleural Effusions in Patients with Various Types of Cancer. *Int. J. Cancer* **1997**, *74*, 245–250.
- (13) Kiyohara, H.; Egami, H.; Kako, H.; Shibata, Y.; Murata, K.; Ohshima, S.; Sei, K.; Suko, S.; Kurano, R.; Ogawa, M. Immunohistochemical Localization of Group II Phospholipase A2 in Human Pancreatic Carcinomas. *Int. J. Pancreatol.* **1993**, *13*, 49–57.
- (14) Jiang, J.; Neubauer, B. L.; Graff, J. R.; Chedid, M.; Thomas, J. E.; Roehm, N. W.; Zhang, S.; Eckert, G. J.; Koch, M. O.; Eble, J. N.; et al. Expression of Group IIA Secretory Phospholipase A2 Is Elevated in Prostatic Intraepithelial Neoplasia and Adenocarcinoma. *Am. J. Pathol.* **2002**, *160*, 667–671.

- (15) Berg, O. G.; Gelb, M. H.; Tsai, M.-D.; Jain, M. K. Interfacial Enzymology: The Secreted Phospholipase A 2 - Paradigm. *Chem. Rev.* **2001**, 101, 2613–2654.
- (16) Jensen, S. Secretory Phospholipase A(2) as a Tumor-Specific Trigger for Targeted Delivery of a Novel Class of Liposomal Prodrug Anticancer Etherlipids. *Mol. Cancer Ther.* **2004**, 3, 1451–1458.
- (17) Linderoth, L.; Fristrup, P.; Hansen, M.; Melander, F.; Madsen, R.; Andresen, T. L.; Peters, G. H. Mechanistic Study of the sPLA2-Mediated Hydrolysis of a Thio-Ester pro Anticancer Ether Lipid. *J. Am. Chem. Soc.* **2009**, 131, 12193–12200.
- (18) Quach, N. D.; Arnold, R. D.; Cummings, B. S. Secretory Phospholipase A2 Enzymes as Pharmacological Targets for Treatment of Disease. *Biochem. Pharmacol.* **2014**, 90, 338–348.
- (19) Davidsen, J.; Vermehren, C.; Frokjaer, S.; Mouritsen, O. G.; Jørgensen, K. Drug Delivery by Phospholipase A2 Degradable Liposomes. *Int. J. Pharm.* **2001**, 214, 67–69.
- (20) Liu, D.; He, C.; Wang, A. Z.; Lin, W. Application of Liposomal Technologies for Delivery of Platinum Analogs in Oncology. *Int. J. Nanomedicine* **2013**, 8, 3309–3319.
- (21) De Jonge, M. J. a; Slingerland, M.; Loos, W. J.; Wiemer, E. a C.; Burger, H.; Mathijssen, R. H. J.; Kroep, J. R.; den Hollander, M. a G.; van der Biessen, D.; Lam, M.-H.; et al. Early Cessation of the Clinical Development of LiPlaCis, a Liposomal Cisplatin Formulation. *Eur. J. Cancer* **2010**, 46, 3016–3021.
- (22) Hope, M. J.; Bally, M. B.; Webb, G.; Cullis, P. R. Production of Large Unilamellar Vesicles by a Rapid Extrusion Procedure: Characterization of Size Distribution, Trapped Volume and Ability to Maintain a Membrane Potential. *Biochim. Biophys. Acta* **1985**, 812, 55 – 65.
- (23) Wacklin, H. P.; Tiberg, F.; Fregneto, G.; Thomas, R. K. Distribution of Reaction Products in Phospholipase A2 Hydrolysis. *Biochim. Biophys. Acta* **2007**, 1768, 1036 – 1049.
- (24) Allen, T. M.; Cullis, P. R. Drug Delivery Systems: Entering the Mainstream. *Science* **2004**, 303, 1818–1822.
- (25) Jørgensen, K.; Davidsen, J.; Mouritsen, O. G. Biophysical Mechanisms of Phospholipase A2 Activation and Their Use in Liposome-Based Drug Delivery. *FEBS Lett.* **2002**, 531, 23–27.
- (26) Saari, K. Group IIPLA(2) Content of Tears in Normal Subjects. *Investig. Ophthalmol. Vis. Sci.* **2001**, 42, 318 – 320.
- (27) Scott, K. F.; Sajinovic, M.; Hein, J.; Nixdorf, S.; Galettis, P.; Liauw, W.; de Souza, P.; Dong, Q.; Graham, G. G.; Russell, P. J. Emerging Roles for Phospholipase A2 Enzymes in Cancer. *Biochimie* **2010**, 92, 601–610.
- (28) Menschikowski, M.; Hagelgans, A.; Fuessel, S.; Mareninova, O. a; Neumeister, V.; Wirth, M. P.; Siegert, G. Serum Levels of Secreted Group IIA Phospholipase A(2) in Benign Prostatic Hyperplasia and Prostate Cancer: A Biomarker for Inflammation or Neoplasia? *Inflammation* **2012**, 35, 1113–1118.
- (29) Buhmeida, a; Bendardaf, R.; Hilska, M.; Laine, J.; Collan, Y.; Laato, M.; Syrjänen, K.; Pyrhönen, S. PLA2 (group IIA Phospholipase A2) as a Prognostic Determinant in Stage II Colorectal Carcinoma. *Ann. Oncol.* **2009**, 20, 1230–1235.

- (30) Kim, Y.-L.; Im, Y.-J.; Ha, N.-C.; Im, D.-S. Albumin Inhibits Cytotoxic Activity of Lysophosphatidylcholine by Direct Binding. *Prostaglandins Other Lipid Mediat.* **2007**, *83*, 130–138.
- (31) McDonald, D. M.; Baluk, P. Significance of Blood Vessel Leakiness in *Cancer*. *CANCER Res.* **2002**, *62*, 5381 – 5385.
- (32) Jain, R. K. Delivery of Molecular and Cellular Medicine to Solid Tumors. *Adv. Drug Deliv. Rev.* **2012**, *64*, 353–365.
- (33) Li, L.; Ahmed, B.; Mehta, K.; Kurzrock, R. Liposomal Curcumin with and without Oxaliplatin: Effects on Cell Growth, Apoptosis, and Angiogenesis in Colorectal Cancer. *Mol. Cancer Ther.* **2007**, *6*, 1276–1282.
- (34) Edhemović, I.; Snoj, M.; Kljun, A.; Golouh, R. Immunohistochemical Localization of Group II Phospholipase A2 in the Tumours and Mucosa of the Colon and Rectum. *Eur. J. Surg. Oncol.* **2001**, *27*, 545–548.
- (35) Buhmeida, A.; Bendardaf, R.; Hilska, M.; Laine, J.; Collan, Y.; Laato, M.; Syrjänen, K.; Pyrhönen, S. PLA2 (group IIA Phospholipase A2) as a Prognostic Determinant in Stage II Colorectal Carcinoma. *Ann. Oncol.* **2009**, *20*, 1230–1235.
- (36) Jain, R. K. Barriers to Drug Delivery in Solid Tumors. *Sci. Am.* **1994**, *271*, 58–65.
- (37) Bhujwala, Z. M.; Artemov, D.; Natarajan, K.; Ackerstaff, E.; Solaiyappan, M. Vascular Differences Detected by MRI for Metastatic Versus Nonmetastatic Breast and Prostate Cancer Xenografts. *Neoplasia* **2001**, *3*, 143–153.
- (38) Kennedy, B. P.; Payette, P.; Mudgett, J.; Vadas, P.; Pruzanski, W.; Kwan, M.; Tang, C.; Rancourt, D. E.; Cromlish, W. a. A Natural Disruption of the Secretory Group II Phospholipase A2 Gene in Inbred Mouse Strains. *J. Biol. Chem.* **1995**, *270*, 22378–22385.
- (39) Yang, C.; Liu, H. Z.; Fu, Z. X.; Lu, W. D. Oxaliplatin Long-Circulating Liposomes Improved Therapeutic Index of Colorectal Carcinoma. *BMC Biotechnol.* **2011**, *11*, 21.
- (40) Zamboni, W. C.; Gervais, A. C.; Egorin, M. J.; Schellens, J. H. M.; Zuhowski, E. G.; Pluim, D.; Joseph, E.; Hamburger, D. R.; Working, P. K.; Colbern, G.; et al. Systemic and Tumor Disposition of Platinum after Administration of Cisplatin or STEALTH Liposomal-Cisplatin Formulations (SPI-077 and SPI-077 B103) in a Preclinical Tumor Model of Melanoma. *Cancer Chemother. Pharmacol.* **2004**, *53*, 329–336.





## General conclusions

Lipid molecules can form numerous supramolecular structures through their self-assembly properties displayed within aqueous environments. One of the most explored structures, the liposome, are formed when lamellar bilayers bend into closed vesicles containing an aqueous core. This particular structural organization, offering hydrophilic (core) and hydrophobic (within the membrane) environments to carry both polar and non-polar molecules, have garnered enormous interest among scientists of several disciplines. In addition, as lipids constitute part of the naturally-occurring biomolecules present in any living organism, liposomes benefit from biocompatible, biodegradable and non-immunogenic properties. Consequently, liposomes have been extensively established as versatile tools in a large number of applications including pharmaceuticals, cosmetics, food technology, models as biological membranes, signal amplifiers in analytical sciences, nanoreactors, and diagnosing tools amongst others.

Metallic nanoparticles have garnered huge interest in the last decades due to their size- and shape-dependant unique properties. Several strategies have been proposed for the controlled synthesis which rely in the use of surfactant templates for the preparation of nanoparticles in a more controlled way. However, these approaches commonly exploit non-sustainable procedures using harsh chemicals and elevated temperature conditions. As an alternative, we have developed an environmentally-friendly method for the controlled synthesis of metallic nanoparticles exploiting the use of liposomes and other lipid supramolecular structures as nano-sized reactors or templates.

We have firstly proposed the use of glycerol as green catalyst for the reduction of palladium into small nanoparticles within liposomal nanoreactors, and demonstrated that the functional liposomal nanoreactors with glycerol incorporated within the core were able to modulate the reduction kinetics by confining a determined number of palladium ions per glycerol molecules. The produced palladium nanoparticles were compared with those prepared without the use of liposomal nanoreactors under the same conditions, and a clear control of the nanoparticle's size and shape was rendered by the liposome nanoreactors.

The membrane of the liposome plays a very important role in nanoparticle synthesis, acting as a route for the precursors to enter the nanoreactor. The membrane permeability of the liposomal nanoreactors towards glycerol molecules provides a semi-mobile environment to glycerol for modulating the reaction by increasing the reducer-to-palladium ratio, thus increasing the number of nucleation points and moderating the nanoparticle growth. Nanoreactor membranes in their liquid phase at a working temperature above their main  $T_m$ , were demonstrated to yield nanoparticles with reduced sizes due to their enhanced permeability towards glycerol to move from the bulk solution inside the liposomes and keep a high glycerol/palladium ratio. However, liposomes prepared with lipids displaying a gel phase behaviour that provides highly ordered and dense bilayers reduced the capacity of glycerol to flow inside the liposome core, leading to a lower OH/Pd ratio and thus producing larger palladium nanoparticles. Small and homogeneous palladium nanoparticles ( $2.6 \pm 0.7$  nm) were produced within glycerol-incorporated DOPG liposomes. This can be explained by the presence of a higher number of glycerol molecules in the lipid headgroup which gives a higher number of available hydroxyl groups to reduce the palladium ions and stabilize the synthesized palladium nanoparticles inside the nanoreactors. In addition, we have explored the role of glycerol acting

as capping agent by demonstrating the presence of glycerol over the palladium nanoparticles using FTIR and SERS. Finally, we have also demonstrated the catalytic activity of the prepared palladium nanoparticles in the reduction of p-nitrophenolate to p-aminophenol in the presence of sodium borohydride.

A similar green glycerol-incorporated liposomal nanoreactor system was employed for the preparation of gold nanoparticles. After optimization of the liposomal membrane composition, DOPG liposomes were used in order to provide the best nanoreactor conditions. In this case, several reaction parameters including temperature, glycerol concentration, presence of capping agent, were also studied to elucidate their effect on the final size and homogeneity of the gold nanoparticles produced. Increasing concentrations of glycerol incorporated to the liposomal nanoreactors resulted in a decrease in nanoparticle size, and in contrast with palladium nanoparticles, the further addition of MCH as strong capping agent reduced the gold nanoparticle size almost by half. Moreover, a drastic decrease in the nanoparticle size at constant concentrations of capping agent and glycerol was observed when the temperature was increased from of 4 to 25 °C, and very few until 50 °C. Overall, small and homogeneous gold nanoparticles ( $2.9 \pm 0.2$  nm) were prepared within DOPG liposomal nanoreactors with 15 % glycerol concentration (v/v) in the presence of MCH capping agent.

Once the ability of glycerol-incorporated liposomal nanoreactors to control the size during the synthesis and produce very small nanoparticles was demonstrated, different lipid structures were explored as templates for the shape controlled synthesis of gold nanoparticles. Several lipid structures with changing polar head groups and different tail lengths were demonstrated as templates for the preparation of gold nanoparticles, where their shape was directly linked to the template geometry.

Templates were prepared of DPPC and LysoPC at 45 and 25 °C for the rectangular and hexagonal-shaped templates, and of DMPG and LysoPC at 25 °C for the ribbon-like lipid nanowires. The synthesis of rectangular and hexagonal-shaped gold nanoparticles was performed through the content exchange after fusion of preformed lipid structures containing citrate and gold loaded lipid structures, forming homogeneous populations of disk-like gold nanoparticles and heterogeneous mix of hexagonal gold disks respectively.

In the case of lipid twisted ribbons made up of negatively charged DMPG lipids, different approaches were carried out:  $\text{HAuCl}_4$  loaded twisted lipid ribbon template was immersed in (1) PBS, (2) citrate in PBS or (3) mixed with citrate encapsulating twisted lipid ribbons. The last method (4), consisted in citrate encapsulating twisted ribbons template immersed in  $\text{HAuCl}_4$  in PBS. Template immersed in PBS gave ribbon-like shaped structures (1) in which the addition of citrate to the template increased the appearance of the ribbon shape gold structures as a result of reduction reaction (2). Mixing both templates encapsulating the gold and citrate (3), as well as when immersing the citrate loaded template in the  $\text{HAuCl}_4$  solution (4), resulted in organizations of tiny gold nanoparticles aligned in a way guided by the lipid template structure. The possible assembling mechanism showed a high dependence in the administration route of the reactants and thus were discussed in terms of the resulting gold nanostructures obtained. In conclusion, self-assembled lipid based nanostructures were demonstrated to be promising tools for the synthesis of metal nanoparticles of controlled morphology and size. The possibility to prepare diversely shaped and sized nanoparticles under mild conditions should find a plethora of potential applications in catalysis, plasmonics and electronics.

Dietary polyphenols have been reported to modulate the intracellular levels of labile zinc, in consequence affecting the activity of numerous signalling and metabolic cellular pathways. Numerous studies have suggested the therapeutic effect of several of those dietary polyphenols in the prevention of cancers, diabetes, and cardiovascular and neurodegenerative diseases. We have demonstrated the capacity of two of the most consumed phenolic compounds present in the human diet, quercetin and epigallocatechin-gallate, to increase the amount of labile zinc within mouse hepatocarcinoma Hepa 1-6 cells, and compared the results with the well-reported ionophore clioquinol. However, in order to confirm that the polyphenols transport zinc cations across the plasma membrane independently of cell transport mechanisms, such as zinc transporters or endocytosis, we explored the use of FluoZin-3 loaded liposomes as simple membrane systems that mimic the cell membrane. The zinc ionophore activity of quercetin and epigallocatechin-gallate was demonstrated as their capacity of polyphenols to transport zinc inside the liposomes and increase the zinc-specific fluorescence of the encapsulated fluorophore FluoZin-3. Both polyphenols displayed a strong zinc ionophore activity and thus was confirmed by dynamic light scattering, zeta potential, and confocal and transmission electron microscopy in order to confirm that the fluorescent signal emerges from the inner part of the liposomes and to check their stability after treatments.

The efficient liposomal system was also used for screening the zinc ionophore activity of a selected library consisting of the most relevant dietary polyphenols. At first, the zinc-chelating strength of the phenolic compounds was tested in a competition assay based on the fluorescence quenching of zinc-dependent fluorescence emitted by zinc-FluoZin-3 complex. On the other hand, we have classified the phenolic compounds by their ionophore activity by means of fluorescence coming from FluoZin-3 encapsulated within liposomes. Finally we were able to show the correlation between the chelation capacity and ionophore activity, thus underlining the different behaviours that the phenolic compounds can display, sequestering or ionophore, thus, giving us a better knowledge of the importance of the structural conformation versus their biological activity.

Exploiting the application of liposomes as drug delivery carriers, an enzyme-sensitive pegylated liposome drug delivery system was developed for the site-specific delivery of oxaliplatin, a chemotherapeutic agent, for the treatment of colon cancer. Long circulating pegylated liposomal oxaliplatin confirmed to have the ability to confine the drug, thus limiting its toxic side-effects, and to enhance drug accumulation in the tumor tissue by the EPR effect. The membrane composition of the liposome carrier was carefully formulated to enhance the enzyme-sensitivity towards its degradation by secretory phospholipase A<sub>2</sub> (sPLA<sub>2</sub>), an overexpressed enzyme in many cancer cells, thus resulting in a site-specific release of oxaliplatin only in cancer tissue. At first, we demonstrated in a calcein release study that modulating the ratio between DPPC and DPPG lipid present in the liposome membrane we were able to tune its sensitivity towards sPLA<sub>2</sub> activity and modify the drug release profile. *In vitro* treatment of cancer cell lines with sPLA<sub>2</sub>-sensitive liposomes loaded with oxaliplatin resulted in a superior growth inhibition compared to free drug or loaded within conventional liposomes. In addition, we have shown that the hydrolysis by-products formed by sPLA<sub>2</sub>, lysolipids and fatty acids, are capable of acting as cell permeability enhancers and display toxic effect. Finally, *in vivo* studies performed in nude mice with sPLA<sub>2</sub>-secreting human colon cancer xenograft models resulted in an improvement in tumor growth delay compared to the free drug, but not to conventional liposomal drug. In conclusion, the developed enzyme-sensitive liposomal oxaliplatin carrier was able to effectively enhance the pharmacokinetics of the drug, but suffered from a reduced triggered release response in the complex *in vivo* scenario.

In summary, the work presented in this doctoral thesis strengthens the view of liposomes as versatile tools that can be used in many different applications. Liposomes were exploited as nanoreactors or templates for the shape and size controlled synthesis of metal nanoparticles. Furthermore, liposomes were used as membrane models that mimic the cell plasma membrane for the determination of zinc ionophore activity of several dietary phenolic compounds. Ultimately, the ability of liposomes to carry and delivery drugs was explored in order to investigate the potential of enzyme-degradable liposomes as drug carriers for the encapsulation of oxaliplatin for the treatment of colon cancer.



